Investigating the Molecular Regulation and Morphological Dynamics of the Visceral Endoderm



Sharon Ruane

St. Edmund Hall

Department of Physiology, Anatomy and Genetics
University of Oxford

Oxford, United Kingdom

July 2016

This thesis is dedicated to my mother, the best person I know.

Declaration

I declare that this thesis is entirely my own work. This dissertation has not in whole, or in part, been previously submitted for a higher degree.

Sharon Ruane

Acknowledgements

I gratefully acknowledge the Wellcome Trust for funding the majority of this PhD, and the Department of Physiology, Anatomy and Genetics for providing additional funding in my final year. I would like to express my very great appreciation to my supervisor, Dr. Shankar Srinivas, for his professional guidance throughout my PhD. I would also like to thank our collaborators in the Vanhaesebroeck lab, who performed the mass spectrometry described in Chapter 5 of the thesis. I am also grateful to Prof. Tony Delaney who provided advice on the statistical analysis used in this work.

I would also like to extend my thanks to past and current members of the Srinivas lab, who provided advice and friendship during the course of this thesis. I am particularly grateful to Dr. Bradley Joyce, who shared experience of microscopy and mouse husbandry at the start of my PhD. I am eternally indebted to Antonio Miranda, a wonderful friend and excellent scientist, who kept me sane through my final year.

I wish to acknowledge the encouragement of Chris Garvey, whose excellent classes convinced a grumpy teenager to study science. In a similar vein I would like to thank Dr. Vincent Kelly, whose confidence in me convinced me to shoot further than I had previously considered.

I am entirely sure that without my friends I would never have made it though the more turbulent periods of the past few years. I am extremely grateful to Dr. Eilis Carroll, whose support, both personal and academic, has been invaluable. I would also like to thank Fiona Morrin and Mary Lindsay for their friendship during my academic career and long before. I am also

grateful to Dr. Matthew Carrigan and Dr. Kevin Powell for their encouragement and companionship.

Finally, I would like to express my appreciation to my family for their support during this PhD and the rest of my academic studies. To my sister Rosie, I am thankful to have such a wonderful person in my family.
And to my mother, who inspires me in ways far more numerous than can be listed here, I would like to extend my deepest thanks. I cannot imagine a kinder or more encouraging parent. For that and a thousand other things, I am truly grateful.

Abstract

Cell migration is of huge importance in the field of development, where the correct positioning of signaling centers and functional structures is of paramount importance. An example of this occurs within the Visceral Endoderm (VE), an extra-embryonic epithelium that is involved in patterning the embryo. A specialized subset of VE cells known as the anterior visceral endoderm (AVE) is induced at the distal tip of the egg-cylinder, and is responsible for specifying anterior embryo pattern. AVE cells migrate in a stereotypic manner towards the prospective anterior. Failure of this migration leads to dramatic mis-patterning of the primary body axis and renders the embryo unviable. The main aim of my D.Phil is to investigate cell movements throughout the VE, in order to understand the behaviour of both the AVE and non-AVE cells and to give insight into the global cell dynamics of reorganizing epithelial tissues during development.

After using DIC and fluorescence microscopy to visualize migratory processes I then applied cell-tracking analysis to the resultant data. Confirming and furthering work that quantified cell movement on the anterior face of the embryo, I performed time-lapse microscopy to visualize the entire surface of the embryo as the AVE migrated, in higher temporal and axial resolution than has been demonstrated to date. Cell-tracking analysis of this data indicates that these areas exhibit different cell behaviour to that previously quantified for the anterior side of the embryo. Further to this, I have developed a novel method of imaging the distal tip of the egg-cylinder embryo. Using this technique, I have generated high definition time-lapse sequences of induced AVE cells prior to migration, allowing previously uncharacterized behavior to be described.

In order to fully understand the cell dynamics of the VE, I took extremely high spatial resolution fluorescence microscopy of the VE from live embryos in culture and manually segmented the tissue in 3D. This allowed the description of regional differences of cell shape within the tissue.

The Wnt/PCP pathway has been implicated in coordinating AVE migration. The second major aim of my project is to investigate how Planar Cell Polarity (PCP) signaling controls the behaviour of cells in the VE. I investigated the PCP core component Vangl2 using mice that contain a dominant negative version of this protein, and determined that there was no overt AVE migration defects in mutant embryos. In order to investigate the role of the Vangl2-binding PCP component Dvl-2, specifically examining whether localized recruitment of Dvl-2 in the VE is obligatory for normal AVE migration, I have generated genetic tools for use in transient transgenics. Further to this, I have demonstrated a role for the Dvl-2-binding protein β-arrestin2 in AVE migration using mice null for this protein.

Table of Contents

Declaration ii
Acknowledgements iii
Abstract v

Chapter 1: General Introduction

1.1 Cell migration 7

1.2 Early mouse embryogenesis 9

1.2.1 Pre-implantation development 11
1.2.2 Implantation and generation of the egg cylinder stage embryo 14
1.2.3 Patterning the egg-cylinder stage embryo 16
1.2.4 Induction of the AVE 17
1.2.5 The AVE as a signalling centre in the E5.5 mouse embryo 19
1.2.6 AVE migration 21
1.2.7 Coordination of AVE migration 22
1.2.8 The hypoblast – an AVE signalling centre equivalent 24
1.2.9 Failure of AVE migration 24
1.2.10 The Visceral Endoderm epithelium during AVE migration 25

1.3 Planar Cell Polarity Signalling 27

1.3.1 The PCP Pathway 27
1.3.2 Vertebrate PCP 30
1.3.3 PCP signalling in AVE migration

Chapter 2: Materials and Methods

2.1 Animal husbandry 38

2.1.1 Mouse lines 38
2.1.2 Genotyping 38
2.1.2.1 Standard DNA purification protocol 40
2.1.2.2 DNA preparation by crude lysis 40
2.1.2.3 Standard PCR genotyping conditions 42

2.2 Embryo dissection 44

2.2.1 Culture medium 44

2.3 Time-lapse Imaging of Cell Movements in the Egg Cylinder Embryo 45
2.3.1 Individual time-lapse experimental set-up adaptions 46
2.3.2 Time-lapse Imaging Parameters 49
2.4 High resolution 3D imaging 52
2.4.1 Imaging parameters for generation of high resolution 3D images from Lifeact embryos 52
2.5 Gene Cloning 52
2.5.1 Transformation of DNA into Bacteria 52
2.5.2 Isolation of plasmid DNA from bacteria 53
2.5.3 Cloning strategy for Dvl2 mislocalisation constructs. 54
2.6 RT-PCR 64
2.6.1 b-arrestin primers used in RT-PCR 64
2.6.2 RT-PCR reagents 64
2.6.3 RT-PCR Turbo DNA-Free Protocol 64
2.6.3 Main RT-PCR protocol 66
2.7 Immunohistochemistry 67
Chapter 3: Time-lapse Imaging and Quantification of Visceral Endoderm Cell Dynamics
3.1 Introduction 71
3.1.1 Visualising the AVE at E5.5 73
3.1.2 Visualising larger areas of the Visceral Endoderm at E5.5 74
3.2 Results 77
3.2.1 Cell Movement 77
3.2.2 Cell Displacement 81
3.2.3 Angle of cell movement 85
3.2.4 Shape factor 87
3.2.5 Neighbour Exchange 91
3.2.6 Apical Surface Area 95
3.3 Discussion 98
3.3.1 Cell Movement 98
3.3.2 Cell Displacement 99
3.3.3 Angle of migration 100
3.3.4 Shape Factor 100
3.3.5 Neighbour Exchange 101

3.3.6 Apical Surface Area 103
3.3.7 Assessment of DIC microscopy as a method for quantification of cell behavior 103

Chapter 4: Quantitative 3D Analysis Of The Visceral Endoderm

4.1 Introduction 111

4.1.1 Variation between Z-levels in Epi-VE imaging 112
4.1.2 Differences in 3D within regions of the Visceral Endoderm 116
4.1.3 The LifeAct peptide

4.2 Results 118

4.2.1 Establishing viability of the LifeAct mouse line for 3D live imaging 118
4.2.2 Manual outlining of imaged embryos 118
4.2.3 Regional Comparisons in Live Visceral Endoderm cells 122
4.2.3.1 Cells outlined in 3D show visual differences in size, 3D shape and cell height 122
4.2.3.2 Cells outlined in 3D show regional differences in cell Surface Area
4.2.3.3 Cells outlined in 3D show regional differences in cell Volume 124
4.2.3.4 Cells outlined in 3D show regional differences in Surface Area to Volume ratio. 127
4.2.3.5 Cells outlined in 3D show regional differences in Sphericity 129
4.2.4. Investigation of the effect of fixation on cell shape within the Visceral Endoderm 131
4.2.4.1 Fixed and live Visceral Endoderm cells show differences in cell Surface Area 131
4.2.4.2 Fixed and live Visceral Endoderm cells show differences in cell Volume 132
4.2.4.3 Fixed and live Visceral Endoderm cells show differences in Surface Area to Volume ratio 132
4.2.4.4 Fixed and live Visceral Endoderm cells show differences in Sphericity 136

4.3 Discussion 139

4.3.1 Regional Comparisons in Live Visceral Endoderm cells 139
4.3.1.1 Cells outlined in 3D show visual differences in 3D shape and cell height 139
4.3.1.2 Cells outlined in 3D show regional differences in cell Surface AreA
4.3.1.3 Cells of the lateral Epi-VE are larger than those of the anterior Epi-VE 140
4.3.1.4 Cells outlined in 3D show regional differences in cell Volume, which do not correspond directly to differences in cell Surface Area 141
4.3.1.5 Cells outlined in 3D show regional differences in Surface Area to Volume ratio 142
4.3.1.6 Cells outlined in 3D show regional differences in Sphericity 142

4.3.2 Investigation of the effects of fixation on the cells of the Visceral Endoderm 145

4.4 Chapter Conclusion 146

Chapter 5: Investigating Cellular Protrusions in the AVE

5.1 Introduction 147

5.1.1 Protrusive behavior during AVE migration 149
5.1.2 Pre-migratory protrusive behavior 150

5.2 Results 152

5.2.1 Protrusions continue into the ExE-VE after migration has halted 152
5.2.2 Laminin staining is increased on the anterior side of the E5.75 embryo
5.2.3 Development of a novel method for imaging the distal tip of the E5.5 mouse embryo 156
5.2.4 High resolution imaging of cells at the distal tip reveals several types of protrusions 159
5.2.4.1 Apical protrusions are present at the distal tip 159
5.2.4.2 Basal protrusions are present at the distal tip 159
5.2.4.3 Tall protrusions are present at the distal tip 160

5.3 Discussion 165

5.3.1 Protrusions continue into the ExE-VE after migration has halted 165
5.3.2 Laminin-a1 is upregualted under the cells of the migrating AVE 165
5.3.3 Imaging cell behavior at the distal tip of the egg cylinder stage embryo 167
5.3.3.1 Apical protrusions are present at the distal tip 167
5.3.3.2 Basal protrusions are present at the distal tip but do not exhibit a filipodial tipped or bifurcated nature 167
5.3.3.3 Tall protrusions are present at the distal tip 168

5.4 Chapter conclusion 170

Chapter 6: Proteomic Analysis of the Egg-cylinder Stage Embryo

6.1 Introduction 171

6.1.1 Proteomic research in the early mouse embryo 171
6.1.2 Phospho-proteomic research in the early mouse embryo 172
6.1.3 Mass spectrometry as a protein and phospho-protein characterization tool 174

6.2 Results 176

6.2.1 Regional Protein Expression and Phosphorylation differences are present in the E6.25 mouse embryo 176
6.2.2 Analysis of the Mass Spectrometry data 180
6.2.2.1 STRING analysis 180
6.2.2.2 Gene Ontology Analysis 186
6.2.2.3 Comparison of Mass Spectrometry Results to a Previously Published Screen 203
6.2.2.4 Searching the data for proteins known to cause an NTD 203
6.2.2.5 Established antibodies were identified for several proteins of interest from each dataset 206
6.2.3 Investigation of candidate proteins by Immunohistochemistry 209
6.2.3.1 Profilin Immunohistochemistry 209
6.2.3.2 Stathmin and p-Stathmin immunohistochemistry 217

6.3 Discussion 222

6.3.1 String analysis 222
6.3.2 Gene Ontology Analysis 224
6.3.3 Comparison of Mass Spectrometry Results to a previously published screen 229
6.3.4 Searching the Mass Spectrmoetry Results For Genes known to be involved with NTDs 235
6.3.5 Secreted Protein Analysis 230
6.3.6 Profilin Immunohistochemistry 232
6.3.7 Stathmin and Phospho-Stathmin Immunohistochemistry 236

6.4 Chapter conclusion 240

Chapter 7: Investigating the role of Planar Cell Polarity Signalling in Visceral Endoderm Cell Behavior

7.1 Introduction 241

7.1.1 The role of Vangl2 in PCP signalling 244
7.1.1.1 Vangl2 protein 244
7.1.1.2 Vangl2 function in vertebrates 246
7.1.1.3 Looptail mice exhibit a strong PCP phenotype 247
7.1.2 The role of Dvl2 in PCP signalling 248
7.1.2.1 Dishevelled protein 250
7.1.2.2 Dvl analogues in the mouse 251
7.1.2.3 Dvl2 is active in PCP signalling at E5.5 252
7.1.3 The role of b-arrrestin2 in Dvl2 signalling 255
7.1.3.1 b-arrestin2 in the early mouse embryo 256

7.2. Results 257

7.2.1 Investigating the role of Vangl2 in migration of the AVE 257
7.2.1.1 *Vangl2*$^{LP/LP}$ mutants do not display defective AVE migration 257
7.2.1.2 Some *Vangl2*$^{LP/LP}$ embryos exhibit delayed development 258
7.2.2 Investigating the role of b-arrestin2 in migration of the AVE 260
7.2.2.1 b-arrestin2 is expressed in E5.5 and E6.5 embryos 260
7.2.2.2 b-arrestin2 immunohistochemistry could not be achieved at the egg cylinder stage 262
7.2.2.3 Some b-arrestin2$^{-/-}$ mice exhibit overmigration of the AVE 265
7.2.3 Disrupting the subcellular localisation of Dvl-2. 267
7.2.3.1 Dvl2 mislocalisation constructs function correctly in mammalian cells 272

7.3 Discussion 275

7.3.1 Investigation of the role of Vangl2 during AVE migration 275
7.3.1.1 Looptail mutants do not display defective AVE migration 276
7.3.1.2 Some *Vangl2*$^{LP/LP}$ embryos exhibit delayed development 277
7.3.2 Investigating a role for b-arrestin2 in AVE migration 279
7.3.2.1 b-arrestin immunohistochemistry 279
7.3.2.2 Some b-arrestin2$^{-/-}$ mutants exhibit AVE overmigration 279
7.3.3 Generation of Dvl2 localisation constructs 283

7.4 Chapter conclusion 286

Chapter 8: General Conclusion 289

References 293
Appendices 327

1

General Introduction

1.1 Cell migration

Cell migration is a fundamental process in development, where the precise spatial positioning of tissues must be generated and maintained to ensure correct embryo development. In order for directed migration to occur, a large number of processes must be coordinated within individual cells. This includes activation and relocalisation of cellular messengers, scaffold proteins, kinases, motor proteins and cytoskeleton components, which work collaboratively to effect the required changes to cell behaviour. Defective migration during development can have disastrous consequences such as embryonic lethality or birth defects such as spina bifida [1], [2].

Cell migration usually occurs as one of two types; the movement of individual cells, where inter-cell boundaries are downregulated and cells move as single units, or as collective cell migration, where groups of cells maintain cell-cell contact and move as a group, influencing their migration partners as they move (reviewed in [3]). Collective cell migration can occur in both mesenchymal and epithelial cell types, with mesenchymal cells maintaining cell contact via loose adherens junctions, and epithelial cells maintaining more stable adherens junctions and retaining their characteristic apical basal polarity during the course of migration [4], [5].

Examples of mesenchymal collective migration include the movement of neural crest cells, which migrate throughout the embryo after delaminating from neighbouring cells and undergoing an epithelial to mesenchymal (EMT) transition [6]. Examples of collective cell migration within epithelia can be seen throughout developmental biology and include the convergent extension seen in Xenopus neurulation, the branching morphogenesis seen in the Drosophila trachea and the migration of the Zebrafish posterior lateral line primordium (pLLP) [7]–[9]. This work focuses on the collective cell migration that occurs within the mouse Visceral Endoderm, utilizing this tissue as a model for collective cell migration within the context of an intact epithelial sheet.

1.2 Early mouse embryogenesis

In order for an embryo to develop successfully, cell growth and differentiation must be strictly regulated. Despite the large differences in the shape and gestation periods of different vertebrate species, many of the protein signalling mechanisms that govern cell lineage allocation and axis patterning are conserved throughout evolution, such as the Wnt, transforming growth factor-β (TGFβ), bone morphogenic protein (BMP) and fibroblast growth factor (FGF) pathways. Mouse embryogenesis is an extensive multifaceted process, involving coordination of cell growth, cell communication and cell rearrangement across many stages (Figure 1.1).

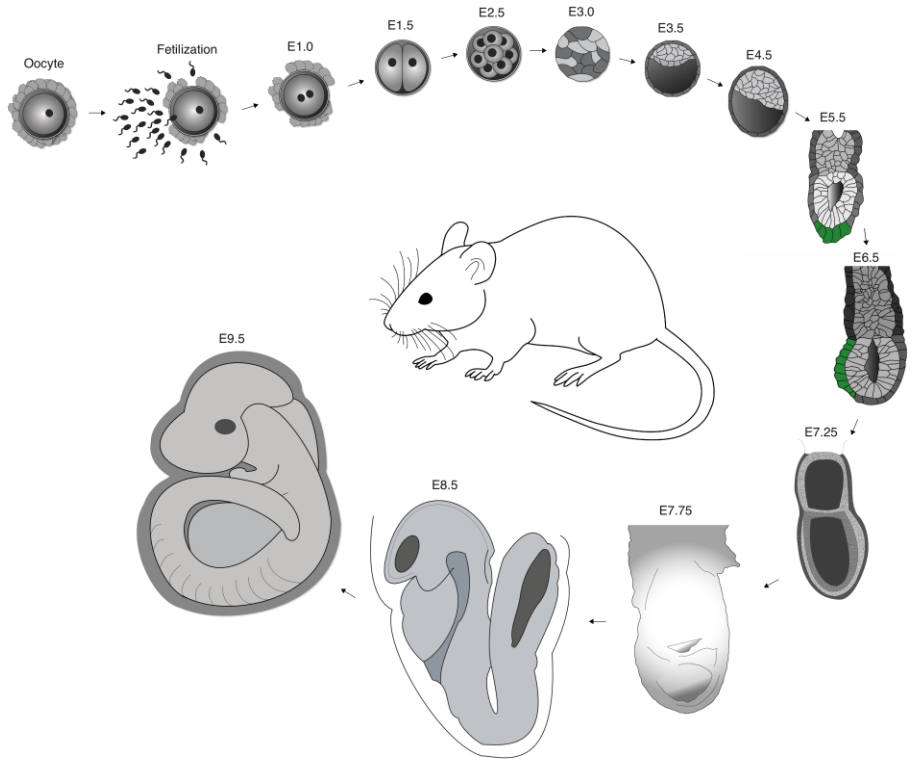


Figure 1.1: Early mouse embryogenesis

Stages of mouse embryogenesis from E0 to E9.5. AVE cells can be seen in green at E5.5 and E6.5. Stages are not to scale.
Mouse vector diagram (centre) adapted from [10].

1.2.1 Pre-implantation development

The mouse embryo develops from a single cell at fertilisation and initially undergoes three rounds of cell cleavage. This generates eight cells by E2.5, referred to as blastomeres, which appear morphologically identical. Initially all eight blastomeres have overlapping expression of caudal-type homeobox protein 2 (Cdx2) and octamer binding transcription factor 3/4 (Oct3/4; also known as Pou5F1), both of which are well-understood transcription factors. These two transcription factors are responsible for the first binary cell fate decision the cells of the new embryo must undergo: the decision to form either of the tissues known as trophectoderm (TE) or inner cell mass (ICM) (Figure 1.1) [11]–[14].

During the first six cell divisions, the cell divisions do not change the overall volume of the embryo. Subsequently at the morula stage, the embryo undergoes its first round of cell divisions to change individual cell volume. Larger cells locate to the outside face of the embryo with smaller cells inside. This is achieved via asymmetric cell division and cell rearrangement.

While initially all cells express both Oct3/4 and Cdx2, a mutually exclusive pattern is then established. Cdx2 is then present in outer blastomeres, now fully established as larger, polarized TE. Oct3/4 is expressed only in inner blastomeres, now known as ICM, and is required to maintain pluripotency of these cells [11], [14]. There has been much debate over the generation of this cell segregation, with two models, the 'inside–outside' model and the 'polarity' model heavily investigated. The inner-outer model proposed that a cell's location and environmental exposure controlled its fate, while the polarity model proposes that the amount of polarized apical surface inherited by daughter cells of dividing outer cells determines their fate [15], [16]. Recently work by the Srinivas lab quantifying cell movement of dividing cells at the 16-

cell stage, showed that the angle of division had little effect on the fate of daughter cells in the developing blastocyst. This indicates a stronger role for location of a cell in determining cell fate at this stage [17].

Nanog, along with Sal-like 4, maintains pluripotency of the ICM, which is the precursor for the epiblast [18]–[20]. A subpopulation of cells expressing Gata6 cells differentiate to become the Primitive Endoderm (PrE), a tissue that lies above the ICM facing the cavity of the blastocyst (Figure 1.2) [21]. This is the precursor to the Visceral Endoderm. Embryos that do not express the upstream components of Gata6 signalling, such as Grb2, Fgf4 or FGF receptor 2 (Fgfr2) fail to express Gata6 and as such do not generate PrE [21]–[23]. The mechanism of cell rearrangements that ensures the correct localisation of the Gata6- expressing cohort of cells to the blastocoel-facing surface of the ICM is not yet fully elucidated. Differences in cell movements and adhesion properties between ICM and PrE cells are thought to function in combination with selective apoptosis [24]. By E3.5 the embryo has specified the three distinct tissues described, the TE, ICM and PrE, as well as undergone cavitation. It is now referred to as a blastocyst (Figure 1.2) (reviewed in [25]).

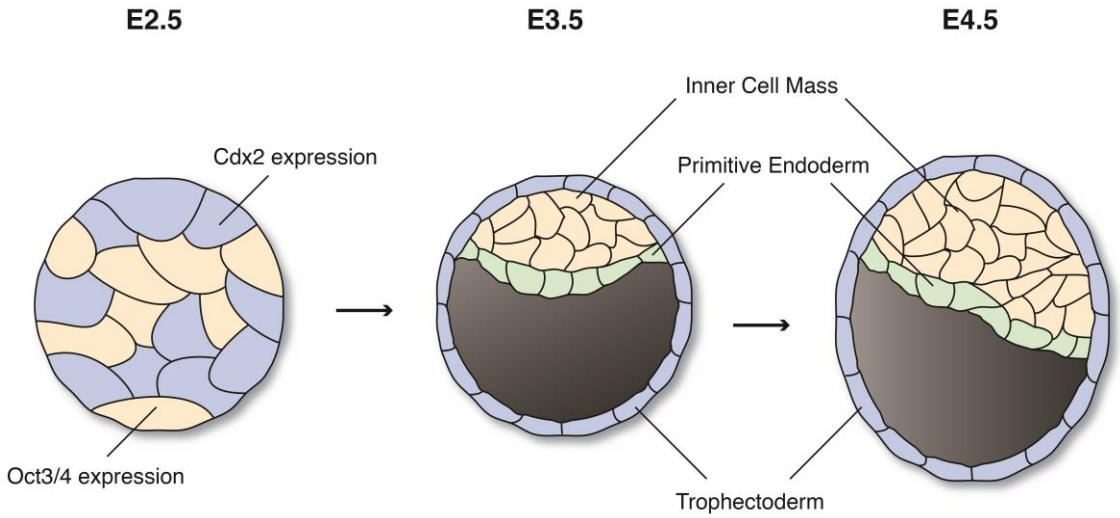


Figure 1.2: Stages of early mouse development E2.5 – E4.5

At E2.5 the mouse embryo shows a mixed population of Cdx2 expressing and Oct3/4 expressing cells. These cells adopt cell fates of Trophectoderm (TE) and Inner Cell Mass (ICM), respectively by E3.5. A portion of Gata6 expressing ICM cells then segregates to form the Primitive Endoderm, which will ultimately generate the Visceral Endoderm (VE) after implantation.

1.2.2 Implantation and generation of the egg cylinder stage embryo

At E4.5 the late blastocyst undergoes implantation. This is facilitated by the TE, which connects the embryo to the uterus. Trophectoderm and ICM growth into the blastocoel cavity drastically alters the overall shape of the embryo, producing egg cylinder stage (Figure 1.3). The TE will differentiate to become the Extra-embryonic Ectoderm (ExE) and the ectoplacental cone, which are the progenitors of the placenta [26].

The remaining cells of the ICM, which did not become PrE, become the Epiblast. These cells continue to retain their pluripotency and will ultimately generate both the somatic tissues and the germ cell lineage of the foetus. Additionally at this stage, they form a cavity within the Epiblast.

The PrE also diversifies, generating the Parietal Endoderm (PE) and the Visceral Endoderm (VE). The parietal endoderm migrates from the epiblast surface so that it directly contacts the maternal tissue. The VE, an epithelial sheet of tissue, remains in contact with the Epiblast and later overlays the surface of the ExE and Epiblast [27]. Later the VE will generate the visceral yolk sac as well as contribute to the gut endoderm by intercalating with the definitive endoderm [28].

Reciprocal signalling between these tissues is required for their maintenance and function, as discussed below. Along with Fgf4, which is secreted by the epiblast, Nodal maintains the pool of trophoblast progenitors [29]. Similarly, signals from the ExE tissue, such as BMPs, are needed to pattern the proximal epiblast and the VE [30].

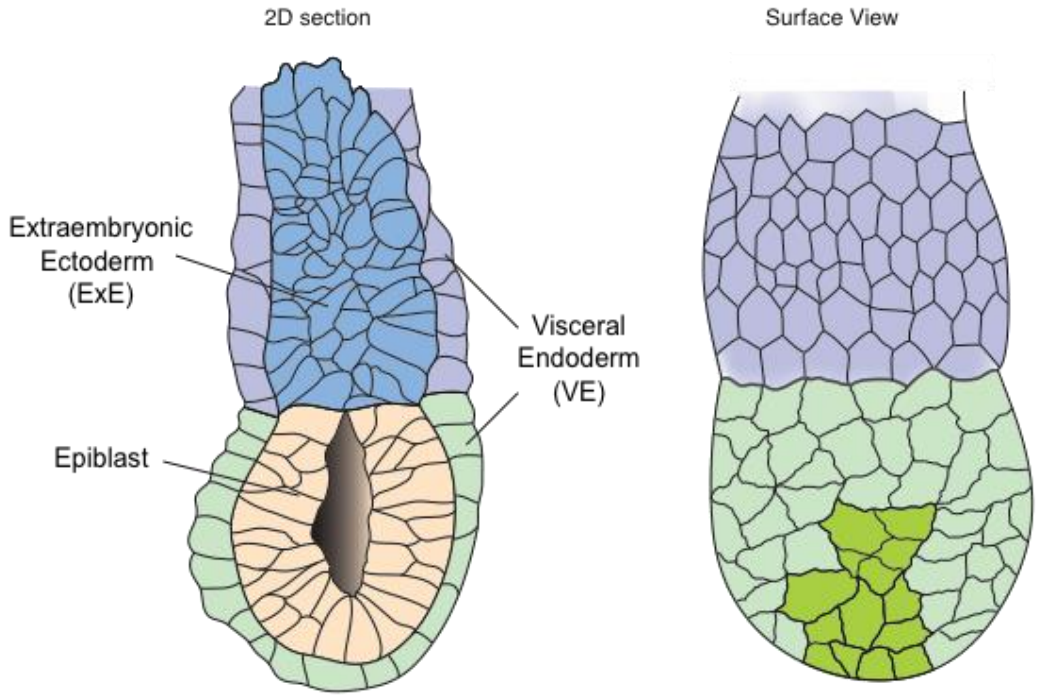


Figure 1.3: The egg-cylinder stage embryo

Diagram of an E5.5 mouse embryo. A 2D section of the embryo is shown (left) depicting the Extra-embryonic Ectoderm (ExE) (blue) and Epiblast (yellow) tissues enveloped by the Visceral Endoderm (Green and Purple). A surface view (right) reveals only the outer layer of Visceral Endoderm.
Figure adapted from [31].

1.2.3 Patterning the egg-cylinder stage embryo

At this stage, the proximodistal (PD) axis is the only axis clearly specified. The PD axis runs from the ExE to the Epiblast, making the egg cylinder stage embryo radially symmetrical. The axis is maintained by localised gene expression patterns in each of the epiblast, ExE and VE cell populations. Mutual and reciprocal signalling via secreted growth factors such as nodal and bone morphogenetic protein (BMP) regulate this expression [30], [32]. The Wnt and FGF families are also essential for appropriate PD axis patterning [33]–[35].

At E5.5 a gradient of nodal signalling levels preconfigures the proximal-distal axis, becoming active through prodomain cleavage [36]. Nodal produced by the Epiblast upregulates the levels of Bone Morphogenetic Protein 4 (BMP4) in the Extra-embryonic Ectoderm, which in turn signals back to the epiblast to enhance Wnt3 expression [36].

Cripto, Nodal and Brachyury (T) are typically expressed in a ring around the most proximal part of the epiblast [37]–[39]. In embryos where the ExE has been removed expression of these three genes is lost, indicating that the ExE is needed to maintain several aspects of epiblast positional signalling. These ExE explants also showed normal expression of Nodal for 2.5 hours after extraction but after 5 hours in culture it is downregulated, indicating that signalling from the ExE is likely to be required for maintaining Nodal expression [30]. Additionally, Nodal mutants are unable to maintain expression of ExE markers Eomes and BMP4, indicating that the reciprocal relationship between the epiblast and maintenance of the ExE has been lost [40].

Nodal signalling from the epiblast is also required for the correct specification of the Visceral Endoderm, which has been shown using Epiblast specific Nodal mutants [41] .

1.2.4 Induction of the AVE

Growth of the epiblast results in the elongation of egg cylinder embryo, increasing the distance between the ExE and distal VE cells. It is thought that as a result of this elongation the most distal VE cells are move beyond the repressive effect of the ExE, allowing the distal VE to differentiate into the anterior visceral endoderm (AVE) [41].

A few cells at the distal tip of the E5.5 embryo become specified as anterior visceral endoderm (AVE) cells. These cells begin to express extracellular Nodal and Wnt-signalling inhibitors Ccerberus-like-1 (Cer1) and Lefty1, decreasing local Nodal signalling in the adjacent epiblast and contributing to the proximal–distal Nodal signalling gradient [34], [42].

The induction of the AVE has been shown to require Nodal signalling, with Nodal-null embryos failing to express markers of the AVE including Hex and Lefty1 [40]. However, despite the fact that Nodal is expressed throughout the epiblast, induction of the AVE is restricted to the distal tip of the egg cylinder. This is caused by repressive signals from the ExE. Embryonic explants in which the ExE is removed show expansion of the AVE markers Hex and Cer1 throughout the Epi-VE and the loss of proximal epiblast marker gene expression, [30]. If the ExE region is removed after migration the upregualtion of these markers does not occur [30].

Further evidence for the role of the ExE in specifying the AVE was seen when

ectopic transplantation of ExE, allowing the suspected inhibitory signals to reach the distal tip, inhibited AVE formation and leads to expansion of the posterior marker Brachyury (T) [43]. BMP4 is expressed in the cells of the ExE and strong evidence points to a role for this protein as an AVE inhibitory factor. It was shown that culturing embryos in the presence of BMP4 causes the loss of *Hex, Lefty1* and *Cer1* expression in the distal tip and that using the BMP4 inhibitor Noggin causes the AVE region of wild type embryos to expand in a manner which phenocopies removal of the ExE [43]. Further, Yamamoto et al. demonstrated using a combination of embryonic explants and null mutants for BMP and Nodal receptors, BMPR and Alk1, respectively that antagonism between BMP-Smad1 and Nodal-Smad2 signalling exists in the VE. It was shown that the reciprocal regulation of these two signalling molecules establishes exclusive signalling of Nodal-activated Smad-2 in the distal-most tip of the embryo and thus determines the site of AVE formation [43].

Smad2 null embryos do maintain expression of *Wnt3*, *Cripto* and *Eomes*, but do not express AVE markers *Lefty1* and *Hex*, further indicating formation of the AVE is dependent upon Smad2-dependant Nodal signalling [40]. This indicates that the role of Nodal signalling in the AVE is likely distinct to that of its role in establishment and maintenance of the characteristic expression patterns seen in the early egg cylinder, and is regulated by Smad2, while earlier roles are Smad2-independant.

1.2.5 The AVE as a signalling centre in the E5.5 mouse embryo

The VE can be categorized into two sub-populations, depending on the tissue it overlays, giving the ExE-VE and the Epi-VE. The AVE is a distinct sub-population of the Epi-VE [5]. The AVE was first established as a signalling centre by Thomas and Beddington, when the region was microsurgically removed in gastrulating embryos [44]. This results in the loss of the forebrain marker Hesx1 in the neurectoderm of early somite stage embryos, at approx. E8.0. *Hesx1* expression was shown to be restricted to the distal tip in a few cells of the VE [44], [45].

In 1998 Thomas and Beddington showed the expression of Hex in the AVE [46]. Initially expressed in the primitive endoderm of implanting blastocyst, by E5.5 Hex is present only in the distal tip. Using lineage tracing analysis with DiI it was shown that the cells in the distal tip at E5.5 are present in the future anterior of the embryo at E5.75. It was also shown by in-situ hybridization that they continue to express *Hex* throughout the time of migration [46].

Hex is a homeobox gene typically known to be expressed in a range of multipotent haematopoietic and endothelial cell lines, being massively down regulated during terminal cell differentiation. It initially emerged as a potential candidate for investigation during early mouse development when Harrison et al. made a cDNA library for specific germ layers in gastrulating embryo and searched it for homeobox genes [47].

Cer1 (also known as Cerl1) expression has also been shown to localise to the distal tip of the VE at E5.5, and the future anterior of the embryo several hours later [42], [48]. Later, *Lefty1* expression was also seen localised to the AVE [49]. Both Cer1 and Lefty1 are established Nodal inhibitors, which gave

further evidence that the AVE was a signalling centre, which functioned via inhibition of Nodal signalling [42], [50].

Prior to the discovery of the asymmetric expression of these markers, the earliest morphological indicator of an A–P axis was the appearance of the Primitive Streak (PS). This coincides with the posteriorly localised expression of streak markers such as Brachyury (T) and Nodal [38], [39]. As no earlier asymmetric markers had been seen it was thought that anterior features were a result of patterning by primitive streak (PS) derivatives. Together, the localisation of Hex, Cer1 and Lefty1 on the anterior of the embryo one day prior to PS formation indicated that the AVE was responsible for specifying the A-P axis of the embryo, localizing the PS to the posterior side. It was also confirmed that the AVE has roles in addition to specifying this axis, as when the AVE was removed during gastrulation the development of the CNS became compromised.

1.2.6 AVE migration

Once migrated the AVE cells pattern the underlying epiblast by expression of diffusible Nodal antagonists Lefty1 and Cer1, which restrict Nodal signalling to the opposite side of the embryo [34]. As a result of this, the Primitive Streak forms opposite the newly specified anterior, generating a correctly positioned anterior-posterior (AP) axis. This process must occur for the embryo to continue development.

While the original experiments that showed the relocalisation of Hex expressing cells were carried out using DiI, more recent investigation using a fluorescent Hex-GFP reporter mouse line has revealed that the cells of the AVE actively migrate to their destination on the future anterior of the cell. [46], [51]. AVE cells were shown using live imaging to migrate proximally towards the future anterior of the cell, stopping mid-way though the Visceral Endoderm above the point where the Epiblast meets the ExE, known as the embryonic/abembryonic boundary. Upon reaching this point, cells spread laterally in both directions [51]

The first published live imaging of migrating AVE cells also showed that filopodia emerged from moving AVE cells in the direction in which they are travelling [51]. It was further demonstrated by Migeotte et al. that leading AVE cells extend long basal protrusions that span several cell diameters and are polarized in the direction of cell movement. These projections are tipped by filopodia-like structures that appear to probe and sample the local environment [52].

The behaviour described above is indicative of an Epithelial to Mesenchymal (EMT) transition. Here cells of an originally epithelial nature express a large cohort of transcription factors, reorganise their cytoskeleton and cell

adhesiveness and produce enzymes that will degrade local Extra Cellular Matrix (reviewed in [53]). However, it was later determined that throughout AVE migration the VE remains a cohesive epithelium, with E-cadherin and ZO-1 stains constant in all regions of the embryo [5]. As such the standard model of EMT cannot be taking place.

Differential Interference Microscopy (DIC) imaging has shown cells of the anterior surface of the VE remodel cell-cell junctions to accommodate the migration of the AVE cells [5]. This indicates that junctional remodelling similar to that seen in Drosophila germ-band extension is occurring in the Visceral Endoderm during AVE migration. This was supported by evidence indicating that non-Hex-GFP expressing cells surrounding labelled Hex-GFP-positive cells were also undergoing directional migration, indicating a coordinated migratory movement within an intact epithelial sheet.

1.2.7 Coordination of AVE migration

The cause of directed AVE is still not fully elucidated. Typically collective migration occurs in response to a chemoattractant, such as in the Zebrafish posterior lateral line primordium (pLLP). Here, directional migration of an epithelial placode along the developing embryo correctly positions sensory organs known as neuromasts [7], [54], [55]. This migration occurs along a gradient of the chemokine Sdf-1a, which is released by the horizontal myoseptum underlying its future path. Within the (pLLP) localized expression of receptors Cxcr4b and Cxcr7 differentially modulate the response of cells within the primordium to the chemoattractant [56].

Some evidence for the role of chemoattractant in the migration of the AVE has been seen. AVE cells have been shown to migrate in response to guidance cues

from the Wnt antagonist Dkk1, though the loss of dkk1 does not affect AVE induction and migration [57], [58]. Further evidence for the role of a chemo attractant comes from Omelchenko et al. who note complex bifucated protrusions emerging from migrating AVE cells. This type of protrusion is associated with cells migrating in a shallow chemical gradient [59], [60].

Asymmetric cell proliferation has also been proposed as a mechanism for driving AVE migration. Experiments using BrdU appeared to show variance in regional proliferation within the VE, which was proposed to be regulated by Nodal [49]. However, later investigation of cells in various phases of the cell cycle around the egg cylinder stage embryo revealed that there is no difference in cell proliferation in the VE, though there is a large amount of proliferation in the epiblast at this stage. As such, asymmetric cell proliferation does not play a role in the migration of the AVE.

Haptotaxis is the migration of cells along an increasing gradient of adhesiveness. It has been established in vitro and in vivo for a wide range of cells, including epithelial cells [61]–[65]. *In vivo* this adhesiveness gradient is usually provided by Extra-Cellular Matrix proteins, such as laminin and fibronectin [66]–[69]. Protrusions such as filopodia and lamellipodia have been shown to be involved in the migratory process [61], [63].

Laminins are large heterotrimeric glycoproteins, comprised of an α, β, and γ chain, each of which has several isoforms. Several papers have shown the presence of laminins in the basement membrane of the Visceral Endoderm of the egg cylinder stage mouse embryo [41], [70], [71]. As such, a role for haptotaxis in AVE migration remains a strong possibility.

1.2.8 The Hypoblast – an AVE signalling centre equivalent

A similarly behaving tissue, the hypoblast, exists in the early chick embryo. Like the AVE, this tissue is an extra-embryonic cell layer that lies next to the Epiblast, undergoes migration and positions the Primitive Streak, The two tissues also express a cohort of identical genes, including *Otx2*, *Hex* and *Rpx* [44], [72]–[76]. Both tissues also express nodal inhibitors, which are thought to be the manner in which the Primitive Streak is restricted to the correct location [77], [78]. The hypoblast is considered to be the chick equivalent of the mouse AVE for these reasons.

While the hypoblast initially lies over the entire epiblast and moves anteriorly, being displaced by newly formed endoblast (reviewed in [79]). Whether this is an active migration in either tissue has yet to be elucidated, and while the hypoblast shares many features with the mouse AVE, an overlap in this characteristic has yet to be established.

1.2.9 Failure of AVE migration

Due to its essential function in embryonic patterning, failure to specify the AVE and carry out successful migration to the prospective anterior results in embryonic lethality [35], [37], [52], [80]–[82]. *Rac1*$^{-/-}$ mutants specify an AVE but fail to migrate and consequently die soon after migration failure, with markers of the posterior embryo Wnt3 and Brachyury (T) unrestricted and remaining in a ring around the embryonic surface [52]. Both *Cripto* and *Otx2* knockout mice similarly specify an AVE, but fail to migrate or undergo gastrulation [37], [82]. Mutants mice such as *Nodal* knockouts, *Smad2* knockouts and *APC* knockout mice do not specify an AVE and are embryonic lethal [32], [33], [41].

1.2.10 The Visceral Endoderm epithelium during AVE migration

1.2.10.1 Cellular behaviour in the VE

The establishment that cells of the Visceral Endoderm remain an intact epithelial sheet throughout AVE migration raises the question of how non-AVE cells of the Visceral Endoderm accommodate this migration. Using DIC, it has been established that the migrating non-Hex-GFP positive cells of the anterior face of the embryo also halt at the embryonic/abembryonic boundary, in the same manner as Hex-GFP positive cells [5]. This indicates that other cells of the VE have a role in AVE migration.

Time-lapse microscopy of the surface of the VE cells reveals a difference in neighbour exchange in the two regions of the VE on the anterior face of the embryo. More neighbour exchange is observed in the Visceral Endoderm overlying the Epiblast (Epi-VE) compared to the Visceral Endoderm overlying the ExE (ExE-VE), which remains relatively static [5]. This has been proposed as the ExE-VE behaving as a physical barrier to the migration of the AVE cells, causing them to halt migration at the point where the VE beings to overlie the ExE.

Using DIC imaging, the T1-T2-T3 process of intercalation was seen among cells anterior Visceral Endoderm [5], [83]. Here coordinated junctional remodelling occurs among four cells to rearrange cell boundaries shortening a boundary along one axis to bring to new cells together, then widening the distance between the two cells that have been separated. This type of movement occurs on a large scale in morphological lengthening events, such as germ-band extension in Drosophila [84]b. While there is not a tissue extension event occurring here, smaller scale use of the T1-T2-T3 junctional remodelling process is clearly utilized to effect AVE migration.

Additionally multicellular rosettes are often observed during AVE migration [31]. Rosettes are cell structures where five or more cells meet at a single central point. These are also seen frequently in Drosophila germband extension, where they form and resolve in a directional manner, contributing to the overall lengthening effect during characteristic convergent extension movements [85]. As the Visceral Endoderm is not undergoing a morphological extension, and the majority of rosettes are seen to form outside those of the AVE, it is highly likely that rosettes function to facilitate AVE migration within the rest of the Visceral Endoderm.

In several mutants where the AVE does not migrate, rosettes are not seen. These include *Nodal*$^{\Delta 600/lacZ}$, *Cripto*$^{-/-}$ and *β-catenin*$^{-/-}$ mutants [31]. ROSA26$^{\text{Lyn-Celsr1}}$ mice have defective PCP signalling and also show lowered numbers of rosettes. AVE in these mice migrates, though not as coherently as wild type mice. This indicates a role for the PCP pathway in rosette formation and the migration of the AVE [86].

1.2.10.2 Cytoskeletal behaviour in the VE

F-actin and non-muscle Myosin IIA can work in conjunction in order to exert forces on the cell, generating changes in cell shape [83], [87]. Both F-actin and Myosin IIA are initially localized to the lateral membranes of the VE prior to and at AVE induction. As the AVE begins to migrate, the ExE-VE develops an atypical shroud of F-actin and to a lesser extent Myosin IIA [5].

This may be a contributing factor to the difference in cell shape exhibited by the ExE-VE and Epi-VE and may have a role in preventing junctional remodelling by preventing movement of ExE-VE cells, via stabilization of this area of the tissue.

1.3 Planar Cell Polarity Signalling

Planar polarity refers to the arrangement of complexes across an established plane. Biologically, this can refer to cells polarized within a specific tissue or proteins and cell components organized within an individual cell. The plane in question is perpendicular to the apical-basal axis of the cell or tissue. The cohort of proteins that establish and maintain this polarity within and across cells is called the Planar Cell Polarity (PCP) signalling pathway. This cohort of proteins have a wide range of functions ranging from cellular organization, orientation of cell divisions and hair follicle position [88]–[94]. PCP signalling has been shown to play a role in the mouse embryo and components of the PCP pathway are investigated in this thesis [5]. As such, the PCP pathway is introduced and discussed below.

1.3.1 The PCP Pathway

Initially, the PCP pathway was discovered and studied in Drosophila, where the core proteins of the pathway were identified. Mutants of members of this core pathway exhibited highly irregular disruption of epithelia, such as pupal wing cells [95], [96]. In the eye, defective PCP signalling results in the failure to correctly organise photoreceptors.

PCP signalling occurs through a set of cooperating proteins. These include transmembrane proteins Strabismus/Vang and Frizzled, the intracellular proteins Dishevelled and Prickle, an atypical cadherin Flamingo, also known as Starry night, Diego and the cadherin-related proteins Fat and Dachous [97]–[103]. In the Drosophila wing blade, members of this group of proteins interact with each other and downstream effectors to establish and maintain planar cell polarity within individual cells and across tissues.

Polarity is first set up at the cell membrane, where core PCP proteins are asymmetrically localized. In Drosophila this occurs at proximal and distal adherens junctions [101], [104], [105]. Frizzled, Dishevelled, Diego and Flamingo interact, localizing to one side of the cell while Strabismus, Prickle and Flamingo localize to the other [105]. Dishevelled is also known to bind Strabismus and Prickle and competition between the protein complexes for binding of the downstream effector is thought to regulate Frizzled signalling [106], [107]. Flamingo, enriched on both sides of the cell is thought to stabilizing both complexes across cell membranes via homophilic binding [103] In addition to being seen in Drosophila wing cells, this asymmetric localisation is seen in several other contexts, such as photoreceptor precursor cells and the sensory organ precursor cells [108], [109].

The asymmetrically localized PCP proteins rely on their cross-cell counterpart complexes to maintain asymmetric localisation. This can be seen upon removal of single core PCP component, which causes loss of asymmetry among the others [105], [110]. This indicates that PCP is set up through a reciprocal exclusion mechanism that requires all components to be present to correctly establish polarity.

In addition to reciprocal exclusion, directed transport of core PCP components has been established as a mechanism for setting up polarity within a cell. This was visualised in Drosophila pupal wings, where Frizzled and Dishevelled filled vesicles moved directionally across the cell [111], [112].

Downstream signalling from Frizzled is carried out via Dishevelled protein, through the small GTPase Rho. Ultimately the goal of PCP signalling is the rearrangement of the cytoskeleton to facilitate a new polar orientation. This occurs through downstream effectors such as non-muscle-Myosin II [113], [114].

The overt external signals that regulate orientation of PCP signalling are not fully understood to date. In flies, polarity appears to be set up along molecular gradients, as an induced gradient of Frizzled expression in the drosophila wing caused polarity to orient towards the point of highest expression [115]. While Wnt signalling is established as a regulator of PCP signalling in vertebrates, less data on Wnt signalling as an overall PCP controlling morphogen is available in flies [116], [117][118].

1.3.2 Vertebrate PCP

Recently research has been carried out showing that this pathway is highly important in vertebrate development. While the vertebrate PCP field is much less well established than that of Drosophila, many homologues of the Drosophila PCP pathway have been shown to both exist in vertebrates and perform similar functions.

PCP signalling has been shown to be involved in vertebrate gastrulation and neurulation [8], [119]–[121]. Mutations in homologs of PCP proteins such as Flamingo and Strabismus disturb the orientation of stereociliary bundles in sensory hair cells of the inner ear [122], [123]. PCP is also involved in the orientation of hairs, with mutations in an analogue of Drosophila Frizzled, Fz6, generating disruptions in the correct alignment of mouse fur [124]. Further, defects in human PCP genes such as Vangl2, Scrib and Celsr1 are known to cause neural tube defects [2].

A strongly investigated vertebrate role for PCP is that of convergent extension (CE), a mechanism of cell intercalation. Disruption of the Xenopus homolog of Dishevelled caused a failure of CE, a stereotypical process involving the shortening of the mediolateral axis and concomitant extension along the anterior–posterior axis. This failure was shown to be due to defects in cell polarization and intercalatory activities [119]. PCP proteins were also shown to be required for the generation of stable protrusions during Xenopus CE.
The Xenopus and Zebrafish homologs of Strabismus was also shown to play a role in CE, in their respective species, with mutated or incorrectly expressed protein causing defects in the Xenopus neural fold and Zebrafish gastrulation [120], [125].

Downstream signalling of the PCP pathway has also been investigated in vertebrates. Celsr1, the mouse homologue of Flamingo was shown to recruit the formin DAAM1 via Dvl, the mouse homologue to Dishevelled. This was then shown to activate a RhoGEF, a protein known to interact with RhoA, regulating cytoskeletal events [126]. A diagram depicting PCP signalling can be seen in Figure 1.4. Further discussion of vertebrate PCP can be found in Chapter 7.

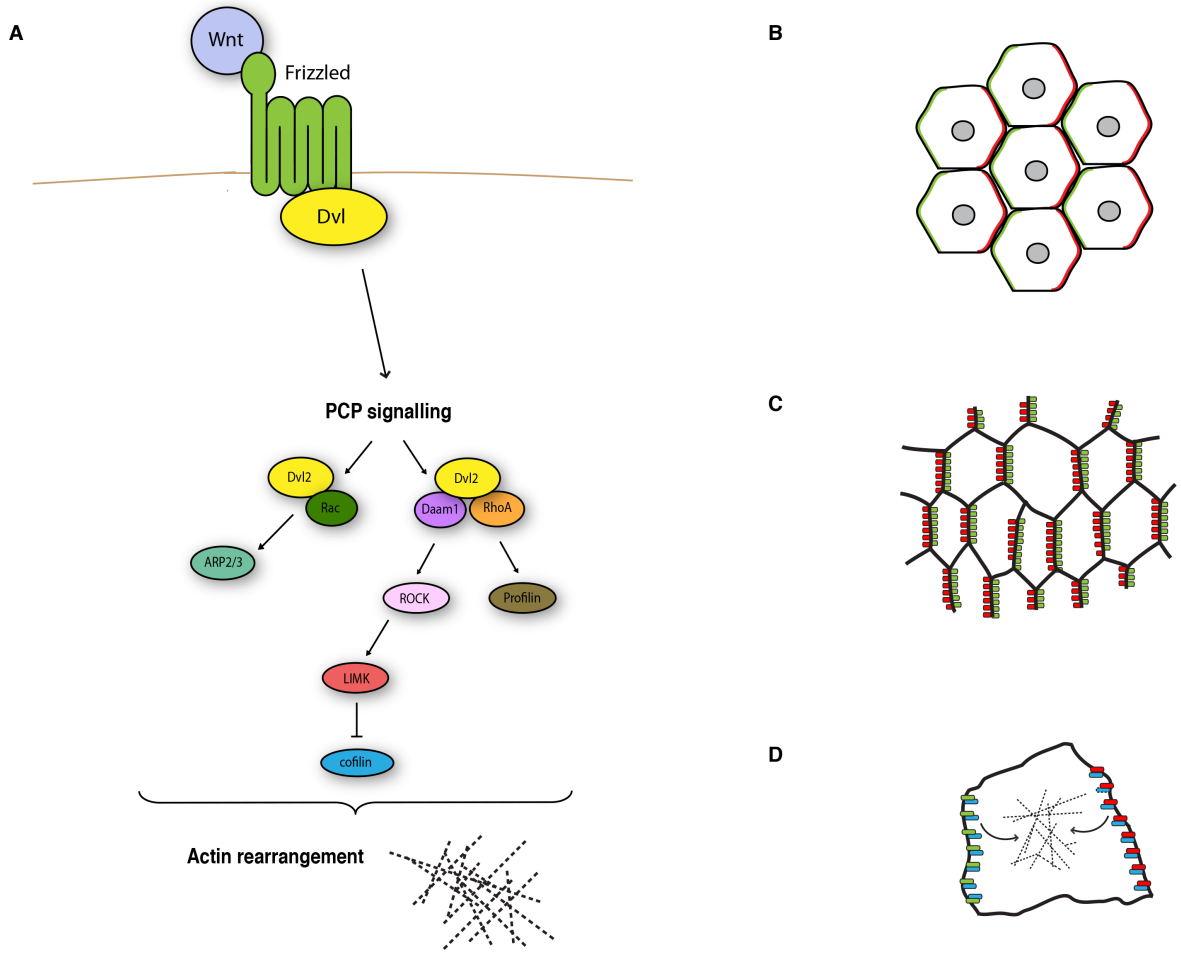


Figure 1.4: PCP signalling and asymmetric distribution of core PCP components

(A) PCP pathway components

(B) A representation of epithelial cells. PCP components are asymmetrically localised across the plane of the cell, represented by green and red colouration.

(C) Asymmetric distribution of proteins within an epithelial sheet. Strabismus protein (green) is localized to a cell wall adjacent to a neighbouring cell with localized Frizzled (red). This pattern is repeated globally across the sheet of cells.

(D) Within an individual cell, the asymmetrically distributed PCP proteins regulate downstream cytoskeletal activity.

1.3.3 *PCP* signalling in AVE migration

Extensive junction remodelling occurs during AVE migration in the cells of the VE. This coordinated cell movement requires long-range signals across the whole epithelium, a process that is known to be modulated by the Planar Cell Polarity pathway in other contexts, such as Drosophila germband extension. Here, the formation and directional resolution of rosettes discussed above was shown to be regulated by the PCP pathway [85].

ROSA26$^{Lyn\text{-}Celsr1}$ mice have defective PCP signalling and also show lowered numbers of rosettes. AVE in these mice migrates, though not as coherently as wild type mice [31]. This supports a role for the PCP pathway in rosette formation and the migration of the AVE.

In wild-type mice, the core PCP protein Dvl (Dishevelled) exhibits regional location specificity within the VE [5]. This can be seen in Figure 1.5. While at E5.5 Dvl2 staining can be found in all regions of the VE, during the migration of AVE cells Dvl2 is gradually downregulated in the ExE-VE, where it exhibits exclusion from the cell membrane. It also becomes noticeably more enriched in the cell membrane of the Epi-VE. *ROSA26*$^{Lyn\text{-}Celsr1}$ mice also show disrupted expression patterns of Dvl2, correlating to the extent of AVE migration abnormalities.

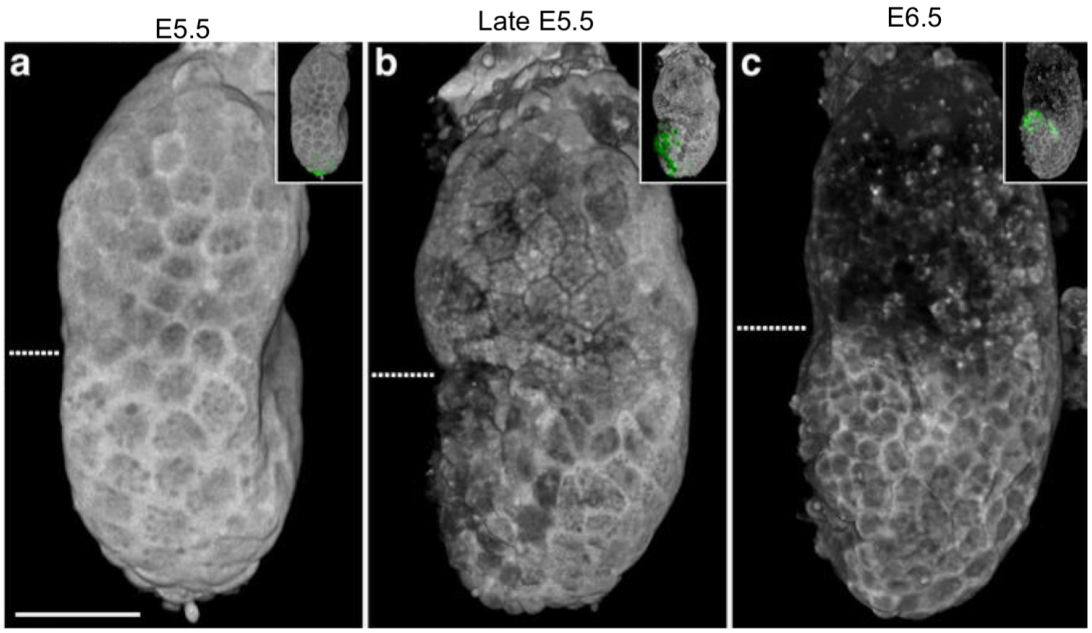


Figure 1.5: Volume rendering of Dvl2 protein in wild-type embryos.

Dvl2 is initially membrane localized throughout the VE. During AVE migration and after, Dvl2 is progressively downregulated in the ExE-VE and excluded from the cell membrane.

Dotted line indicates Epiblast/ExE boundary. Scale Bar = 50μm

Adapted from [5]

AVE migration is well established as an essential developmental process and has much in common with many other types of migration. However, it is highly unusual in many ways. Typically migration that involves an intact epithelial sheet, such as convergent extension, aims to elongate a tissue, or carry out changes in the 3D shape of the tissue, such as neurulation [127], [128]. AVE cells are actively migrating within the plane of an epithelium and appear to be utilizing similar mechanisms to those of large scale coordinated tissue rearrangements such as those seen in Drosophila germband extension, but exhibit directed migration of a small group of cells [85].

In order to fully understand the migration of the AVE, the other cells of the intact Visceral Endoderm tissue must be assessed. Whether these are migrating in a global coordinated movement or facilitating the migration of the AVE via junctional rearrangements has been touched upon in recent research, but to date the behaviour of the cells of the lateral and posterior Visceral Endoderm has not been investigated. To address this, I have used DIC and fluorescent microscopy to image the cells on all Proximal-Distal faces of the embryo, and performed analysis of cell behaviour in multiple regions.

Directed filopodia and lamellipodia are seen in the AVE, which when lost result in a failure of AVE migration [129]. Additionally the loss of protrusional directionality also results in a failure of AVE migration [59]. When these protrusions begin and whether they possess directionality from the time of AVE induction has not been investigated to date. To investigate this, I have developed a novel method of imaging the distal tip of the embryo, and generated high-resolution images of projections forming at this stage.

A role for haptotaxis has not been established in the regulation of AVE migration, despite basement membrane proteins having established roles at

this stage [130]. To address this I have investigated the location of basement membrane protein Laminin-α1.

Despite an established role for PCP signalling in the migration of the AVE, very little is known about the extent of this role. Whether PCP signalling is merely generating permissiveness to migration, how PCP establishes regional localisation of Dvl2 within the VE, and how downstream effectors are mediated to control cell migration are questions that remain unanswered. To begin to address this, I have investigated mice that harbour mutations in a core PCP protein Vangl2, the vertebrate homolog of Strabismus. I have also examined null mutants of β-arrestin2, a protein known to bind and regulate core PCP protein Dvl2. Finally, I have generated transgenic constructs that can be used to relocalise Dvl2, which will facilitate future investigation of this protein.

2

Materials and Methods

2.1 Animal husbandry

All work involving animals was undertaken in accordance with the Animals Scientific Act (1986). Mice were held under the project licenses 30/2309 up to 30th September 2011 and 30/2887 from the 1st Oct 2011 onwards. PIL 30/7527 (Ms. Sharon Ruane) carried out all regulated procedures.

Mice were maintained on a 6.30am – 6.30pm light - dark cycle until August 2012 and were maintained on a 7.30am – 7.30pm light from August 2012 onwards. Mice were mated and checked daily for vaginal plugs. 1pm of the day on which vaginal plugs were observed was designated E0.5 days and embryos were staged accordingly.
Prior to embryo dissection pregnant females were culled by cervical dislocation in accordance with schedule one of the Animals Scientific Procedures Act (1986).

2.1.1 Mouse lines

The mouse lines used during the course of this thesis are shown in Table 2.1.

2.1.2 Genotyping

Mice were ear biopsied using standard husbandry procedures. DNA for PCR genotyping was purified using a standard DNA purification protocol for most mouse strains. For generating wild-type DNA to use as a control and for genotyping embryos an alternative crude lysis protocol was used.

Table 2.1: Mouse lines used during the course of this study

Name	Official Name	Brief description
Hex-GFP	Tg(Hhex-EGFP)#Rbe	GFP is expressed under the Hex promoter acting as a marker for AVE cells [131].
Vangl2	JAX ® Strain 000220 LPT/LeJ	A mutation in the Vangl2 protein (S464N) disrupts both Vangl2 and Vangl1 localisation to the plasma membrane [132]–[134].
Arrb2	JAX ® Strain 011130 Arrb2tm1Rjl/J	Functional deletion of the β-arrestin 2 gene [135].
LifeAct-EGFP	Not available from Jax database	The 17 N-terminal amino acids from *Saccharomyces cerevisae* actin binding protein Abp140, was fused to EGFP. This allows actin mechanics to be visualized [136].
CD1	Crl:CD1(ICR)	Wild-type mice [137], [138]
Flam	ROSA26$^{Lyn\text{-}Celsr1}$	A membrane-tethered portion of the Zebrafish Celsr1 C-terminal domain is expressed under the ubiquitously expressed *ROSA26* locus. This disrupts several PCP dependent processes [5].
Vangl2-Hex-GFP	N/A	Homozygous for both 'Hex-GFP' and 'Vangl2' as described above
Arrb2-HexGFP	N/A	Homozygous for both 'Hex-GFP' and 'Arrb2' as described above

2.1.2.1 Standard DNA purification protocol

Ear biopsies were lysed in 150µl Lysis Buffer 1 +0.5µl Proteinase K overnight at 55°C. The lysate was incubated at 95°C for 15 minutes to heat inactivate Proteinase K and 90µl of saturated $NaCl_2$ was added. Samples were then centrifuged at 14000rpm for 10 minutes and the supernatant was removed to a new eppendorf. 160µl isopropanol was added and samples were inverted 6-8 times to mix. Samples were cooled to -20°C for 30 minutes, then centrifuged at 14000rpm for 10 minutes. The supernatant was removed carefully to ensure that the DNA pellet was not dislodged and the remaining pellet was washed with 100µl of 70% ethanol. Samples were then centrifuged 14000rpm for 1 minute. The supernatant was removed carefully to ensure that the DNA pellet was not dislodged and the pellet was allowed to air dry for 30 minutes at room temperature. The resulting purified DNA was re-suspended in 40µl H_2O and stored at -20°C.

2.1.2.2 DNA preparation by crude lysis

Ear biopsies were lysed in 150µl lysis buffer 2 + 0.5µl Proteinase K overnight at 55°C. For embryos, 15µl Lysis Buffer 2 + 0.05µl Proteinase K was used. Embryonic DNA samples were lysed for 1 hour, and the lysate was then incubated at 95°C for 15 minutes to heat inactivate proteinase K. Samples were centrifuged at 14000rpm for 10 minutes and the resulting purified DNA was then re-suspended in 40µl H_2O and stored at -20°C.

2.1.2.1.1 Lysis Buffer 1:

Batches were syringe filtered, aliquoted and store at -20°C

Reagent	Concentration required	Stock solution	Volume used
H_2O	-	-	174ml
$NaCl_2$	0.1M	5M	4ml
SDS	0.5%	10%	10ml
Tris	10mM	1M pH 8.0	2ml
EDTA	25mM	0.5M	10ml
Total			**200ml**

2.1.2.1.1 Lysis Buffer 2:

Batches were syringe filtered, aliquoted and store at -20°C.

Reagent	Concentration required	Stock solution	Volume used
H_2O	-	-	94.3ml
Tris-HCl	50mM	1M (pH 8-8.5)	5ml
EDTA	1mM	0.5M	200µl
Tween	0.5%	20%	500µl
Total			**200ml**

2.1.2.3 Standard PCR genotyping conditions

Using the appropriate primers detailed in Table 2.2 genotyping was achieved using the following reagents per PCR reaction. If more than 2 primers are used, 0.5 µl less water was added to maintain the correct end volume.

Reagent	**Volume**
H_2O (MilliQ)	19.125µl
10x Buffer (Sigma)	2.5µl
Primer 1	0.5µl
Primer 2	0.5µl
$MgCl_2$	0.5µl
dNTPs	0.5µl
Taq DNA Polymerase (Sigma D1806)	0.625µl
DNA	1.0µl
Total	**25.0µl**

Table 2.1: Genotyping conditions for mutant mice

'PCR' refers to the mutant line being genotyped, 'Start' refers to the initial steps of the PCR, 'Loop' refers to the repeated part of the PCR containing the denaturing, annealing and elongation steps. 'Rep' details how many times the 'Loop' stage should be repeated. 'Primers' gives the sequence of primers used for the reaction. The 'Band' column gives the size of the resultant PCR products when run on an SDS PAGE gel.

PCR	Start	Loop	Rep	End	Primers	Band
Vangl2	94° - 4 min	94° - 30 sec 61° - 60 sec	35	72° - 7 min 4° - 3 min	**WT Forward:** CAAACAGTGGACCTTGGTGTG **Mutant Forward:** CAAACAGTGGACCTTGGTGTA **Reverse:** TGGCAGAAATGTGTCAGGG	300bp *
Arrb2	94° - 3 min	94° - 30 sec 62° - 60 sec 72° - 30 sec	30	72° - 3 min 4° - 3 min	**WT Forward:** GATCAAAGCCCTCGATGATC **Mut Forward:** GCTAAAGCGCATGCTCCAGA' **Reverse:** ACAGGGTCCACTTTGTCCA	**Mut:** 300bp **WT:** 600bp
TdTom	94° - 3 min	94° - 30 sec 65° - 30 sec 72° - 45 sec	30	72° - 3 min 4° - 3 min	**Forward** CAGTTCATGTACGGCTCCAA **Reverse:** GAGGTGATGTCCAGCTTGGT	419bp

**Note: As the Looptail (Vangl2) mutant results from a point mutation, the products of the mutant and wild-type bands are the same size. As such, the PCRs must be done separately*

2.2 Embryo dissection

Dissections were performed as described by the CSH protocols publication "Imaging Cell Movements in Egg-Cylinder Stage Mouse Embryos" [139]. Briefly, embryos were dissected in M2 media. Dissection was completed using fine forceps to remove the decidua from the uterus and the embryo from the decidua. Tungsten needles were used to mechanically remove the Reichart's membrane. Once dissected embryos were fixed for immunohistochemistry or moved into pre-equilibrated culture media.

2.2.1 Culture medium

Embryos were cultured in media made up of 50% mouse serum (homemade) or KnockOut serum and 50% CMRL supplemented with 1mM L-Glutamine. Embryos were cultured at 37°C with 5% CO_2.

Mouse serum was prepared as described by Srinivas *et al.* [139]. Blood was collected from culled mice and immediately centrifuged to separate the blood cells from the serum. The serum was then refrigerated before being centrifuged again and was promptly aliquoted and stored at -80oC.

From 2012 onwards KnockOut serum (Thermo-Fisher Scientific Catalog number: 10828-028) was used in place of mouse serum. All experiments were conducted with consistent culture conditions within sets of experiments.

2.3 Time-lapse Imaging of Cell Movements in the Egg Cylinder Embryo

All imaging was carried out using a Zeiss Axiovert 200 spinning disc confocal microscope.

Preparation:

Two batches of 500μL of culture medium were incubated in an eight-well Lab-Tek II cover glass-bottomed dish for a minimum of 2-3 hours and a maximum of 6 hours at 37°C and 5% CO_2 in a tissue culture incubator. The confocal microscope environmental chamber was equilibrated to 37°C for a minimum of 6 hours.

Embryos were dissected promptly to preserve health and minimize time outside of culture. Excess M2 medium was removed by transferring the embryos to be imaged into a drop of culture medium and the embryos were then transferred into 500 μL of culture medium in one well of the eight-well Lab-Tek II cover glass-bottomed dish and allowed to recover for 30 minutes in the tissue culture incubator.

Approx. 300 μL of culture medium from the second well was transferred to a MatTek dish. If imaging for an extended period, the medium was overlaid with embryo-tested mineral oil to prevent evaporation of the media.

2.3.1 Individual time-lapse experimental set-up adaptions

For each type of imaging experiment performed during the course of the thesis, an adaption was made to the protocol to optimize for the varied desired outcome.

2.3.1.1 Adaptions for DIC imaging

For the DIC imaging described in Chapter 3, a MatTek dish containing glass rods was used to stabilize the embryos during imaging and prevent rolling. A diagram of this dish can be seen in Fig 2.1. These dishes were made using hand-pulled glass rods that were cut to the appropriate size and glued in place using non-toxic glass glue. Smaller glass rod pieces were used as spacers to keep these rods at the appropriate width apart while they were drying. Dishes were left to set for at least 24 hours in daylight, to facilitate the UV bonding of the glue and kept at all times until use in a clear sterile plastic bag to prevent dust contamination.

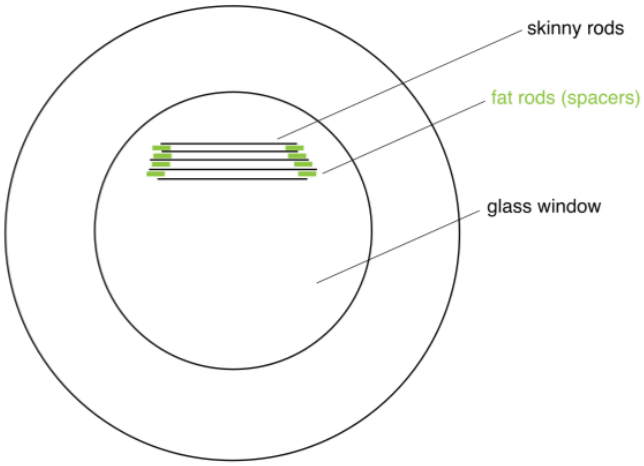


Figure 2.1 Diagram of glass rod dish used for DIC imaging.

A MatTek dish was adapted using hand-pulled glass rods. These were glued into place with spacers of smaller glass rods to hold them apart while drying.

2.3.1.2 Adaptions for fluorescent imaging of AVE migration

For the fluorescent imaging described in Chapter 3, imaging was carried out in the eight-well Lab-Tek II cover glass-bottomed dish, as they were imaged for a much shorter period and did not require special positioning.

2.3.1.2 Adaptions for distal tip fluorescent imaging

For the fluorescent imaging described in Chapter 3, imaging was carried out in a MatTek dish containing a mesh framework. These dishes were made using Millipore nylon net filters (100μm) and affixed to MatTek 30mm glass bottomed Petri dishes using non-toxic glass glue. Dishes were left to set for at least 24 hours in daylight, to facilitate the UV bonding of the glue and kept at all times until use in a clear sterile plastic bag to prevent dust contamination.

2.3.2 Time-lapse Imaging Parameters

2.3.2.1 DIC imaging parameters

Embryos were imaged using a 488nm laser to generate a DIC image of the Visceral Endoderm using the TPMT channel and simultaneously identify any Hex GFP positive cells. To reduce photo toxicity laser intensity was kept at a very low setting and the pinhole increased to capture a wider optical section of the fluorescent reporter. 6-8 optical sections were taken, depending on the size of the embryos so that the most accurate outline of VE cells could be achieved and multiple embryos cold be imaged using the same settings. This greatly increased the number of embryos that could be imaged per session and made it possible for enough embryos of outlinable quality to be attained.

Embryos were imaged every 10 minutes so that accurate tracking of the moving cells could be achieved. At the end of the culture period a high-resolution image of the entire embryo was captured so that the final position of the AVE could be identified and thus the location of the VE cells imaged (anterior, lateral or posterior).

2.3.2.2 Fluorescent imaging parameters

Both pre-migratory and post migratory time-lapse imaging was carried out under the same conditions and with the same imaging parameters. EGFP marking AVE cells was excited at 488 nm. A Z-stack of 8 focal planes was captured every 3 or 4 minutes using 40x objective. Embryos that had been imaged every 4 minutes were used for projection counting, while embryos that were imaged every three minutes were examined for projections that occurred between the shortened time periods. Interval distance between Z-stacks varied between samples depending on size.

2.3.3 Time-lapse Image Analysis

2.3.3.1 DIC image analysis

The time-lapse DIC movies of embryos during AVE migration were spliced together in the Volocity program and then exported as tiff files. These were then realigned in Adobe Photoshop. To do this the deepest Z- level, usually Z-level 6, was used to visualize the outline of the embryo.

For each time point, the deepest Z-level was rotated and shifted in the X-Y axis. The 'pinch' between the ExE and Epiblast regions was used as a central point to align the embryos to.

These adjustments were recorded using the Photoshop 'Action' function and applied to all Z-levels of that time-point (both DIC and GFP channels). This allowed the movement of cells to be tracked reliably. Then, using the most apical Z-section in which cell outlines could be clearly discerned, cells of the VE were outlined in Adobe Photoshop using the Brush tool.

Once outlining was completed, the tiff images were re-imported into Volocity. The manual cell-tracking tool of Volocity was then used to track each individual outlined cell over the time points it was visible for. Individual cell parameter data was then exported and handled as .csv files in Excel. Parameters are detailed in Chapter 3.

Fluorescent image analysis

Cells of the distal tip were assessed for projection type, stability and direction. Projection type was classified visually. Stability assessment counted the time point of the first appearance of the projection to the time point where it had fully receded as the duration of the projection. As the direction of interest of

cellular protrusions at the distal tip was 'Outwards' (proximal) vs. 'Inwards' towards other DVE cells, this meant that standard degree-based directional assessments could not be used. Instead projections were classified as being 'Outwards' (away from the direction of another Hex positive cell) or not. Cells were also assessed for the presence of bifurcated projections.

2.4 High resolution 3D imaging

2.4.1 Imaging parameters for generation of high resolution 3D images from LifeAct embryos

LifeAct embryos were imaged using the 488nm laser. Confocal microscope settings including laser power, gain and digital offset were adjusted for each embryo. Z-stacks were taken every 0.5μm. Outlining of individual cells was carried out using Imaris software, which allowed cells to be rendered in 3D.

2.5 Gene Cloning

Competent DH5α bacteria were used throughout all cloning processes. Transformed bacteria were grown on LB plates and in LB media containing the appropriate antibiotic.

2.5.1 Transformation of DNA into Bacteria

Bacteria were defrosted on ice for 30 minutes and DNA was cooled on ice for five minutes. Bacteria were then added to the DNA and kept on ice for a further 30 minutes. The bacteria were heat shocked at 42°C for 30 seconds and then left on ice for a further two minutes. The bacteria were then incubated in 500μl LB media (without ampicillin) at 37°C for 30 minutes. The incubated bacteria were plated on LB plates with appropriate selection media.

2.5.2 Isolation of plasmid DNA from bacteria

Plasmid DNA was isolated and purified from bacterial cultures using Qiagen Miniprep, Midiprep and Maxiprep kits. PCR of DNA from plasmids PCR was used to clone specific DNA fragments from plasmids. Cloning primers were designed with 5' overhangs to incorporate new restriction enzyme sites into the DNA to aid in subsequent cloning.

Phusion DNA polymerase is a proof reading DNA polymerase that reduces the potential for sequence errors. Phusion DNA polymerase was used for PCR amplification of products for cloning. Using the primers and conditions outlined in Table 2.1, amplification of target DNA sequences was achieved. The following reagents were used for each PCR reaction:

Reagent	**Volume**
H_2O (MilliQ)	12.3µl
5x Buffer (Phusion)	4.0µl
Primer 1 (10µM)	1.0µl
Primer 2 (10µM)	1.0µl
dNTPs (10µM)	0.4µl
Phusion DNA Polymerase	0.3µl
DNA	1.0µl
Total	**25.0µl**

2.5.3 Cloning strategy for Dvl2 mislocalisation constructs.

The complete cloning strategy for the Dvl2 mis-localisation constructs described in Chapter 6 is shown in this section. Further reasoning behind the use of each constituent sequence can be found in Chapter 6. The constructs required several key sequences to be included. These were:

1. The Dvl2 coding sequence
2. The attachment appropriate mis-localisation sequence to Dvl2 (CAAX and MA)
3. The attachment of an appropriate tag to Dvl-2 to allow for visualization of the constructs (HA tag)
4. The inclusion of a co-expressed fluorescent marker to identify successful transient transgenics easily (TdTomato, co expressed using the 2A sequence)
5. The inclusion of the appropriate promoters (CAG, Hex and TTR)

To summarize the process described below, the constructs were made by PCRing of the various constituent parts (tdTomato2A, Dvl2-CAAX, MA, and the TTR promoter) and inserting them into linker plasmids that contained the CAG promoter and HBG transcriptional termination signal sequences. The linker plasmids were then combined sequentially until the main constructs had been generated. Lastly, the appropriate promoter was inserted.

The previously made plasmid BJ1(CAG-HBG) was utilized as the starting point for the cloning strategy. The BJ1 (CAG-HBG) plasmid contains the lengthy linker sequence shown below, which is rich in restriction sites.

BJ-1 Linker: (42bp)

5'TTAATTAACTCGAGGGGAATTCGTGCGGCCGCGTGGTACCGCTCTAGA
GCACCGGTGGAAGCTTGGGGATCCGGCTGCAGGGCGCGCCGAGCTC3'

This reads, in terms of restriction sites, as:
Pac1 Xho1 *O* EcoR1 Not1 Kpn1 Xba1 Age1 HindIII BamH1 *X* Pst1 Asc1 Sac1

In the above restriction site sequence *O* corresponds to a CAG promoter sequence (1734bp) which was present. The *X* corresponds to the HBG sequence (1680bp).

2.5.3.1 Enzymes used in the cloning strategy

All enzymes used in the cloning strategy for the Dvl2 mislocalisation constructs are shown and described in Table 2.2. In all cases NEB CutSmart Buffer and corresponding NEB enzymes were used.

Table 2.2 Enzymes used in the cloning plan for Dvl2 mislocalisation constructs
The bold/unbold distinction in the "Restriction Site" column corresponds the exact base of site cutting. The 'Amino Acids' column describes the amino acids this sequence would be translated as, if any.

Enzyme	Restriction Site	Amino Acids
PacI	**TTAAT**TAA	-
AgeI	**A**CCGGT	Thr- Gly
HindIII	**A**AGCTT	Lys- Leu
Bam HI	**G**GATCC	Gly- Ser
KpnI	**G**GTACC	Gly- Thr
AscI	**GG**CGCGCC	-
NotI	**GC**GGCCGC	-
MluI	**A**CGCGT	Thr- Ala

2.5.3.2 Td-tom2A insertion into BJ1(CAG-HBG) linker

It was not possible to use several of the available restriction sites due to the complex nature of the final constructs required. PacI was required to cut the construct when ligating into the Hex plasmid as the final step in the cloning plan. It was also necessary to drop out the CAG promoter at the final step to include the appropriate TTR and Hex promoter sequences. AgeI was required to cut the construct when ligating into the Ttr plasmid at a later stage.

As such NotI was utilized to add the PCR into the linker in this step, so that the CAG promoter is not dropped out at this stage. NotI could not be used after this step, as it would cut Dvl2.

Td-tom2A was PCRed up from the Hex-tdtom_2A _iCre-ERT2_HBG in pT1PA plasmid. Xho1, PacI and AgeI sites were to the 5' end (in that order) and inserted into the BJ1(CAG-HBG) linker.

Primers for this step included several additional features in the overhang.

The Kozak sequence (GCCACC) used was included. It corresponds to "ANN ATG G", the most commonly used Kozak sequence in eukaryotic mRNAs. A HindIII site was added to the 3' end of the Td-tom2A fragment using primer overhang, to join Td-tom2A to HA-Dvl2.

The sequence needed at the 5' end was:

(5') CG GCGGCCGC TTAATTAA C ACCGGT GCCACC ATG GTG AGC AAG (3')

Which corresponds to: NotI PacI AgeI Kozak M (start of TdTom)

The sequence needed at the 3' end was:

(5') GGAGAATCCTGGCCCA AAGCTT GTC (3')

This was achieved using the following primers:

Forward: CG GCGGCCGC TTAATTAA C ACCGGT GCCACC ATGGTG AGC AAG

Reverse: GACAAGCTTTGGGCCAGGATTCTCCTCGACGTC

The PCR fragment was cut with NotI and HindIII and inserted into BJ1(CAG-HBG) plasmid, and then sequenced with CAG and HBG primers. This stage can be seen in (Figure 2a).

2.5.3.3 Inserting HA-Dvl2-CAAX into a linker plasmid

HA-Dvl2 was PCRed up from HA-Dvl2_pCDNA3.1 plasmid, which was kindly supplied by the Benz lab, Cambridge.

A HindIII site was added to the 5' end to provide a weak Kozak sequence before HA-Dvl2. This ensured there would not be preferential binding here and 'skipping' of the Tdtom sequence. An MluI site, a 54bp CAAX sequence, a STOP codon (TAG) and a BamHI site were added to the 3' end. MluI provided a cut out point (used with BamHI) to drop out CAAX and ligate in MA.

As the HA-Dvl2 PCR contains the Dvl2 STOP codon, this needed to be removed so that the additional CAAX or MA sequences could be transcribed in the final constructs.

The sequence needed at the 5' end was:

5' - GTC AAGCTT ATGTACCCATACGATGTT - 3'

This corresponds to: HindIII - (Start of HA) - CAAX

The sequence needed at the 3' end was: TTTTTTGTGGATGTTATGAGCAAAGATGGTAAAAAGAAGAAAAAGAAGT CAAAGACAAAGTGTGTAATTATGTAGGGATCCGTC

This corresponds to: End of Dvl2 (No Stop) – MluI – CAAX - STOP – BamHI

This was achieved using the following primers:

Forward: GTCAAGCTT ATGTACCCATACGATGTTC

Reverse: GACGGATCCCTACATAATTACACACTTTGTCTTTGACTTCTTTTT

CTTCTTTTTACCATCTTTGCTACGCGTCATAACA

TCCACAAAAAAACGCGT

The PCR fragment was cut with HindIII and BamHI and inserted into BJ-1 (CAG- HBG) linker, giving a 6348bp fragment. The whole construct thus far was sequenced with CAG and HBG primers. This stage can be seen in (Figure 2b).

2.5.3.4 Inserting MA into a linker plasmid

The required MA fragment was PCRed up from X-mito-Mcherry plasmid, which was kindly supplied by the Gertler lab, MIT. PacI and MluI sites were added to the 5' end and a BamHI site was added to the 3' end. A stop codon was added after the MA site.

The sequence needed at the 5' end was:

GTC TTAATTAA ACGCGT AAACTAATTGCTAAAAGT

This corresponded to PacI-MluI-Start of MA

The sequence needed at the 3' end was:

AATTAAGAAAA AATAATTAGGGATCCGTC

This corresponded to End of MA-STOP – BamHI

This was achieved using the following primers:

Forward: GTCTTAATTAAACGCGTAAACTAATTGCTAAAAGT

Reverse: GACGGATCCCTA ATTATTTTTTCTTAATT

The PCR fragment was then cut with PacI and BamHI and inserted into the BJ-1(CAG-HBG) linker. The PCR fragment generated a 152bp band when cut. The BJ-1(CAG-HBG) lost the CAG promoter and generated a 4562bp band upon cutting. This stage can be seen in (Figure 2c).

2.5.3.5 Inserting the TTR promoter into BJ1(CAG-HBG)

The BJ1(CAG-HBG) plasmid was cut with PacI and NotI to drop out the CAG promoter. The TTR plasmid was also cut with PacI and NotI to isolate TTR promoter. The PacI-TTR promoter –NotI fragment and PacI/NotI cut BJ1 plasmid was then ligated. This gives access to AgeI site for insertion of TdTom-2A-HA-Dvl2- CAAX/MA-BGH which could not previously be inserted as NotI cuts Dvl2. This stage can be seen in (Figure 2d).

2.5.3.6 Combining the constituent parts held in linkers

The BJ1(CAG-TdTom2A-HBG) plasmid was cut with HindIII and BamHI to open the plasmid at Td Tomato, generating 2 fragments. The main 7834bp backbone was kept.

The BJ1(CAG-HA-Dvl2-CAAX-HBG) plasmid was cut with HindIII and BamHI to release HA-Dvl2-CAAX fragment.

The HA-Dvl2-CAAX fragment and the cut BJ1(CAG-TdTom2A-HBG) backbone were ligated. This generated the BJ1(CAG-TdTom2A-HA-Dvl2-CAAX-HBG) plasmid (10163bp).

Half of the newly created BJ1(CAG-TdTom2A-HA-Dvl2-CAAX-HBG) plasmid stock was then cut with MluI and AscI to drop out the CAAX-HBG site, giving an 8405bp fragment. Similarly, BJ1(CAG-MA-HBG) was cut with MluI and AscI to isolate the 1837bp MA- HBG fragment.

The MA-HBG fragment was ligated to the BJ1(CAG-TdTom2A-HA- Dvl2-CAAX-HBG) backbone. This generated BJ1(CAG-TdTom2A-HA-Dvl2-MA-HBG) plasmid.

This provided two of the final six required constructs, BJ1(CAG-TdTom2A-

HA-Dvl2-CAAX-HBG) and BJ1(CAG-TdTom2A-HA-Dvl2-MA-HBG). To generate the other constructs, the CAG promoter was dropped out and the TTR and Hex promoters were ligated in.

2.5.3.7 Adding Hex and TTR promoters

The Hex Plasmid pT1PA was cut with PacI and AscI. BJ1(CAG-TdTom2A-HA-Dvl2-CAAX-HBG) and BJ1(CAG-TdTom2A-HA-Dvl2-MA-HBG) were also cut with PacI and AscI. These were ligated to form Hex-TdTom2A-HA-Dvl2-CAAX-HBG and Hex-TdTom2A-HA-Dvl2-MA-HBG. The final Hex-TdTom-2A-(CAAX or MA)-HBG fragment can be easily removed at local KpnI sites. Plasmids for the final versions can be seen in Figure 6.7.

BJ1(TTR) plasmid was cut with AgeI and AscI. BJ1(CAG-TdTom2A-HA-Dvl2-CAAX-HBG) and BJ1(CAG-TdTom2A-HA-Dvl2-MA-HBG) were also cut with AgeI and AscI. These were ligated to form TTR-TdTom2A-HA-Dvl2-CAAX-HBG and TTR-TdTom2A-HA-Dvl2-MA-HBG. PacI and AscI can be used entire Ttr-TdTom-Ha-Dvl2-Caax/MA- BGH fragment. Plasmids for the final versions can be seen in Figure 6.7.

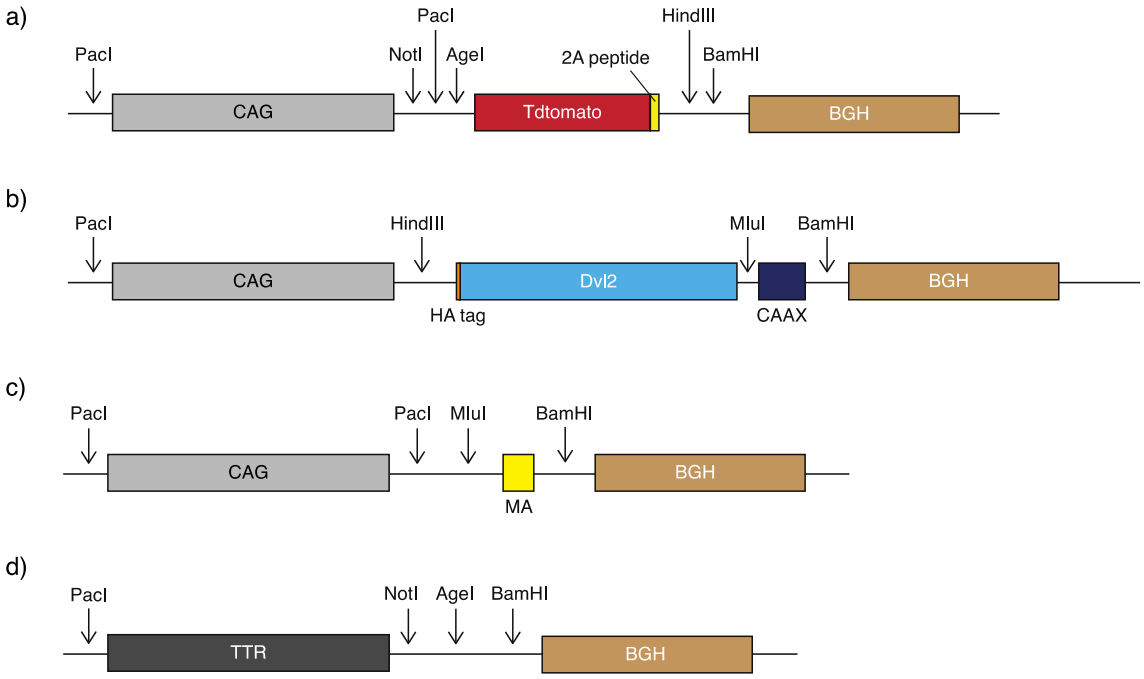


Figure 2.2: Stages of the cloning plan for Dvl2 mislocalisation constructs

(a) Depicts the addition of TdTom to a linker plasmid. (b) Shows the addition of CAAX to the Dvl2 coding sequence. (c) Depicts the positioning of the MA construct in a liner plasmid. (d) Shows the insertion of the TTR promoter into a linker plasmid.

2.6 RT-PCR

2.6.1 β-arrestin primers used in RT-PCR

ARRB2 -1 AATTTGCCTTGTTCCGTCAC

ARRB2 -2 TTGTTGGTGACATGGACGTT

These primers generated an 1116bp fragment between exon 6 and 9 in genomic DNA.

2.6.2 RT-PCR Reagents

Qiagen mini RNeasy kit (74104)

QIAshredder spin column (79654)

TURBO DNase (Ambion AM1907)

Random primer (Invitrogen 48190-011)

Invitrogen Kit 18080-093

2.6.3 RT-PCR Turbo DNA-Free Protocol

The mixture for the DNA-free reaction was prepared as shown below:

Reagent	Volume
H_2O	-
RNA (up to 10μg)	-
10X Turbo DNase buffer	5μl
Turbo DNase	1μl
Total	50μl

This mixture was incubated for 20-30 minutes at 37^{O}C. 5 μL of DNase Inactivation Reagent was added and the preparation was mixed well and then incubated at room temperature for 5 minutes. The mixture was then centrifuged at 10,000 x g for 1.5 min and the remaining RNA was transferred to a fresh tube.

2.6.3 Main RT-PCR protocol

The First-Strand cDNA Synthesis reaction mixture was prepared as follows:

Reagent	Volume
Gene specific primer (2 pmol)	1µl
10µM dNTPs	1µl
RNA	5µl
H_2O	13µl
Total	20µl

This mixture was incubated at 65^{O}C for 5 minute and then incubated on ice for 1 minute. 6 µL of the following preparation was then added to each reaction.

Reagent	Volume
5x First Strand Buffer	1µl
0.1µM DTT	1µl
SuperScript III RT	4µl
Total	20µl

The reactions were mixed gently by pipetting and incubated for 5 minutes at 25^{O}C, followed by 55^{O}C for 1 hour and finally at 70^{O}C for 15 minutes. 1 µL RNaseH was then added and the reactions were incubated at 37^{O}C for 20 minutes. The resulting DNA was then stored at 4^{O}C for future use

2.7 Immunohistochemistry

E5.0-E6.5 embryos were dissected at various stages for the work carried out in this thesis. For immunochemistry, embryos were typically fixed, washed, blocked, stained with primary antibody, washed, stained with secondary antibody, washed and then stained with phalloidin, washed, stained for DAPI and then stored in Vectashield mounting medium.

2.7.1 Fixing Embryos (with PFA)

Embryos were dissected in M2 media and fixed in 4% PFA. E5.5 embryos were fixed for 20 minutes and E6.5 embryos were fixed for 30 minutes.
For some antibodies an alternative 'Buffered fixative' was used, made as described below:

Reagent	Volume
PFA (4%)	1µl
KCl (2.5M)	52µl
0.5M Hepes	50µl
1M MgCl	3µl
25% gluteraldehyde	6µl
Triton-X 100	0.6µl
Total	1µl

Embryos were washed x3 in PBT Triton (0.1%) for 5 minutes (each). Embryos were then washed x1 in PBT Triton (0.25%) for 15 minutes, followed by washing x3 again in PBT Tween (0.1%) for 5 minutes (each).

2.7.2 Blocking:

Embryos were added to blocking solution for a minimum of 1 hour (usually overnight). Blocking Solution was made from 3% BSA 2.5% Horse serum in PBT Tween

2.7.2 Primary Antibody

Embryos were added to a 1/100 or 1/200 solution of appropriate Primary antibody in fresh blocking solution. They were left for 24 hours. Embryos were then washed x5 in PBT Tween (0.1%) for 5 minutes (each). Finally, embryos were washed x1 in PBT Tween (0.1%) for 15 minutes.

2.7.3 Secondary Antibody

Embryos were added to a 1/100 or 1/200 solution of appropriate secondary antibody in PBT Tween (0.1%). They were then left overnight.

2.7.4 Phalloidin + DAPI staining

1/100 Phalloidin was added directly to embryo-containing eppendorf. It was then left for 1 hour. Embryos were washed x5 in PBT Tween (0.1%) for 5 minutes (each).
Embryos were added to 20µl (Vectashield+ DAPI). They were then left for 2 days in a depression slide.

2.7.5 Mounting embryos:

After fixation and staining embryos were individually mounted on slides in a small amount of Vectashield (~2µl). Laboratory tape was used as a spacer between the glass slide and coverslip, to avoid squashing the embryos.

Coverslips were secured in place using nail varnish. Figure 2.3 depicts the steps involved in preparation of mounted embryos for confocal microscopy.

Table 2.3 Primary antibodies

This table lists the primary antibodies used during the course of this study.

Antibody	Source	Host	Fixative
Dishevelled 2	Biomol 4270	Rabbit	Buffered Fix
PhosphoERK	Cell Signalling 9101	Rabbit	4% PFA
Phosphorylated Smad2	Cell Signalling 3108	Rabbit	4% PFA
β-Arrestin 2	Cell Signalling 3857	Rabbit	Both fixes (neither worked)
β-Arrestin 2	Aviva AAP48007	Rabbit	Both fixes (neither worked)
pMLC	Cell Signalling 3761	Rabbit	4% PFA
Rab	ADI-KAP-GP006E	Rabbit	4% PFA
Profilin	Immunoglobe 0022- 01	Rabbit	4% PFA
Stathmin	Sigma Aldrich 00138	Rabbit	4% PFA
P-stathmin	Sigma Aldrich Ab47399	Rabbit	4% PFA
Dkk1	Aviva ARP48015	Rabbit	Both fixes (neither worked)
JMY	Santa Cruz SC- 13020	Rabbit	4% PFA
Ezrin	BD biosciences 610602	Rabbit	4% PFA
Dvl2	Aviva ARP32102	Rabbit	Both fixes (neither worked)
Laminin- alpha1	Sigma L9393	Rabbit	4% PFA

Table 2.4: Secondary antibodies and conjugated dyes

Reactivity	Fluorophore	Source
Donkey anti-rabbit IgG	Alexa Fluor 555	Invitrogen A-31572
Goat anti-rat IgG	Alexa Fluor 633	Invitrogen A-21094
Phalloidin	TRITC 555	Sigma 77418
Phalloidin	Atto 647N	Sigma 65906

2.7.6 Confocal microscopy of fixed embryos

Antibody stains and endogenous fluorescent reporters were imaged using a Zeiss 710 confocal microscope on a 40x (W) (1.2NA) objective. 405nm, 488nm, 561nm and 633nm lasers were used for excitation of fluorophores and the emitted light captured. Confocal microscope settings including laser power, gain and digital offset were adjusted for each embryo. When imaging groups of mutant embryos to compare potential differences all embryos of the group were imaged using the same settings and in the same confocal session. Image analysis including three-dimensional rendering was carried out using Improvision Volocity software.

3

Time-lapse Imaging and Quantification of Visceral Endoderm Cell Dynamics

3.1 Introduction

Until recently, most experiments on AVE migration have only visualized the specific subset of Hex-expressing AVE cells that migrate to the future anterior of the embryo. This is mainly due to the availability of fluorescent reporters expressed specifically in the AVE and the importance of the AVE in patterning the embryo. The Srinivas lab performed time-lapse imaging on the anterior face of the embryo, investigating regional differences in the Visceral

Endoderm [5]. This however, does not address the behaviour of Visceral Endoderm cells in other areas of the embryo. In this chapter, I describe a confirmation and extension of published work, at shorter time intervals, on all faces of the E5.5-E5.75 mouse embryo.

3.1.1 Visualising the AVE at E5.5

As discussed in Chapter 1, the Visceral Endoderm (VE) is a continuous sheet of epithelial tissues that overlies the epiblast and the ExE, forming the outer layer of the embryo. Srinivas et al. performed the original live imaging of this tissue, utilizing a *Hex-GFP* transgenic marker that labelled AVE cells [51]. In this manner it was shown that the cells of the AVE actively migrate towards the prospective anterior of the embryo, extending protrusions in the direction of migration. Additionally, upon reaching a point directly above the boundary between the Epiblast and the ExE, AVE cells migrating to their anterior destination were demonstrated to halt their proximal migration and move laterally. AVE migration has also been shown in greater resolution by Migeotte et al., who saw long cellular protrusions which were often tipped with additional filopodia, which were noted to be basally localized [129]. Bifurcating protrusions were described by Omelchenko et al. in the migrating AVE, further confirming the highly active behaviour of these cells. [59]

3.1.2 Visualising larger areas of the Visceral Endoderm at E5.5

Members of the Srinivas lab have utilized Differential Interference Contrast (DIC) microscopy to examine non-fluorescent cells of the VE during AVE migration (Figure 3.1). From this work it became evident that AVE cells do not move autonomously, but as a part of coordinated intercalatory movement with surrounding cells. Investigation of multiple cell parameters also revealed regions of dramatically different cell behaviour within the intact epithelial sheet of the VE. These regions consist of the VE overlying the epiblast (Epi-VE) and VE overlying the Extra-embryonic Ectoderm (ExE-VE). Cells of the Epi-VE were shown to exhibit robust cell movement; irregular shapes and intercalation, while cells within the ExE-VE behave in a more static manner, with relatively little cell movement and mixing [5].

This variation in regional cell behaviour was proposed to be the cause of the abrupt migratory halt which AVE cells stereotypically exhibit. Cells of the ExE-VE behave as though they are non-permissive to the intercalation that occurs during migration in the AVE. This theory is supported by evidence that the overmigration phenotype seen in *Lefty1* mutants, where cells of the AVE migrate past the embryonic/abembryonic boundary into the ExE-VE, is accompanied by cell shape changes and neighbour exchange behaviour in the ExE-VE that are far more 'Epi-VE like' in nature. Less rigid packing and a higher rate of neighbour exchange indicate that the non-permissive behaviour of the ExE-VE cells has been lost, removing the barrier which the region posed to AVE migration [140].

Because of the importance of the AVE in mouse embryology, previous studies from the Srinivas lab focused on the anterior of the embryo. As such, we do not know how cells in the posterior or lateral VE respond to or influence AVE migration. It stands to reason that within an intact epithelium of finite space,

the other cells of the VE might also migrate to accommodate the migration of the AVE. An alternate explanation for how the other VE cells might behave is the accommodation of movement by changes in cell shape. To address this issue, one needs to visualize in detail cell movements through all regions of the VE during AVE migration.

Two transgenic reporters were tested previously in the lab, CAG-TAG-1 and KIK-GR, but both were found to be unsuitable for this line of imaging [141], [142]. Given Srinivas lab has successfully used DIC optics to discern cell outlines in the past, I performed time-lapse imaging using this method on E5.5 mouse embryos, with the aim of visualizing all faces of the embryo during AVE migration.

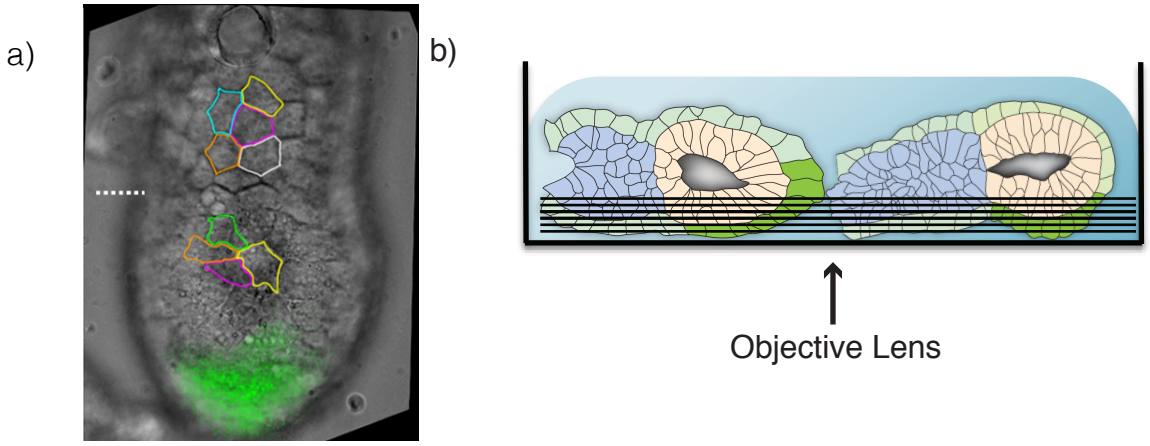


Figure 3.1 DIC imaging of the E5.5 mouse embryo

(a) shows DIC imaging of an E5.5 Hex-GFP mouse embryo. AVE cells (green) are located at the distal tip of the embryo. Tracing and tracking of individual cells is indicated by the coloured outlines in each region. The dotted line indicates the embryonic/abembryonic boundary that the AVE migrates towards and halts upon reaching, before moving laterally.

(b) depicts the embryo imaging setup for DIC. Few Z-stacks were taken to limit photo toxicity and allow healthy migration during imaging. From this set up, the apical surface outlines of Visceral Endoderm cells closest to the objective can be tracked throughout AVE migration..

Image (a) adapted from [5]

3.2 Results

In order to characterise the movement of VE cells in the lateral and posterior of the embryo during AVE migration, I utilized DIC microscopy to acquire time-lapse images of E5.5-E5.75 embryos. These image sequences are of sufficient resolution to quantify cell migration over time. Details of image processing can be found in Chapter 2. I determined the orientation of embryos using Hex-GFP as a marker of the anterior. Embryos are positioned at random in the dish during imaging, generating a distribution of orientations. After capturing time-lapse images, I categorized individual embryos as 'anterior' (n=4), 'lateral' (n=4), or 'posterior' (n=4) facing (Fig 3.1).

3.2.1 Cell Movement

I analysed general cell movement in embryos where the anterior, lateral or posterior side was facing the objective. Using the centroid location of each cell, the distance moved between two time points (or greater period of time) can be calculated and used as a measure of how motile cells are. I determined the amount each cell had migrated in μm per time-point (Fig. 3.2). For this analysis, migration in any direction was assessed. Results can also be found in Table 3.1.

Significant differences in cell movement between the Epi-VE and ExE-VE were seen on the lateral and posterior faces of the embryo. A strong trend showing a difference in the cell movement between the Epi-VE and ExE-VE was seen on the anterior face of the embryo, but this was not significant.

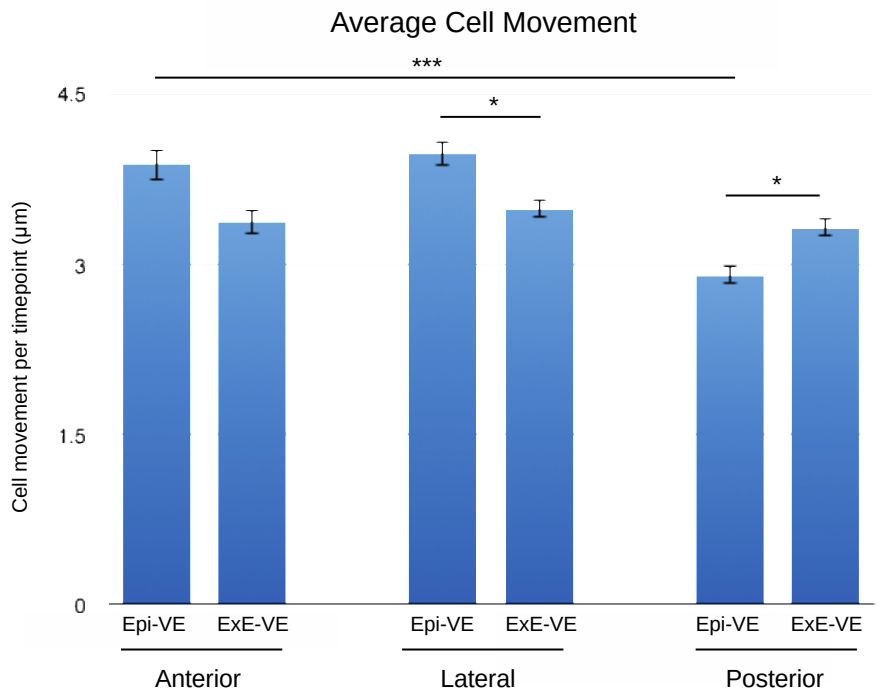


Figure 3.2: Average cell movement in the E5.5-E5.75 Visceral Endoderm

After outlining and tracking cells in Volocity, cell movement was calculated using the centroid location of each cell. The distance a cell moved between two time points was averaged per region. Statistical analysis was performed using a nested ANOVA to account for the differences between individual embryos.

A strong trend was seen between the Epi-VE and ExE-VE on the anterior face of the embryo, with cells moving more in the Epi-VE, though this was not statistically significant ($p = 0.091$).

A statistically significant difference in cell movement was seen between the Epi-VE and ExE-VE on the lateral faces of the embryo ($p = 0.019$)

A strongly statistically significant difference in cell movement was seen between the Epi-VE and ExE-VE on the posterior faces of the embryo ($p = 0.002$)

** indicates $p < 0.05$, ** indicates $p < 0.01$, *** indicates $p < 0.0001$*

Table 3.1: Analysis of cell movement in the E5.5-E5.75 Visceral Endoderm

Data pertaining to the analysis of cell movement in the VE is listed. The 'Face' column lists which side of the embryo was analysed. The 'Region' column lists the area 'Epi-VE' or 'ExE-VE' in question. 'Name' corresponds to the distinct name given to each of the six regions during analysis. Number' details the number of time-point differences analysed. 'µm /TP' is the averaged results of migration per time-point. 'µm /min' is the value of averaged cell migration per minute.

Face	Region	Name	Number	µm/TP	µm /min
Anterior	Epi-VE	AEPI	368	3.8758	0.38758
Anterior	ExE-VE	AEXE	425	3.3718	0.33718
Lateral	Epi-VE	LEPI	586	3.97798	0.397798
Lateral	ExE-VE	LEXE	621	3.48579	0.348579
Posterior	Epi-VE	PEPI	521	2.90279	0.290279
Posterior	ExE-VE	PEXE	538	3.32274	0.332274

3.2.2 Cell Displacement

After analysis of cell movement revealed differences within regions of the VE, I examined the tracking data for differences in directional movement of each region's constituent cells. This was achieved by dividing the total displacement (start vs. end of a track) of a given tracked cell by the number of time-points the cell was tracked for. The average track length was approx. 8 time-points (80 minutes). A high value indicates a migratory behaviour in a cell, while a low value indicates that a cell is not moving in a directed manner. Results of this analysis can be seen in Fig 3.3 and Table 3.2.

Significant regional differences were seen in directed cell movement. The highest rate of movement was seen in the anterior Epi-VE. This was significantly higher than all other regions.

The ExE-VE showed no significant difference in directed cell migration on any face of the embryo. The Epi-VE showed large differences in directed cell movement on different faces of the embryo, with the lateral Epi-VE showing a directed movement similar to that of the global ExE-VE. The posterior Epi-VE exhibited even lower directed movement than the global ExE-VE.

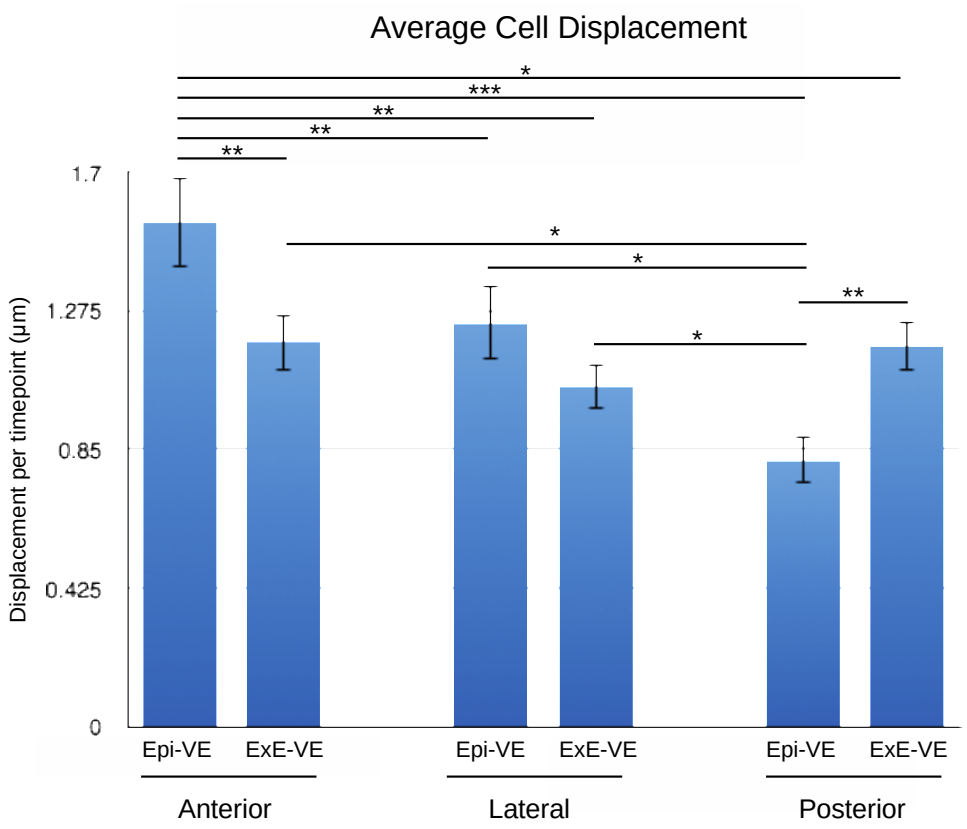


Figure 3.3: Directed cell movement in the E5.5-E5.75 Visceral Endoderm

Cell displacement was calculated by Volocity software using the centroid location of each cell at the first and last time-points in any given track. The distance a cell moved between these two time points then divided by the number of time-points of the cell track. Statistical analysis was performed using a nested ANOVA to account for the differences between individual embryos.

A statistically significant difference in directed cell movement was seen between the Epi-VE and ExE-VE on the anterior face of the embryo ($p < 0.01$). A similar difference was also seen between the Epi-VE and ExE-VE on the posterior faces of the embryo ($p < 0.01$). Anterior, lateral and posterior regions of the Epi-VE showed significantly different levels of directed cell

movement in all combinations. No difference was seen in directed movement between the ExE-VE regions of the anterior, lateral and posterior faces of the embryo.

** indicates $p < 0.05$, ** indicates $p < 0.01$, *** indicates $p < 0.0001$*

Table 3.2*: Analysis of directed movement in the E5.5-E5.75 Visceral Endoderm*

Data pertaining to the analysis of directed cell movement in the VE is listed. The 'Face' column lists which side of the embryo was analysed. The 'Region' column lists the area 'Epi-VE' or 'ExE-VE' in question. 'Name' corresponds to the distinct name given to each of the six regions during analysis. 'Number' details the number of tracks analysed. 'Mig/TP' is the averaged results of migration per time-point. 'Mig/min' is the value of averaged cell migration per minute.

Face	Region	Name	Number	Mig/TP	Mig/min
Anterior	Epi-VE	AEPI	42	1.543	0.1543
Anterior	ExE-VE	AEXE	41	1.178	0.1178
Lateral	Epi-VE	LEPI	69	1.238	0.1238
Lateral	ExE-VE	LEXE	65	1.046	0.1046
Posterior	Epi-VE	PEPI	51	0.817	0.0817
Posterior	ExE-VE	PEXE	55	1.168	0.1168

3.2.3 Angle of cell movement

Some directed movement was seen in all regions of the embryo, however, it is not apparent from this that the directed movement is coordinated in the same direction. In order to analyse which directions cells of each region were moving in, I reoriented the time-lapse images to position the embryos along the Proximal to Distal axis, and quantified the cell migratory tracks on angle of movement between time-points.

When averaged and compared directly, no significant difference could be seen between the regions due to the high variability of the movement. However, when binned into regions of 20 degrees and plotted visually, the cells of the anterior Epi-VE can be seen to have a clear bias towards proximal migration, while other regions migrate in a far more evenly dispersed radial manner (Fig 3.4).

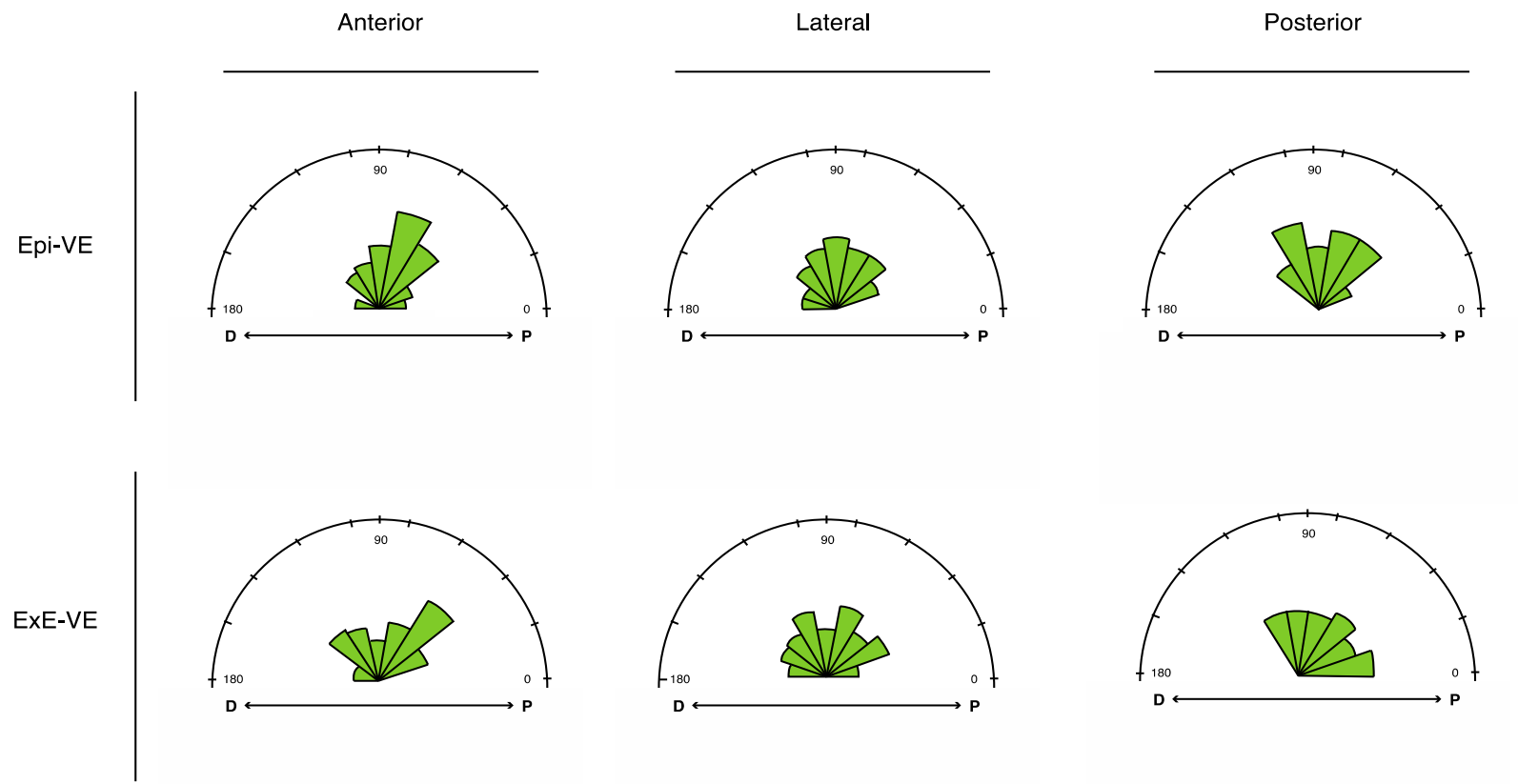


Figure 3.4: Angle of migration within regions of the Visceral Endoderm

Embryos were oriented along the proximal-distal (PD) axis and the angle between the line generated by a traced cell between two time-points and the PD axis (0 to 180 degrees) was deemed the angle of movement. Results were binned in 20-degree increments and plotted as rose plots. Heavily proximal movement was seen in the Anterior Epi-VE and to a lesser extent the posterior ExE-VE)

3.2.4 Shape factor

Given the differences in cell shape seen on the anterior in previously published data, I investigated the shape factor of cells of the Visceral Endoderm on all faces of the embryo.
Shape factor, described in Chapter 2, is a numeric value between 0 and 1. Shape factor gives a measure of the distortedness of a cell's shape, with shapes such as hexagons and pentagons scoring closer to 1 than flattened or irregular shapes. A straight line scores a shape factor of 0 and a circle scores a value of 1.

Results for shape factor analysis can be found in Figure 3.5 and Table 3.3.

Shape factor was lower in the Epi-VE than the ExE-VE in all regions of the embryo, however lateral Epi-VE showed a marked increase over the Epi-VE on the other faces. Similarly, lateral ExE-VE showed a marked increase in shape factor over the other two faces.

a)

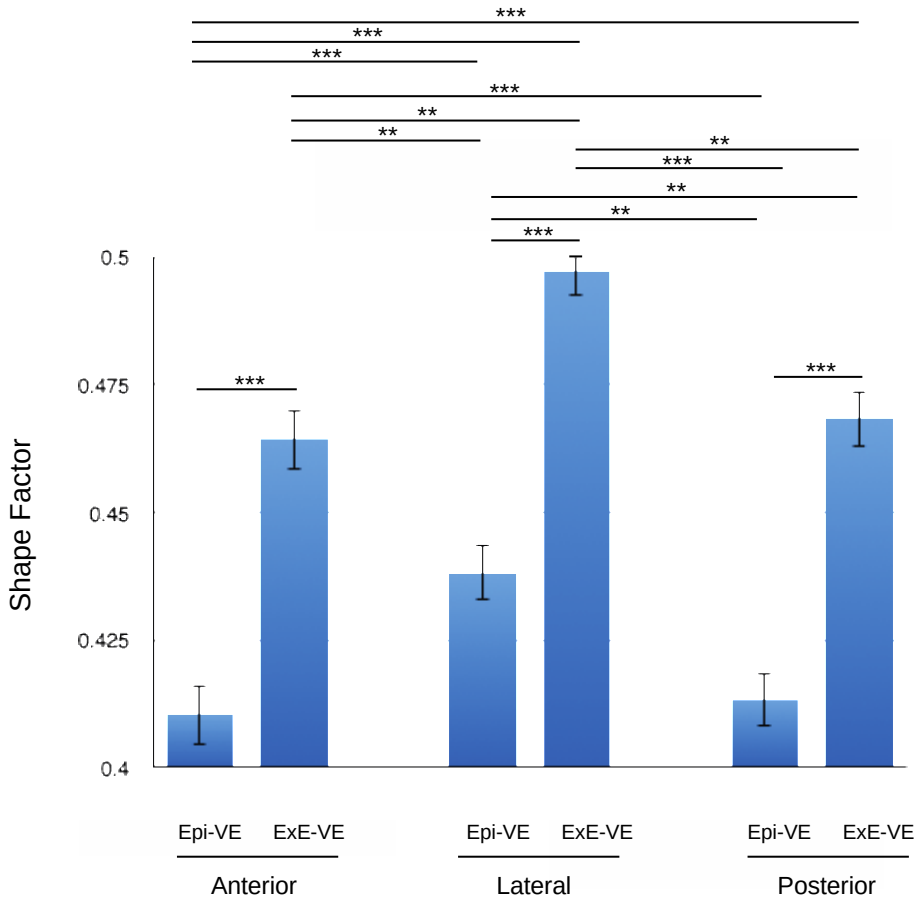


Figure 3.5: Analysis of shape factor in the E5.5-E5.75 Visceral Endoderm

*Shape factor was calculated by dividing 4*π*(cell area) by (cell perimeter)². A higher shape factor indicates a more rounded shape. Statistical analysis was performed using a nested ANOVA to account for the differences between individual embryos.*

A statistically significant difference in shape factor was seen between the Epi-VE and ExE-VE on the all faces of the embryo. A statistically significant difference in shape factor was seen between the lateral and anterior faces of the Epi-VE, and the lateral and posterior faces of the Epi-VE.

Similarly, a statistically significant difference in shape factor was seen between the lateral and anterior faces of the ExE-VE, and the lateral and posterior faces of the ExE-VE.

** indicates $p < 0.05$, ** indicates $p < 0.01$, *** indicates $p < 0.0001$.*

Table 3.3*: Analysis of shape factor in the E5.5-E5.75 Visceral Endoderm*

Data pertaining to the analysis of shape factor in the VE is listed. The 'Face' column lists which side of the embryo was analysed. The 'Region' column lists the area 'Epi-VE' or 'ExE-VE' in question. 'Name' corresponds to the distinct name given to each of the six regions during analysis. 'Number' details the number of tracks analysed. 'Shape' indicates the average value determined for shape factor in a given region.

Face	Region	Name	Number	Shape
Anterior	Epi-VE	AEPI	447	0.4103
Anterior	ExE-VE	AEXE	487	0.4642
Lateral	Epi-VE	LEPI	568	0.4382
Lateral	ExE-VE	LEXE	593	0.4972
Posterior	Epi-VE	PEPI	582	0.4133
Posterior	ExE-VE	PEXE	520	0.4684

3.2.5 Neighbour Exchange

In order to move within an epithelial sheet, a large degree of neighbour exchange must occur. Here, cells alter which other cells they share cell boundaries with.

Neighbour exchange was examined on all faces and regions of the VE at E5.5 (Figure 3.6). Results can also be seen in Table 3.4.

Neighbour exchange was higher in the Epi-VE than the ExE-VE in all regions of the embryo, but highest in the anterior Epi-VE. In the ExE-VE there was no difference in neighbour exchange between faces of the embryo.

Table 3.4: Analysis of neighbour exchange in the E5.5-E5.75 Visceral Endoderm

Data pertaining to the analysis of neighbour exchange in the VE is listed. The 'Face' column lists which side of the embryo was analysed. The 'Region' column lists the area 'Epi-VE' or 'ExE-VE' in question. 'Name' corresponds to the distinct name given to each of the six regions during analysis. 'Number' details the number of time-points where NE was counted between all visible cells. 'NE' indicates the average value determined for neighbour exchange per time point per cell in a given region.

Face	Region	Name	Number	NE
Anterior	Epi-VE	AEPI	22	0.3612
Anterior	ExE-VE	AEXE	22	0.1259
Lateral	Epi-VE	LEPI	53	0.2143
Lateral	ExE-VE	LEXE	53	0.05476
Posterior	Epi-VE	PEPI	48	0.2337
Posterior	ExE-VE	PEXE	48	0.1031

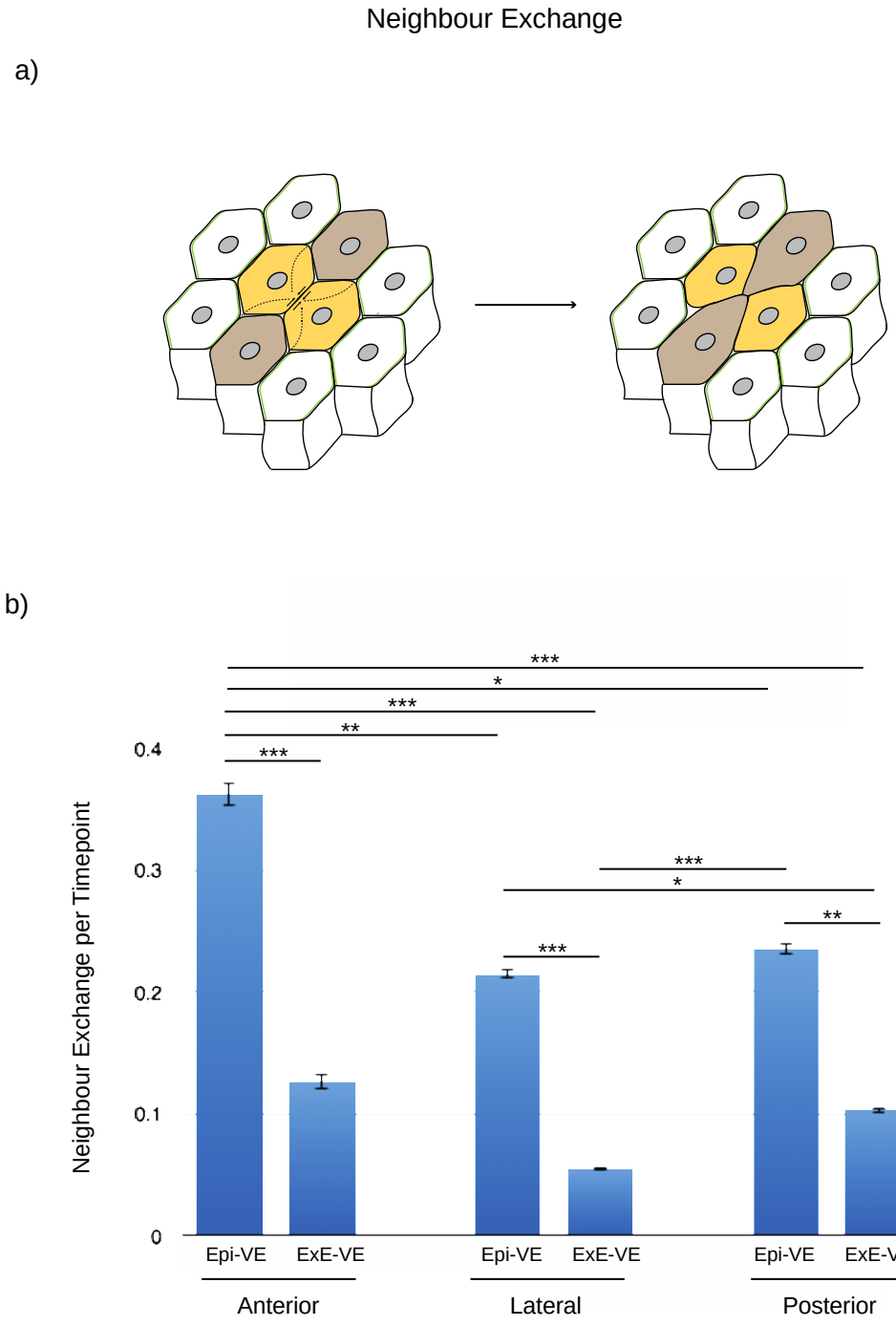


Figure 3.6: Analysis of neighbour exchange in the E5.5-E5.75 Visceral Endoderm *(legend overleaf)*

** indicates p < 0.05, ** indicates p < 0.01, *** indicates p < 0.0001*

Figure 3.6: Analysis of neighbour exchange in the E5.5-E5.75 Visceral Endoderm

(a) Cartoon depiction of neighbour exchange occurring. In this event, brown cells become neighbours, and orange cells are no longer neighbours.

(b) Statistical analysis of neighbour exchange across the VE during AVE migration. Statistical analysis was performed using a nested ANOVA to account for the differences between individual embryos.

A significant difference in neighbour exchange was seen between the Epi-VE and the ExE-VE on all faces of the embryo.

No difference was seen among regions of the ExE-VE on all faces of the embryo.

** indicates $p < 0.05$, ** indicates $p < 0.01$, *** indicates $p < 0.0001$*

3.2.6 Apical Surface Area

Given that the apical region of the Visceral Endoderm was imaged and the cell perimeters were outlined, this gave an approximation of the apical cell surface individual cells. I utilized this to compare regional differences in apical cell surface area.

Across all faces of the embryo, the ExE-VE cells showed a larger apical surface area than those of the Epi-VE. This was most prominent in the posterior region where cells of the posterior ExE-VE were shown to be the largest of any region.

There was also a statistically significant difference in apical cell surface between the cells of the anterior Epi-VE and lateral Epi-VE.

Table 3.6*: Analysis of the apical surface area of cells in the E5.5-E5.75 Visceral Endoderm*

Data pertaining to the analysis of neighbour exchange in the VE is listed. The 'Face' column lists which side of the embryo was analysed. The 'Region' column lists the area 'Epi-VE' or 'ExE-VE' in question. 'Name' corresponds to the distinct name given to each of the six regions during analysis. 'Number' details the number of cells analysed. 'Area' indicates the average value determined for apical surface area in a given region, measured in μm^2.

Face	Region	Name	Number	Area
Anterior	Epi-VE	AEPI	447	195.05
Anterior	ExE-VE	AEXE	487	220.21
Lateral	Epi-VE	LEPI	568	213.21
Lateral	ExE-VE	LEXE	593	223.62
Posterior	Epi-VE	PEPI	582	194.81
Posterior	ExE-VE	PEXE	520	267.15

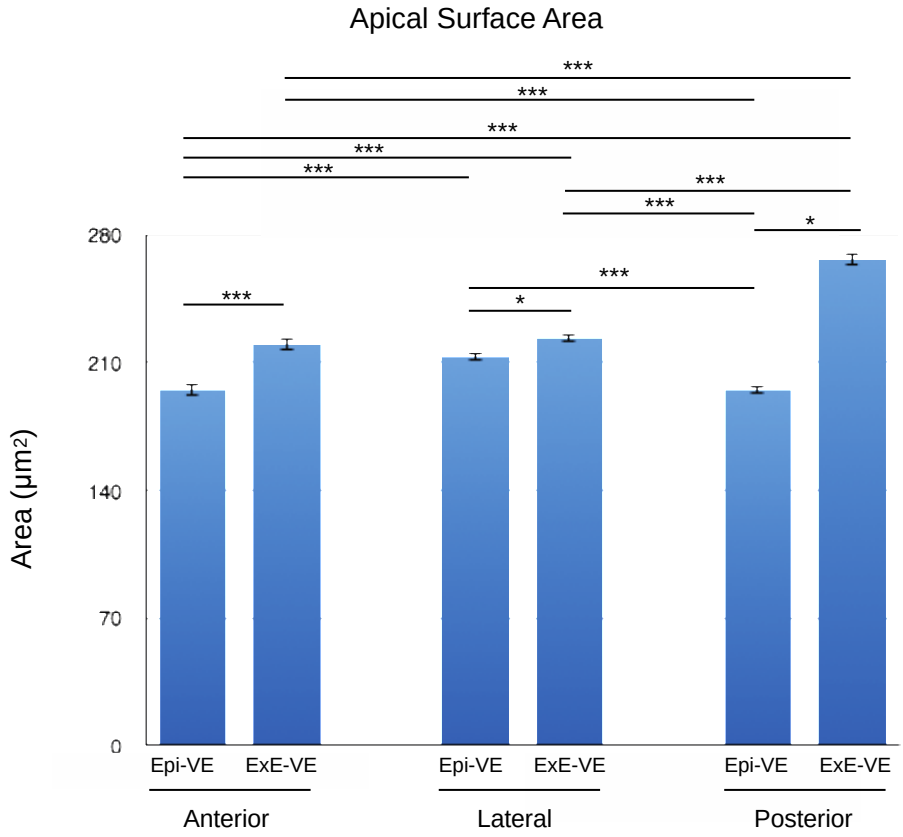


Figure 3.7: Analysis of apical cell surface area in the E5.5-E5.75 Visceral Endoderm

Statistical analysis of apical cell surface area across the VE during AVE migration. Cell surface area was generated by tracing the perimeter of imaged embryos in image analysis software Volocity. Statistical analysis was performed using a nested ANOVA to account for the differences between individual embryos.

A significant difference in cell surface area was seen between the Epi-VE and the ExE-VE on all faces of the embryo, with the ExE-VE being consistently larger. A significant difference was also seen between cells of the lateral Epi-VE and both other Epi-VE regions.

** indicates $p < 0.05$, ** indicates $p < 0.01$, *** indicates $p < 0.0001$*

3.3 Discussion

3.3.1 Cell Movement

The lack of significant difference between cell movement in the Epi-VE and ExE-VE on the anterior side of the embryo was notable, given that previously published data has shown a significant difference between these two regions ($p < 0.005$). However, the trend between the two regions is consistent with the previously published data. The data previously published for cell movement on the Epi-VE shows a movement of approx. 0.37μm/min for the ExE and 0.42μm/min for the Epi-VE. This is in contrast to the results found here, which were approx. 0.34μm/min in the ExE-VE and 0.39μm/min in the Epi-VE. The difference in results could be due to variation between embryos. However, these two sets of results generate an ExE-VE to Epi-VE ratio of 0.88 and 0.87 respectively, indicating that the results are quite comparable.

Additionally, the data published by Trichas et al. was calculated using a Student's *t*-test, which as I detail in Chapter 2, is not the optimal statistical test for this analysis due to the large variation seen between embryos. In order to account for this variation, a nested ANOVA must be performed. If a Student's t-test is performed on the cell migration data in this thesis, the result is strongly significant with a value of $p = 0.0033$.

When compared to data published by Omelchenko et al. for Hex-GFP cells of the AVE only, the anterior Epi-VE rate of 0.39μm/min seen in this work is higher than that reported, at 0.28μm/min. This could be due to the inclusion of other non-Hex GFP cells in the analysis or due to variations among embryos used [59].

Overall, the data for cell movement is highly interesting. There is no significant difference and no visible trend difference in the cell movement between the ExE on all faces of the embryo. The cells of the anterior Epi-VE and Lateral Epi-VE show no difference in movement, indicating that the cells of the lateral Epi-VE are moving as much as those of the anterior. This is highly interesting, indicating a potential role in AVE migration for cells that are not on the anterior face of the embryo. Finally, there is a very large difference ($p < 0.0005$) in the movement of the cells of the anterior (and lateral) Epi-VE and the cells of the posterior Epi-VE. The cells of the posterior Epi-VE are moving even less than those of the global ExE-VE. This indicates that the cells of the posterior are likely mostly stationary during AVE migration.

3.3.2 Cell Displacement

Analysis of cell movement was highly informative. The cells of the revealed ExE-VE showed no significant difference in directed cell migration on any face of the embryo. This, in comparison with the cell movement data, indicates a highly consistent cell movement behaviour spanning the ExE-VE.

The highest rate of directed movement was seen in the anterior Epi-VE, with the cells of the lateral Epi-VE showing directed movement comparable to the ExE-VE around the embryo. This is interesting given that the general movement of the two regions was very similar.

The posterior Epi-VE showed a strikingly low level of movement, strongly significantly lower than even that of the ExE-VE. From this, and the low levels of general cell movement, it is highly likely that these cells are not contributing to VE rearrangement in any migratory manner.

3.3.3 Angle of migration

The directed movement data indicated that there was directed movement in several regions of the embryo, with the most seen in the anterior. However this is only an indication that the cells are moving in a persistent manner in their own particular direction, not that they are collectively migrating in a single direction. In order to examine if the directed migration seen in the embryo was coordinated in specific directions, I compared the angles of migration for each cell movement. As shown in Figure 3.3 only the Anterior Epi-VE and Posterior ExE-VE show any bias towards a particular direction. Both show a bias towards the proximal end of the embryo. Taken with the data regarding cell migration, where the posterior is seen to be involved in a very small amount general and directed migration, it is unlikely that is having a large effect. Contrasting this, the high levels of directed migration shown by the Epi-VE coupled with a bias in direction is a clear indication of directed migration.

While this agrees with fluorescent imaging analysis of the AVE and adds weight to the reliability of this type of analysis, it again raises the question of the behaviour of the lateral cells of the VE, where more significantly more general movement occurs than the global ExE-VE, yet little directional migration occurs, in comparison to the anterior Epi-VE. Further, from the angle of migration it can be seen that any directed migration that does occur does not occur in any directionally specific coordinated manner.

3.3.4 Shape Factor

Previously published data for the anterior of the embryo found the average shape factor in the Epi-VE to be 0.391, and average shape factor to be 0.45 in the ExE-VE. In the data presented in this chapter, a value of 0.41 was found

for the Epi-VE and 0.46 was found for the ExE-VE. These follow the same trend of being higher in the Epi-VE, and the two sets of results generate an ExE-VE to Epi-VE ratio of 0.87 and 0.89 respectively, indicating the difference between regions is reliably conserved between datasets.

The globally lower difference in the shape factor of the cells of the Epi-VE to those of the ExE-VE supports the theory put forward by Trichas et al., that the whole Epi-VE is a permissive environment for migration. There is however a significantly higher shape factor in the lateral Epi-VE when compared to the anterior or posterior Epi-VE. It is unlikely that this is due to the cells of the anterior having an altered shape factor due to active migration alone, as cells of the posterior are not migrating, and these also have a lower shape factor. This could indicate a role for the cells of the lateral Epi-VE to bias intercalation of the anterior cells with other cells on the anterior side, by being less permissive to movement than alternative neighbouring anterior cells.

3.3.5 Neighbour Exchange

Previously published data for the anterior of the embryo found the average rate of neighbour exchange in the Epi-VE to be 0.15, and average neighbour exchange to be approx. 0.02 in the ExE-VE. In the data presented in this chapter, a value of 0.3612 was found for the Epi-VE and 0.1259 was found for the ExE-VE. While these follow the same trend of being higher in the Epi-VE, they are significantly different in magnitude of the difference. This could be generated by the larger number of cells analysed per time point in this study, which averaged approx. 20 per time-point per embryo, while the published data averaged 7. As cells can only be counted for neighbour exchange analysis with other outlined cells, a smaller sample per time-point would amplify the differences between the two regions.

Overall the neighbour exchange analysis was extremely interesting. There was no significant difference in neighbour exchange in the ExE on any face of the embryo. This further confirms the consistent global nature of the ExE-VE around the entire egg cylinder.

While the highest neighbour exchange rate occurred on the anterior face of the embryo, all regions of the Epi-VE showed a significantly higher rate of neighbour exchange over that of the ExE-VE, further supporting the theory that the Epi-VE is more permissive to movement throughout the entire region.

Strikingly, there was no significant difference between the lateral and posterior Epi-VE regions of the embryo, meaning an increase in movement to facilitate neighbour exchange is not the cause of the increased movement seen in the lateral Epi-VE compared to the posterior Epi-VE. It is possible that the movement seen on the lateral Epi-VE is a result of increased pressure placed upon them from the moving AVE cells, which does not require more neighbour exchange than is done in the posterior VE to accommodate, but does result in an increased level of directionless movement.

The particularly high neighbour exchange rate in the anterior VE is also highly notable, given that Trichas et al. have described the majority of rosette formation, a process that involves several neighbour exchange events, occurs infrequently in the cells of the AVE [31]. As cells of the anterior Epi-VE exhibit high levels of neighbour exchange and migration but low levels of rosette formation, this data supports the theory put forward in that paper that rosette formation is not a major feature of AVE migration, but is required within the other cells of the Epi-VE, whose role it is to facilitate the movement of the AVE.

3.3.6 Apical Surface Area

On all faces of the embryo the apical surface of the ExE-VE was shown to be consistently larger. Additionally, cells of the lateral Epi-VE showed a higher apical surface area than the Epi-VE of the anterior and posterior Epi-VE. This mirrored the increased shape factor differences seen in these regions.

Additionally, the cells of the posterior ExE-VE showed the highest apical surface area. These differences in surface area couple with the differences in Shape factor to show that while the ExE might be behaviourally similar in some aspects, in this case, movement, directed migration and neighbour exchange, they can have very different features regarding their cell shape and size. These differences may have an effect on the migratory behaviour of other cells. Similarly, while the lateral and posterior Epi-VE show very similar neighbour exchange patterns, they clearly show very different shape factor and surface area values.

Whether the apical surface area differences are a result of local cell shape differences or differences in cell volume cannot be assessed without investigating the 3D nature of the embryo, which is the topic of Chapter 4.

3.3.7 Assessment of DIC microscopy as a method for quantification of cell behaviour

Differential Interference Contrast microscopy generates an image based on interference to a path of polarized light caused by sub-cellular structures such as the cell membrane. In this manner, an image of the Visceral Endoderm surface can be generated while using minimal laser power, reducing the photo-

toxicity the imaging process. As E5.5 embryos are vulnerable to photo-toxic damage, this is a highly beneficial feature of the technique. Further, DIC can be carried out in combination with fluorescent confocal microscopy with a single laser, further reducing overall photo-damage. This allowed the generation of time-lapse movies of up to 10 hours, while maintaining healthy embryos in culture.

As a result of the difference in cell membrane composition it emerged throughout the imaging process that a severe limitation of using DIC microscopy for VE visualization is the ability to image the Epi-VE. Boundaries between the Epi-VE cells are far more difficult to discern and outline than those of the ExE-VE. As a result generating sufficient embryos to perform analysis was a difficult task.

Another limitation of this technique is the relatively small region of the VE which generates clear images; the regions closest to the objective. This means it is impossible to image cells around the surface of the same embryo. As migration happens over a period of approx. 4 hours and visible cell outlines are often only visible for a fraction of this period, it cannot be ensured that the same period is outlined in different regions. In this study this is overcome by using a large number of tracks from several periods of migration in several embryos. However, this means the ability to compare different points in migration to each other is lost.

Lastly, it is not possible to use an automated program to track cell movement in the time-lapse sequences. This is due to several complications that impede the types of auto-segmentation typically performed in this line of work:

1. Boundary recognition is far easier to accomplish in images where the two objects of interest are not touching. In the case of an epithelial sheet,

the cells are by definition all touching, adding additional complication to the automatic generation of individual cell boundaries.

2. DIC microscopy reveals cell boundaries clearly (from a human perspective) but cells are also full of many organelles that also generate contrast. Image processing algorithms do not deal well with this additional noise source.

Images were therefore exported and cells were traced by hand. This is extremely time-consuming meaning that large numbers of embryos cannot be analysed for cell tracking. It also increases the opportunity for human error.

3.3.8 Future visualization of the Visceral Endoderm

As described above, DIC imaging has both strong benefits and benefits and drawbacks. Ideally, all of the cells of the Visceral Endoderm would be simultaneously imaged with high spatial resolution, in 3D, throughout the entire embryo for the duration of AVE migration and for several hours afterwards to confirm survival. This is not currently feasible for a number of reasons.

Live time-lapse 3D imaging of cells would require a vastly prohibitive level of laser exposure, and the resultant photo-toxicity would not allow embryo survival for the duration of AVE migration. While this can be overcome utilizing a less damaging type of imaging, this is a difficult and arduous process to install and optimize, which is beyond the scope of this D.Phil.

Light sheet microscopy is one such type of minimally photo-toxic microscopy and has been investigated by the Srinivas lab, with promising results [143], [144]. However imaging of the entirety of the embryo with equally clear cell outlines has not been achieved to date. Further to this, integration of the visual data when multiple objectives are used poses a barrier to analysis of the resultant images. Lastly, there is no method for automatically outlining and tracking cells of this dataset and manually performing such a task would be unfeasible.

A further downside to the use of light sheet imaging is that only one embryo can be imaged at any given time, which poses a large problem if mutant lines need to be analysed, given that these mutants need to be removed from agarose and genotyped afterwards, making a large number of successful imaging experiments necessary for any significant number of successful mutant imaging experiments to be confirmed. DIC allows many embryos to be imaged

simultaneously, which can then be removed individually by mouth pipette to labelled tubes for genotyping. This allows the comparison of batch-mates within a mutant line, which is useful for confirming phenotypes.

DIC also provides the advantage that Hex-GFP can be used to track cells of the AVE with no additional laser usage to that of the TPMT. This independence from fluorescence as a cell outline is particularly useful in time-lapse cell imaging, where often a fluorescent line is available, but ultimately is not bright enough under the low-laser levels needed to maintain a healthy embryo for the duration of imaging. An example of this is the LifeAct line, which will be discussed in Chapter 4.

Ultimately DIC allowed analysis of regional differences in cell shape, size and behaviour in a very large number of cells. By a very large amount, the rate-limiting factor on this experiment was the processing and outlining of the cells within the migratory time-lapse videos, as opposed to the dissection, culture and imaging of biological samples. If this problem could be tackled, the use of DIC as an imaging technique at this stage would be far more recompensing.

In addition to increased wild-type tracking, the ability to outline and track cells within an embryo without lengthy manual outlining would allow a far larger number of embryos to be considered in future experiments and would free up the field to use this technique to analyse the effects of various inhibitors on AVE migration, as well as the phenotypes of a wide range of known mutant mice with relative ease. This type of analysis was performed on the anterior side only of *Lefty1*$^{-/-}$ and *ROSA26*^{LynCelsr1} mutant mice but was a similarly lengthy process [140]. If comparison to mutants such as the β-arrestin2 homozygous null mutant described in Chapter 6 were to be carried out, it would likely require improvements in other forms of imaging have emerged if outlining of DIC images cannot be automated.

This poses the question of how such images might be automatically outlined. In recent years the emergence of machine learning techniques as a tool for image analysis, particular those of neural networks, has reopened the possibility that this type of image might be automatically segmented, and this automatically tracked over time.

Machine learning has been gaining prominence in biological studies in recent years, with a focus on classification. Automatic identification of different cell types or cancerous cells within a population is achievable [145]. Indeed, Mango et al demonstrated as far back as 1994, that a neural network system could differentiate normal cells from malignant ones [146].

Using machine learning to teach computers to automatically segment and outline cells of the Visceral Endoderm could be the key to making DIC imaging of AVE migration a more recompensing process. As discussed above, supervised machine learning utilizes a test data set to train the computer to recognize patterns in a data set. Using a very large data set to train the machine learning algorithms would allow for an accurate program that generated correct cell outlines to be achieved. The tracked dataset generated for this thesis and described in this chapter would be ideal for this.

The machine learning in question would not be trained to classify objects, as much of machine learning in biology to date has attempted, but to use its feature recognition capabilities to generate an outline from a raw DIC, indication the locations of the cell outlines. Computational neural networks are field of machine learning that have been utilized heavily in image analysis, including being used to reduce over-segmentation issues seen with typical cell image segmentation by several groups, including Mao et al. [147].[148]

Convolutional neural networks (CNN), in particular are likely to be of use for this task, having emerged as an excellent tool for image recognition and analysis [148], [149]. Excellent correct detection rates were seen (99.77%) using CNNs from the MNIST database of handwritten digits, and a detection rate of 97.6% on was possible when identifying more than 10 items from several thousand images [150].

If this could be optimized for DIC imaging, the outlined image data set traced for the work presented in this chapter could be put to further use to train a neural network to identify cell outlines. This would allow analysis of many mutant lines, as well as the effects of small molecule inhibitors on cell behaviour in the Visceral Endoderm, in a far more time efficient manner.

3.4 Chapter conclusion

In this chapter I have described the generation and analysis of a dataset that describes the migratory behaviour, apical cell shape and apical surface area of Visceral Endoderm cells on all faces of the embryo. Overall, the data from this chapter indicates that the cells of the anterior Epi-VE are the only cells within the VE that are migrating in a directed manner during AVE migration. The high levels of neighbour exchange in the lateral and posterior regions of the Epi-VE indicate that the cells of these regions facilitate the movement of the AVE through rearrangements of their own. These rearrangements are likely a result of the redistribution of the mechanically unfavourable cell configurations undertaken by the AVE as it moves.

4

Quantitative 3D Analysis of the Visceral Endoderm

4.1 Introduction

During the analysis of the DIC data described in Chapter 3, it became apparent that the cells of the Epi-VE were particularly difficult to outline due to an apparently squamous nature. This was initially discovered when different optical sections of the same time-point showed different outlines. This, along with differences in the apical cell Surface Area and shape factor of cells in various regions of the Visceral Endoderm prompted questions on the potential differences between the ExE-VE and Epi-VE in a 3D context. In this chapter I

discuss the generation and examination of high-resolution 3D images of E5.75 embryos. This was carried out in both fixed and live embryos to facilitate the first established comparison of the effect of fixation on the cells of the embryo at this stage.

4.1.1 Variation between Z-levels in Epi-VE imaging

While the DIC method of imaging gives very interesting data regarding cell movement, the data it provides regarding cell shape is restricted to the apical cell surface. This is due to the fact that DIC does not allow for high resolution optical sectioning so it is not possible to obtain good quality images at depth.

The DIC images did however give an indication of a difference in the 3D shape of the cells. In the ExE-VE the 6-8 optical sections of each cell membrane almost always overlapped, while in the Epi-VE it became apparent that often the boundaries of the cell differed in the Z-dimension (Figure 4.1, 4.2). To ensure this did not affect data collection, the same Z-stack was consistently used while outlining. Further, DIC imaging didn't allow the comparison of multiple faces/regions of the same embryo. In DIC, only the small region of the VE closest the objective generates sufficiently clear images to allow analysis.

In order to tackle these issues, the ideal solution would be to perform time-lapse imaging on embryos expressing a fluorescent labelled protein that clearly labels the cell outlines of the VE. This had been tried in the lab previously using two different lines. The CAG-TAG line that had previously been used to great effect at the blastocyst stage was unsuccessful at the E5.5 stage, as the fluorescent membrane protein is very highly expressed in the epiblast and not in the VE, leading to movies of unusable quality for any meaningful interpretation. The LifeAct line was also used to generate time-lapse movies,

but the fluorescent protein was weak and the high laser power required to generate images of required quality for outlining was highly detrimental to the embryo, particularly if more than a small apical surface was imaged.

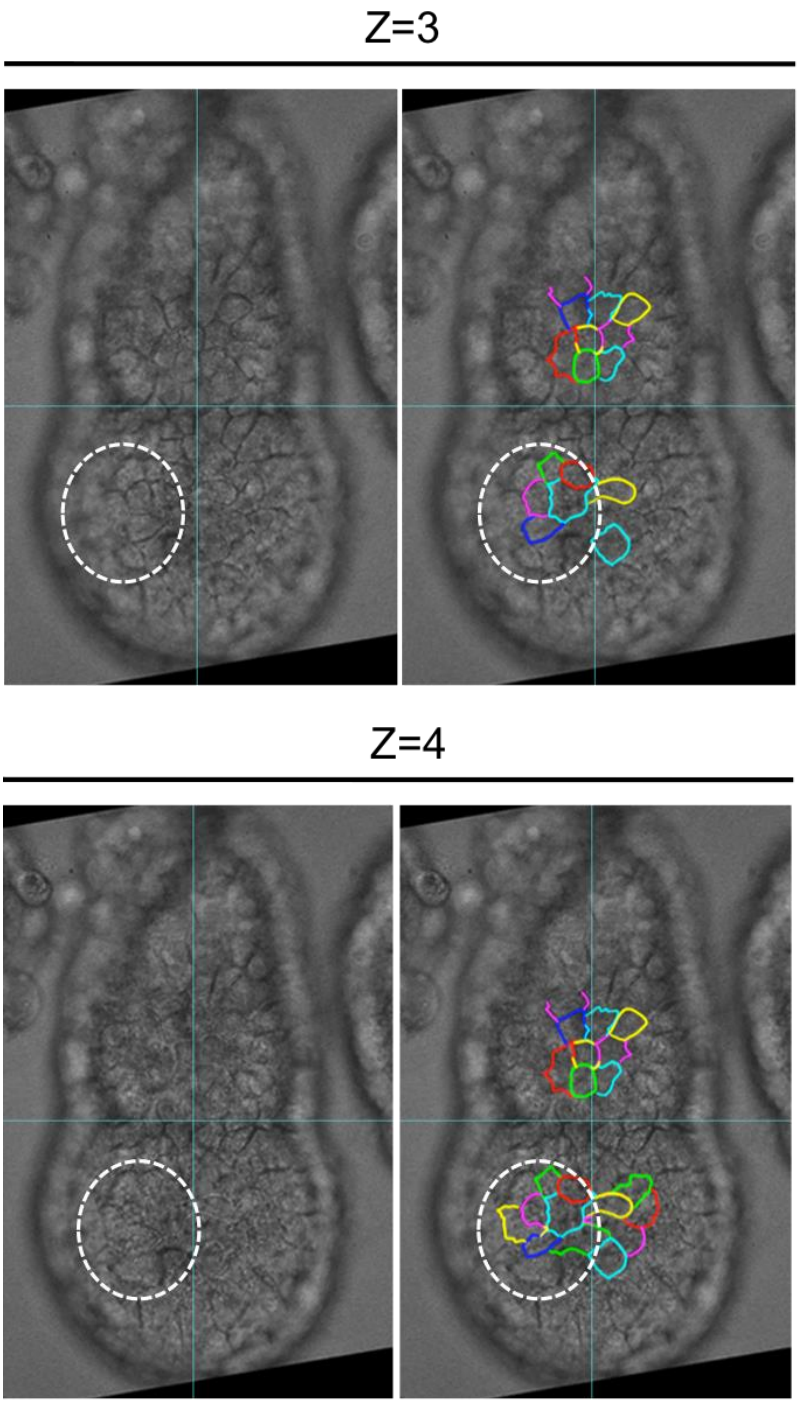
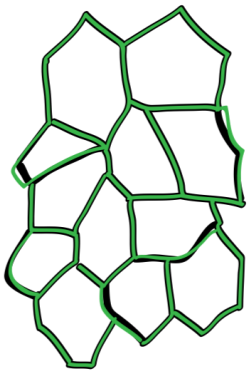


Figure 4.1: Z-level differences in the Epi-VE

Z-stack #3 (top) depicts cells (blue and pink) as neighbours. In Z-stack #4 (bottom) the blue and pink cells can be seen separated by the yellow cell. Z-stacks #3 and #4 are 4.5um apart.

a)



b)

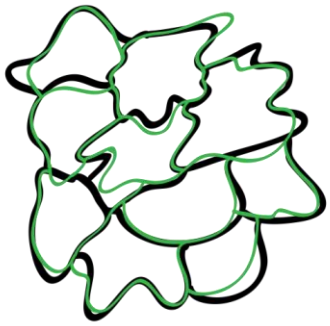


Figure 4.2: Representation of regional Z-level differences in the cells of the Visceral Endoderm

(a) Depicts 2 Z-levels typically seen in the ExE-VE (black and green lines), which overlap almost perfectly

(b) Depicts 2 Z-levels typically seen in the Epi-VE (black and green lines), which do not overlap in many instances.

4.1.2 Differences in 3D within regions of the Visceral Endoderm

The overlapping Z-stacks seen in the cells of the VE indicated a columnar shape within these cells. Contrasting this, the variance seen within the Epi-VE implies a more squamous 3D shape in this region. In addition to this, the DIC analysis performed in Chapter 3 indicated regional differences in the apical cell shape, with cells of the ExE-VE having a much higher shape factor value, than those of the Epi-VE, as well as regional differences in shape factor within the VE itself. Further to this, apical cell surface was much larger in the ExE-region and showed differences across anterior, posterior and lateral faces of the embryo in both the ExE-VE and Epi-VE regions.

To examine the extent of the 3D differences in regions of the Visceral Endoderm, I utilized LifeAct mice to generate high-resolution 3D images of live E5.75 embryos that were undergoing AVE migration. I then manually outlined these in 3D at a very high spatial resolution, before quantifying multiple 3D cell parameters. Further, this analysis provided an opportunity to examine the effect of fixation on the cells of the Visceral Endoderm. As such, embryos of LifeAct mice were compared to fixed wild-type cells stained with phalloidin.

4.1.3 The LifeAct peptide

The LifeAct peptide consists of the 17 N-terminal amino acids from Abp140, an actin binding protein present in Saccharomyces cerevisiae [136]. This was fused to EGFP, allowing actin mechanics to be visualised in live cells. A number of processes, including interactions between vesicles and the cell cortex, adherens junctions dynamics and cell motility, were initially examined using this line [151]–[154].

In this project I utilized a mouse line that ubiquitously expresses the LifeAct-EGFP fusion protein for a comparative characterisation of regional VE cellular morphology in E5.75 embryos.

4.2 Results

4.2.1 Establishing viability of the LifeAct mouse line for 3D live imaging

I imaged live E5.75 LifeAct embryos by point scanning confocal microscopy and tested the brightness that could be achieved at a single time-point. I discovered that a high-resolution 3D image of the embryo could be made, though the embryo would begin to deteriorate after repeated exposure to such high intensity excitation illumination. This gave high-resolution 3D data of a live embryo at a single time-point which to date had not been generated and could be highly informative.

It emerged however that the side of the embryo furthest from the microscope objective was dimmer than that closest, which is a common occurrence in confocal imaging. Additionally, LifeAct embryos do not have an AVE marker and were stage matched visually using the distinctive cellular morphology of the AVE. As a result of these two factors, it was impossible to guarantee stage matching of embryos in which the posterior of embryo was facing the objective. Therefore, only anterior and lateral cells were considered in this study.

4.2.2 Manual outlining of imaged embryos

Visceral Endoderm cells from fixed and living samples were manually segmented in Imaris imaging software. Cells were then rendered in 3D (Figure 4.3). Numbers of cells outlined in each region can be found in Table 4.1.

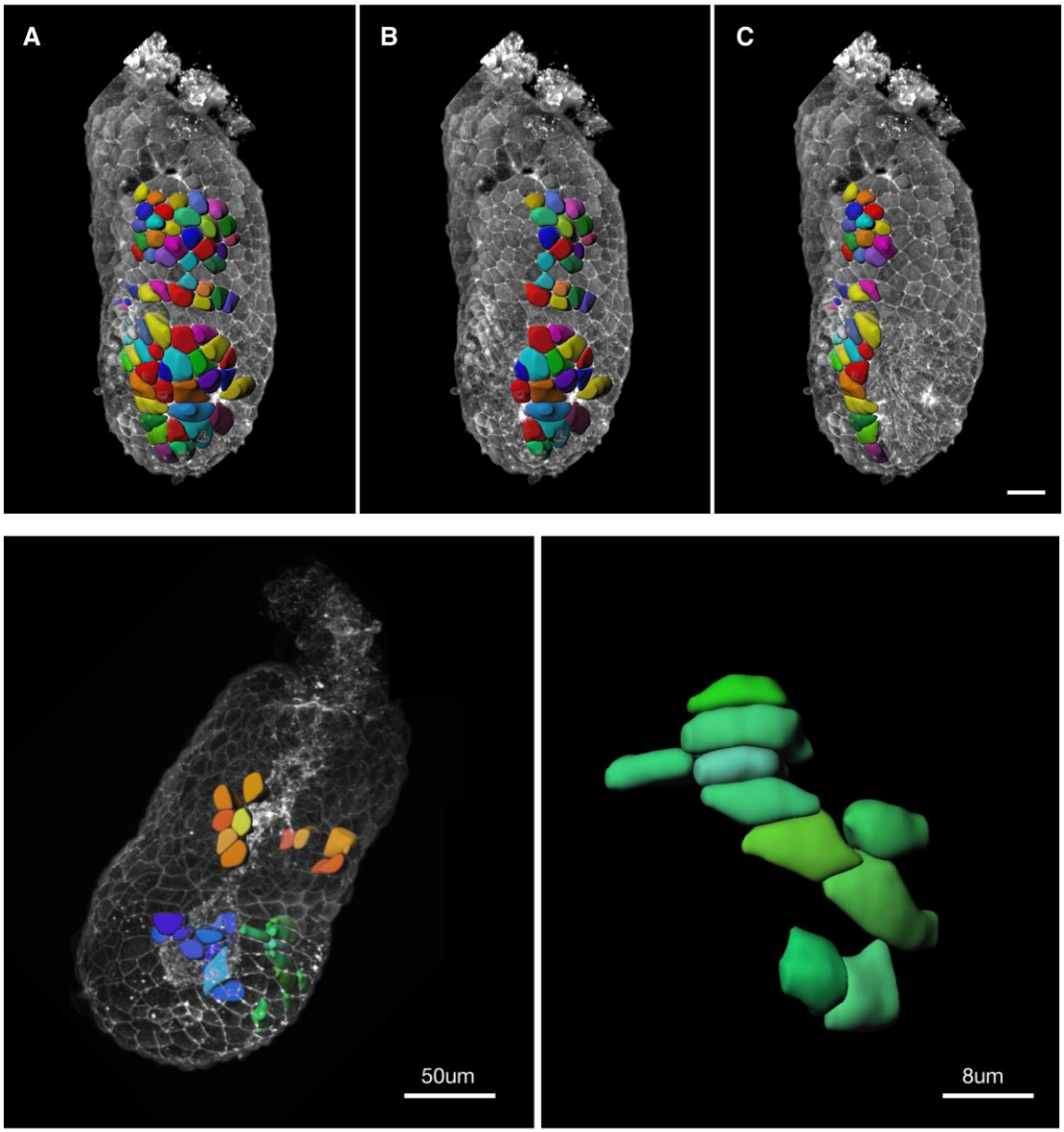


Figure 4.3: 3D cells outlined in Imaris

(a-c) Depict live LifeAct embryos, scale bar 25µm. (d-e) Depict cells outlined from fixed phalloidin-stained embryos. [L SEP]

(Legend continued overleaf.)

Figure 4.3: 3D cells outlined in Imaris

(a) Cells rendered in 3D in both lateral and anterior regions.
(b) Lateral cells only.
(c) Anterior cells displayed only.
(d) Selected cells from regions outlined in phalloidin-stained embryos, scale bar = 50μm
(e) Sample of AVE cells from outlined embryos showing an irregular and squamous nature, scale bar = 8μm

Table 4.1: 3D Cells outlined in Imaris

Data pertaining to the analysis of fixation on cells of the Visceral Endoderm and the analysis of the differences in the 3D cell shape of various Visceral Endoderm regions. 'Fix/Live' refers to the fixation state of the embryo in question. Face refers to the side of the embryo the outlined cell was contained in. Region refers to the Visceral Endoderm region (ExE-VE vs. Epi-VE) the outlined cell was contained in. 'Number' refers to the number of cells counted in each category.

Fix/Live	Face	Region	Number
Fixed	Anterior	ExE-VE	34
Fixed	Anterior	Epi-VE	39
Fixed	Lateral	ExE-VE	44
Fixed	Lateral	Epi-VE	19
Live	Anterior	ExE-VE	85
Live	Anterior	Epi-VE	99
Live	Anterior	Mid-VE	28
Live	Lateral	ExE-VE	35
Live	Lateral	Epi-VE	47
Live	Lateral	Mid-VE	8

4.2.3 Regional Comparisons in Live Visceral Endoderm cells

Outlined cells from live samples were assessed for regional differences in cell appearance, Surface Area, Volume, cell shape (Sphericity) and Surface Area to Volume ratio (SA:V).
While Surface Area and Volume give information on the comparative size of cells in each region, Sphericity and Surface Area:Volume (SA:V) ratio give a readout of cell shape and behaviour in three dimensions.

It was noted upon outlining that cells of the upper Epi-VE were more squamous that other cells of the Epi-VE. To test if this was a significant difference, these cells were assigned a new regional label of 'Mid-VE'. These cells constitute Epi-VE cells that are at the boundary of the ExE and Epiblast, but remain on the side of the Epi-VE

4.2.3.1 Cells outlined in 3D show visual differences in size, 3D shape and cell height

Cells outlined from a live LifeAct embryo can be seen in Figure 4.4. It is clear from these images that the cells of the Epi-VE are far more squamous in nature. The cells of the ExE-VE are far more regular in shape, exhibiting a columnar appearance. The cells of the ExE-VE are also far more consistent in shape between cells, while those of the Epi-VE show a wide range of shapes.

The height (apical-basal) of the cells cannot be determined from the 3D outlining process, so outlined embryos were assessed visually. In all live cases, cells of the ExE-VE appear taller than those of the Epi-VE.

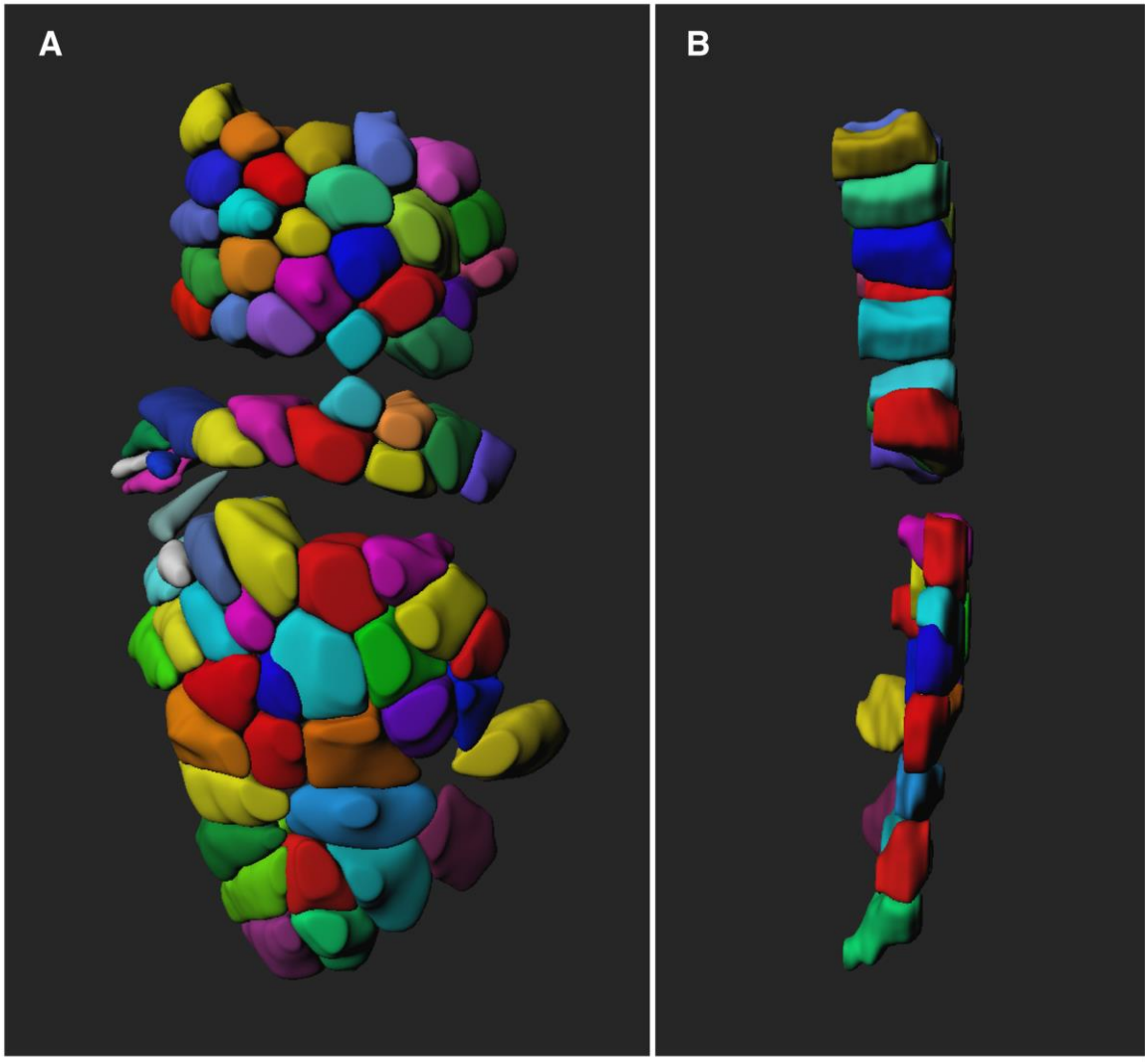


Figure 4.4: Cells outlined in 3D show differences in 3D cell shape and cell height

(a) Front view of 3D rendered cells in an E5.75 embryo. ExE-VE (top), Mid-VE (middle) and Epi-VE (bottom) regions are shown with gaps between them.

(b) Side view of selected cells from (a). Here, only lateral cells are shown due to the curvature of the embryo blocking this view when all are visible.

4.2.3.2 Cells outlined in 3D show regional differences in cell Surface Area

Cell Surface Area data was generated from the 3D outlined cells by Imaris software (Figure 4.5a). Statistically significant differences were seen in cell Surface Area between the Epi-VE and ExE-VE on the anterior face of the embryo ($p < 0.001$). However, no significant difference was seen between the Epi-VE and ExE-VE on the lateral face of the embryo.

Cells of the anterior Epi-VE showed significantly smaller Surface Area than cells of the lateral Epi-VE ($p < 0.001$).

Cells of the Epi-VE and Mid-VE did not show any differences in cell Surface Area on either the anterior or lateral faces of the embryo.

4.2.3.3 Cells outlined in 3D show regional differences in cell Volume

Cell Volume data was also generated from the 3D outlined cells by Imaris software. This data can be seen in Figure 4.5b. In the anterior of the embryo, similar to the cell Surface Area, a large significant difference was seen between cells of the anterior Epi-VE and ExE-VE ($p < 0.001$). In contrast to the cell Surface Area, differences were seen on the lateral face of the embryo between lateral Epi-VE and ExE-VE cell Volume ($p < 0.05$). This indicated a change in the 3D shape of the cells between the anterior and lateral faces of the embryo. Where these changes are require using additional parameters to investigate regional cell shape.

Cells of the Epi-VE and Mid-VE did not show any differences in cell Surface Area on either the anterior face of the embryo, but did show a significant difference on the lateral side of the embryo.

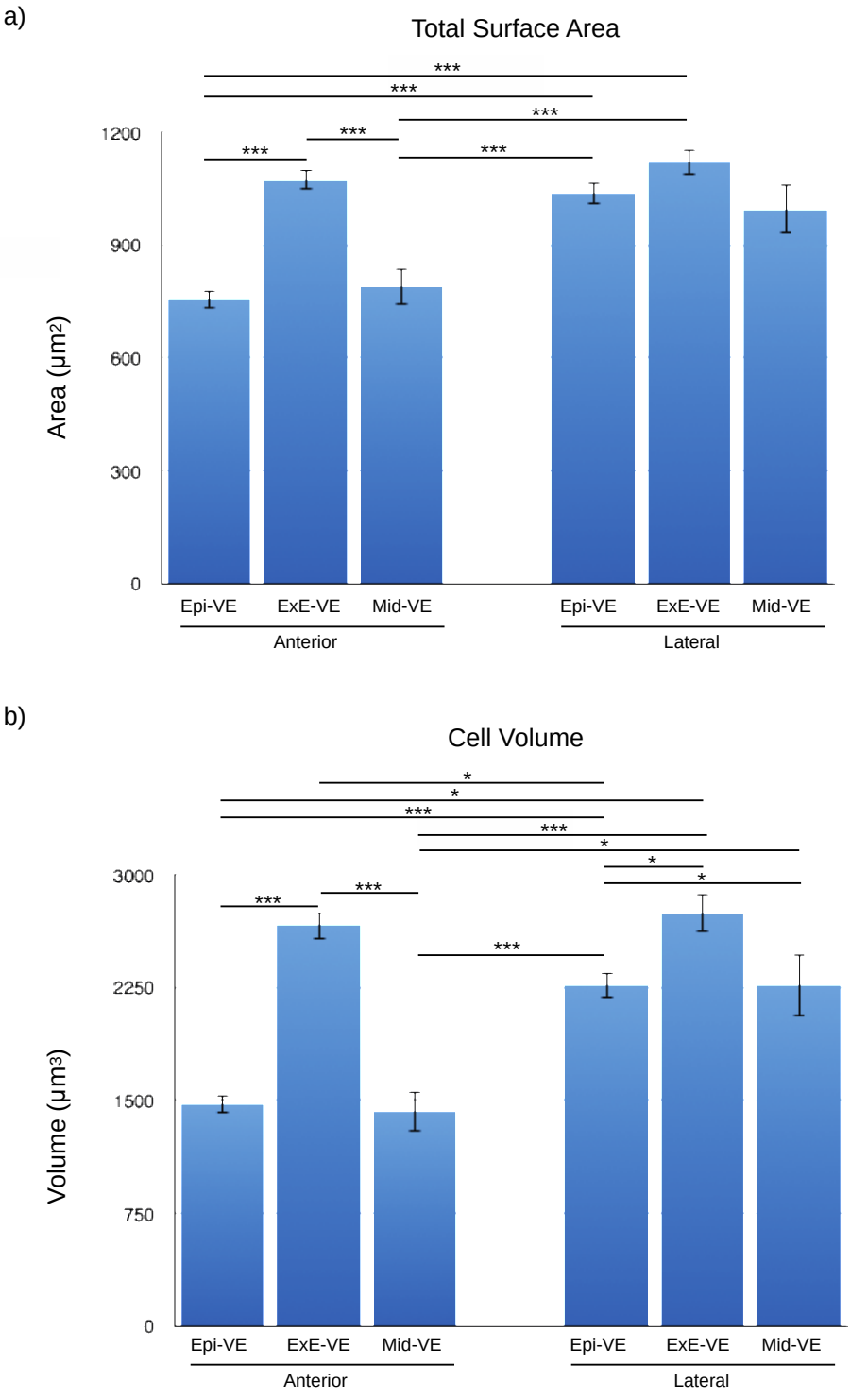


Figure 4.5: Regional differences in total cell Surface Area and Volume in Visceral Endoderm cells *(Legend Overleaf)*

Figure 4.5: Regional differences in total cell Surface Area and Volume in Visceral Endoderm cells

(a) Statistical analysis of total cell Surface Area of live Visceral Endoderm cells in various regions of the tissue. A nested ANOVA was used to compare samples to account for the variances between individual embryos.

A statistically significant difference was anterior and lateral Epi-VE cells. Additionally, a statistically significant difference was seen between Epi-VE and ExE-VE cells on the anterior side of the embryo. This was not seen on the lateral face of the embryo.

(b) Statistical analysis of the cell Volume of live Visceral Endoderm cells in various regions of the tissue. A nested ANOVA was used to compare samples to account for the variances between individual embryos.

A statistically significant difference was seen in anterior and lateral Epi-VE cell Volume. The statistically significant difference seen between Epi-VE and ExE-VE cells on the anterior side of the embryo in cell Surface Area was recapitulated in the Volume data, however a difference was seen in lateral cells between the Epi-VE and ExE-VE which was not seen in cell Surface Area, indicating differences in cell shape between regions.

* indicates ($p < 0.05$), ** indicates ($p < 0.01$), *** indicates ($p < 0.001$)

4.2.3.4 Cells outlined in 3D show regional differences in Surface Area to Volume ratio.

Surface Area to Volume ratio (SA:V) is the amount of Surface Area per unit Volume of an object. For a given Volume, the object with the smallest Surface Area is the sphere. Cells with a high Surface Area to Volume ratio are likely to be more squamous and irregularly shaped.

There were differences between all regions of the anterior face of the embryo when compared for SA:V. Epi-VE, Mid-VE and ExE-VE showed significance of $p < 0.001$ in all combinations. Strikingly, no significant difference was seen on the lateral side, when regions were compared within this face of the embryo.

A strongly significant difference was also seen between all cells of the Epi-VE (classed as Epi-VE and Mid-VE) on the anterior face and cells of the Epi-VE of the lateral side. This indicates that there are differences in how squamous the cells are within the global Epi-VE. No difference was seen between anterior and lateral ExE-VE regions (Figure 4.6).

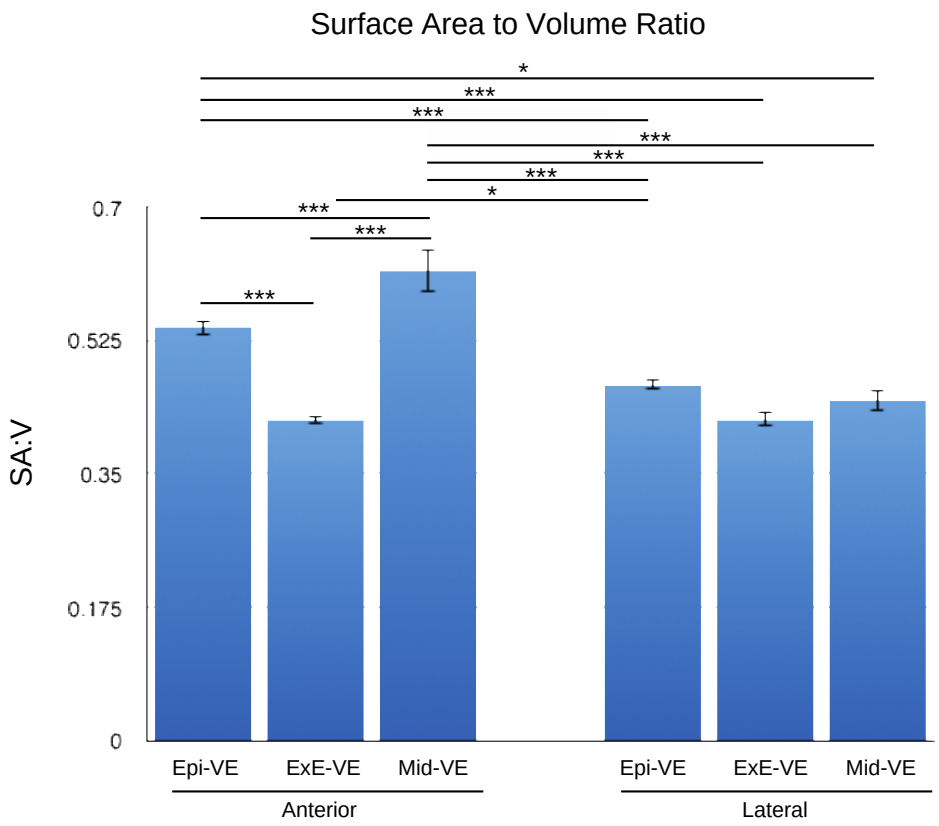


Figure 4.6: Regional differences in Surface Area to Volume ratio (SA:V) in Visceral Endoderm cells

Statistical analysis of Surface Area to Volume ratio (SA:V) of live Visceral Endoderm cells in various regions of the tissue. A nested ANOVA was used to compare samples to account for the variances between individual embryos.

Statistically significant differences were seen between all combinations of Epi-VE, Mid-VE and ExE-VE cells on the anterior side of the embryo. This was not seen on the lateral face of the embryo.

A statistically significant difference in Surface Area to Volume ratio was seen between anterior and lateral Epi-VE cells.

* indicates ($p < 0.05$), ** indicates ($p < 0.01$), *** indicates ($p < 0.001$)

4.2.3.5 Cells outlined in 3D show regional differences in Sphericity

Sphericity is the ratio of the Surface Area of the particle in question to that of a sphere with the same Volume. Like Surface Area to Volume ratio, it describes the 3D shape of the cell. Cells with a lower Sphericity value are more irregular in nature. Comparison of regional differences in Sphericity in live embryos can be found in Figure 4.7.

Like the analysis for SA:V, there were differences between all regions of the anterior face of the embryo when compared for Sphericity. Epi-VE, Mid-VE and ExE-VE showed significance of $p < 0.001$ in all combinations.

Overall trends in Sphericity mirror that of Surface Area to Volume, as expected. However, Sphericity appears more sensitive to cell shape changes in the lateral Epi-VE, as differences not seen between the ExE-VE and Epi-VE using a SA:V comparison can be seen in Sphericity analysis.

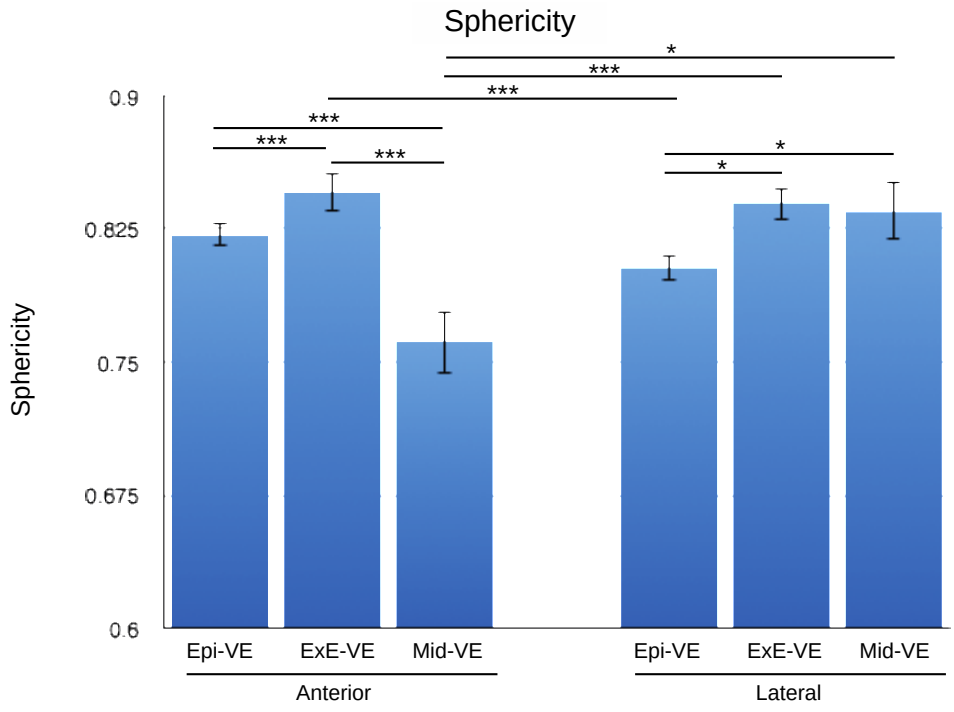


Figure 4.7: Regional differences in Sphericity in Visceral Endoderm cells

Statistical analysis of Sphericity of live Visceral Endoderm cells in various regions of the tissue. A nested ANOVA was used to compare samples to account for the variances between individual embryos.

Statistically significant differences were seen between all combinations of Epi-VE, Mid-VE and ExE-VE cells on the anterior side of the embryo. This was seen between Epi-VE and ExE-regions on the lateral face of the embryo, in contrast to the values for Surface Area to Volume ratio.

A statistically significant difference in Surface Area to Volume ratio was seen between anterior and lateral Epi-VE cells.

* indicates ($p < 0.05$), ** indicates ($p < 0.01$), *** indicates ($p < 0.001$)

4.2.4. Investigation of the effect of fixation on cell shape within the Visceral Endoderm

A large amount of research on the cells of the AVE is conducted on fixed samples. In order to investigate the effects of fixation on E5.75 embryos I compared cells from fixed and live embryos using the parameters described in for live comparison in Section 4.2.3. Outlined cells from fixed and live samples were assessed for differences in Surface Area, Volume, cell shape (Sphericity) and Surface Area to Volume ratio (SA:V). All fixed vs. live results can be found in Table 4.2.

4.2.4.1 Fixed and live Visceral Endoderm cells show differences in cell Surface Area

When Surface Area was compared between fixed and live cells, using a nested ANOVA an overall significant effect was seen between all pooled groups ($p < 0.001$). In subsequent post-hoc analysis, the individual differences between the groups were seen. There was no significant difference in the cells of the Epi-VE and ExE-VE on the anterior of the embryo between fixed and live cells, but there was a significant difference between fixed and live Surface Area in the cells of the lateral Epi-VE and ExE-VE (both $p < 0.001$), where cell Surface Area was dramatically reduced (Figure 4.8a). Additionally, interesting significant differences between regions seen in live embryos, such as the difference between Epi-VE on the anterior and lateral faces of the Visceral Endoderm are lost in the fixed samples.

4.2.4.2 Fixed and live Visceral Endoderm cells show differences in cell Volume

Investigation of cell Volume revealed the same results as that of cell Surface Area, with an overall significant difference between the cells that has been fixed and those that were live ($p < 0.001$). This was seen to be a result of Volume changes in fixed and live cells of the lateral Epi-VE and ExE-VE (both $p < 0.001$), which showed a decrease in size upon fixation. Additionally, a reduction in the size of cells in the anterior ExE-VE was seen, though this was not statistically significant.

4.2.4.3 Fixed and live Visceral Endoderm cells show differences in Surface Area to Volume ratio.

Significant differences in SA:V were seen in anterior ExE-VE ($p < 0.05$) and lateral Epi-VE ($p < 0.001$). This indicates changes in cell shape upon fixation. It must also be noted that different regions appear changed in SA:V comparisons to that of cell Surface Area and cell Volume. This indicates that not only are changes present, but fixation affects different regions differently. A factorial ANOVA to test whether there is an interaction between the effects of fixation and the region of the embryo is found in confirmed that this is indeed the case ($p < 0.001$) (Figure 4.9).

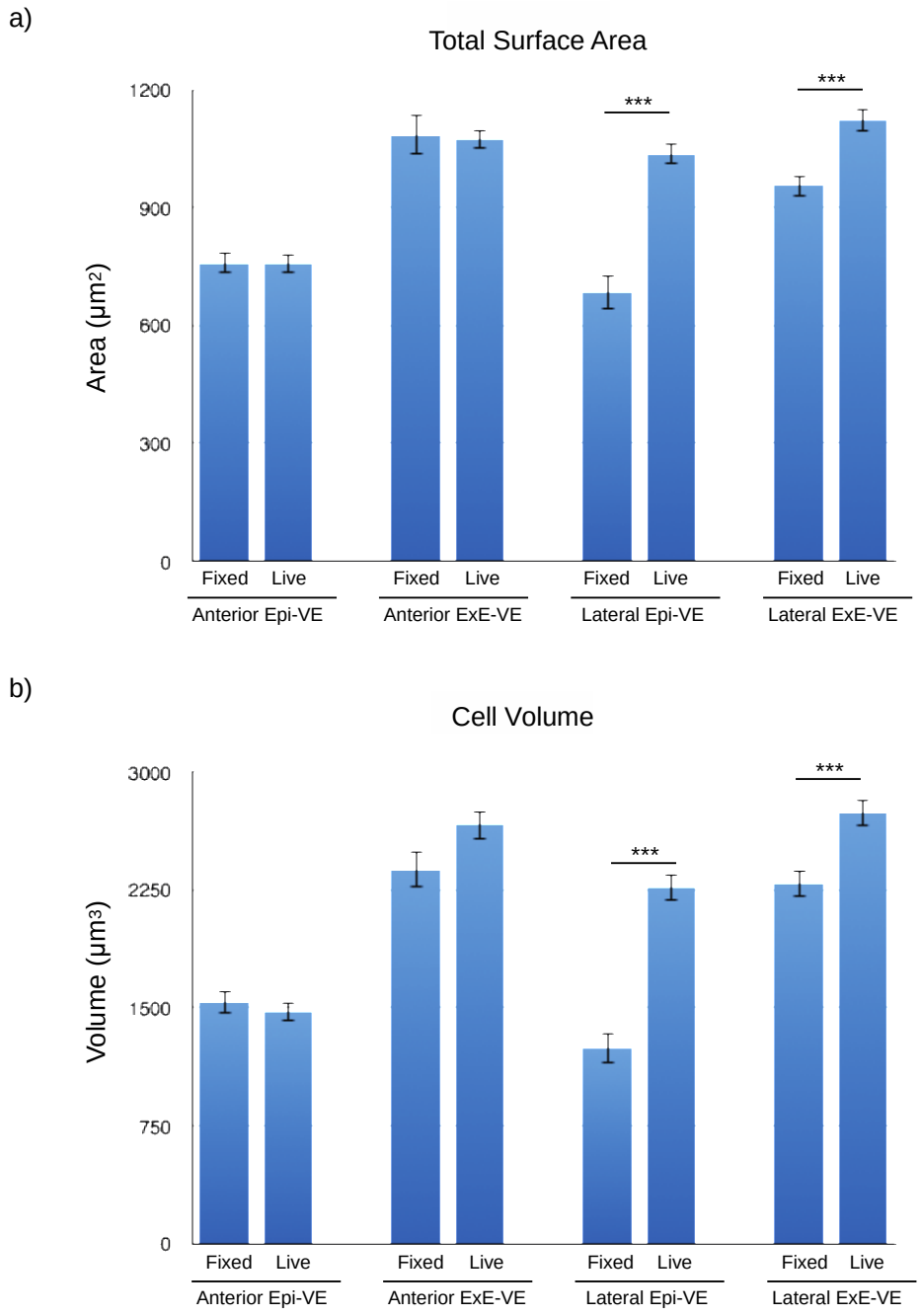


Figure 4.8: Fixed and live Visceral Endoderm cells show differences in cell Surface Area and Volume (Legend overleaf)

Figure 4.8: Fixed and live Visceral Endoderm cells show differences in cell Surface Area and Volume

(a) Statistical analysis of cell Surface Area in fixed and live Visceral Endoderm cells. A nested ANOVA was used to compare samples to account for the variances between individual embryos.

A statistically significant difference was between fixed and lived cells in both the Epi-VE and ExE-VE of the lateral face of the embryo.

(b) Statistical analysis of cell Volume in fixed and live Visceral Endoderm cells. A nested ANOVA was used to compare samples to account for the variances between individual embryos.

A statistically significant difference was between fixed and lived cells in both the Epi-VE and ExE-VE of the lateral face of the embryo.

Additionally, a change in the Volume of anterior ExE-VE cells can be seen, though this is not statistically significant.

*** indicates ($p < 0.001$)

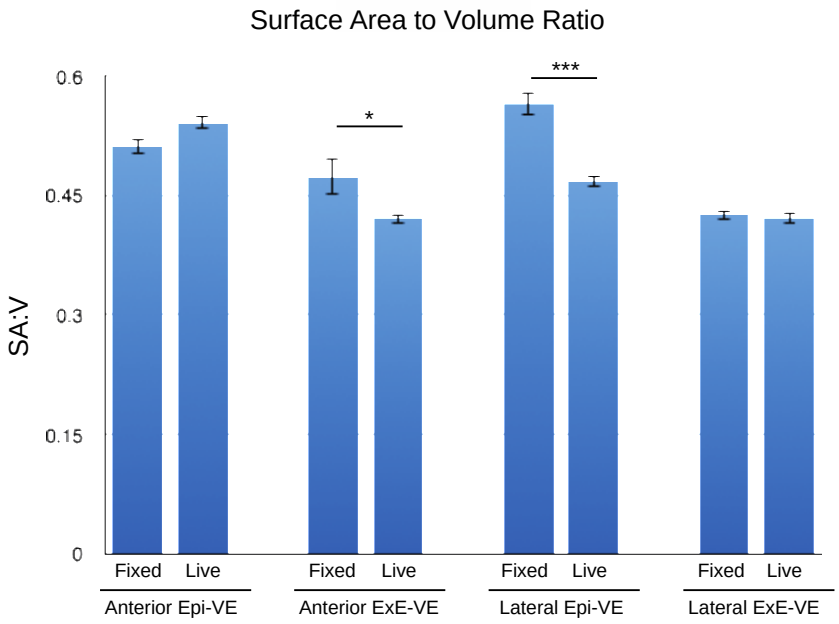


Figure 4.8: Fixed and live Visceral Endoderm cells show differences in Surface Area to Volume ratio (*SA:V)***

Statistical analysis of Surface Area to Volume ratio in fixed and live Visceral Endoderm cells. A nested ANOVA was used to compare samples to account for the variances between individual embryos.

A statistically significant difference was between fixed and lived cells in the ExE-VE of the anterior face of the embryo. Additionally, a statistically significant in SA:V was seen in the Volume of lateral Epi-VE cells can be seen.

* indicates ($p < 0.05$), *** indicates ($p < 0.001$)

4.2.4.4 Fixed and live Visceral Endoderm cells show differences in Sphericity

Fixation showed a significant effect on the Lateral ExE-VE. As with other parameters, significant effects seen in live, such as the change in Sphericity shown between the anterior Epi-VE and lateral ExE-VE are lost in fixed samples. Additionally, using a factorial ANOVA, fixation was again shown to impact different regions of the embryo differently ($p < 0.001$). Results for the effects of fixation on Sphericity can be found in Figure 4.9.

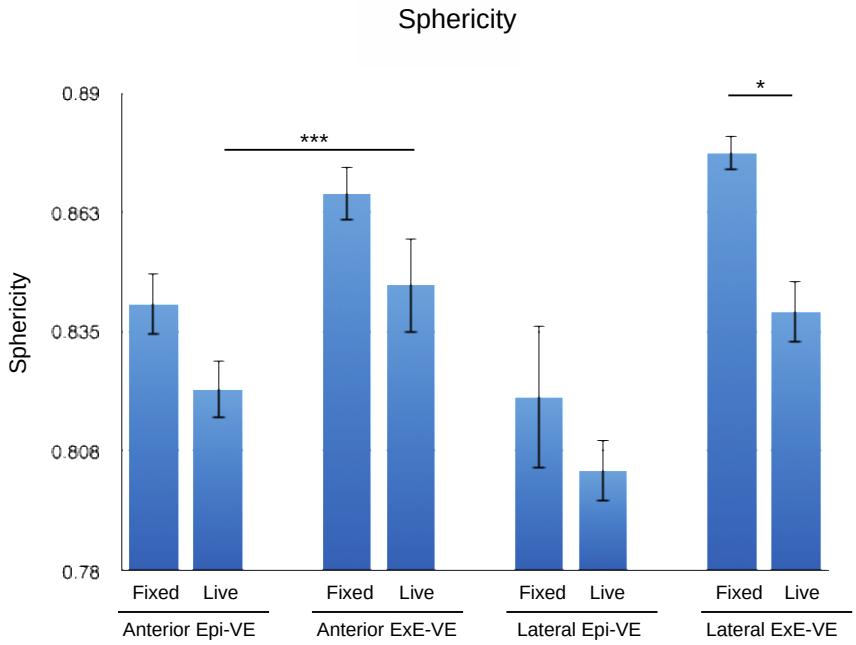


Figure 4.9: **Fixed and live Visceral Endoderm cells show differences in Sphericity.**

Statistical analysis of Sphericity in fixed and live Visceral Endoderm cells. A nested ANOVA was used to compare samples to account for the variances between individual embryos.

A statistically significant difference was between fixed and lived cells in the ExE-VE of the lateral face of the embryo.

* indicates ($p < 0.05$), *** indicates ($p < 0.001$)

Table 4.2: Comparison of Fixed and live embryos across multiple parameters

Results from all comparisons of fixed vs. live regional data are shown. 'F/L' column describes whether the cells averaged for the result were from fixed or live samples. 'Face' indicates the side of the embryos where the cells were located. 'Region' indicates whether the cells were in the ExE-VE or Epi-VE. 'Area' indicates the average cell Surface Area of cells in each category, while 'Vol' corresponds to the average Volume. 'SA:V' describes the Surface Area to Volume ratio. The 'Sph' column gives the average Sphericity of each category.

F/L	Face	Region	Area	Vol	SA:V	Sph
Fixed	Ant	Epi-VE	759.31	1531.01	0.51	0.84
Live	Ant	Epi-VE	756.27	1470.20	0.54	0.82
Fixed	Ant	ExE-VE	1084.90	2379.63	0.47	0.87
Live	Ant	ExE-VE	1072.93	2664.95	0.42	0.85
Fixed	Lat	Epi-VE	683.92	1240.33	0.57	0.82
Live	Lat	Epi-VE	1036.62	2268.29	0.47	0.80
Fixed	Lat	ExE-VE	954.44	2289.72	0.43	0.88
Live	Lat	ExE-VE	1122.33	2743.79	0.42	0.84

4.3 Discussion

4.3.1 Regional Comparisons in Live Visceral Endoderm cells

Large differences were seen between regions in multiple parameters when cells were examined in 3D. Below, I discuss these differences and where relevant, compare the results to those seen from DIC imaging described in Chapter 3 and relevant other work.

4.3.1.1 Cells outlined in 3D show visual differences in 3D shape and cell height

While it can be seen in E5.75 immunohistochemistry that the cells of the ExE-VE are larger than those of the Epi-VE, this has not yet been fully confirmed in live embryos and in 3D. Data describing the less rigidly packed nature of the Epi-VE has to date only come from apically restricted DIC data[5], [140]. It is clear however from this data the cells of the Epi-VE are far more squamous in nature, confirming the cause of the variation within Z-stacks during DIC imaging. The cells of the ExE-VE are far more regular in shape, exhibiting a columnar appearance, and are also far more consistent in shape between cells, while those of the Epi-VE show a wide range of shapes. This agrees with the 2D data previously published for these regions.

The apical-basal height of the cells cannot be determined from the 3D outlining process, as the cells are curved around the embryo. This prevents the Imaris software from determining the 'bottom' of a cell. When assessed visually however, all cells of the ExE-VE were larger than any seen in any region of the Epi-VE. It is possible that the difference in cell height limits contacts between the cells of the Epi-VE, allowing easier rearrangement of cell boundaries

during the migration process.

4.3.1.2 Cells outlined in 3D show regional differences in cell Surface Area

A large difference was seen between the total cell Surface Area of the Epi-VE and ExE-VE on the anterior face of the embryo. However, no significant difference was seen between the Epi-VE and ExE-VE on the lateral face of the embryo. This agrees with the apical Surface Area data seen in Chapter 3, for the anterior face, where a large significant difference was also seen, but not for the lateral side. This indicates that the proportion of total Surface Area presented apically differs between regions on the apical and lateral regions, which would mean that the cells are a different shape in these areas.

4.3.1.3 Cells of the lateral Epi-VE are larger than those of the anterior Epi-VE

While there is no significant difference between cells of the anterior ExE-VE and lateral ExE-VE, there is a very large difference between the anterior and lateral Epi-VE. Cells of the lateral Epi-VE are much larger than their anterior counterparts. This is in agreement with the data seen in Chapter 3, which showed that cells of the lateral Epi-VE had a much larger apical Surface Area than cells of the anterior Epi-VE. This has large implications, given that the corresponding apical Surface Area data for the posterior cells indicated that cells of the posterior Epi-VE were the same size as the anterior Epi-VE.

Why only the cells of the lateral Epi-VE are comparable in size to the global ExE-VE is a difficult question to answer. The larger Surface Area of the cells could increase cell-cell contact, making the overall cell adhesiveness of cells on the lateral side of the embryo different to that of the cells of the anterior face,

biasing intercalation of anterior Epi-VE cells with each other, rather than with those of the lateral Epi-VE. Cellular sorting between two populations of cells which possess different levels adhesiveness has been conclusively shown with the tissue of lower surface tension enveloping the tissue of higher surface tension, and this phenomenon has been described using the Differential Adhesion Hypothesis [155]. This states that cells will rearrange themselves to maximize contact with cells of similar adhesiveness to generate the most energetically stable configuration of the mixed cell population.

Whether the cells of the anterior Epi-VE shrink relative to their size prior to migration of AVE cells or cells of the lateral Epi-VE become larger would be relatively easy to assess, using 3D outlining of Visceral Endoderm cells at E5.5, which had not begun to migrate. If a regional difference in cell size on one face of the embryo was present it is possible that this could bias the direction of movement and thus direct the asymmetric migration of the AVE cells.

4.3.1.4 Cells outlined in 3D show regional differences in cell Volume, which do not correspond directly to differences in cell Surface Area

While the trends differences in cell Surface Area on the anterior face are recapitulated in the cell Volume data, there is a marked difference in the proportional difference in area and cell Volume between the Epi-VE and ExE-VE. Additionally on the lateral face of the embryo, the difference in cell Volume between the Epi-VE and ExE regions became significant. This indicated a change in the 3D shape of the cells between the anterior and lateral faces of the embryo, but could not indicate what this change might be, or how it might affect cell behaviour. As such, cell shape parameters were applied to the 3D data to further investigate changes in regional cell shape.

Cells of the Mid-VE on the anterior and lateral faces of the embryo did not show any differences cell Surface Area when compared to other cells of the Epi-VE. A small significant difference was seen in the cell Volume of lateral Mid-VE cells, but from cell surface and Volume data alone, no conclusions about these cells could be made.

4.3.1.5 Cells outlined in 3D show regional differences in Surface Area to Volume ratio.

Surface Area to Volume ratio (SA:V), the amount of Surface Area per unit Volume of an object, showed significant differences within regions on the anterior face of the embryo, but not on the lateral face of the embryo. This was highly interesting.

All regions of the lateral Visceral Endoderm were comparable in SA:V to cells of the anterior ExE-VE, which indicates that these cells are comparably shaped and far less irregular than that seen in the anterior Epi-VE. This does not agree with the data seen in Chapter 3, where the shape factor analysis on the apical surface of the embryo indicated that there was a strong difference between the lateral Epi-VE and lateral ExE-VE. This difference could be because only the apical surface of the cells were considered in DIC analysis, or could be because SA:V is not sufficiently sensitive to cell shape changes to detect any within the lateral face of the embryo at this stage. The latter is likely the case, as is seen in the following section, where regional differences in the lateral VE were detected in Sphericity analysis.

4.3.1.6 Cells outlined in 3D show regional differences in Sphericity

Sphericity, the ratio of the Surface Area of an object to that of a sphere with the same Volume, measures how irregular a 3D shape is. Theoretically trends

in Sphericity and Surface Area to Volume should have an inverse relationship, which is reflected in the results seen. However, they do not measure exactly the same features of cell shape, and so can give different insight into cell behaviour.

Regional examination of Sphericity within the Visceral Endoderm revealed that the anterior differences seen using Surface Area to Volume ratio were recapitulated, but additional differences could be seen between Epi-VE and ExE-VE cells on the lateral face of the embryo. Here, the Epi-VE was seen to be more irregularly shaped that that of the ExE-VE, which corresponds to the data seen in Chapter 3, where a similar effect was seen between regions in Shape factor.

Collectively taking the Surface Area and Sphericity results describing 3D cell shape in the embryo, it is clear that the cells of the anterior Epi-VE are highly irregularly shaped. The majority of this structural irregularity is likely due to the migratory nature of these cells. However, cells of the lateral VE can be seen to be significantly more irregular in shape in the Sphericity analysis performed in this chapter, and the shape factor analysis performed in Chapter 3. It is likely that the more irregular nature of the lateral Epi-VE cells allows the cells of the Anterior Epi-VE to migrate in a more efficient manner. This supports the theory that while all the cells of the Epi-VE are more permissive to movement than the cells of the ExE-VE, only the cells of the anterior are actively migrating.

Additionally, an interesting result can be seen when the cells of the Mid-VE are compared to those of the rest of the Epi-VE. These cells comprise those at the closest point to the ExE-VE boundary, which could be visually seen to have a cell shape even more irregular than other cells of the Epi-VE. This was

confirmed in both SA:V and Sphericity analysis. This is likely as a result of being compressed against the more robust cells of the ExE-VE while surrounding cells of the anterior Epi-VE continue to migrate anteriorly. This supports the previously published cell behavioural data that indicated that the ExE-VE was acting as a physical barrier to AVE migration.

4.3.2 Investigation of the effects of fixation on the cells of the Visceral Endoderm

In all parameters analysed, fixation had an effect on cells of the Visceral Endoderm. From both the cell Surface Area and Volume comparisons, it can be seen that cell size is affected by fixation, and that this affects certain regions more than others, in particular, the larger cells of the lateral face of the embryo seen in live analysis are drastically reduced in size. Additionally, both Sphericity and Surface Area to Volume ratio are affected, indicating that cell shape is altered upon fixation.

As a result of this analysis, it can be determined that analysis of cell shape from fixed embryos cannot be performed reliably. This is likely the case for many developmental processes, and it should be noted that any analysis of cell shape behaviour during migration must be performed live to ensure results which reflect the true parameters of the biological processes studied.

4.4 Chapter Conclusion

In this chapter I have compared the regional differences in 3D cell size and shape across regions of the Visceral Endoderm, and shown multiple differences between regions. In particular, I have shown that the cells of the lateral Epi-VE are far larger than those of the anterior Epi-VE, and that the cells of the anterior Epi-VE show a more squamous nature than the cells of the lateral Epi-VE region, with the ExE-VE showing a more regular columnar appearance. I have also shown that the cells bordering the ExE-VE on the anterior of the embryo exhibit a very highly irregular cell shapes, supporting previously published evidence that the ExE-VE acts as a physical barrier to migrating AVE cells.

Additionally, I have examined the effect of fixation on cells of the Visceral Endoderm and determined that fixation has a significant effect on the size and shape of cells.

5

Investigating cellular protrusions in the AVE

5.1 Introduction

As discussed in Chapters 1 and 3, original imaging of Hex-GFP embryos during AVE migration revealed dynamic protrusions emerging from the migrating AVE cells in the direction of movement [51]. These were later characterised as basal projections by Migeotte et al. and shown to be dependent on Rac1 signalling, and directionally dependent on the Rho-GEF protein β-Pix [59], [81], [156].

In this chapter, I examine several aspects of these cellular projections during AVE migration. This includes the previously uncharacterized distal tip region, where AVE cells are located prior to migration towards the prospective anterior of the embryo. Additionally, I have used immunohistochemistry to investigate the role of haptotaxis in the migrating AVE, in particular, the role of Laminin-α1.

The emergence of protrusions from migrating cells is a phenomenon typically associated with mesenchymal cell migration, where cells lose cell adhesiveness and contact with neighbouring cells, and migrate individually towards a specific point. However, directed cellular projections have been seen in examples of collective cell movement within an epithelial sheet.

In Xenopus convergent extension involves directed cell protrusions, including lamellipodia and filopodia, a process which is regulated by the PCP pathway [157], [158]. These projections are mediolaterally polarised and make contact with other nearby cells prior to intercalation of cells in the region, and resultant extension of the anteroposterior axis [159]–[161]. In the migration of the posterior lateral line primordium (pLLP) of the Zebrafish large protrusions of both a lamellipodial and filopodial nature extend from the cells at the front of the primordium [7], [55]. Additionally, during migration in the Drosophila trachea, large protrusions are seen from apparent leader cells [162].

5.1.1 Protrusive behaviour during AVE migration

The protrusions of the AVE have been proposed to be in response to a chemoattractant, which drives migration towards the prospective anterior side of the embryo. There is strong evidence for this, as AVE cells are known to migrate directionally in response to localised Dkk1 protein, a Wnt antagonist [58]. While the loss of *Dkk1* does not affect AVE induction and migration, this could be due to a redundancy in the signalling pathway [57].

An alternative, or potentially complimentary mechanism of migration is haptotaxis, where cells migrate along a gradient of adhesion [64], [66]. This method of migration also involves protrusive behaviour in migrating cells [61], [63]. Given the known presence of several isoforms of the protein Laminin in the basement membrane of E5.5 mouse embryos, I examined the presence of Laminin-α1, a common Laminin subunit, under the cells of the migrating AVE.

It has been reported that the cells of the AVE stop sending forward protrusions upon reaching the embryonic/abembryonic boundary [129]. Given that any chemoattractant present is either secreted by the ExE region (consisting of the ExE and ExE-VE) or is an incredibly local source of attractant molecule at the embryonic/abembryonic boundary, this cessation of protrusive behaviour is unexpected.

If a chemical signal were present from the ExE region, protrusions would attempt to move into the region. If haptotaxis were in effect, the embryonic/abembryonic boundary would need to exhibit a stark regional difference in adhesive protein localisation in order to cause such an abrupt stop in protrusive behaviour. In order to investigate this, I visualized Hex-GFP embryos at the end of AVE migration and assessed the cells there for protrusive behaviour.

5.1.2 Pre-migratory protrusive behaviour

Due their cylindrical nature, E5.5 embryos fall to their anterior, lateral or posterior faces during time-lapse imaging experiments. To date, live imaging work on the Visceral Endoderm has focused on the cells of the migrating AVE. Published work, and earlier chapters of this thesis have examined the anterior, lateral and posterior faces of the egg cylinder stage embryo. Very little, however is known about the behaviour of cells at the distal tip of the embryo.

While imaging the posterior and lateral sides of the egg-cylinder can be achieved using established methods, visualizing the distal tip is more problematic. Due to the high curvature of the distal tip and sides of the egg cylinder, it is generally only a relatively limited region of VE directly facing the objective that is in focus. To visualize all the cells of the VE, one has to capture a confocal image volume of the entire embryo and use it to build a surface rendering. With the embryo traditionally imaged lying flat, the distal tip portion of the rendered image relies heavily on the Z-axis resolution. This however is reduced to a third of that provided by the XY-axis, due to elongation of the Point Spread Function (PSF) orthogonal to the optical plane. As such, generating a surface rendering of high-resolution with current technology leads to levels of photo-damage incompatible with the survival and development of the embryo.

Given the functional constraints associated with current imaging methods, I have investigated the viability of positioning the developing embryo so that the distal tip could be imaged in greater detail. Supporting the embryo so that it remained vertical for the entire imaging process would allow the objective to be placed directly under the distal tip, placing the DVE cells in focus as they

are induced. This orientation would also overcome issue of less efficient imaging in the Z-axis.

I developed a novel method of maintaining E5.5 embryos vertically, which does not damage the embryo, or impede migration. I have used this method to identify different types of protrusive behaviour prior to migration in the E5.5 mouse embryo.

5.2 Results

5.2.1 Protrusions continue into the ExE-VE after migration has halted

In order to examine the role of the ExE-VE cells as a physical boundary to AVE migration, cells of the AVE were imaged past the point where they had reached the Epi-VE and ExE boundary. They were then assessed for whether protrusions continued into the ExE-VE region. AVE cells were examined for projections for two hours after reaching the embryonic/abembryonic boundary. Upon reaching the ExE-VE, AVE cells were observed to send protrusions into the area ahead, without moving into the ExE region (n = 4 embryos). An example of this can be seen in Figure 5.1.

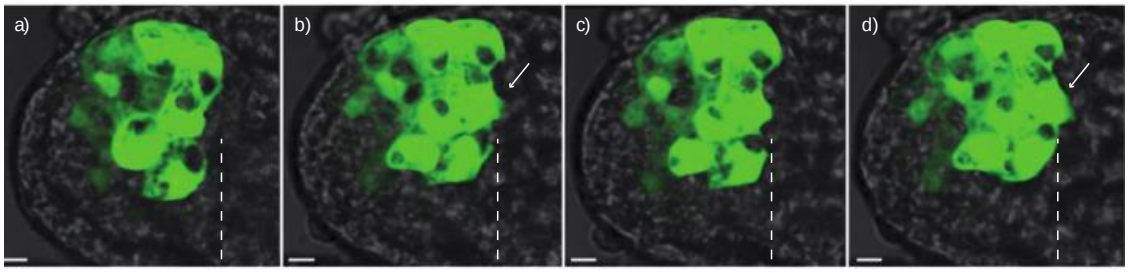


Figure 5.1: Projections continue after migration to the Epiblast-ExE boundary is complete

Fully migrated cells of the AVE continue to send protrusions into the ExE-VE upon reaching the Epiblast-ExE boundary.

Images (a) – (d) show the cells of the VE sending projections into ExE region but not continuing to migrate one hour after reaching the Epiblast-ExE boundary. Each image depicts an increase of 40 mins after the one previous.

Time-point (a) depicts 1 hour after the cells reached the Epiblast-ExE boundary and is designated 0h in terms of post-migration projection analysis. (n=4)

Scale bar = 10µm

5.2.2 Laminin staining is increased on the anterior side of the E5.75 embryo

I investigated the role of haptotaxis in the migration of the AVE, staining for Laminin-α1, a basement membrane protein. Here, a distinct difference was seen during AVE migration, with Laminin-α1 staining on the anterior side of the embryo far more intense than that of the posterior side (n= 15). This can be seen in Figure 5.2.

The basement membrane of the ExE-VE showed a higher level of laminin stain than that of the Epi-VE, which was again higher on the anterior side of the embryo (n= 15).

In all samples Laminin-α1 between cells of the anterior VE showed higher intensity than those of the posterior VE. This can be seen in in Figure 5.2a.

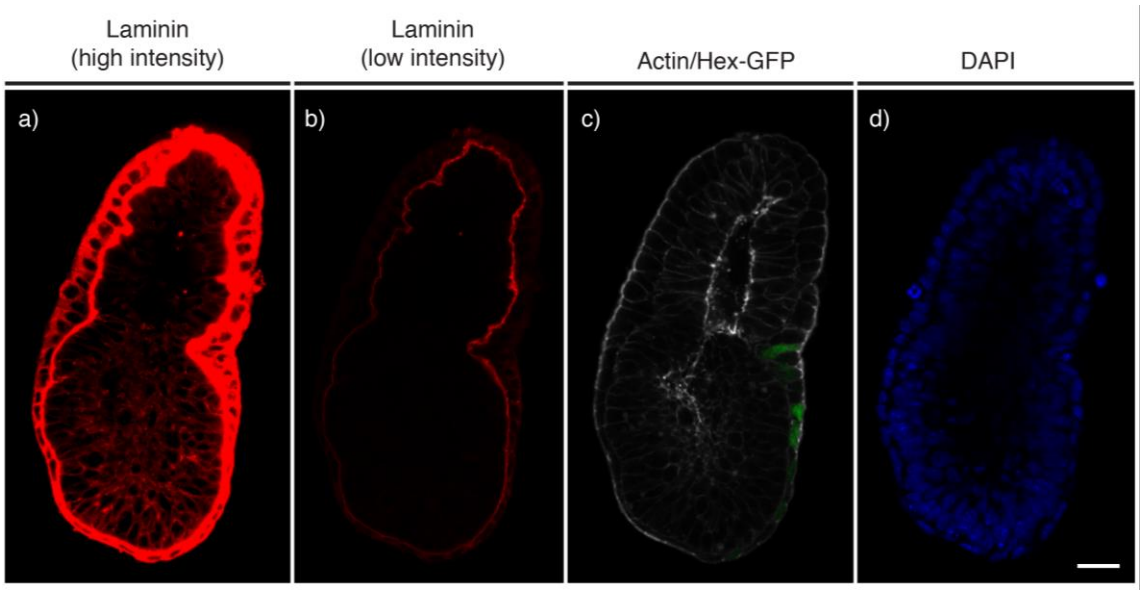


Figure 5.2: Laminin-α1 immunohistochemistry in the E5.75 mouse embryo

E5.75 Hex-GFP embryos stained for Laminin-α1, phalloidin and DAPI. Laminin staining was enriched on the anterior side of the embryo in all samples (n = 15)

(a) shows Laminin staining under high laser power, allowing Laminin between individual AVE and Epiblast cells to be seen (b) shows Laminin staining under lower laser power, emphasizing the increased staining on the anterior side of the embryo (c) shows actin and Hex-GFP, (d) shows DAPI staining

5.2.3 Development of a novel method for imaging the distal tip of the E5.5 mouse embryo

In order to visualize the distal tip of the embryo at a resolution that has not been achieved using confocal microscopy in the past, I developed a novel method of maintaining E5.5 embryos vertically, which does not damage the embryo, or impede migration.

The system utilizes nylon woven net filters, which provide a better solution than other tested materials for multiple reasons. The fibres of the mesh generate square holes that have 100μm sides, allowing the embryo to sit inside the pores in an upright position. A double layer of these net filters generates a thicker mesh, holding the embryo firmly, and preventing movement during imaging. The double layer allows for growth of the embryo, which had been shown to destabilize the positioning of the sample in previous models. The mesh, by design, allows the free flow of culture media and consequently allows the embryos access to the required nutrients provided by the media, and dispersal of any waste products. The nylon is non-toxic, and proved the best of all tested models in facilitating normal embryo development.

Multiple methods of attaching the nylon mesh to the surface of the imaging dish used were investigated, and UV glass glue proved to be the adhesive which least affects the embryos. Minimal amounts of glue are used to attach the mesh. I have tested this method and shown that individual cells can be distinguished, using mice bred in a Hex-GFP background. An overview of this method can be seen in Figure 5.3.

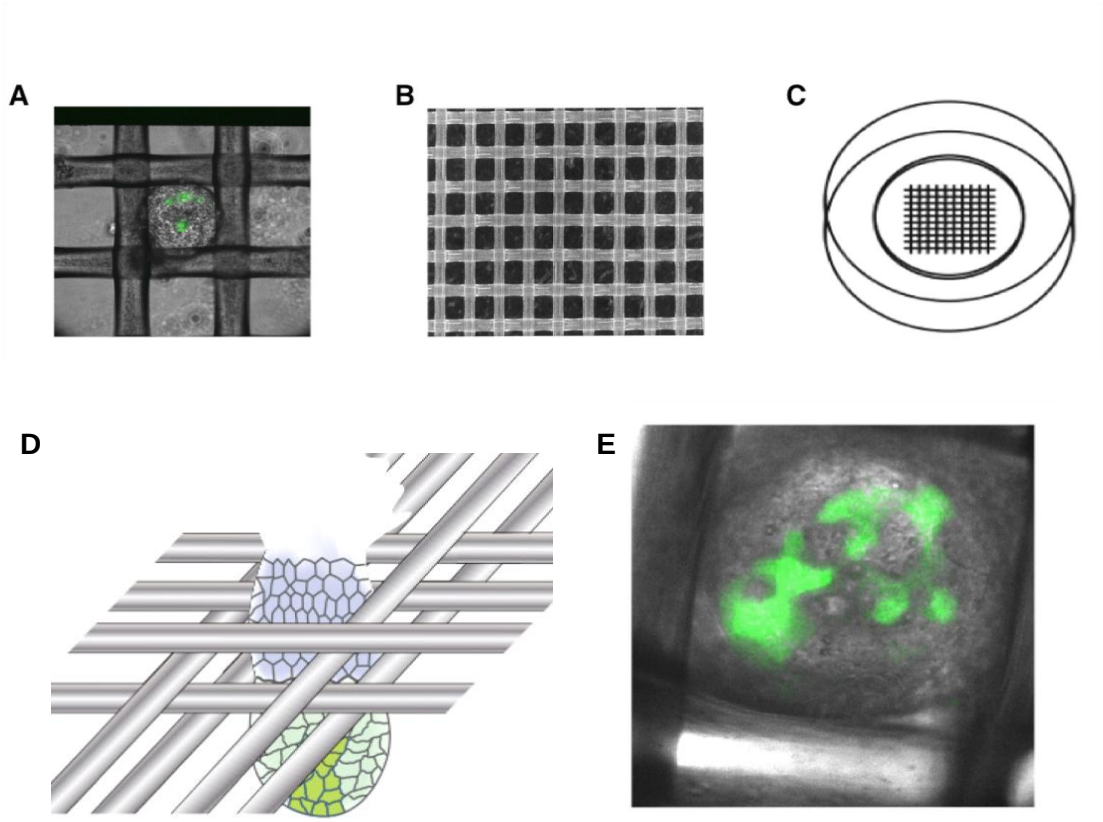


Figure 5.3: Novel method of imaging the E5.5 distal tip.

(A) E5.5 Hex-GFP embryo mounted between the fibres of the nylon mesh, imaged with a 20X objective

(B) Image of nylon mesh, holes between fibres are 100µm²

(C) Cartoon depiction of dish design

(D) Cartoon of embryo held in a double layer mesh.

(E) E5.5 Hex GFP embryo mounted between the fibres of the nylon mesh, imaged with a 40X objective

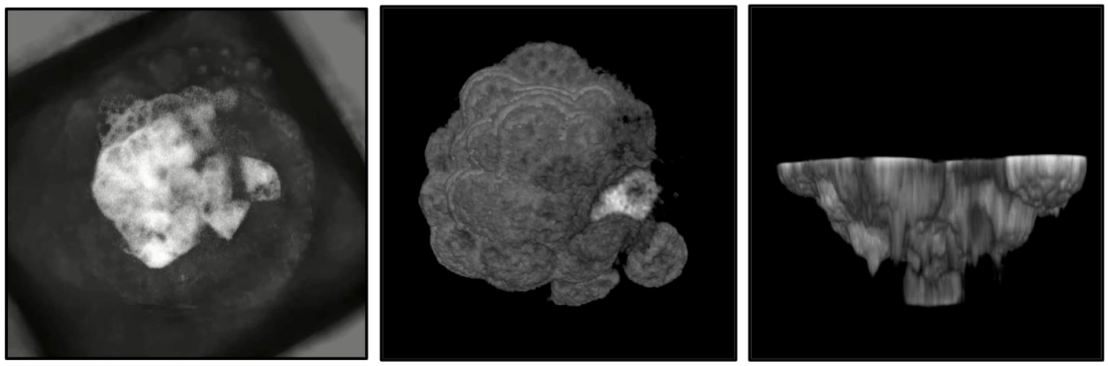


Figure 5.4: High-resolution imaging at the distal tip of the E5.5 mouse embryo

Induced AVE cells that had yet to migrate were imaged at the distal tip of the embryo using the novel imaging dish.

GFP and brightfield image of an E5.5 Hex-GFP mouse is shown (left), rendered in 3D (middle) and rotated in 3D (right). Apical protrusions can be seen in Hex positive cells of the distal tip prior to migration. These protrusions were highly variable, ranging up to 8μm in length (n= 25 protrusions, n= 3 embryos).

5.2.4 High resolution imaging of cells at the distal tip reveals several types of protrusions

Imaging from this position provides enough resolution to visualize protrusions emerging from individual AVE cells. Cellular protrusions have been previously observed in migrating AVE cells, but never before at this stage. Many of these can be seen in Figures 5.5 and 5.6.

5.2.4.1 Apical protrusions are present at the distal tip

Perpendicular filopodia-like protrusions were seen emerging from the apical surface of Hex-GFP cells at the distal tip. These protrusions were extremely dynamic, and were not stable enough to be efficiently measured for duration, often appearing only for a single 3-minute time-point. They ranged up to 8μm in height, measuring from the surface of the cell (projection n= 45, cell n = 20, embryo n = 3). An example of these can be seen in Figure 5.4.

5.2.4.2 Basal protrusions are present at the distal tip

Basal, lamellipodial protrusions can be seen at the distal tip. These were assessed for stability, and on average took 11.43 minutes to extend and retract (protrusions n= 104, cells n = 86, embryos n= 18). Examples of these can be seen in Figure 5.5.

Protrusions were also assessed for a bifurcated nature, or the filopodial tipped protrusion behaviour seen in studies on the migrating AVE. No lamellipodial projection showed either of these characteristics (protrusions n= 104, cells n = 86, embryos n= 18) (Figure 5.7).

5.2.4.3 Tall protrusions are present at the distal tip

In addition to apical and flat basal projections, an additional type of projection was seen. These often encompassed the entire height of the cell along the apical basal axis and repeatedly touched similar tall projections at the sides of other cells. These were deemed 'Tall' projections and were seen in all embryos analysed (n=28)

Some Tall protrusions were the entire height of the apical-basal axis of the protrusive cell. Others were less tall, but were clearly taller than the basal lamellipodial protrusion, and behaved in the same manner. As such, these were classed as 'Tall' protrusions along with those of the full apical-basal cell height. Examples of these tall protrusions can been seen in Figure 5.5, indicated by a white arrow and a red circle.

Tall protrusions were also assessed for stability, and on average took 6.72 minutes to extend and retract *(protrusions* n= 67, cells n = 86, embryos n= 18) (Figure 5.7).

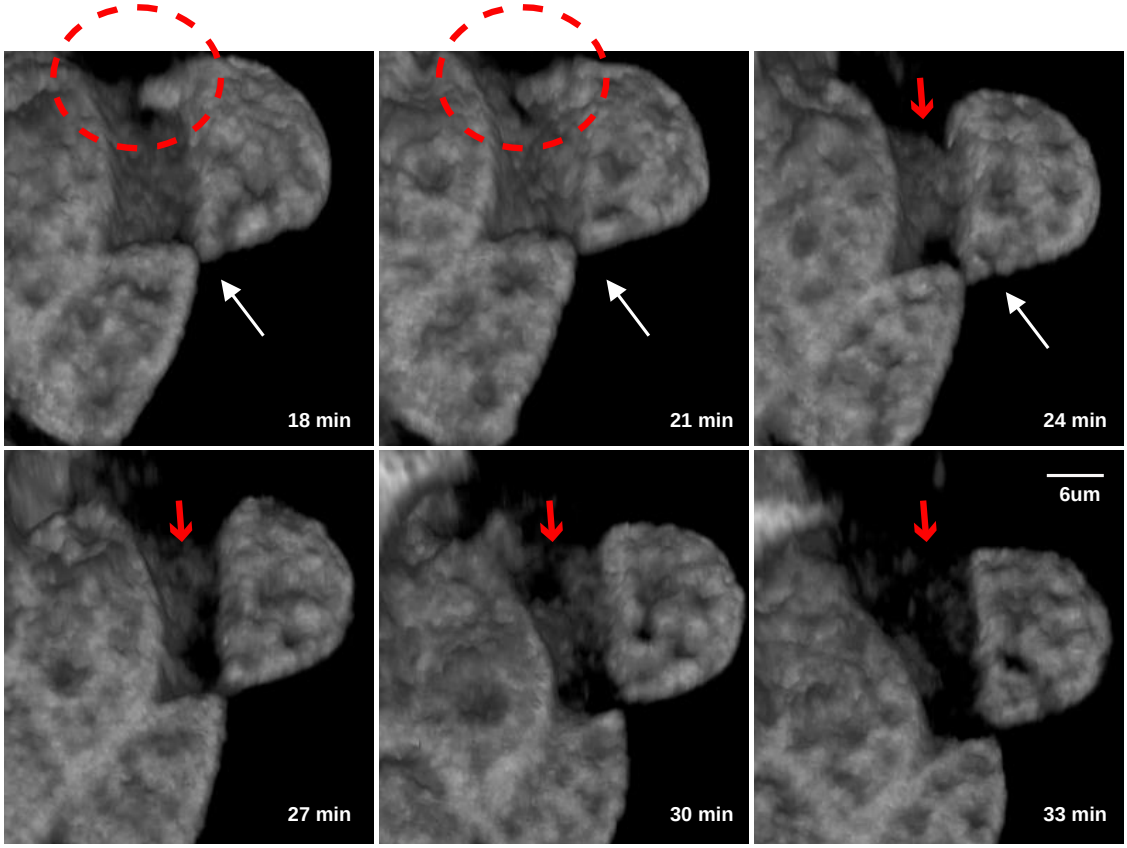


Figure 5.5: Induced AVE cells at the distal tip extend multiple types of projections prior to migration (A)

Time-lapse 3D rendering of Hex-GFP cells at the distal tip of an E5.5 mouse embryo, prior to AVE migration. Images were taken every 3 minutes for two hours.

After induction, cells of the distal tip send projections towards each other. These include basal lamellipodial projections (red arrow) and 'Tall' projections, which protrude between the boundaries of other cells and are not restricted to the basal side of the projecting cell (red circle) and filopodial protrusions.

(Continued overleaf)

Basal cells protrude under the other cells of the distal tip. No bifurcated cellular projections or lamellar projections with filopodial tips were seen.

Basal protrusions extend and retract over the course of 11.43 minutes on average (protrusions n= 104, cells n = 86, embryos n= 18*).*

Tall protrusions extend and retract over the course of 6.72 minutes on average Projections do not extend outwards away from the centre of the distal tip (protrusions n= 67, cells n = 86, embryos n= 18*).*

(Counted cell n = 140, embryo n = 28). Scale bar = 6μm

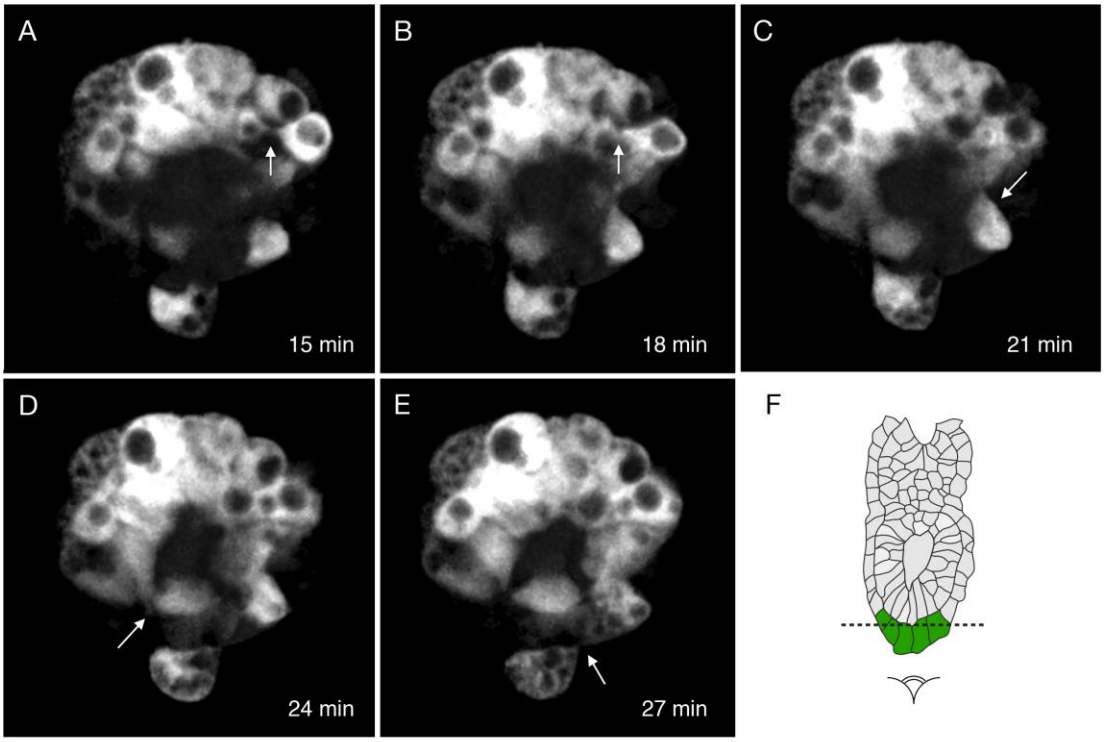


Figure 5.6: Induced AVE cells at the distal tip extend multiple types of projections prior to migration (B)

Optical section of Hex-GFP cells at the distal tip of an E5.5 mouse embryo, prior to AVE migration. Images were taken every 3 minutes for two hours.

(A-E) show the same cells over the course of 12 minutes. Arrows indicate projections, all of which extend or change over the course of the time-lapse shown.

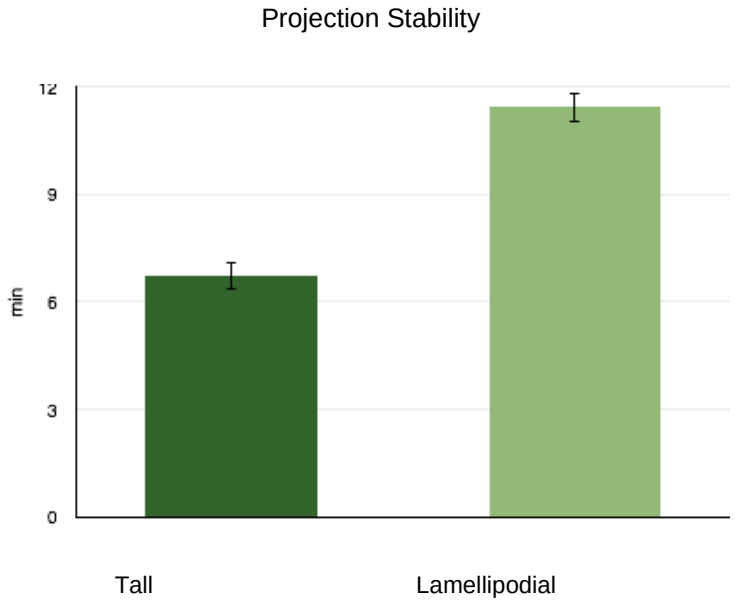


Figure 5.7: Duration of Tall and Lamellipodial projections at the distal tip of the E5.5 mouse embryo

Tall and lamellipodial projections were timed from the first time-point of observation until the time-point where the projection had receded fully. This was taken as the duration of the projection.

Tall protrusions emerged and fully receded within 6.72 minutes, on average (protrusions n= 67, cells n = 86, embryos n= 18).

Lamellipodial protrusions emerged and fully receded within 11.43 minutes, on average (protrusions n= 104, cells n = 86, embryos n= 18).

5.3 Discussion

5.3.1 Protrusions continue into the ExE-VE after migration has halted

Upon reaching the ExE-VE, embryos were observed to send protrusions into the area ahead, without moving into the ExE region.

This supports the theory that the ExE-VE is acting as a physical barrier to migration, but also indicates that the cause of migration of the AVE, whether chemotaxis, haptotaxis or both, extends into the ExE-VE. Data from *Lefty1*$^{-/-}$ embryos where over-migration is seen has indicated that that loss of the distinct differences between Epi-VE and ExE-VE behaviour is the cause of AVE cell overmigration. This data supports this, as AVE cells clearly send projections into the ExE-VE, but are unable to migrate within these cells.

5.3.2 Laminin-α1 is upregulated under the cells of the migrating AVE

Laminins are heterotrimeric proteins made up of three chains, each of which has multiple genetic variants. Laminins are named according to which variants they are composed of (i.e.: Laminin-111 is composed of α1, β1 and γ1 chains) Different chains show different tissue distributions, indicating different roles *in vivo,* though this aspect of the field is largely uninvestigated [163]. Laminin-111 is known to be present in the early mouse embryo, as is Laminin-511 [164] and as such Laminin-α1 was selected for investigation at the egg-cylinder stage.

The increased presence of laminin in the basement membrane underneath the migrating cells of the AVE was highly striking. This is a clear indication that haptotaxis plays a role in the migration of the AVE, and may be the cause of

the projections seen at this stage.

While the Laminin stain is clearly more intense in the basement membrane overlying the ExE-VE, intensity was not seen to be in a gradient along the Proximal-Distal axis of the Epi-VE, when assessed visually.

Whether the increased levels of Laminin-α1 on the anterior side of the embryo generate the directed protrusions seen during AVE migration would be very difficult to assess, as mutants for Laminin chain genes expressed at this stage are highly perturbed at and prior to E5.5. Mutants for Laminin α1- die by E6.5 but overall tissue organization defects are seen at E5.5, including Visceral Endoderm differentiation defects [165]. Laminin γ1-chain mutants do not survive past E5.5 due to lack of basement membrane and proper Primitive Endoderm formation [130]. Laminin β1-chain mutants have a very strong phenotype, possessing no basement membrane at E5.5 and having subsequent large-scale shape and specification defects.

Laminin β1 has been shown to be expressed by the cells of the AVE however, in a screen [166]. It is possible that the cells of the AVE are expressing and depositing specific basement membrane components to assist their own migration. This could be investigated using a Visceral Endoderm specific deletion of *Lamb1*, the Laminin-β1-chain encoding gene.

5.3.3 Imaging cell behaviour at the distal tip of the egg cylinder stage embryo

I examined high-resolution Hex-GFP fluorescence imaging movies to investigate the cell behaviour in pre-migration embryos, establishing a novel method of imaging to accomplish this. This method of imaging allows for more frequent image capture than previous methods, with time-points gained as often as every three minutes, for up to two hours. Several types of protrusions were seen prior to the induction of migration. These included Apical, Lamellipodial and Tall protrusions.

5.3.3.1 Apical protrusions are present at the distal tip

Apical projections protruded out of the embryo and varied greatly in size. These were highly dynamic, changing in size between 3-minute time-points. Additionally apical protrusions can be seen in LifeAct embryos (unpublished data from the Srinivas group), both at the distal tip of the embryo and during AVE migration. A role for these protrusions, if any, is unknown. Investigation of various faces of the E5.5 mouse embryo, as well as later stages using the LifeAct mouse line, or another established membrane marker would establish whether these protrusions are a standard, but previously described feature of Visceral Endoderm cells or if they are a feature of the AVE.

5.3.3.2 Basal protrusions are present at the distal tip but do not exhibit a filopodial tipped or bifurcated nature

Migeotte et al. described the protrusions seen in AVE migration as basal, and similar lamellipodial projections can be seen at the distal tip. This can be seen clearly in 3D even without the use of a depth filter. Lamellipodial protrusions varied in length and stability, with some only visible for a single time point,

but averaged at 11.43 minutes in total duration (extension and retraction). These protrusions extended towards other Hex-GFP cells, with two protrusions often touching each other beneath a non-fluorescent cell.

No cell investigated showed a bifurcated or a filopodial tipped protrusion, which are seen when imaging the migrating AVE [59], [129]. Bifurcated protrusions have been noted as characteristic of cells migrating in a shallow gradient of a chemoattractant [60]. This points toward the cells of the distal tip being primed to respond to a chemoattractant at this stage, but having yet to receive such a migratory signal.

5.3.3.3 Tall protrusions are present at the distal tip

A novel type of cell protrusion was seen at the distal tip. These protrusions originated at the intersection point between several cells and inserted from the protruding cell in between cell boundaries of other cells. Often these touched tall protruding processes from other cells. An example of this is indicated by the white arrow in in Figure 5.5. Occasionally these protrusions were not the entire apical height of the cell, but were classed as Tall projections due to being taller than the basal lamellar protrusions and behaving in the same manner as apical protrusions which were the full apical-basal height of the protruding cell. An example of a mid-sized Tall protrusion is circled in Fig 5.5.

Mid-migration embryos were examined for Tall protrusions, however cells have become far more squamous as a result of AVE migration, and as such Tall projections cannot be reliably distinguished from small filopodia when rendered in 3D.
On average, Tall projections in the distal tip extended and retracted within

approx. 6.4 minutes. Duration analysis is not ideal, as projections must be counted from the first time-point seen to the last seen. Several projections were seen in only one time-point, indicating duration shorter than the three minute imaging frequency, indicating that using 3-minute units of time to calculate projection parameters is less than ideal. However, a general sense of how long the projections of each time take to extend and retract can be gained from this analysis, and it was evident that basal Lamellipodial protrusions were more stable than Tall protrusions. While the role of basal protrusions is potentially that of a precursor to migration along a chemoattractant or adhesion gradient, the presence of Tall protrusions far more likely to play a role in the neighbour exchange seen during AVE migration. This is because the cells appear to be transiently attempting to create new interactions with cells they are not directly touching, pushing through the cell-cell boundaries of current neighbour cells. As such, Tall projections are likely not a feature of only the distal tip, but can be visualized here due to the more columnar nature of the cells.

A mosaically expressed fluorescent reporter expressed under the TTR promoter could be used to test whether non Hex-GFP cells in the distal tip, lateral and posterior Visceral Endoderm are also sending these tall protrusions. It would be highly interesting to see if this exploratory pre-intercalatory behaviour is occurring throughout the Epi-VE and ExE-VE. A difference solely between regions could give insight into the generation of the ExE-VE behaviour that ensures a physical boundary to the migrating AVE cells.

5.4 Chapter conclusion

Overall, the presence of directed protrusions could be indicative of several types of behaviour in the cells of the migrating AVE. As discussed above, chemoattractant based migration, haptotaxis based migration and intercalatory behaviour all exhibit protrusions, making those seen in the AVE very difficult to interpret.

Taking both the lack of bifurcated and tipped projections prior to migration and the increased presence of Laminin-α1 underneath the AVE into consideration, evidence from this chapter advocates for both chemotaxis and haptotaxis playing a role in the migration of the AVE. Further investigation of other basement membrane proteins at this stage would be very informative to explore the extent of the role of haptotaxis at this stage.

6

Proteomic Analysis of Egg Cylinder Stage Embryos

6.1 Introduction

6.1.1 Proteomic research in the early mouse embryo

One major difficulty that arises frequently when studying the E5.5 mouse embryo is the relatively small amount of previously conducted research in this area, when compared to later stages. Often no data is available regarding a protein of interest during early embryonic stages. An example of this is seen in Chapter 6, where the earliest established β-arrestin2 expression data prior to this work was as late as E14.5.

Further to this, most research that has been completed at this stage has focused on signalling proteins and transcription factors that might regulate pattern formation. As a result there is very little information regarding proteins involved in cellular processes such as migration, making choosing probable candidates for investigation of AVE migration and general Visceral Endoderm behaviour very difficult.

As discussed in Chapter 1, several labs have begun elucidating key factors in the regulation of cell mechanics during this process, a process that would be greatly benefit from an improved understanding of the protein content of the regions under observation [5], [31], [59], [81], [156]. This has been addressed specifically in the cells of the AVE region in a screen by Gonçalves et al., which investigated RNA levels in the AVE region of embryos [166]. While this was informative, this screen did not give any information on expression in the ExE, Epiblast or ExE-VE, meaning important candidates regulating the behaviour of the entire VE may have been overlooked. Overall, choosing candidate proteins to investigate regulation cell behaviour and migration in the egg cylinder stage embryo would greatly benefit from an improved understanding of the protein content of the regions under observation.

6.1.2 Phospho-proteomic research in the early mouse embryo

Very little research has been conducted to data on the regulation of phosphorylation at the egg cylinder stage, due to the lack of antibodies suitable for immunofluorescence staining. Phosphorylation, the enzymatically mediated addition of a phosphate group ($^{-}PO_4$) to an amino acid, is a major mechanism of protein regulation, and is the most widely studied post-translational regulation. Given that this protein modification can lead to changes in function, activity, location or stability of proteins, improved insight

into the regional differences of protein phosphorylation in would be of great benefit in the study of the egg cylinder stage embryo.

Phosphorylation is a reversible process that occurs on a rapid timescale, which can act on all, or more likely, a subset of a given protein in a cell. This makes it an ideal molecular system for regulating cellular processes. It can act as a binary ON/OFF switch for many proteins, as well as act in tandem with other phosphorylation sites, allowing for complex regulation of cellular machinery and the intra/extra cell signal transduction [167].

The proportion a given protein's phosphorylation will change depending on the type and life-cycle stage of the cell in question. This provides a far more adaptable method of controlling protein activity than relying on translation alone. For example, a cell can have a large amount of protein transcribed and held in an inactive state, of which a selected amount can be phosphorylated and active with a reaction time of seconds to minutes, while translation can require 30 minutes to several hours to take effect (reviewed in [167]).

Important phosphorylation dependent pathways during development include the canonical β-catenin pathway, where canonical β-catenin is degraded when phosphorylated [168], [169]. APC mutants where this phosphorylation pathway is not effective are embryonic lethal [80]. Regulation of cell proliferation is hugely important in development, and the cell cycle itself is regulated by cell cycle kinases at multiple stages, which all require phosphorylation regulation to manage cell cycle progression (reviewed in [170]). Apoptosis is a key player in development, and phosphorylation plays a key role in the control of cell survival vs. cell death via kinases such as AKT [171].

Phosphorylation is also highly important during migration. Most conventional

non-muscle and smooth muscle myosins are regulated by phosphorylation of their regulatory light chains [172]–[174]. Many proteins involved in cell migration are kinases, such as PAK and LIMK [175]–[177]. Migratory function, not cell proliferation or survival functions, of the phosphatase Pten is required for the normal migration of AVE cells [81]. Given that phosphorylation is known to play multiple roles in cell migration, it is highly likely to be involved in multiple aspects controlling the migration of the AVE.
Various proteins play vastly different roles and are activated in unique combinations in different types of migration. Given that AVE cells seem to migrate in a manner that does not fit any typical description of various migration types, understanding which proteins are differentially activated or suppressed by post-translational modification in the AVE cells would be a large step towards understanding the migration of this region.

6.1.3 Mass spectrometry as a protein and phospho-protein characterization tool

Mass spectrometry provides a solution to both the lack of both protein and phosphorylation state characterization in the early mouse embryo.
The capabilities of the technique in the field of protein detection have been established for over two decades, while in recent years, major advances have been made in the optimization of mass spectrometry for identification of specific phospho-peptides [178]. Both areas have benefitted from improved mass spectrometry technique allowing more detailed, smaller particles to be identified, while phospho-peptide identification has seen improvements in preparatory methods and in the improvement of software that allows specific phosphorylation sites to be identified [175], [179].

The ability to enhance the efficiency of phospho-protein detection within a small biological sample facilitates the use of mass spectrometry for phospho-protein detection in this project, where the tissues in question are particularly small.

Given the capabilities of the technique, I decided to use mass spectrometry to investigate which proteins were expressed in the different regions of the E6.25 mouse embryo, and which proteins were differentially phosphorylated. The 'ExE region' and 'Epiblast region' were compared, with the 'ExE region' comprising the entire ExE and the overlying ExE-VE and the 'epiblast region' comprising the entire Epiblast and the overlying Epi-VE. This generated a list of proteins that would act as candidates for potential further research, which is the first proteomic and phospho-proteomic analysis of the embryo at this stage.

6.2 Results

6.2.1 Regional Protein Expression and Phosphorylation differences are present in the E6.25 mouse embryo

I dissected 104 embryos at E6.25 from several pregnant mothers, with the help of Dr. Srinivas during several dissections. The embryos were removed from decidua, had Reichart's membrane removed and were carefully cut in half along the point at which the ExE meets the Epiblast as depicted in Figure 6.1. This was performed as promptly as possible, without compromising dissection quality, to limit exposure of the embryo and any potential changes the cells within might undergo as a result of the embryo perturbation.

The different regions were pooled in two separate tubes and quickly frozen in liquid nitrogen, and stored at -80°C. The two halves of the embryo were deemed 'Epiblast region' referring to the epiblast itself and the overlying Visceral Endoderm tissue and the 'ExE region', referring to the Extra-embryonic Ectoderm and overlying Visceral Endoderm tissue (Figure 6.1).

The sample preparation and mass spectrometry was performed by the Vanhaesebroeck lab, our collaborators at the Centre for Cell Signalling, Barts Cancer Institute, Queen Mary University of London. This was performed in the manner described by Casado et al. [180]. In brief, cells were harvested, lysed and treated with phosphatase inhibitors. Both pools of embryo halves were lysed and further divided into four aliquots that were processed individually, giving four technical replicates each. Further treatment on resultant peptide solutions included enrichment of phosphopeptides via Immobilized metal ion affinity chromatography (IMAC), a very popular method for isolating phosphopeptides [181]. Each sample was run three times and the data for each sample was averaged over the three runs. The data

obtained from the resulting chromatogram was sent to the Srinivas lab. We received 'Total' and 'Phospho-protein' data from the samples, sorted according to the fold difference and significance.

167 proteins were detected at a two-fold or higher difference between the 'Epiblast' and 'ExE' regions (Figure 6.1). The complete list of significant Total Protein results can be found in Appendix 1. 175 proteins showed a two-fold or higher level difference in phosphorylation at specific residues between the 'Epiblast' and 'ExE' regions (Figure 6.1). The complete list of significant Phospho-protein results can be found in Appendix 2.

As exploring such a large number of proteins using a literature review-based approach would be a prohibitively time consuming process, several analysis tools were utilized instead, as described below, to condense the list into a smaller number of candidates for further investigation. The data from both the Total Protein and Phospho-Protein mass spectrometry were assessed for prominence of particular biological functions and molecular processes, enrichment of series of interacting proteins, inclusion of keywords in gene ontology database descriptions. They were also assessed for secretory behaviour and ability to generate neural tube defects.

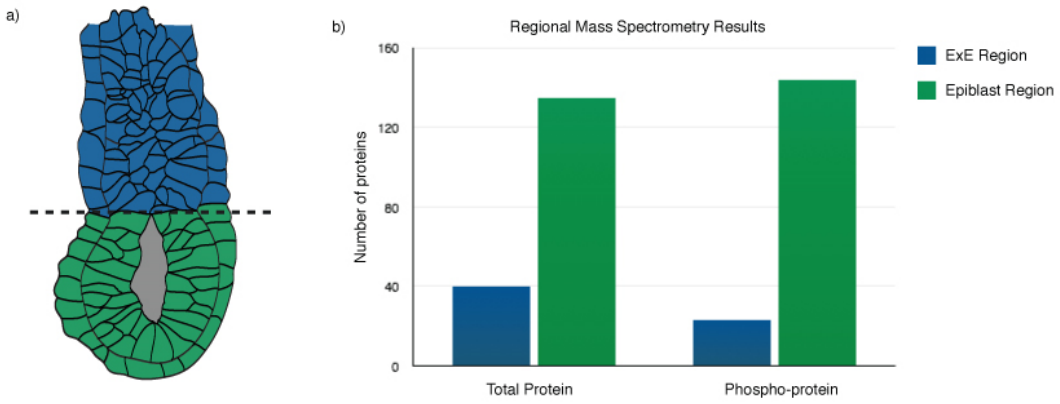


Figure 6.1: Mass spectrometry was performed on 'Epiblast' and 'ExE' regions of E6.25 mouse embryos

a) E6.25 embryos (n = 104) were cut along the boundary between the ExE and Epiblast regions, depicted by a dotted line. This was repeated for multiple pregnant mice. The embryos were frozen in liquid nitrogen and stored at -80C.

b) 167 proteins showed a two-fold or higher difference between the 'Epiblast' and 'ExE' regions. 143 proteins showed a two-fold or higher expression in the Epiblast region. 24 proteins showed a two-fold or higher expression in the ExE region.

c) 176 proteins showed a two-fold or higher level difference in phosphorylation at specific residues between the 'Epiblast' and 'ExE' regions. 135 proteins showed a two-fold or higher level difference in phosphorylation in the Epiblast region. 41 proteins showed a two-fold or higher level difference in phosphorylation in the in the ExE region.

6.2.2 Analysis of the Mass Spectrometry data

6.2.2.1 STRING analysis

In order to test for enrichment of a cohort of interacting proteins in a particular region, STRING analysis was used. STRING (Search Tool for the Retrieval of Interacting Genes/Proteins) is a database of known and predicted protein interactions. The interactions include direct (physical) and indirect (functional) associations.

Both Total protein and Phospho-protein data were examined, with the Epiblast and ExE regions investigated individually for protein connections.

6.2.2.1.1 Total Protein STRING analysis

In the ExE region, the total protein data showed only two groups of connected proteins. These were Anxa5/Tagln2 and Lamβ1/Dab2/Cubilin. This can be seen in Figure 6.2

In the Epiblast region, the total protein showed a great deal of interaction, as seen in Figure 6.3. Some connection pathways such as Mcm2/Mcm3/Prim2/Msh2/Rpa were immediately eliminated from consideration for future investigation, as they were DNA replication or repair pathways. Additionally many proteins were involved in ribosomal activity and maintenance. However, this still left a large number of connections.

Notably Rab5 had a large number of protein interactions (3 direct and a large number of interconnecting pathways as secondary neighbours). Additionally, profilin had many protein interactions (4 direct and a large number of interconnecting pathways as secondary neighbours).

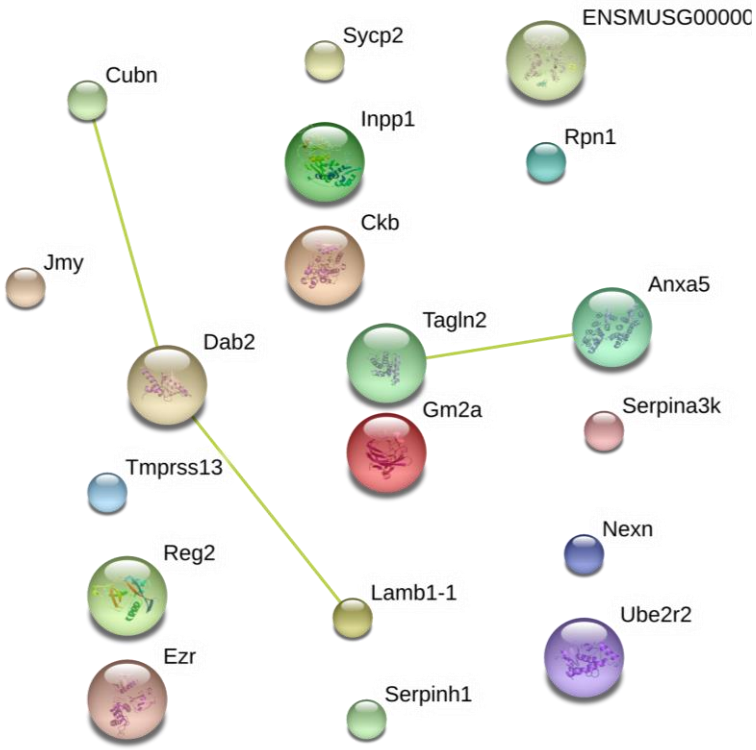


Figure 6.2: Analysis of protein interactions in the ExE region - Total protein mass spectrometry data

STRING evidence based view showing established interactions between proteins that were expressed at a minimum of a two-fold higher level in the ExE region than the Epiblast region

Line colour indicates the evidence source that connects the proteins.
Red = fusion evidence, green = neighbourhood evidence, blue = co-occurrence evidence, purple = experimental evidence, yellow = text mining evidence, light blue = database evidence, black = co-expression evidence.

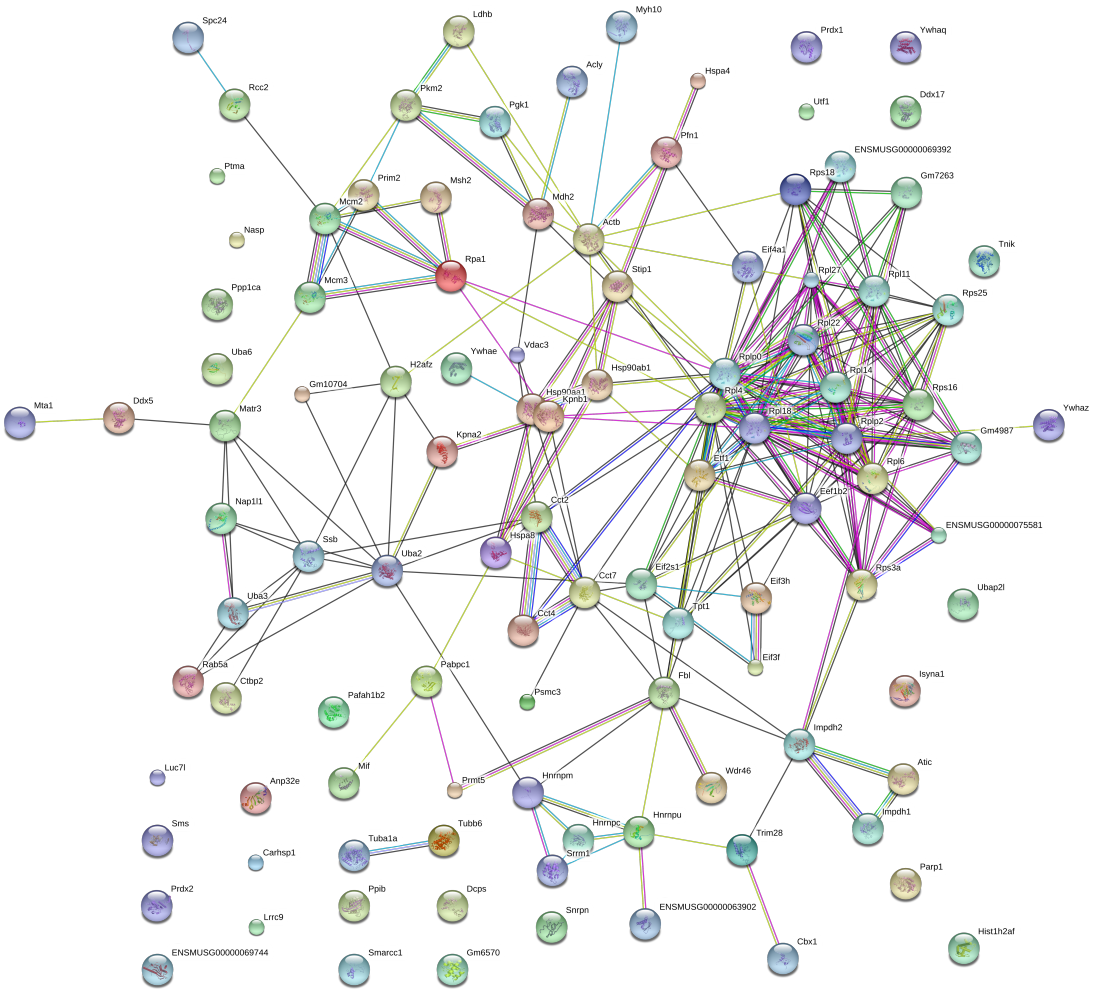


Figure 6.3: Analysis of protein interactions in the Epiblast region - Total protein mass spectrometry data

STRING evidence based view showing established interactions between proteins that were expressed at a minimum of a two-fold higher level in the Epiblast region than the ExE region

Line colour indicates the evidence source that connects the proteins.
Red = fusion evidence, green = neighbourhood evidence, blue = co-occurrence evidence, purple = experimental evidence, yellow = text mining evidence, light blue = database evidence, black = co-expression evidence.

6.2.2.1.2 Phospho-protein STRING analysis

In the ExE region, the phospho-data exhibited only two interactions (Figure 6.4). The Spna2/Epb4.1L3 interaction was highly of interest due to the involvement of these proteins in migration.

In the Epiblast region, there were many interactions, however all but one were eliminated from proteins of interest due to being DNA replication and repair proteins, or being involved in ribosomal regulation. This was the MarcksL1/Marcks interaction (Figure 6.5). These are calmodulin, actin, and synapsin binding proteins.

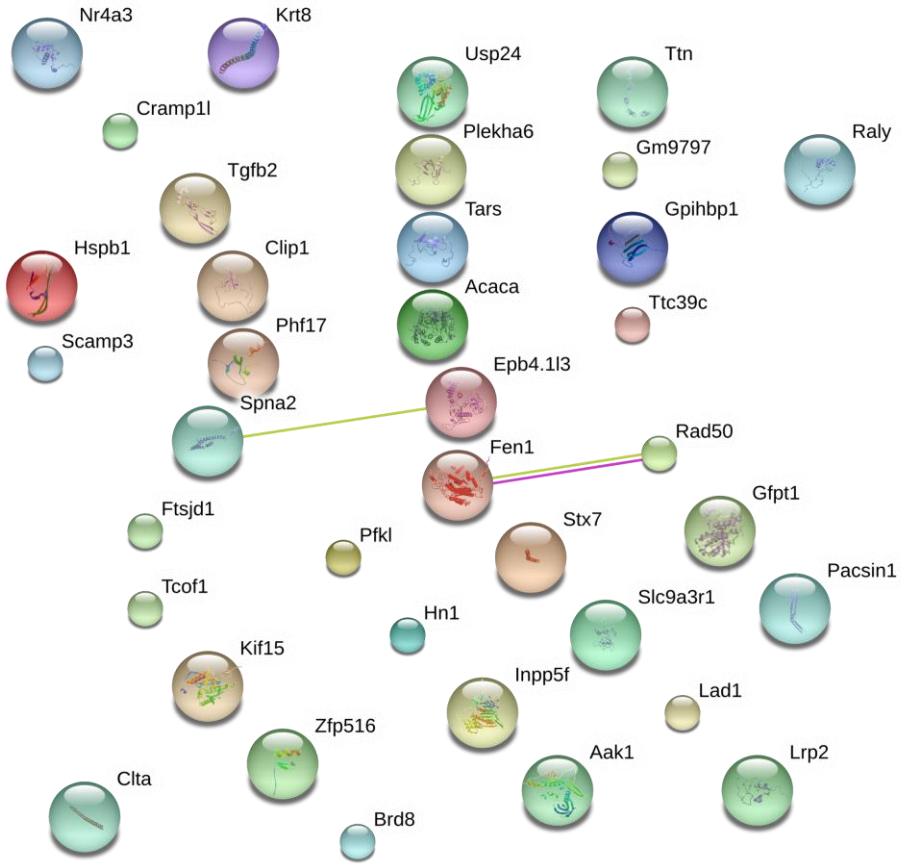


Figure 6.4: Analysis of protein interactions in the ExE region – Phospho-protein mass spectrometry data

STRING evidence based view showing established interactions between proteins that showed a minimum of two-fold higher phosphorylation level at specific regions in the ExE region than the Epiblast region

Line colour indicates the evidence source that connects the proteins.
Red = fusion evidence, green = neighbourhood evidence, blue = co-occurrence evidence, purple = experimental evidence, yellow = text mining evidence, light blue = database evidence, black = co-expression evidence.

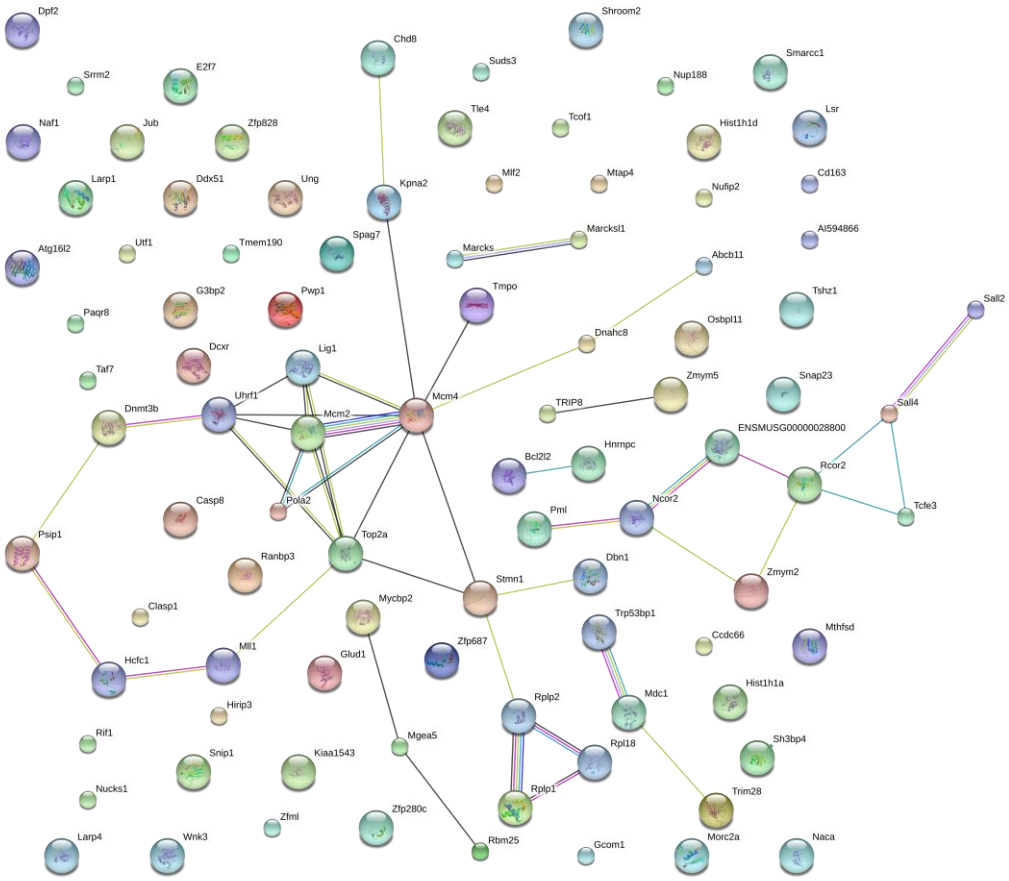


Figure 6.5: Analysis of protein interactions in the Epiblast region – Phospho-protein mass spectrometry data

STRING evidence based view showing established interactions between proteins that showed a two-fold higher phosphorylation level at specific regions in the Epiblast region than the ExE region

Line colour indicates the evidence source that connects the proteins.
Red = fusion evidence, green = neighbourhood evidence, blue = co-occurrence evidence, purple = experimental evidence, yellow = text mining evidence, light blue = database evidence, black = co-expression evidence.

6.2.2.2 Gene Ontology Analysis

6.2.2.2.1 PANTHER analysis

The PANTHER (Protein ANalysis THrough Evolutionary Relationships) Classification System was predominantly used. PANTHER can classify proteins according to their molecular function and the biological process a protein is known to be involved in [182]. Proteins that showed a two-fold higher expression in the ExE or Epiblast regions were analysed for enrichment of a particular molecular function or biological process. The same analysis was carried out for the proteins that showed a two-fold higher level of phosphorylation at a particular phosphorylation site in either region.

6.2.2.2.1.1 Biological Process PANTHER analysis

In both ExE and Epiblast regions of Total and Phospho-protein datasets the most represented category was that of metabolic process, followed by that of cellular process.

Total protein data

In the total protein analysis, the ExE region proportionally showed almost nine times the level of biological adhesion proteins (n = 2 of 43) than the Epiblast region (n = 1 of 193). Further, three times the proportion of proteins that categorized as being involved in developmental processes were seen in the ExE region (4 of 43) than the Epiblast region (7 of 190). No proteins categorized as involved in Reproduction were seen in the ExE region analysis (Figure 6.6).

In the Epiblast region, twice the proportion of proteins were categorized to have a role in metabolic processes (78 of 190), than in the ExE region (n = 11

of 43). Additionally, twice the proportion of proteins (n = 16 of 190) were categorized to have a role in Cellular Component Organisation, than in the ExE region (n = 2 of 43) (Figure 6.7).

In the phospho-protein dataset, there is almost twice the proportion of proteins categorized as being involved in response to stimulus in the ExE region (n = 2 of 31) as in the Epiblast region (n = 5 of 140). There are over twice the proportion of proteins involved in Biological regulation processes in the ExE region (n = 2 of 31) as in the Epiblast region (n = 5 of 140). Similarly, there are over twice the proportion of proteins involved in Cellular Component Organisation processes in the ExE region (n = 2 of 31) as in the Epiblast region (n = 5 of 140). Three times the proportion of proteins were categorized as having a role in localisation of proteins in the ExE region (n = 4 of 31) than the Epiblast region (n = 6 of 140).

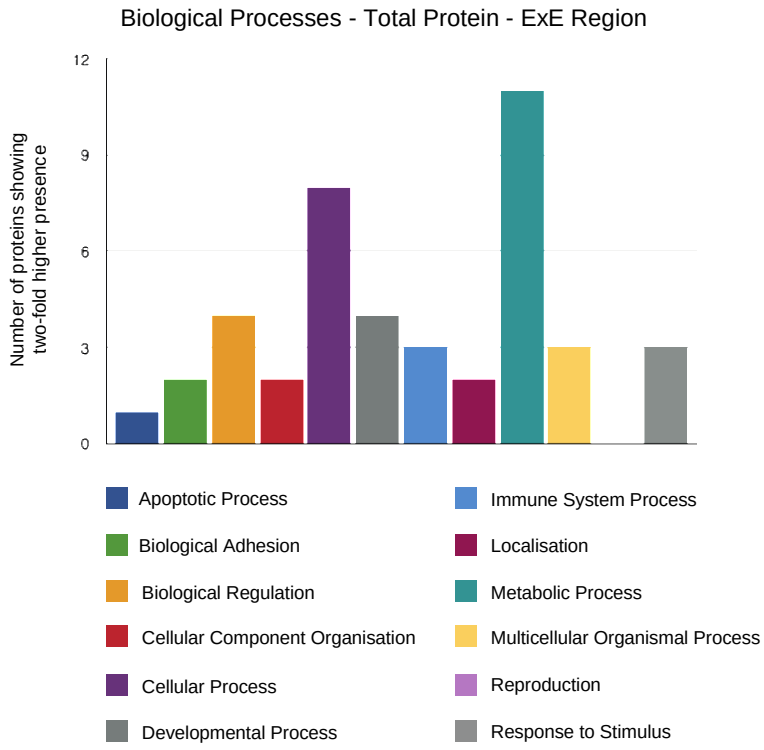


Figure 6.6: Biological Process PANTHER analysis of Total Protein mass spectrometry data - ExE region

PANTHER classification of the proteins that showed a minimum of a two-fold higher expression level in the ExE region than the Epiblast region. Proteins were classified according to Biological Process.

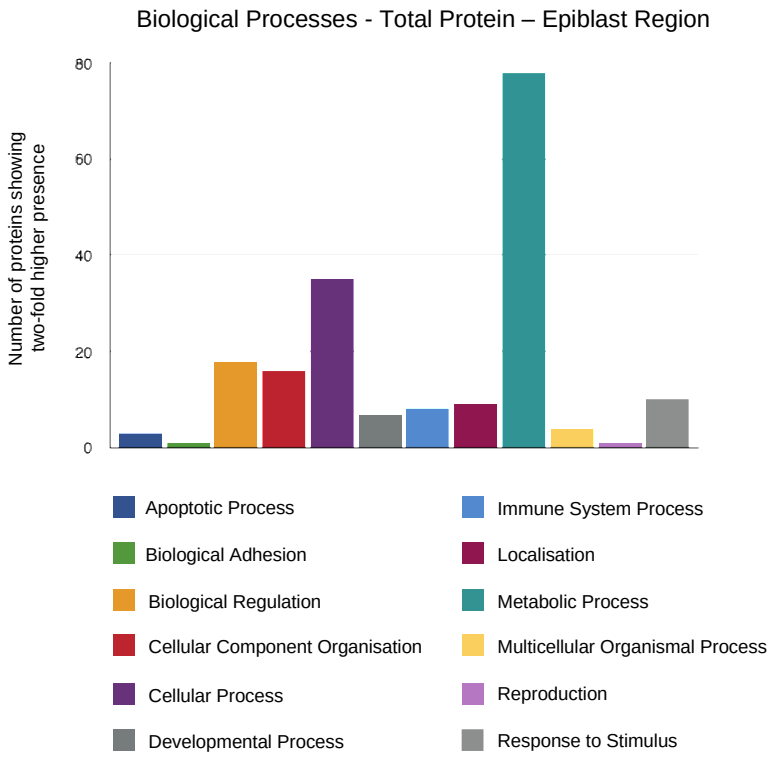


Figure 6.7: Biological Process PANTHER analysis of Total Protein mass spectrometry data - Epiblast region

PANTHER classification of the proteins that showed a minimum of a two-fold higher expression level in the Epiblast region than the ExE region. Proteins were classified according to Biological Process.

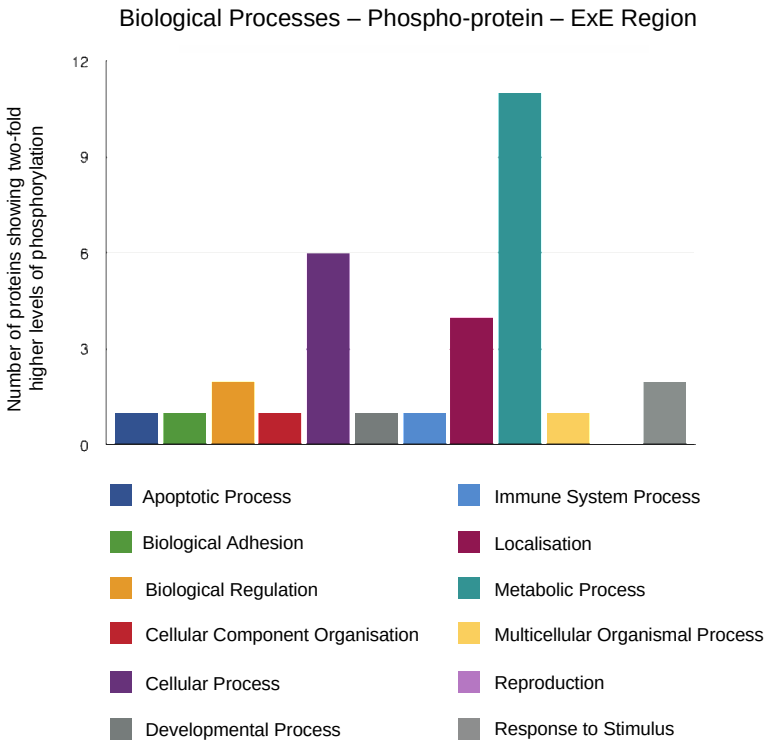


Figure 6.8: Biological Process PANTHER analysis of Phospho-protein mass spectrometry data - ExE region

PANTHER classification of the proteins that showed a minimum of a two-fold higher phosphorylation level at specific regions in the ExE region than the Epiblast region. Proteins were classified according to Biological Process.

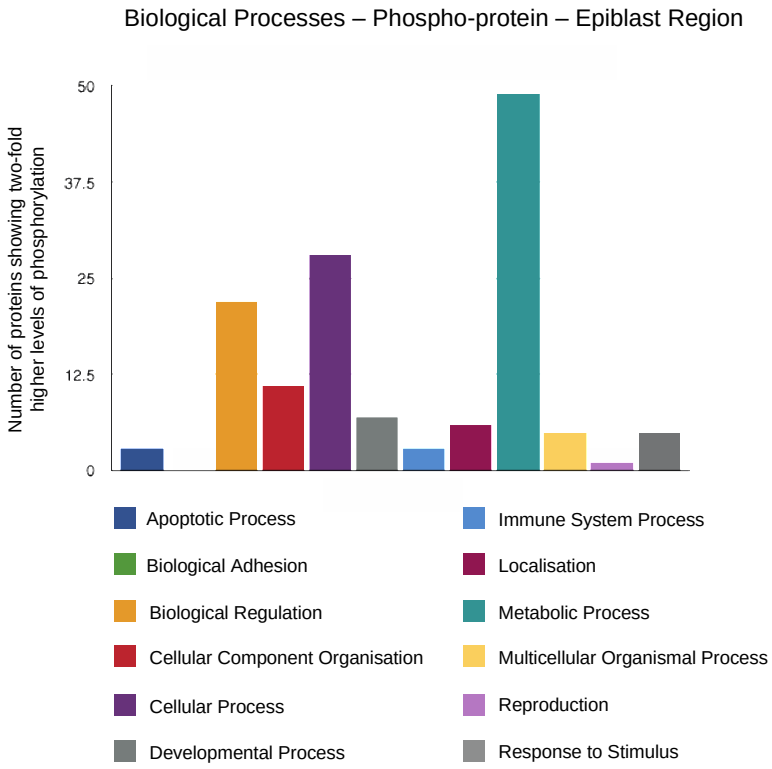


Figure 6.9: Biological Process PANTHER analysis of Phospho-protein mass spectrometry data - Epiblast region

PANTHER classification of the proteins that showed a minimum of a two-fold higher phosphorylation level at specific regions in the Epiblast region than the ExE region. Proteins were classified according to Biological Process.

5.2.2.2.1.2 Molecular Function PANTHER analysis

In both ExE and Epiblast regions of Total and Phospho-protein datasets, the two highest represented categories were that of binding activity and catalytic function.

In the Total protein data, the Epiblast region showed representation in all ten available categories. In the ExE region, enzyme regulator activity and receptor activity were represented at a far higher proportion (n= 4 of 27, both) than in the Epiblast region (n= 4 of 118 and 1 of 118, respectively). In the ExE region no proteins were categorized as having antioxidant activity, nucleic acid binding transcription factor activity, protein binding transcription factor activity, translation regulation activity.

In the Phospho-protein molecular function analysis proteins categorized as having nucleic acid binding transcription factor activity were particularly high in the Epiblast region (n= 18 of 100). Very few proteins emerged from the ExE region analysis as having specific molecular function annotation. Of these, the highest category was catalytic function (n= 5 of 11).

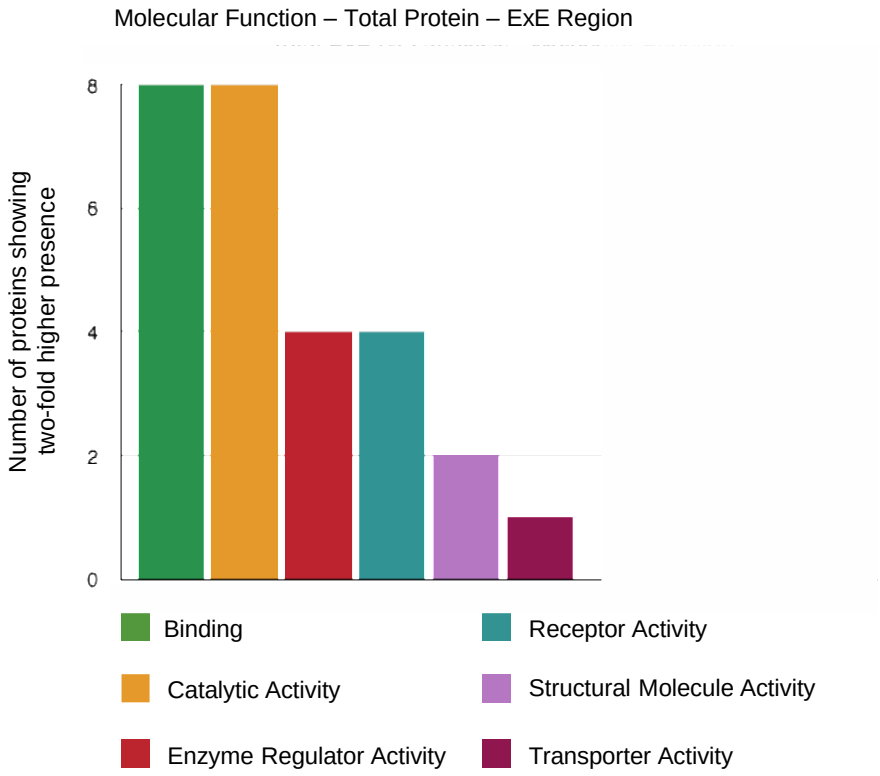


Figure 6.10: Molecular Function PANTHER analysis of Total Protein mass spectrometry data - ExE region

PANTHER classification of the proteins that showed a minimum of a two-fold higher expression level in the ExE region than the Epiblast region. Proteins were classified according to Molecular Function.

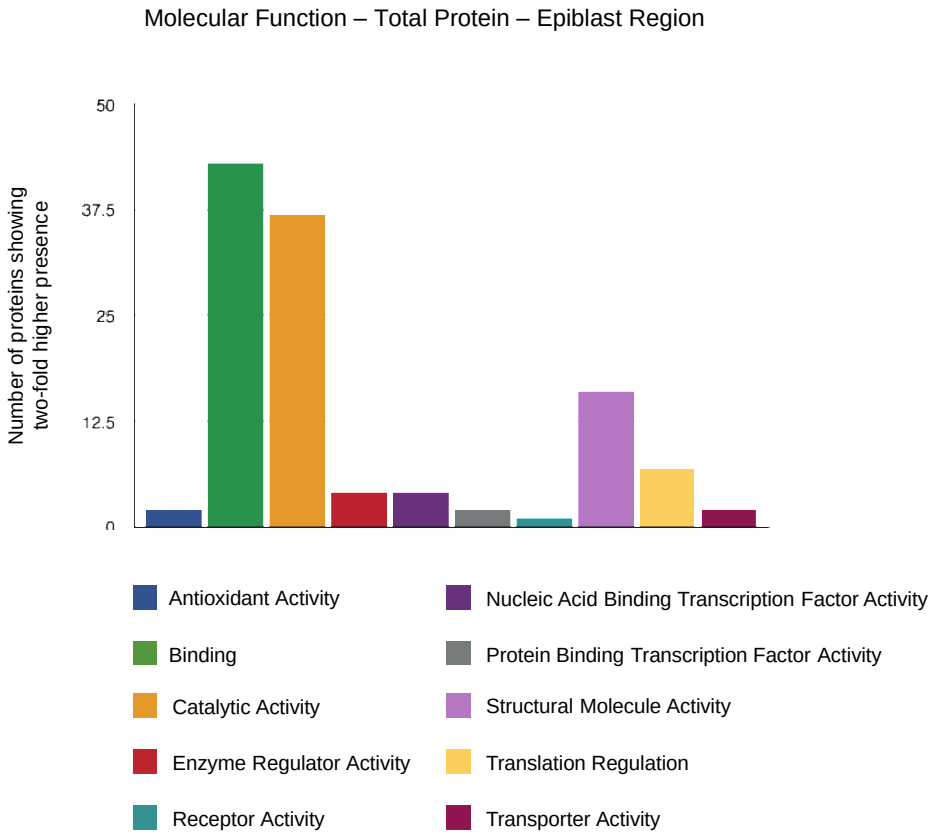


Figure 6.11: Molecular Function PANTHER analysis of Total Protein mass spectrometry data - Epiblast region

PANTHER classification of the proteins that showed a minimum of a two-fold higher expression level in the Epiblast region than the ExE region. Proteins were classified according to Molecular Function

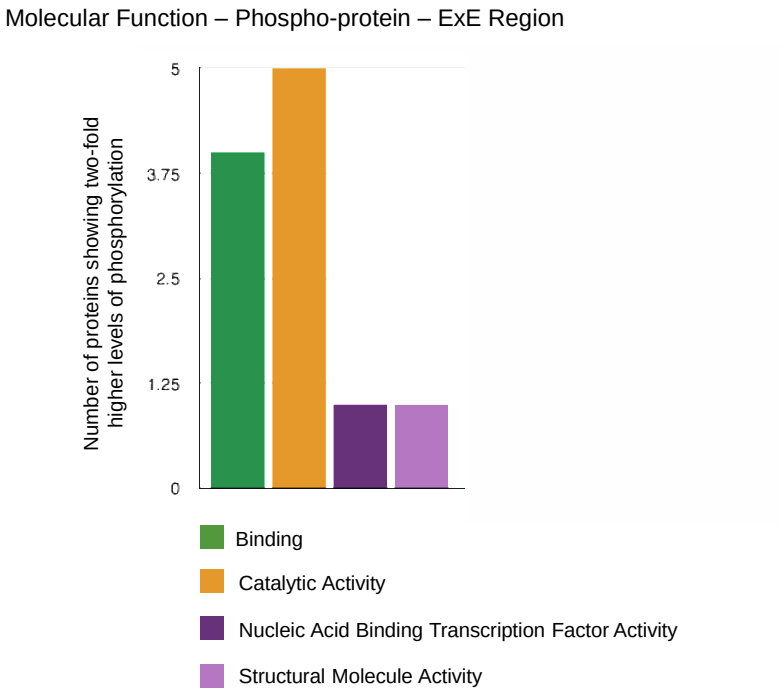


Figure 6.12: Molecular Function PANTHER analysis of Phospho-protein mass spectrometry data - ExE region

PANTHER classification of the proteins that showed a minimum of a two-fold higher phosphorylation level at specific regions in the ExE region than the Epiblast region. Proteins were classified according to Molecular Function

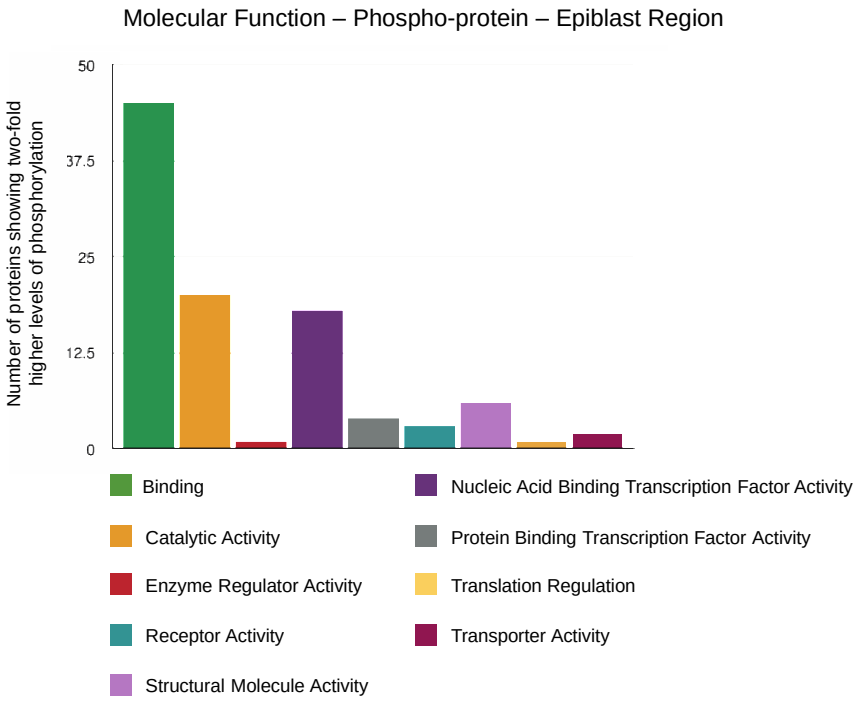


Figure 6.13: Molecular Function PANTHER analysis of Phospho-protein mass spectrometry data - Epiblast region

PANTHER classification of the proteins that showed a minimum of a two-fold higher phosphorylation level at specific regions in the ExE region than the Epiblast region. Proteins were classified according to Molecular Function

6.2.2.2.2 KEGG analysis

Analysis was also performed using the KEGG database (Kyoto Encyclopaedia of Genes and Genomes) to determine if any signalling pathways were systematically upregulated in either region [183], [184]. However, no pathways showed a significantly higher representation in the data.

6.2.2.2.3 Uniprot Database - Secreted Factor Analysis

Secreted factors are of great relevance at this stage of development, with nulls of some secreted proteins being embryonic lethal. These include Nodal and BMP4 [185], [186]. Further, it has been shown that secreted factors from the ExE restrict the induction of the AVE to the distal tip at E5.5. If the ExE is removed, the region of VE induced as AVE expands to cover the whole epiblast [30].

As such I examined the output of the mass spectrometry for known secreted proteins, using the UniProt Database [187][188]. Eight proteins in total came out of the Total and Phospho-protein datasets.

From the Total Protein data, only MIF (Macrophage inhibitory factor) was found in the Epiblast region to be both secreted and have a higher expression level than the ExE region. Four proteins were found to be secreted from the ExE region with a higher expression level than the Epiblast region. These were, Lit2 (Lithostathine-2), Lamβ1 (Laminin subunit beta-1), Serpina3K (Serine protease inhibitor A3K) and GILT (Gamma-interferon-inducible lysosomal thiol reductase).

From the Phospho-protein data, C163A, (Scavenger receptor cysteine-rich type 1) was the only secreted protein detected in the Epiblast region with a higher expression level than the ExE region.

Lad1 (Ladinin-1) and Tgfβ2 (Transforming growth factor beta-2) were secreted phosphorylated proteins detected in the ExE region with a higher expression level than the Epiblast region.

6.2.2.2.4 Gene Ontology Database Keyword Search

In addition to molecular function and biological process classification, PANTHER provides detailed gene ontology descriptions for a given list of proteins, collected from a range of gene ontology databases. This output was searched for keywords related to multiple areas of interest. Proteins involved in cell migration, cytoskeleton rearrangement, endocytosis, vesicle formation/transport, and calcium signalling were deemed "Proteins of Interest". Additionally, the gene ontology database readouts were searched for any reference to 49 key words, including 'PCP', 'LIMK', 'Rho', 'GEF', 'Rac', 'Dvl', 'arrestin', 'profilin', 'formin', and 'myosin'. The full list of terms and gene ontology readouts for proteins that had positive matches can be found in Appendix 3.

The proteins identified as being of interest from the Total Protein data are found in Table 6.1, while the proteins selected from the Phospho-protein data are shown in Table 6.2.

Table 6.1: Proteins of Interest from the Total Protein Mass Spectrometry data

Proteins of interest from the total protein mass spectrometry results. The 'Protein' column refers to the common name of the Protein of Interest. The 'Gene' column is the corresponding Uniprot gene name that was used for analysis in various databases. The 'Area' column refers to the embryo region that showed a minimum of 2x higher expression over the other.

Protein	Gene	Region
T-complex protein 1 subunit delta	TCPD_MOUSE	Epi
Beta-actin-like protein 2	ACTBL_MOUSE	Epi
Profilin-1	PROF1_MOUSE	Epi
SWI/SNF complex subunit SMARCC1	SMRC1_MOUSE	Epi
Tubulin alpha-1A chain	TBA1A_MOUSE	Epi
Calcium-regulated heat stable protein 1	CHSP1_MOUSE	Epi
Translationally-controlled tumour protein	TCTP_MOUSE	Epi
Serine/threonine-protein phosphatase PP1-alpha catalytic subunit	PP1A_MOUSE	Epi
Myosin-10	MYH10_MOUSE	Epi
Nucleosome assembly protein 1-like 1	NP1L1_MOUSE	Epi
TRAF2 and NCK-interacting protein kinase	TNIK_MOUSE	Epi
Heat shock protein HSP 90-beta	HS90B_MOUSE	Epi
Nexilin	NEXN_MOUSE	Exe
Lithostathine-2	LIT2_MOUSE	Exe
Cubilin	CUBN_MOUSE	Exe
Ezrin	EZRI_MOUSE	Exe
Laminin subunit beta-1	LAMB1_MOUSE	Exe
Serpin H1	SERPH_MOUSE	Exe
Junction-mediating and -regulatory protein	JMY_MOUSE	Exe
Serpin H1	SERPH_MOUSE	Exe

Table 6.2: Proteins of Interest from Phospho-protein mass spectrometry data.

The 'Protein' column refers to the common name of the Protein of Interest. The 'Gene' column is the corresponding Uniprot gene name that was used for analysis in various databases. The 'Area' column refers to the embryo region that showed a minimum of 2x higher expression over the other (continued overleaf).

Protein	Gene	Region
Protein ajuba	JUB_MOUSE	Epi
SWI/SNF complex subunit SMARCC1	SMRC1_MOUSE	Epi
MARCKS-related protein	MRP_MOUSE	Epi
Protein Shroom2	SHRM2_MOUSE	Epi
Drebrin	DREB_MOUSE	Epi
Calmodulin-regulated spectrin-associated protein 3	CAMP3_MOUSE	Epi
Stathmin	STMN1_MOUSE	Epi
Microtubule-associated protein 4	MAP4_MOUSE	Epi
Serine/arginine repetitive matrix protein 2	SRRM2_MOUSE	Epi
Dynein heavy chain, axonemal	DYH8_MOUSE	Epi
CLIP-associating protein 1	CLAP1_MOUSE	Epi
MARCKS-related protein	MRP_MOUSE	Epi
Myristoylated alanine-rich C-kinase substrate	MARCS_MOUSE	Epi
Scavenger receptor cysteine-rich type 1 protein M130	C163A_MOUSE	Epi
Protein PML	PML_MOUSE	Epi
Lipolysis-stimulated lipoprotein receptor	LSR_MOUSE	Epi
Smad nuclear-interacting protein 1	SNIP1_MOUSE	Epi
Synaptosomal-associated protein 23	SNP23_MOUSE	Epi

Heat shock protein beta-1	HSPB1_MOUSE	Exe
Na(+)/H(+) exchange regulatory cofactor NHE-RF1	NHRF1_MOUSE	Exe
Band 4.1-like protein 3	E41L3_MOUSE	Exe
Titin	TITIN_MOUSE	Exe
Spectrin alpha chain, brain	SPTA2_MOUSE	Exe
CAP-Gly Domain Containing Linker Protein 1	CLIP1_MOUSE	Exe
Kinesin-like protein KIF15	KIF15_MOUSE	Exe
AP2-associated protein kinase 1	AAK1_MOUSE	Exe
Protein kinase C and casein kinase substrate in neurons protein 1	PACN1_MOUSE	Exe
Low-density lipoprotein receptor-related protein 2	LRP2_MOUSE	Exe
Syntaxin-7	STX7_MOUSE	Exe

6.2.2.3 Comparison of Mass Spectrometry Results to a Previously Published Screen

The microarray performed by Gonçalves et al. that investigated gene expression in AVE cells of E5.5 embryos utilizing Affymetrix GeneChip technology generated a large dataset depicting differences between the Proximal Anterior and Proximal Posterior regions of E5.5-5.75 embryos.
In the phosphorylated data Wnk3, a serine/threonine kinase emerged from both screens. In the total data, Ubp24 (Ubiquitin carboxyl-terminal hydrolase 24) and Lamβ1 (Laminin subunit beta-1) were present in both screens.

6.2.2.4 Searching the data for proteins known to cause an NTD

PCP signalling has been shown to play a role in AVE migration, and defects in PCP signalling are well known to cause neural tube defects in both mouse and human [5], [127] . Because of this link, I compared proteins which showed a two-fold difference in total levels or phosphorylation level between the Epiblast region and ExE regions in the mass spectrometry analysis to a published list of genes known to cause NTD when knocked out or mutated [189]. The results are shown in Tables 6.3 and 6.4.

Table 6.3: Proteins known to be involved in neural tube defects that show a higher protein expression in region of the embryo.

The 'Protein' column refers to the common name of the protein of interest. The 'Gene' column is the corresponding Uniprot gene name that was used for analysis in various databases. The 'Region' column refers to the embryo region that showed a minimum of 2x higher expression over the other. "Epi" refers to the Epiblast and the overlying Epi-VE. No proteins that matched the criteria were found in the 'ExE'.

Protein	Gene	Region
Profilin-1	PROF1_MOUSE	Epi
SWI/SNF complex subunit SMARCC1	SMRC1_MOUSE	Epi

Table 6.4: Proteins known to be involved in neural tube defects that show phosphorylation at a higher rate in one region of the embryo.

The 'Protein' column refers to the common name of the Protein of Interest. The 'Gene' column is the corresponding Uniprot gene name that was used for analysis in various databases. The 'Area' column refers to the embryo region that showed a minimum of 2x higher phosphorylation over the other. "Epi" refers to the epiblast and the overlying Epi-VE. No proteins that matched the criteria were found in the 'ExE' region.

Protein	Gene	Region
SWI/SNF Related Matrix Associated Actin Dependent Regulator Of Chromatin	SMCA4_MOUSE	Epi
SWI/SNF complex subunit SMARCC1	SMRC1_MOUSE	Epi
DNA (cytosine-5)-methyltransferase 3B	DNM3B_MOUSE	Epi
Treacher Collins-Franceschetti Syndrome protein	TCOF_MOUSE	Epi

6.2.2.5 Established antibodies were identified for several proteins of interest from each dataset

All of the proteins which showed were known to be secreted, showed interactions not related to DNA in the STRING analysis were added to the list of 'Proteins of Interest' from GO analysis of the Total and Phospho-protein data. A literature review and extensive antibody database search was then performed to identify the existence of a previously established functioning antibody for each protein.

From the Total protein data, antibodies were available for five proteins in the ExE region, and four in the Epiblast region were identified. Several of these were tested, as detailed below, however several remain to be investigated at a later date. These can be found in Table 6.5.

From the Phospho-protein data, no antibodies could be found which were established to function within the early mouse embryo. However two were found which had been established in mammalian cells. These can be found in Table 6.6.

Table 6.5: Proteins of Interest from the Total Protein Mass Spectrometry dataset for which a validated antibody can be found in the literature

The 'Protein' column refers to the common name of the protein of interest. The 'Gene' column is the corresponding Uniprot gene name that was used for analysis in various databases. 'Knockout' refers to the phenotype of a knockout mutant of the protein in question, if it has been established. 'Region' refers to the embryo region that showed a minimum of 2x higher expression over the other.

Protein	Gene	Knockout	Region
Profilin-1	PROF1_MOUSE	Lives to 2 cell	Epi
Myosin-10	MYH10_MOUSE	Unknown	Epi
Heat shock protein HSP 90-beta	HS90B_MOUSE	Lives to 9.0	Epi
TRAF2 and NCK- interacting protein kinase	TNIK_MOUSE	Fully viable – cognitive defects	Epi
T-complex protein 1 subunit delta	TCPD_MOUSE	Unknown	Epi
Ezrin	EZRI_MOUSE	Dies just after birth	ExE
Junction-mediating and regulatory protein	JMY_MOUSE	Unknown	ExE
Nexilin	NEXN_MOUSE	Unknown	ExE
Serine protease inhibitor A3K	SPA3K_MOUSE	Unknown	ExE
Serpin H1	SERPH_MOUSE	Dies at 11.5	ExE
Ezrin	EZRI_MOUSE	Dies just after birth	ExE
Junction-mediating and regulatory protein	JMY_MOUSE	Unknown	ExE

Table 6.6: Proteins of Interest from the Phospho-protein Mass Spectrometry dataset for which a validated antibody can be found in the literature

The 'Protein' column refers to the common name of the protein of interest. The 'Gene' column is the corresponding Uniprot gene name that was used for analysis in various databases. 'Knockout' refers to the phenotype of a knockout mutant of the protein in question, if it has been established. The 'Region' column refers to the embryo region that showed a minimum of 2x higher expression over the other.

Protein	Gene	Knockout	Region
Stathmin	STMN1_MOUSE	Viable	Epi
Heat shock protein beta-1	HSPB1_MOUSE	Unknown	ExE

6.2.3 Investigation of candidate proteins by Immunohistochemistry

From the established antibodies, Profilin and Rab5 were chosen from the Total protein data further investigation and to validate the mass spectrometry results. p-Stathmin(Ser38) was chosen from the Phospho-protein data.
Unfortunately, the Rab5 antibody could not be optimized, and showed inconsistent staining across batches (n=33, of 5 batches). Profilin, Stathmin and p-Stathmin(Ser38) antibodies showed a reliable stain.

6.2.3.1 Profilin Immunohistochemistry

Profilin is a cytoskeletal regulatory protein. It can sequester monomeric actin in a 1:1 ratio and can inhibit actin polymerization. Under certain conditions, it can also enhance actin polymerization. The results of the mass spectrometry indicated that this protein was present at a 2.09-fold higher level in the Epiblast region than the ExE region at E6.25.

Embryos were initially immunostained for profilin at E6.25 to test the antibody and check for reliability of the protein mass spectrometry screen. In all cases the Epiblast region showed a higher level of profilin signal than the ExE region (n=17), which correlated with the results of the mass spectrometry (Figure 6.14).

When stained at a stage later than E6.25, E6.5 (n=18) and E6.75 (n=4), embryos showed slightly brighter profilin signal in the epiblast region, though this was far less pronounced than at E6.25 (Figure 6.15). Notably, at E6.5 the profilin stain appeared absent in the Epi-VE, but present in the ExE-VE.

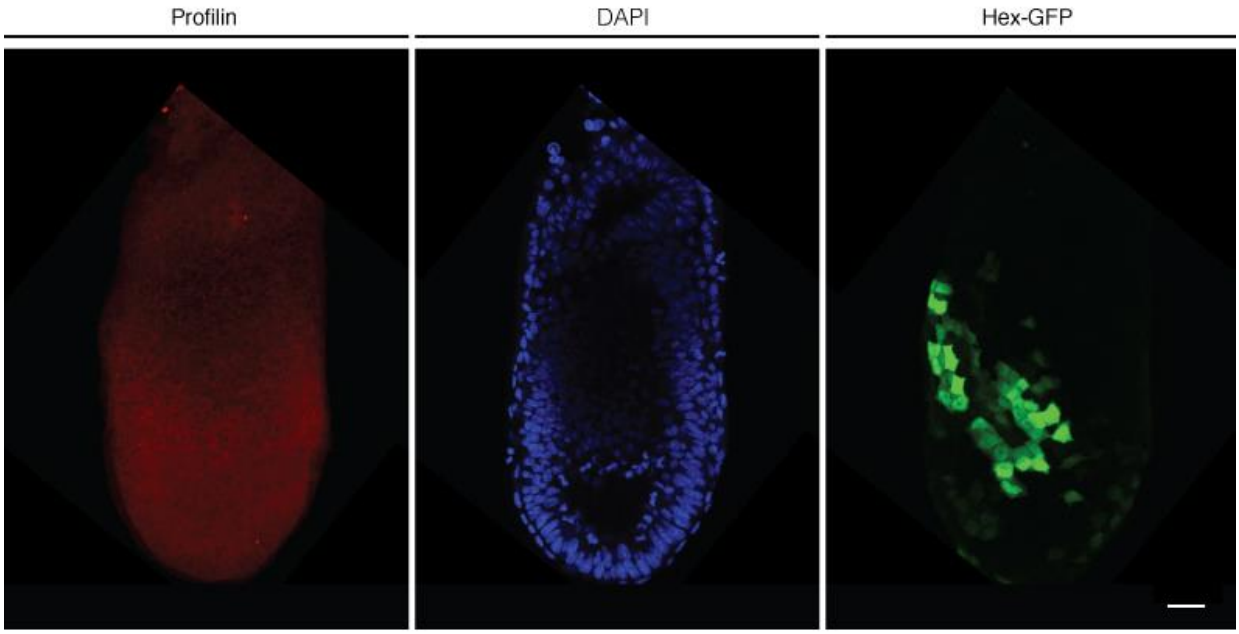


Figure 6.14: Profilin staining is stronger in the Epiblast region at E6.25.

Maximum intensity projection view of an E6.25 Hex-GFP embryo stained for Profilin and DAPI. Profilin staining intensity is higher in the Epiblast region than the ExE region (n = 17).

Profilin is shown in red (left), Hex-GFP indicates the cells of the AVE, shown in green (right). DAPI staining is also shown (middle). Scale bar = 35 μm

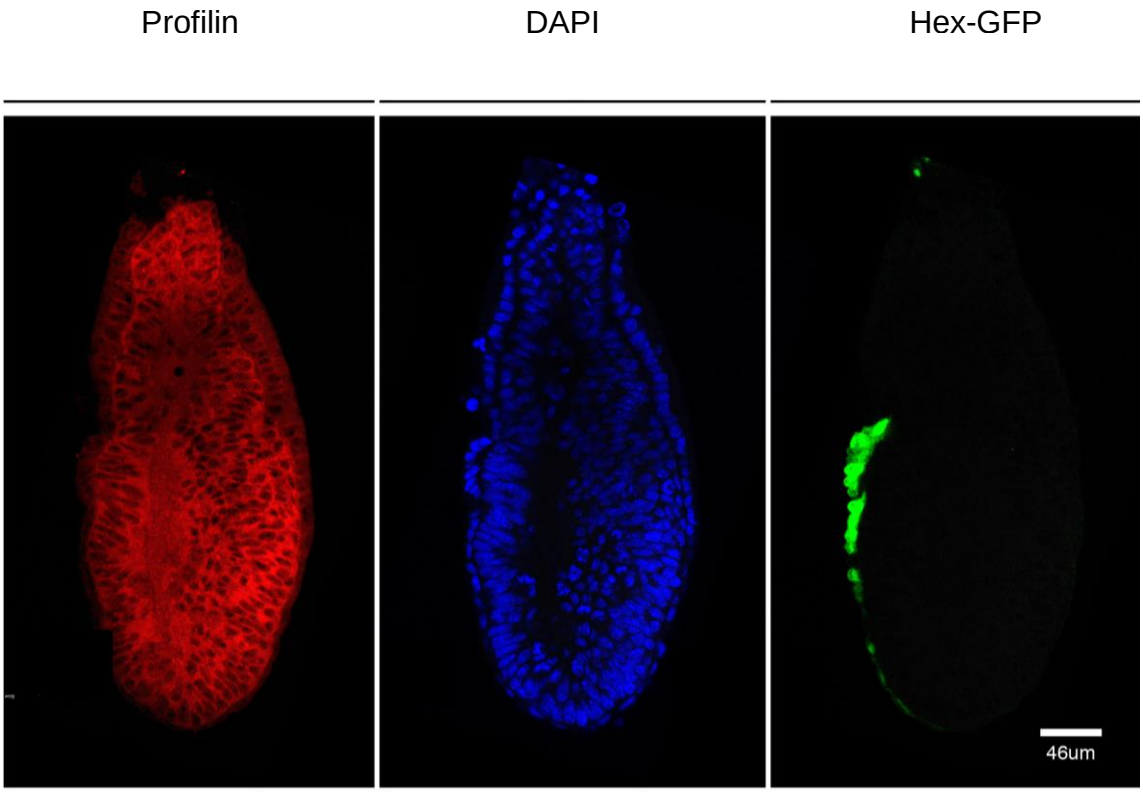


Figure 6.15: Profilin immunostaining in the E6.5 Hex-GFP embryo

Optical section view of an E6.5 Hex-GFP embryo stained for Profilin and DAPI. Profilin staining intensity is slightly higher in the Epiblast region than the ExE region (n = 18).

Profilin is shown in red (left), Hex-GFP indicates the cells of the AVE, shown in green (right). DAPI staining is also shown (middle). Scale bar = 46 μm

Embryos were then immunostained for profilin at E6.0, and E5.5. At E6.0 the difference between the two regions was far more pronounced (Figure 6.16). Strong signal was seen in the epiblast, particularly beneath the basement membrane of the VE. When optical sections were examined it could be seen that in contrast to E6.25 the Epi-VE exhibited a stronger staining than the ExE-VE (Figure 6.17). Though some signal was present in the ExE-VE in all samples, little to no signal was seen in the ExE (n=12).

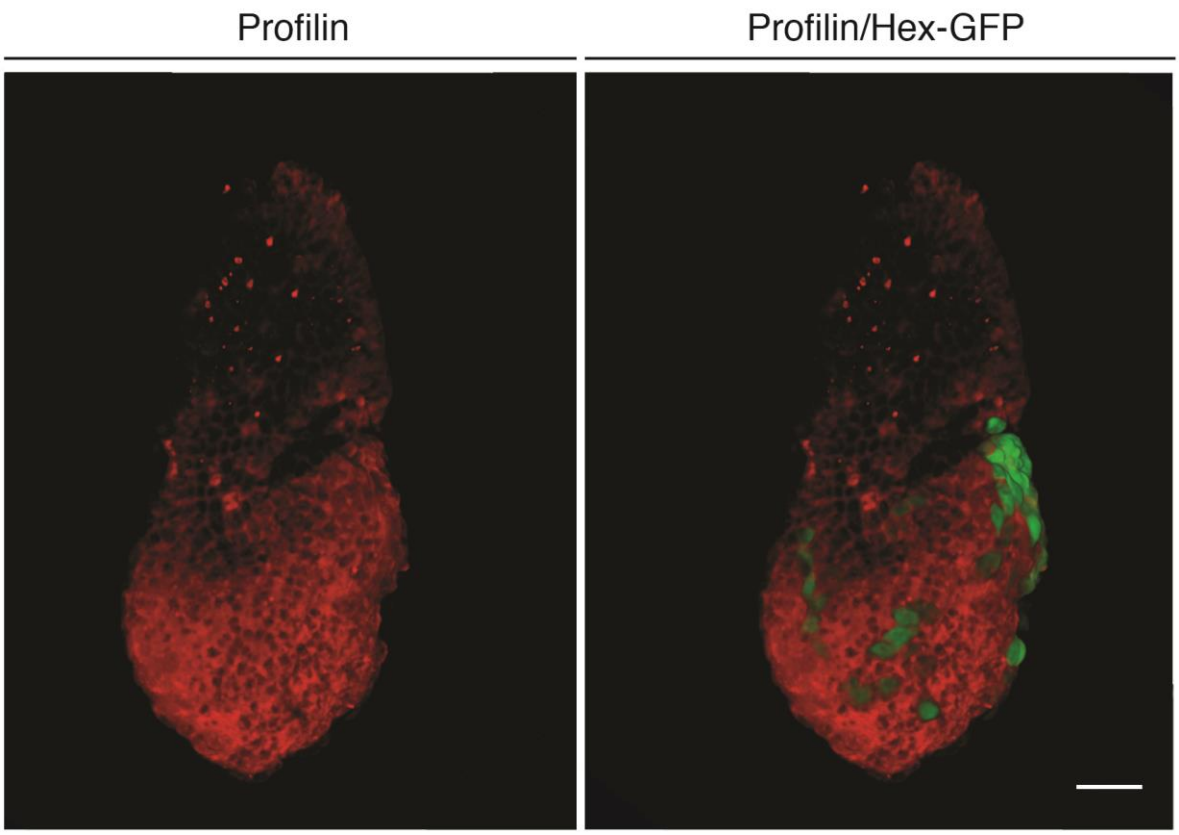


Figure 6.16: Profilin staining is stronger in the Epiblast region at E6.0.

Maximum intensity projection view of an E6.0 Hex-GFP embryo stained for Profilin and DAPI. Profilin staining intensity is higher in the Epiblast region than the ExE region (n = 12).

Profilin is shown in red (left), Hex-GFP indicates the cells of the AVE, shown in green (right). Scale bar = 35 μm

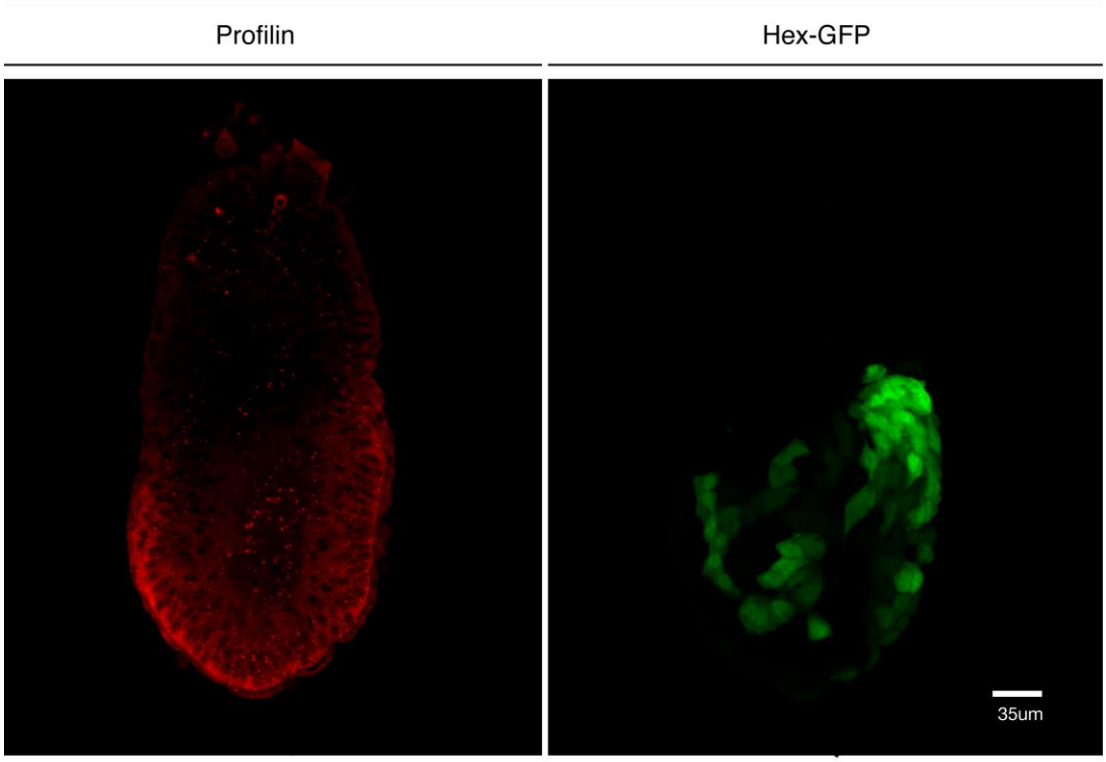


Figure 6.17: Profilin immunostaining in the E6.0 Hex-GFP embryo

Optical section view of an E6.0 Hex-GFP embryo stained for Profilin. Profilin staining intensity is present in the Epiblast and absent in the ExE (n = 12). Profilin is shown in red (left), Hex-GFP indicates the cells of the AVE, shown in green (right). Scale bar = 35 μm

At E5.5, the profilin signal is only very slightly higher in the Epiblast than the ExE, as can be seen in Figure 6.18. Profilin is predominantly absent in the cells of the Visceral Endoderm (n=14).

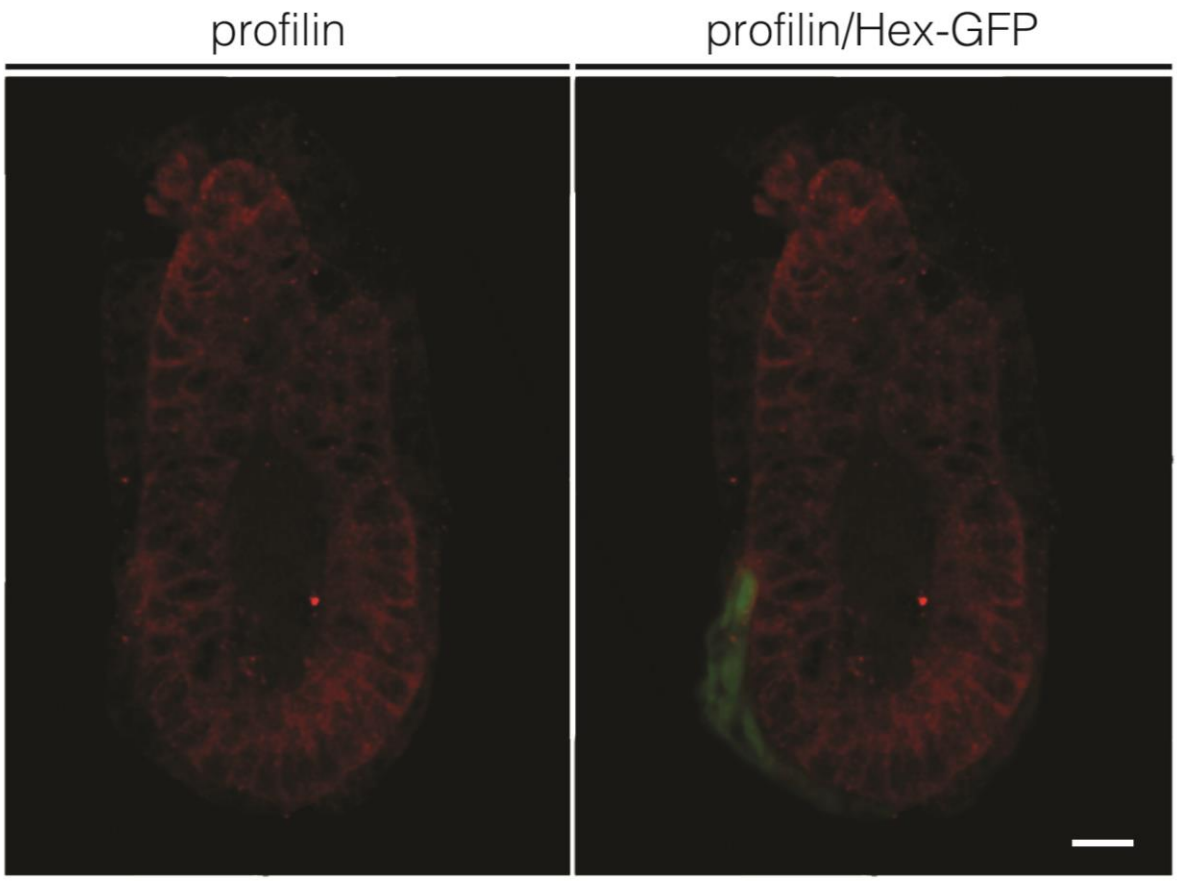


Figure 6.18: Profilin staining in the E5.5 Hex-GFP embryo.

Optical section projection view of an E5.5 Hex-GFP embryo stained for Profilin. Profilin staining intensity is slightly higher in the Epiblast region than the ExE region (n = 12).

Profilin is shown in red (left), Hex-GFP indicates the cells of the AVE, shown in green (right). Scale bar = 35 μm

Prior to AVE migration, the E5.25 embryo showed a striking inversion of the relative profilin enrichment seen at the later stages (Figure 6.19). The profilin was stronger in the ExE in all samples where the AVE had yet to migrate (n=6).

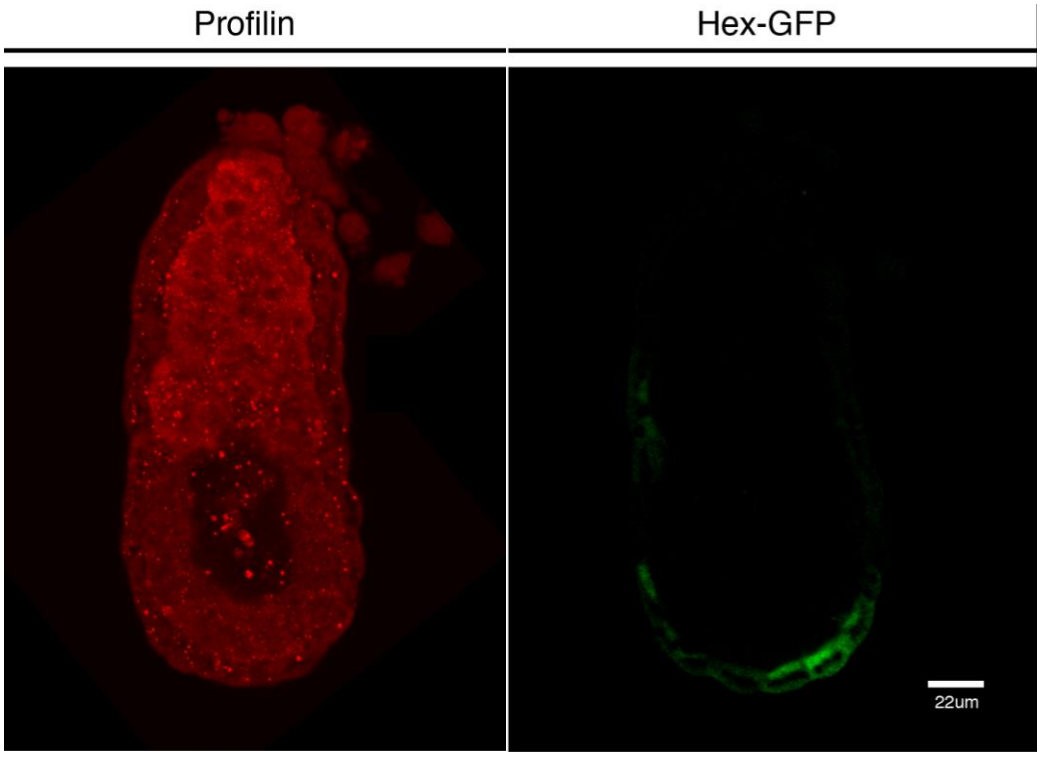


Figure 6.19: Profilin staining in the E5.25 Hex-GFP embryo.

Optical section projection view of an E5.0 Hex-GFP embryo stained for Profilin. Profilin staining intensity is higher in the ExE region than the Epiblast region (n = 12).

Profilin is shown in red (left), Hex-GFP indicates the cells of the AVE, shown in green (right). Scale bar = 22 μm

6.2.3.2 Stathmin and p-Stathmin immunohistochemistry

An antibody for non-phosphorylated Stathmin was available in addition to the antibody from p-Stathmin(Ser38), which was utilized as a comparison to the stainings for the phosphorylated protein.
Embryos were stained at E.5.5 and E6.25 with the Stathmin antibody. At E6.25, Stathmin appeared localized to the Epiblast, underlying the basement membrane of the Visceral Endoderm (n=5) (Figure 6.20). At E5.25 no visible difference was seen between the intensity of staining between the Epiblast or ExE tissues. Stathmin showed increased localisation in the AVE in several embryos (n= 3 of 7) (Figure 6.21).

When stained for an antibody against p-Stathmin(Ser38), signal was heavily seen in the epiblast at all stages investigated. (Figure 6.22 and Figure 6.23)
The results of this at the E6.25 stage (n=9) match that of the mass spectrometry screen, giving weight/credence to the reliability of the Phospho-proteomic data (Figure 6.22).
At E5.5 some embryos showed a slightly higher p-Stathmin(Ser38) signal in the AVE than the rest of the VE though this was not a significant portion of the stained embryos (n=15).

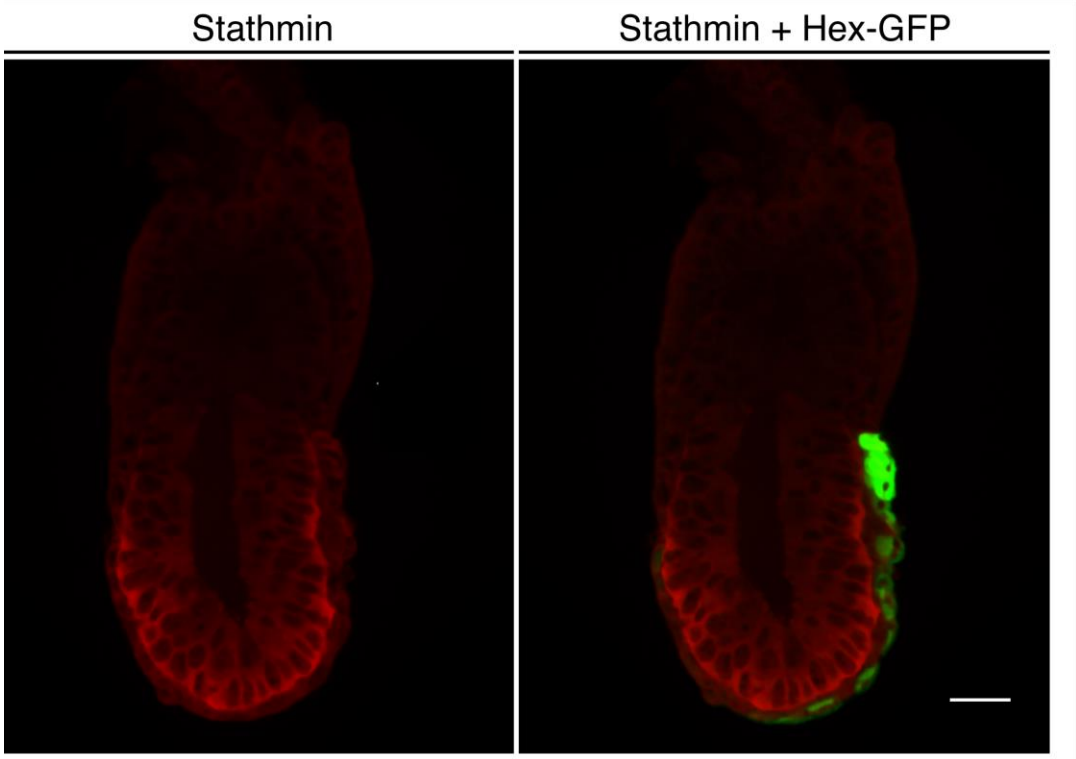


Figure 6.20: Stathmin staining in the E6.25 Hex-GFP embryo

Optical section projection view of an E6.25 Hex-GFP embryo stained for non-phosphorylated Stathmin.

Stathmin staining intensity is highest in the Epiblast. (n = 5).

Stathmin is shown in red (left), Hex-GFP indicates the cells of the AVE, shown in green (right). Scale bar = 22 μm

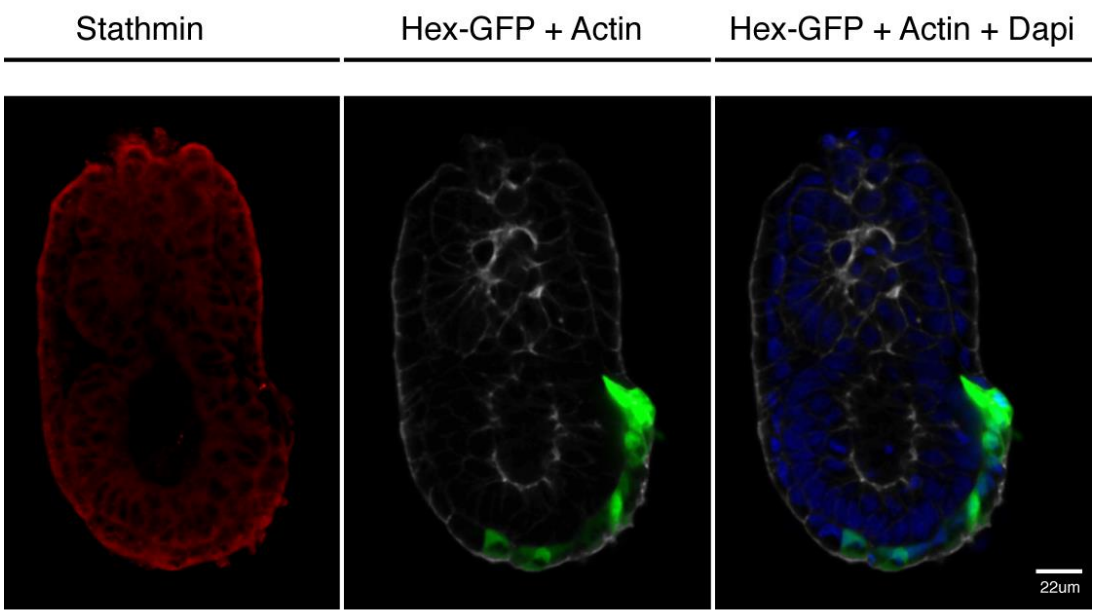


Figure 6.21: Stathmin staining in the E5.5 Hex-GFP embryo

Optical section projection view of an E5.5 Hex-GFP embryo stained for non-phosphorylated Stathmin, phalloidin and DAPI. (n=7)

Stathmin is shown in red (left), Hex-GFP indicates the cells of the AVE, shown in green (middle, right). DAPI is also shown (right). Scale bar = 22 μm

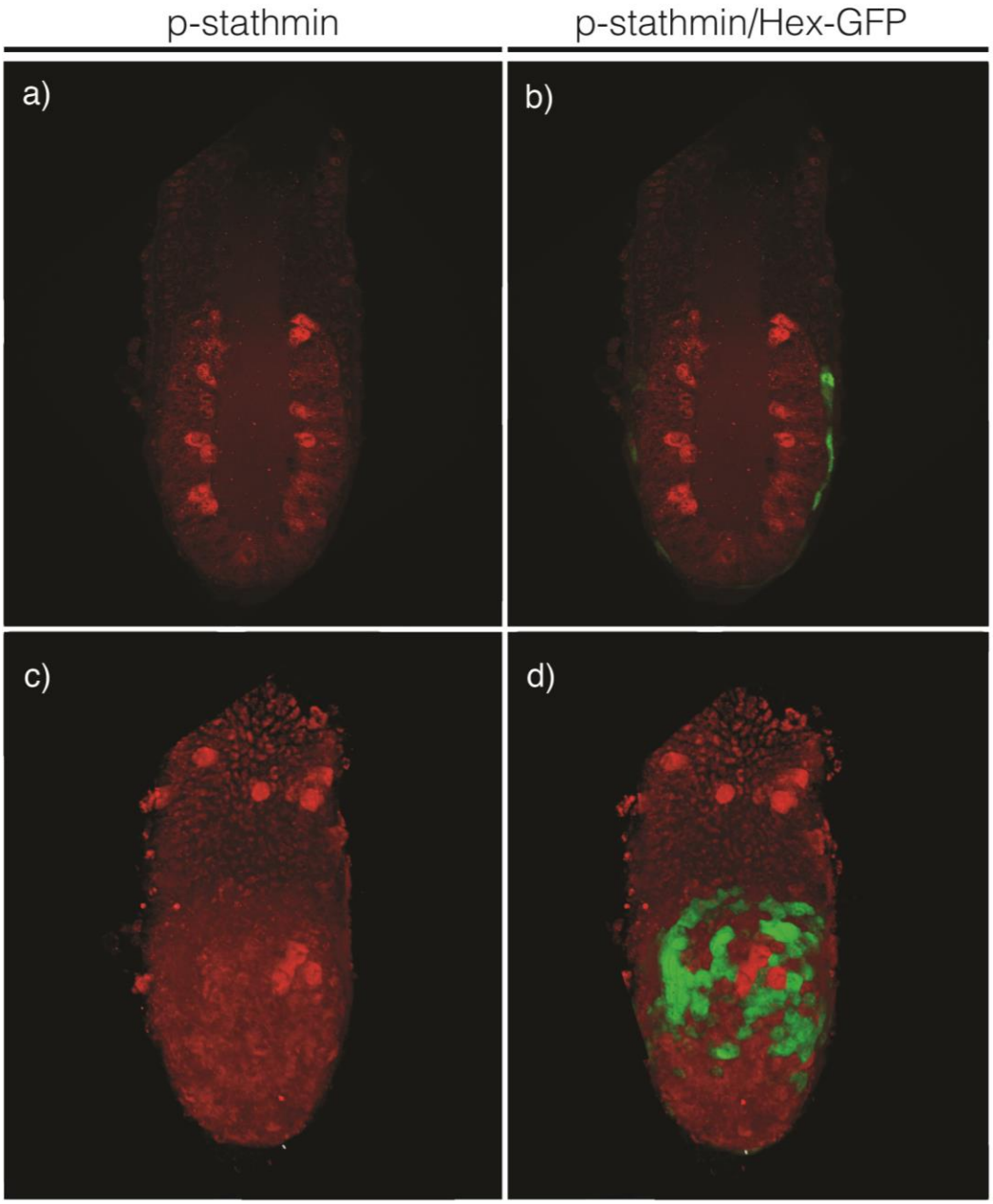


Figure 6.22: Phospho-Stathmin staining in the E6.25 Hex-GFP embryo.

(a) and (b) show optical section views of an E6.25 Hex-GFP embryo stained for phosphorylated Stathmin (n=9).

(c) and (d) show maximum intensity projection views of the same E6.25 Hex-GFP embryo stained for phosphorylated Stathmin (n=9).

In both rows, Stathmin is shown in red (left), Hex-GFP indicates the cells of the AVE, shown in green (middle, right).

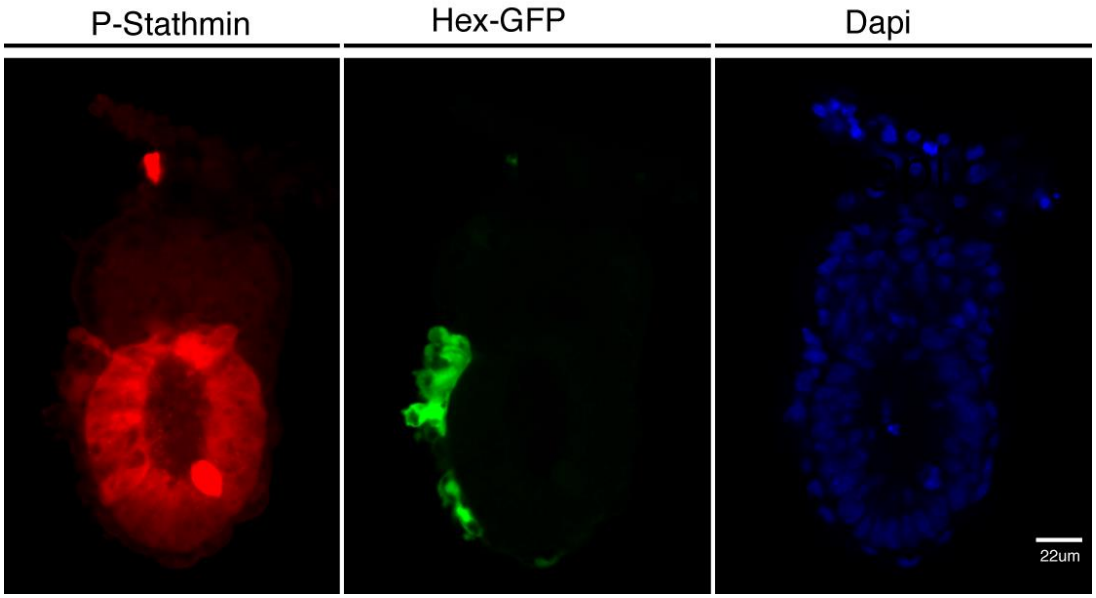


Figure 6.23: Phospho-Stathmin staining in the E5.5 Hex-GFP embryo.

Optical section views of an E6.25 Hex-GFP embryo stained for phosphorylated Stathmin and DAPI. (n=15).

Stathmin is shown in red (left). Hex-GFP indicates the cells of the AVE, shown in green (middle). DAPI is also shown (right). Scale bar = 22 μm

6.3 Discussion

Ideally, cells of the ExE, Epiblast, Epi-VE, ExE-VE and AVE would have been compared. This however, would have required a huge number of embryos to generate the minimum number of cells needed for mass spectrometry. Additionally, they would have needed to be sorted efficiently. Potentially, flow cytometry could have been used to separate the cells, but this would have resulted in some loss of sample material while sorting, further increasing the number of embryos used. Finally, the use of flow cytometry would require that transgenic mice were used, which were fluorescent in the different regions of the embryo. As these mice are not currently available to us, this would have drastically increased the length and difficulty of the project, taking it out of the scope of this PhD. Flow cytometry was avoided by Gonçalves et al. in their AVE cell screen, while maintaining a high level of regional specificity [166]. However, this meant that very small regions had to be dissected from transgenic embryos, which would drastically raise the ratio of damaged to healthy cells that were analysed. As phosphorylation is a rapid post-translational modification that affects many proteins upon cell damage, this was not an appropriate approach for this project. For these reasons a mid-way approach was used, where key proteins were identified using mass spectrometry performed on halved embryos.

6.3.1 String analysis

Increased expression in the case of total protein data, or alternative regulation of a protein in different regions of an embryo is an indication of different behaviour in the constituent cells. However, data generating large protein lists can be difficult to interpret, due to the high numbers of factors to consider, and the complex nature of proteins which may be involved in a number of signalling cascades, scaffolding functions and regulatory processes. The systematic

upregualtion of several components of a particular pathway can reveal patterns of activity within the data. To probe the data for protein interactions between the unregulated and differently phosphorylated proteins I used STRING analysis.

Total protein data

In the ExE region, the total protein data showed only two groups of connected proteins. These were ANXA5/TAGLN2 and Lamβ1/Dab2/Cubilin. AnxA5 (Annexin) is an anticoagulant protein, involved in the blood coagulation and very little is known about Taglnn2 (Transgelin) so these proteins were not followed up. Lamβ1 is a basement membrane protein, which made this interaction highly of interest, due to the role of tension on actin behaviour [190]. Lamβ1 was investigated for an established antibody, however none was found.

In the Epiblast region, the Total protein showed a great deal of interaction. Some connection pathways such as Mcm2/Mcm3/Prim2/Msh2/Rpa were not followed up as they were DNA replication or repair pathways. Additionally many proteins were involved in ribosomal activity and maintenance. This still left a large number of connections.

Rab5 and Profilin showed a high number of interactions, which contributed strongly to these proteins being chosen for further characterization.

Phospho-protein data

In the STRING analysis of the Phospho protein data there were only two interactions in the ExE, Fen1/Rad50 and Spna2/Epb4.1L3. The Fen1/Rad50 link was not considered further as they are DNA damage repair proteins. The Spna2/Epb4.1L3 interaction, however, is highly of interest. Spectrin interacts with calmodulin in a calcium-dependent manner and is a candidate for the

calcium-dependent movement of the cytoskeleton at the membrane. Epb4.1L3 (erythrocyte protein band 4.1-like 3 Gene; Isoform 2) interacts with spectrin and actin [187]. This interaction could be involved in the stationary behaviour of the Visceral Endoderm cells, and the maintenance of the actin shroud, which is visible during AVE migration. It was not investigated however as no antibodies for either protein at the correct phosphorylation sites were available.

In the Epiblast region a very high number of interactions were seen but only one, the interaction between Marcksl1/Marcks, was found that was not likely upregulated due to a role in DNA replication or repair. This is understandable due to the high level of cell division occurring in the Epiblast at this stage, and the prominent role of phosphorylation in cell cycle regulation (reviewed in [170]). Marcksl1 and Marcks are calmodulin, actin, and synapsin binding proteins [187]. Further investigation of these proteins would be highly of interest, however no antibodies for either protein at the correct phosphorylation sites were available.

6.3.2 Gene Ontology Analysis

6.3.2.1 PANTHER Gene Ontology Analysis

Biological Process Analysis

In the biological process GO analysis of the total protein data, twice the proportion of categorized proteins showed a metabolic role in the Epiblast region than the ExE region. Given the high level of division and activity in the cells of the Epiblast, this further lends weight to the reliability of the mass spectrometry data. Further to this higher levels of proteins deemed as having a role in developmental processes were seen in the ExE region, which is expected as these cells are specified and involved in patterning, while the

Epiblast cells that make up the majority of the Epiblast region are undifferentiated.

In the biological process GO analysis of the Phospho-protein data, a much higher proportion of proteins were classified as having a role in localisation. This might reflect an increased level of endocytosis in the ExE-VE, implied by the increased amounts of microvilli seen in this region [191].

Molecular Function Analysis

In the molecular function GO analysis of the Total Protein data, No proteins in the ExE sample were categorized as having antioxidant activity, nucleic acid binding transcription factor activity, protein binding transcription factor activity or translation regulation activity and the most represented categories in both regions were binding and catalytic activities.

The absence of nucleic acid binding transcription factor activity, protein binding transcription factor activity and translation regulation activity proteins in the ExE region is unsurprising given that the majority of cell division is occurring in the epiblast at this stage, and cells of the ExE are more differentiated than those of the epiblast. This adds confidence that the mass spectrometry data reflects the real protein content of the two regions.

In the molecular function GO analysis of the Phospho-protein data, the Epiblast region the fraction of proteins categorized as having catalytic activity was far lower than that of the binding region, which in the Phospho-protein ExE region and both regions in the Total protein results had consistently shown comparable levels. This is unusual, as the increased activity associated with the Epiblast at this stage implies that large amounts of catalytic functions

would be taking place. It may be the case that phosphorylation plays more of a role in targeting localisation of proteins, or marking them for degradation than would be initially expected at this stage.
Proportionally high levels of proteins categorized as having nucleic acid binding transcription factor activity were present in the Epiblast, which corresponds to the large amount of DNA replication occurring in this region. Very few proteins emerged from the ExE region analysis as having specific molecular function annotation. Of these, the highest category was catalytic function.

While the PANTHER analysis of function was highly of interest and supportive of the validity of the mass spectrometry results, the categorization was heavily dominated by the functions of the larger tissues, the epiblast and the ExE in each region. While the behaviour of these tissues is interesting, in order to find potential candidates for the behaviour of the Visceral Endoderm, other types of analysis were performed on the data.

6.3.3 Comparison of Mass Spectrometry Results to a Previously Published Screen

The microarray performed by Gonçalves et al. that investigated gene expression in AVE cells of E5.5 embryos utilizing Affymetrix GeneChip technology generated a large dataset depicting differences between the Proximal Anterior and Proximal Posterior regions of E5.5-5.75 embryos. Upregulation of many known AVE markers such as *Lefty1*, *Cer1*, *Gsc*, *Hesx1*, *Lhx1* (*Lim1*), *Foxa2* and *Otx2* were seen to be present in the AVE region of the embryo [192]–[195]. In total Gonçalves et al. found 175 genes upregulated in the mid-migrating AVE region and 36 genes unregulated in the upper-posterior region sample.

As the AVE region is contained within the distal/epiblast embryo region of my screen, it stands to reason that several of the proteins may appear in both screens. It is unlikely that all (or most) of the genes expressed would be present in the epiblast region, as the Gonçalves screen compares two regions of the distal half of the embryo, and a difference between these two regions might appear in the Gonçalves screen, while a similar non-localised presence of that gene expressed in the ExE would exclude it from my screen, which compares the two halves of the embryo.

It is possible that there is not enough expression within the AVE cells to appear in my screen, and that the mass spec was not sensitive enough to detect many of the proteins.

However, if a protein were to be present in both screens, it could be argued that these are highly expressed proteins of the AVE cells, as they are enough to register as present in a two-fold higher manner throughout the entire distal half of the embryo, and are expressed only in the anterior VE. I therefore

compared both screens using the UniProt designations of the genes and proteins.

In the phosphorylated data Wnk3, a serine/threonine kinase emerged from both screens. In the total data, Ubp24 (Ubiquitin carboxyl-terminal hydrolase 24) and Lamβ1 (Laminin subunit beta-1) were present in both screens.

Laminin subunit beta-1 is the most interesting of these proteins, as its binding partners, laminin alpha and gamma did not come out of the Mass spectrometry screen and laminin alpha did not come out of the microarray screen.

As discussed in Chapter 5, laminins are heterotrimeric proteins that contain an α-chain, a β-chain and a γ-chain, each of which has several genetic variants. Different chains show different tissue distributions, indicating different roles *in vivo,* though this aspect of the field is largely uninvestigated [163]. Given the evidence presented in Chapter 5 that haptotaxis, migration along a gradient of adhesion, plays a role in the migration of the AVE, it is possible that an increased adhesive basement membrane caused by a particular form of laminin which contains the β1 subunit, is also involved in directed AVE migration.

It is however, particularly striking that the Lamβ1 emerged in both screens, as the Gonçalves screen took samples from two regions of the epiblast, and my Lamβ1 was shown to have over a two-fold higher presence in the ExE in the mass spectroscopy data. It could be that the levels of this protein change regionally between E5.5 and E6.25. However it is more likely that the far higher levels of Lamβ1 in the ExE overshadow the presence of Lamβ1 in the Epiblast in my screen.

6.3.4 Searching the data for proteins known to cause an NTD

Due to the role of PCP proteins in the migration of the AVE, I was particularly interested in finding candidates that might be linked to this pathway, either upstream of downstream. PCP proteins are well known to cause neural tube defects (NTDs). Because of this link, I compared proteins from the mass spectrometry analysis to a published list of genes known to cause NTDs [189]. SWI/SNF complex subunit SMARCC1 and Profilin-1 were hits from the total protein data. SWI/SNF Related Matrix Associated Actin Dependent Regulator Of Chromatin, Subfamily A Member, DNA (cytosine-5)-methyltransferase 3B, SWI/SNF complex subunit SMARCC1 and Treacher Collins-Franceschetti Syndrome protein emerged from the Phospho-protein data.

This generated several interesting candidates for further investigation. From reviews of the literature, most likely of these to have a strong phenotype during AVE migration is Profilin, a regulator of the actin cytoskeleton.

SMARCA4 (SWI/SNF Related, Matrix Associated, Actin Dependent Regulator Of Chromatin, Subfamily A, Member) is a protein that showed over a 2x difference in phosphorylation between the Epiblast region and the ExE region, being more highly phosphorylated in the Epiblast region. It is a member of the SWI/SNF family of proteins.

Another member of the SWI/SNF family, SMARCC1 (SWI/SNF Related, Matrix Associated, Actin Dependent Regulator Of Chromatin, Subfamily C, Member 1) was also present in both the total and phosphorylation categories. Being more highly expressed and more highly phosphorylated in the Epiblast region. The SWI/SNF family of proteins display helicase and ATPase activities, which are thought to regulate transcription of certain genes by altering the chromatin structure around those genes [196].

Given the larger amount of cell division in the epiblast, it is not entirely surprising that transcription proteins are expressed and activated in a higher amount in the epiblast. Given that differing rates of cell division were shown not to be involved in the AVE migration these candidates were not investigated further[197].

DNMT3B is involved in genome-wide de novo methylation, is also upregulated in the Epiblast region, Given that it is also likely to be upregulated in a region with more dividing cells it was not investigated for the same reason.

Treacher Collins-Franceschetti Syndrome protein, also known as Treacle is suspected to be involved in nucleolar-cytoplasmic transport and to play a role in development of the craniofacial complex. It is not heavily investigated to date, and was not followed up due to time constraints on the project.

6.3.5 Secreted Protein Analysis

Several secreted proteins have been shown to be vital for patterning the embryo at this stage. Secreted factors from the ExE restrict the induction of the AVE to the distal tip at E5.5. If the ExE is removed, the region of VE induced as AVE expands to cover the whole epiblast. BMP signalling has been shown to be involved in this process, via secreted protein regulation of Smad signalling in affected areas [43], [198]. In addition to this, any potential candidate for an AVE migration chemoattractant would be a secreted molecule. As such I analysed both Total and Phospho-protein mass spectrometry datasets for proteins classified as secreted proteins by the Uniprot Database [187].

Of the proteins that emerged from this analysis, TGFβ2 and SPA3K are most likely to have a role in AVE formation and to act as an inhibitory signal. As detailed earlier, TGFβ family proteins are heavily involved at this stage of development in tissue patterning function, and include Nodal and BMP proteins. SPA3K is known to be a serene protease inhibitor, which is more likely to have a localised regulatory effect on other secreted proteins than the other secreted proteins, which have less direct effects or are involved in the basement membrane. As an antibody is available for this protein, further investigation could be very informative. Additionally, experiments similar to those performed by Yamamoto et al. that demonstrated BMP4 signalling as an inhibitory influence on AVE induction using the inhibitor noggin and recombinant BMP4 protein could be performed using recombinant SPA3K protein to determine if location of this protein could affect induction, completion or direction of AVE migration.

6.3.6 Profilin Immunohistochemistry

Profilin was chosen as a candidate for further investigation for several reasons. The protein had a large number of interacting proteins within the screen and was present in the comparison of mass spectrometry data to a published list of genes that cause NTDs when mutated or knocked out. Further, it was deemed a 'Protein of Interest' in the gene ontology analysis due to its established role in the regulation of actin and thus plays a likely role in cell migration and cellular behaviour within the Visceral Endoderm.

Originally discovered as a protein that co-crystallized with actin, Profilin was later discovered to sequester monomeric actin in a 1:1 ratio, and to inhibit actin polymerization. It is a ubiquitously expressed protein. In the mouse embryo, Profilin is essential from the earliest divisions[199]. A knockout generated by Witke et al. showed that without Profilin, embryos die as early as the two-cell stage. Heterozygous mice, however, are viable and fertile [200].

The role of Profilin in actin dynamics has been heavily studied. It is clear that Profilin interacts with actin in both its ADP- and ATP bound forms and the rate of filamentous actin growth or shrinkage is affected by levels of the protein. It is clear from the numerous studies reinvestigating the role(s) and functions of Profilin that its effects are highly context dependent. Plasma membrane composition, localisation, actin concentration, extracellular signals, and concentrations of other actin regulatory proteins will all impact on the effects Profilin has on actin polymerization.

Pantaloni and Carlier demonstrated that Profilin would accelerate actin filament growth in conditions where new free barbed ends were formed *in vitro* [201]. Further, Finkel et al., showed that injection of human Profilin I into CHO cells would promote formation of filamentous actin indicating that

Profilin could function to encourage actin polymerization *in vivo* [202].

ATP also heavily regulates actin dynamics. Profilin has been shown to play a role in this interaction as well [203]. Blanchoin and Pollard showed that Profilin enhances the exchange of ADP for ATP in a pool of actin monomers in a concentration dependent manner. Increased pools of available ATP-actin would promote growth of actin filaments [204]. Whether the hydrolysis of ATP is utilized by Profilin to add monomers preferentially to the barbed end, effectively lowering the critical concentration of actin at the barbed end, has been heavily debated. It has also been debated whether Profilin utilizes the hydrolysis of ATP to accelerate growth at the barbed end, and the role of thymosin B4, an actin binding partner, has in mediating Profilin's effects [204].

Profilin is also known to bind several other proteins that are known to control the actin cytoskeleton in various ways. These include: mDIA, VASP & MENA, Drebrin, Gephyrin, and SMN and has been shown to enhance cdc42 nucleation of actin [205], [206].

Because of the numerous connections of Profilin to actin regulation, both direct and indirect, it was hypothesized that Profilin would show an upregualtion in the cells of the AVE. However, this was not seen in when immunohistochemistry was performed at migratory stages. Profilin did show an increase of the protein in the epiblast region, which correlates with the mass spectrometry screen.

The most striking result of the Profilin immunohistochemistry was the stark regional differences seen in different time-stages of the embryo. At E5.25, prior to migration of the AVE, Profilin was shown to be upregulated in the ExE. At E5.5 this difference is reversed, with slightly higher staining in the Epiblast. At E6.0 there is strikingly higher Profilin staining in the Epiblast, with almost

total downregulation in the ExE. At E6.25 staining in the ExE has begun to return, and at E6.5 Profilin intensity is bright in the ExE again, though not as bright as the Epiblast.

The cause of this dramatic temporal change in the regional expression of Profilin between the ExE and Epiblast is difficult to assess. Increased expression could be a driver of cell movement. Cells of the Epiblast are known to move amongst themselves prior to gastrulation, and the increase in Profilin could be an indication of this. However, this does not explain the downregulation in ExE expression of the protein. It could be an indication that the cells of the ExE are altering their actin cytoskeleton in order to effect changes on the cells above through changes in cell shape and tension. The high staining of Profilin in the Epiblast adjacent to the Visceral Endoderm basement membrane also supports a role for Profilin in the interaction between the two tissues, though this apparently not a direct role in the generation of asymmetry, as the stainings appear even on future anterior and posterior sides.

Additionally, Profilin was strikingly absent from the Visceral Endoderm at E5.5, despite being present in a uniform manner throughout the Epi-VE and ExE-VE at E5.25 and being present again at E6.0. Given the activity of the AVE cells at this stage, and the F-actin shroud often seen in the ExE-VE, this is highly unusual [5]. It would be highly interesting to see if Epiblast specific and ExE specific conditional mutants of *Prof1* showed disrupted AVE migration. If conditional ExE *Prof1* mutants showed an AVE overmigration phenotype, this would indicate that the cell behaviour of the ExE cells, most likely the cell shape, is a driving factor in the behaviour of the overlying Visceral Endoderm cells. If conditional Epiblast *Prof1* mutants failed to migrate, this could indicate that the cells underneath either need to possess a particular shape, or require Profilin-coordinated movements to facilitate the

above AVE cell movement. Which of these two was the case could be determined by Epiblast cell movements in the conditional mutants and comparing them to that of wild-type.

Overall, the Profilin immunohistochemistry performed demonstrates the highly dynamic behaviour of this protein during the egg cylinder stage of embryo development, and supports the results of the mass spectrometry screen.

6.3.7 Stathmin and Phospho-Stathmin Immunohistochemistry

For the Phospho-protein data, the existence of a previously established functioning antibody for the particular phosphorylation site in question was investigated. Along with this, a previously established antibody for the unphosphorylated protein was also sought as a suitable control. Ideally both the phosphorylated antibody and its unphosphorylated counterpart would both be previously shown to work in the early mouse embryo, as was the required criteria for the Total Protein antibody search.

Unfortunately, this combination was not available for any of the Proteins of interest. This was mainly due to the specificity of the antibodies required. Relatively few antibodies exist for specific phosphorylation states in comparison to those for a standard protein. Additionally, many of the Phosphorylation states picked up in our mass spectrometry experiment have only ever been seen in other mass spectrometry experiments and have not been researched individually. Further, most antibodies against phosphorylated states are only recommended for western blots and are unsuitable for immunofluorescence. Further research indicated that this option was only available for two of the 178 proteins that had come out of the Phosphorylation screen.

These two proteins were Stathmin, phosphorylated at serine 38 in at a higher rate in the Epiblast region, and HSPB1 (Heat shock protein beta-1) phosphorylated at serine 86, at a higher level in the ExE region. Ultimately, Stathmin was studied due to time restraints on the project.

I selected Stathmin over HSPB1 as it was more likely to be involved in migration or cell behaviour, and was shown to have a role in regulation of microtubules in the GO analysis. Additionally more was known about the

particular phosphorylation that was detected.

Further, I am strongly interested in AVE migration and HSPB1 was phosphorylated at a higher level in the ExE region, while Stathmin was phosphorylated in the Epiblast region. Stathmin also had a much higher fold-difference in phosphorylation between the regions (6.5 fold difference vs. 2.4 fold difference, respectively).

Stathmin is 17kD highly conserved regulator of microtubule dynamics. Though they are typically given less researched than actin, microtubules are known to play a large role in cell structure, motility and migration. Stathmin interacts with two molecules of dimeric α,β-tubulin, the subunit that makes up microtubules, to sequester tubulin in the cytoplasm and prevent its polymerization. This drives the overall equilibrium of the microtubule/tubulin population to favour depolymerized tubulin.

Several lines of evidence indicate that Stathmin is involved in cell motility. It is expressed in high levels in a wide variety of human malignancies and Stathmin overexpression correlates with increased cell motility and invasion of human sarcomas in vivo. Further is was shown that approximately 50% of genes up or down regulated by a factor of two in STMN1$^{-/-}$ mouse embryo fibroblasts function broadly in cell adhesion and motility. Surprisingly, however, Stathmin null mice are viable and don't display a developmental phenotype.

The phosphorylation at Ser38 found in the screen is one of four known phosphorylation site of Stathmin, with the others at Ser16, Ser25 and Ser63. Many instances of these modifications are cell cycle specific, as cells must assemble the mitotic spindle for the mitotic phase to occur. All four phosphorylation events cause the Stathmin-tubulin interaction to weaken.

Ser38 was the only phosphorylation state of Stathmin that displayed a twofold higher rate of phosphorylation in one region than the other.

Phospho-Stathmin

When stained at E5.5 and E6.25, p-Stathmin(Ser38) was found predominantly in dividing cells of the embryo, with no consistent upregulated staining in the cells of the AVE. p-Stathmin(Ser38) appeared excluded from the cytoplasm of cells in the ExE at E6.25, while it was present in the cytoplasm and nucleus of the cells of the Epiblast. While the Ser38 phosphorylation has been shown to be involved in migration, many of the cells in which signal for p-Stathmin(Ser38) is highly present are clearly dividing. As such, its strong presence in the epiblast is likely to be a result of Stathmins cell-cycle function. It was not entirely surprising that the phosphorylation detected in the screen was shown via antibody staining to be cell-division related and not migration, as it is known that there are high levels of division in the Epiblast. The stainings did however confirm the results shown in the screen.

Non-Phosphorylated Stathmin

The non-phosphorylated Stathmin immunohistochemistry was performed as a control for the specificity of the p-Stathmin(Ser38) antibody. However, several interesting features were seen in this staining. Apical enrichment of non-phosphorylated Stathmin was seen in the VE at E5.5, which was not seen at E6.5. Non-phosphorylated Stathmin was higher in Epi-VE than the ExE-VE in both E5.5 and E6.5 embryos, though this was more pronounced in E6.5 embryos.

At E6.5 non-phosphorylated Stathmin was found to be enriched in the epiblast, directly under the Epi-VE. This enrichment increased along the P-D axis, being brightest at the distal region of the epiblast. This could be indicative of a

structural role for Stathmin in the epiblast cells, perhaps communicating with the Epi-VE via tensile forces. Additional investigation using small molecule inhibitors for Stathmin, such as Taxol or Vinblastine on E5.5 mouse embryos would be highly of interest to further explore the role of this protein at the egg cylinder stage [207]–[210].

In the phosphorylation screen, HSBP1 was the only other protein for which there is an available proven antibody, so staining for this is a logical next step for this project. Overall, however, the distinct lack of antibodies for the identified phosphorylation states of most of the proteins interest that emerged from the screen is a huge barrier to further investigation of candidates.

Generating purpose made antibodies is a solution to this, though it was far beyond the scope of this project.

6.4 Chapter conclusion

Overall, the gene ontology classification and the immunocytochemistry stainings carried out support the mass spectrometry data. As such, this study gives regional proteomic data for the egg-cylinder stage embryo, which is the first investigation of this nature at this stage. This gives a large range of candidates for investigation. It emerged that the rate-limiting factor on the usefulness of this data was the lack of established antibodies for many of the proteins, particularly those of the phosphorylation data.

It also emerged that location of proteins of interest are highly different depending on the time point that the embryo is taken at. While the mass spectrometry screen provided an excellent method for generating interesting candidates for investigation at this stage, it certainly cannot be taken to be an indication of the protein state of temporally close stages of egg-cylinder embryos.

While none of the investigated proteins showed an interesting localisation absence or change in intensity in the AVE, several observations can be made from the stainings. In particular, the striking upregulation of Profilin beginning at E5.5 in the Epiblast warrants further investigation. In addition to this, several other candidates generated from the initial protein analysis would be highly interesting to investigate at this stage, particularly Rab5 and Lamβ1. Investigation of JMY (Junction mediating and regulatory protein), a candidate from the ExE region of the Total Protein data has already begun in the Srinivas lab.

7

Investigating the role of the Planar Cell Polarity pathway in Visceral Endoderm cell behaviour

7.1 Introduction

The Planar Cell Polarity (PCP) pathway consists of the cohort of proteins that establish and maintain polarity in individual cells and across entire tissues in the plane perpendicular to the apical-basal axis. As discussed in Chapter 1, the PCP pathway is one of several known non-canonical pathways modulated by Wnt signalling. Initially discovered and studied in Drosophila, the PCP

pathway has been shown in recent years to be highly important in vertebrate development

PCP was shown to be required for the junctional remodelling that occurs during development of the Drosophila axis extension, the intercalation and protrusive activity exhibited in Xenopus gastrulation, and in coordinated epithelial elongation required for development of kidney tubules in Xenopus and mouse embryos [84], [119], [211]. Extensive junction remodelling occurs during AVE migration in the cells of the VE, which led to the investigation of a potential role for PCP signalling at this stage. To date, several lines of evidence have emerged to support this, including mutant mice that have disrupted PCP signalling.

In the *ROSA26*$^{Lyn\text{-}Celsr1}$ mouse line PCP is disrupted. In this line the AVE crossed the normal boundary between the ExE and Epiblast and the cells migrated in a non-coordinated manner. Additionally, these dominant negative mutants showed a dramatic decrease in the number of rosettes observed, which impairs the ability of the tissue to reorganize cell junctions effectively. This impairment of migration does not affect viability of the mice. *ROSA26*$^{Lyn\text{-}Celsr1}$ mice also show disrupted subcellular localisation of Dvl2, correlating to the extent of AVE migration abnormalities. In addition to this, in the *Lefty1* null mutant shows abnormal subcellular localisation of Dvl2, a core component of the PCP pathway in addition to an AVE overmigration phenotype. Similar disruption of Dvl2 localisation can be seen in *Nodal* null embryos [5].

Great use has been made to date of mutant mouse embryos that exhibit disrupted migration to further understand the behaviour of the AVE, rather than those who fail to induce the AVE or fail to initiate migration. While the latter categories can tell us much about the signalling pathways that induce cell identity and pattern, mutants that migrate incorrectly give information on

the mechanisms coordinating physical cell movement. Examples include mice null for the phosphatase *Pten,* which exhibit an uncharacteristically dispersed AVE cell phenotype and *Rac1* null embryos, which do not undergo migration or send the protrusions typically associated with the AVE [81], [156].

To further explore the role of the PCP pathway in the coordination of AVE migration, I investigated mutants for the core PCP protein Vangl2. To further understand the role of Dvl2 on cell coordination I examined knockout mutants for β-arrestin2, a protein known to bind Dvl2 and facilitate its internalization and downstream function. Additionally I have produced gene constructs that disrupt Dvl2 localisation in the VE during AVE migration in a targeted manner. The background of each of these approaches is discussed below.

7.1.1 The role of Vangl2 in PCP signalling

In recent years, many mouse genetic mutants have been shown to exhibit defects in cranial or spinal formation, including numerous members of the PCP pathway. The most extreme of these is the open neural tube defect referred to as craniorachischisis; a complete failure of neural tube closure at all three established stages [127].

The Looptail (Lp) mutant mouse line exhibits this phenotype. The line was first described in 1949 by Strong et al. as having the looped tail phenotype which has now become associated with mutants of the PCP pathway [132]. A genetic mapping and positional cloning approach later identified *Lpp1*, a homologue of the Drosophila protein Strabismus/Van Gogh (Vang) as the gene responsible for the distinctive looped tail phenotype. The human orthologue of the *Lpp1* gene*, LPP1*, shares 89% identity with its murine counterpart, Vangl2, at the nucleotide level and 99% identity at the amino acid level [212], [213]. Due to the presence of *craniorachischisis* and its potential as a model for NTDs, the mouse line has been extensively investigated and has proved an extremely valuable tool in the understanding of the Vangl2 protein, PCP signalling in a range of processes and the interaction of the PCP pathway with other signalling pathways [214], [215].

7.1.1.1 Vangl2 protein

Vangl2 is a four-pass transmembrane protein that contains a PDZ binding domain at the C-terminus [216], [217]. It was first discovered in Drosophila, where Strabismus, the Vangl2 homolog was shown to be required to establish polarity in the eye, leg and bristles. In Drosophila Strabismus has been shown to bind planar polarity proteins Prickle and Dishevelled, directing them to the

plasma membrane. In the absence of Strabismus activity, Prickle and Dishevelled show abnormal cellular localisation [105], [218], [219].

7.1.1.2 Vangl2 function in vertebrates

In vertebrates Vangl2 has also been shown to have multiple functions. The over expression of the Xenopus Vangl2 homologue, *XStbm*, in early Xenopus embryos results in failure of convergent extension, generating severely shortened trunk structures [220]. It was later shown that depletion of *XStbm* function also negatively affected convergent extension [221]. Strabismus was also implicated as the affected protein in Zebrafish *trilobite* mutant embryos, which have defects in gastrulation movements. Impaired mediolateral cell polarity was shown to be the cause of the observed impaired gastrulation in this line [120].

In mice, the most striking phenotype associated Vangl2 is the craniorachischisis seen in mouse embryos. Enlargement of the floor plate region in homozygous Looptail embryos has been proposed to drive this failure of neurulation. Disrupted PCP signalling as a result of mutant Vangl2 impedes midline bending, which generates neural folds spaced further apart than those of wild-type mice, ultimately causing the failure of neural tube closure [222].

Additionally, several other phenotypes have been associated with disruption of Vangl2. It has been shown that mutation of Vangl2 disturbs polarization of stereociliary bundles in mouse cochlea [122]. This was carried out using the Looptail mouse line, however mice null for Vangl2 also exhibit *c*raniorachischisis and other PCP defects [223]. In the mouse node, PCP signalling coordinates the collective alignment of rotating cilia, facilitating leftward flow of nodal ligand and subsequent left-right patterning of the embryo. Here, Vangl2 is localized at one side of the cell, while Dvl2 is localized to the other [89], [224]. Left-Right asymmetry defects occur when either protein activity is reduced and many cilia are not correctly positioned.

7.1.1.3 Looptail mice exhibit a strong PCP phenotype

In Looptail mutants, a serine to arginine mutation in the cytoplasmic domain of the Vangl2 protein (S464N) causes Vangl2 to be retained in the endoplasmic reticulum instead of being delivered to the plasma membrane. It also severely reduces the levels of Vangl2 protein [225]. It was then noted by Yin et al. that the Looptail mutant phenotype was stronger than that seen in the *Vangl2* knockout mouse line. This was determined to be caused by a dominant negative function on Vangl1. In the presence of Vangl2^{S464N} expression, both Vangl2 and Vangl1 trafficking to the membrane are reduced [223]. This effect is likely to be due to the binding of the mutant Vangl2 to Vangl1 and sequestering it, as the existence of Vangl2/Vangl1 heterodimers has been shown [226].

It was later shown that Vangl2 is sorted in the endoplasmic reticulum by Sec24b, a cargo loading protein, while Vangl2^{S464N} is not. This suggests the mutated cytoplasmic region of the protein is necessary for sorting, generating the lack of membrane localisation of both Vangl2 and Vangl1 seen in Looptail mutant embryos [227], [228].

In wild-type embryos Vangl2 is membrane enriched in the Epi-VE and more cytoplasmically located in the ExE-VE. In *ROSA26*$^{Lyn\text{-}Celsr1}$ embryos, Vangl2 is downregulated and not membrane enriched in the Epi-VE [5]. Given this regional expression pattern, coupled with a localisation effect in a known PCP mutant, I considered Vangl2 a prime candidate for a role in the migration of the AVE and the regulation of Visceral Endoderm cell behaviour. I hypothesized that Vangl2 enrichment in the Epi-VE was required to facilitate cell movement. To investigate this I utilised the Looptail mutant.

7.1.2 The role of Dvl2 in PCP signalling

Dishevelled protein relays Wnt signals from receptors to downstream effectors, being most well-known for its role in the canonical Wnt signalling pathway, regulating nuclear activity of β-catenin [229], [230].

The Planar Cell Polarity (PCP) pathway is regulated on a tissue scale by external Wnt proteins, constituting an alternative pathway to canonical Wnt signalling and acting independently of β-catenin, despite sharing common upstream pathway components. Like, Vangl2/Strabismus, Dishevelled (also known as Dsh in Drosophila, Xdsh in Xenopus and Dvl in vertebrates) was first discovered in Drosophila, where it disrupts body and wing hair orientation [231]. Dvl was later established as a core member of the PCP pathway, after being shown to regulate cell polarity in flies [232], [233].

Dvl binds over 60 other proteins (reviewed in [234]) and in addition to its function in canonical and PCP signalling it is known to have roles in Wnt-calcium signalling, Wnt-RYK signalling, Wnt-atypical PKC signalling and Wnt-GSK3 signalling [235]–[238].

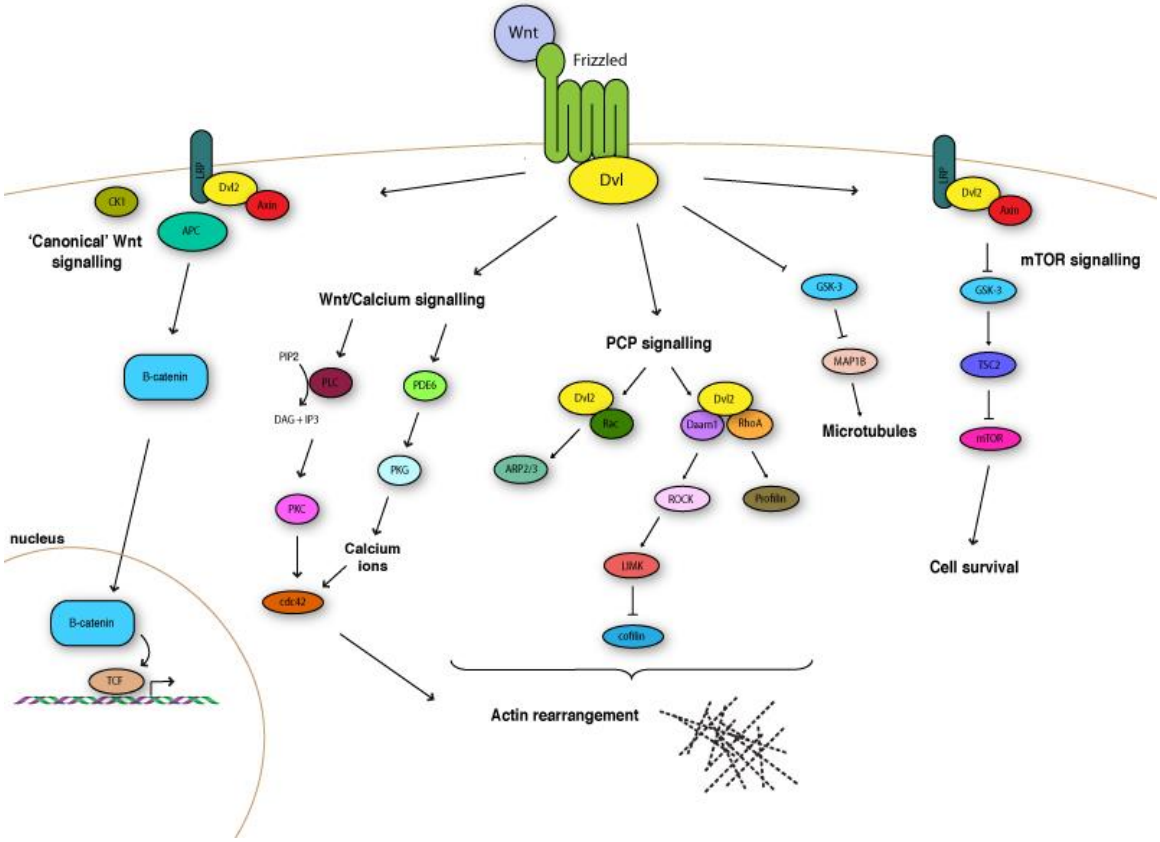


Figure 7.1: Multiple downstream functions of Dishevelled

In addition to the canonical Wnt signalling pathway (depicted far left), several other non-canonical Wnt signalling pathways also require Dvl activation. The most well-known and their respective downstream functions are shown. These are (left to right) the Wnt-calcium signalling, Planar Cell Polarity signalling and the mTOR signalling pathways.

7.1.2.1 Dishevelled protein

Dishevelled protein contains three conserved domains. These are an amino-terminal DIX domain necessary for canonical signalling via Axin binding, a PDZ domain, which binds Frizzled to transmit downstream signalling, and a carboxyl-terminal DEP domain. There is also a proline-rich region and a basic and serine/threonine-rich region [239]–[244].

It was first shown in Drosophila that the DEP domain is essential for planar polarity signalling, while the DIX domain is not required [245], [246]. The DEP domain both recruits Dvl to the membrane and is responsible for activation of the downstream JNK pathway [247]. The DEP domain is also involved in interactions with the plasma membrane itself, via electrochemical signals interacting with plasma membrane [248].

In PCP signalling, Dvl conducts downstream signals via the scaffold protein formin homology adaptor protein Daam1, ultimately activating cytoskeletal rearrangement through RhoA and Rac1 activation. In Xenopus loss or inhibition of Daam1 non-canonical activation of Rho and disrupts gastrulation movements [113]. Dvl binding disrupts the auto-inhibited state of Daam1 upon binding via its PDZ domain. This triggers Daam1 activation and subsequent Rho/ROCK signalling through interaction with Rho guanine nucleotide exchange factors[249], [250]. ROCK activation leads to cytoskeletal rearrangement (reviewed in [251]).

Dvl is also known to activate Rac signalling, independently of Rho activation. This has been seen in both Xenopus gastrulation and dendrite growth, though the Dvl mediated manner of Rac activation remains unclear [252].

7.1.2.2 Dvl analogues in the mouse

In mice there are three Dvl genes *Dvl1*, *Dvl2* and *Dvl3*. Individual Dvl analogues are known to have specific functions, as evidenced by different phenotypes upon deletion. *Dvl1* knockout mice are viable and fertile, but display social interaction abnormalities and defects in sensorimotor gating [253]. Mice containing null mutations in Dvl2 present with 50% lethality, with approximately 90% of Dvl2$^{-/-}$ mice showing vertebral and rib deformities. A small amount of Dvl2$^{-/-}$ mice (2-3%) exhibit spina bifida [254]. Dvl3$^{-/-}$ mice die perinatally, exhibiting cardiac abnormalities, and misorientated stereocilia in the organ of Corti [255].

There is also evidence for redundancy in several roles, as compound mutants have much stronger phenotypes than single Dvl mutants. *Dvl1*$^{-/-}$; *Dvl2*$^{-/-}$ mutants display craniorachischisis and more pronounced skeletal abnormalities than that of single Dvl2 knockouts. *Dvl2*$^{-/-}$; of *Dvl3*$^{-/-}$ double mutants also display craniorachischisis. *Dvl1*$^{-/-}$ and *Dvl3*$^{-/-}$ single mutants or *Dvl1*$^{-/-}$; *Dvl3*$^{-/-}$ double mutants do not display neural tube defects [253], (unpublished data, referred to in [121]) . This could indicate a stronger role for Dvl2 in PCP signalling.

More severe defects are also seen when either other Dvl analogue is knocked out in addition to Dvl3 [255]. Triple *Dvl1*$^{-/-}$;*Dvl2*$^{-/-}$;*Dvl3*$^{-/-}$ mutants do not gastrulate (unpublished data, referred to in [256]). Further, increasing Dvl levels using Dvl transgenes can compensate for other lost Dvl in knockout mutants, giving healthy development [257].

To date, the relative expression of the three analogues has not been shown in the early mouse embryo. However, mouse F9 and P19 embryonal carcinoma cell lines have been used as a model of the early embryo, and *Dvl2* makes up

95% and 80% respectively of the total Dvl expression in these two cell lines [258].

7.1.2.3 Dvl2 is active in PCP signalling at E5.5

Work by Axelrod et al. showed that localisation of Dvl2 to the cell membrane was a hallmark of PCP signalling [104], [245]. Later, Park et al. showed that the membrane localisation of Xdsh protein is necessary for PCP signalling to occur in the developing Xenopus embryo [259]. This was accomplished by directing wild-type Dishevelled protein specifically to cell membrane or sequestering it in the cytoplasm. It must be noted, however, that PCP is not the only pathway in which membrane recruitment of Dvl is a characteristic [245], [260]. In the case of PCP, membrane recruitment of Dvl protein facilitates downstream events triggering molecular motors to promote and coordinate cytoskeletal rearrangement.

In the egg cylinder stage embryo, there have been conflicting reports on the activity of β-catenin. A small amount was seen in E5.5 embryos using a LacZ transgene that reported TCF/Lef-activity downstream of β-catenin, indicating that the non-canonical pathway is not largely active at this stage [261]. A far brighter and more sensitive GFP reporter line indicated that there was diffuse B-catenin signalling in the Visceral Endoderm of E5.5 embryos during AVE specification, which increased to a salt and pepper pattern over several hours [262].

Dvl2 stains from the Srinivas lab (Chapter 1) have shown global localisation of Dvl2 to the membrane in the Epi-VE region, which is not consistent with the mosaic activation seen by the B-catenin reporter mice. As such it is likely that another Wnt signalling pathway is active at this stage, and acting on all the cells of the Epi-VE.

Evidence for this has also come from an investigation of Wnt isoform expression was carried out by Kemp et al., which demonstrated that canonical signalling is not the predominant form of Wnt signalling occurring at E5.5. Wnt5A and Wnt11, the main Wnt ligands known to be involved in PCP signalling were heavily upregulated at E5.5, despite dramatically lower expression 12 hours before and after this stage. Additionally, Wnt ligands associated with canonical signalling are strongly reduced at E5.5 for a period of 12 hours, and then become highly expressed prior to onset of gastrulation [263].

Given this expression data, it is very likely that the membrane localisation of Dvl2 seen in the Epi-VE is a response to PCP signalling at this stage.

As discussed, the Srinivas lab has shown that the Epi-VE is characterised by the enrichment of Dvl2 to the plasma membrane implying that there is active PCP signalling in this region of the VE. Down-regulation and eventual loss of Dvl2 in the ExE-VE in parallel to this suggests distinct areas of localised PCP signalling corresponding to the two established regions of Visceral Endoderm [5]. Regional differences in the localisation of Dvl2 effector Daam1 also indicated this [140].

Given that membrane enrichment of Dvl2 is a characteristic that varies in different regions of the VE and at different stages of AVE migration, I hypothesized that membrane localisation of Dvl2 protein is directly responsible for regulating the migration of AVE cells. To test this, one would need to alter the localisation of Dvl2 in the mouse embryo. Given that Dvl2 is involved in a wide array of pathways, a permanent mislocalisation of the protein is not ideal as it is highly likely that a mouse line with mislocalised but present Dvl2 protein would be unviable.

Further, given that at E5.5 the main active Wnt signalling isoforms are those regulating PCP signalling, a temporally–isolated relocation of the protein at only this stage would give direct insight into the specific function of Dvl2 localisation during AVE migration. Transient transgenics provide the ideal solution for the purposes of this experiment, as the technique allows temporary expression of genes which would typically result in embryo fatality [264]. To provide tools to test this theory, I generated several constructs that can be used in future experiments to confirm the role of Dvl2 localisation on AVE migration.

7.1.3 The role of β-arrrestin2 in Dvl2 signalling

I have discussed above the previously published evidence to show the importance of localisation of Dvl2 on its function. It is also established, however, that the internalization of Dvl2 plays a role in its activity. There is strong evidence that β-arrrestin2 is a regulator of the localisation and internalization of Dvl2 protein.

Originally discovered as regulators of G-protein receptor desensitization, β-arrestins have more recently been implicated in several other functions, including acting as multi-functional adaptors that link receptors to the machinery of clathrin-mediated endocytosis [265]–[267]. β-arrestin2 has been shown to interact with Dvl2 in vitro and in vivo and mediate its role in the PCP pathway in both human tissue culture and Xenopus embryo models [268], [269].

Kim and Han showed that Xenopus β-arrestin2 (xβarr2) was recruited to phosphorylated Xenopus Dvl2 (xDsh) at the cell membrane of human embryonic kidney 293 (HEK293) cells. Additionally, if xDsh was forcibly localised to the mitochondrial membrane, xβarr2 also relocalised to this area. Evidence that β-arrestin2 regulates Dvl2 internalisation was also seen, with endocytosis of Frizzled 4 shown to be dependent on β-arrestin2, which was only recruited to Fz4 by binding to phosphorylated Dvl2. Functional knockdown of βarr2 relocalised xDsh to the cell membrane and inhibited colocalisation with β2-adaptin in cytoplasm [269].

Depletion of β-arrestin2 severely disrupts convergent extension movements in Xenopus embryos, an indication of disrupted PCP signalling [269]. β-arrestin is necessary for internalization of Fzd7/Dvl/AP-2 complexes, and endocytic function of βarr2 is required for *Xenopus* CE movements [236]. This internalization is required for activation of components of the Wnt/PCP

pathway like RhoA and Rac1, the latter of which has been shown to be important for AVE migration[269].

Additionally removal of xβarr2 did not disrupt Xfz7 triggered localisation of Xdsh to the plasma membrane, adding weight to the previously established evidence that β-arrestin2 is recruited by Dvl2, and is involved in downstream signalling, rather than recruiting Dvl2. Further, xβarr2 was shown to regulate the subcellular localisation of Daam1, a PCP downstream effector, in Xenopus animal cap cells. To date, the combined evidence in cell lines and Xenopus embryos indicates that β-arrestin2 is required for Dishevelled activation downstream of PCP signalling activity, and that this function involves the endocytic function of β-arrestin2[269].

7.1.3.1 β-arrestin2 in the early mouse embryo

Given the established role of PCP in AVE migration, the distinct regional patterns of Dvl2 in the Visceral endoderm, and the role of β-arrestin2 in regulating Dvl2 function, I hypothesized that β-arrestin2 was involved in regulating AVE migration. While a β-arrestin2 knockout mouse line exists, it has not been utilized to study the mouse embryo [135]. The earliest known expression of β-arrestin2 to date is E14.5 [270]. I aimed to establish whether *arrb2,* the gene encoding β-arrestin2, was expressed during AVE migration, determine β-arrestin2 protein localisation and investigate the role of β-arrestin2 in AVE migration by examining knockout mutants at this stage.

7.2. Results

7.2.1 Investigating the role of Vangl2 in migration of the AVE

Given that Vangl2 is a core PCP protein and the Looptail mutant line has such a strong phenotype, I requested the line to assess the role of Vangl2 and Vangl1 in AVE migration.

I crossed the Looptail line the Hex-GFP line described in Chapter 2 so that the AVE cells of these mutants were easily identified. I bred these mice to establish homozygosity of the Hex-GFP transgene, so that a higher proportion of the homozygous *Vangl2*$^{lp/lp}$ embryos would have a labelled AVE. I then assessed these mutants for abnormal AVE migration phenotypes.

7.2.1.1 *Vangl2*$^{lp/lp}$ mutants do not display defective AVE migration

Eight mutant homozygous *Vangl2*$^{lp/lp}$ embryos were confirmed by genotyping. Of these, seven embryos exhibited normal migration. One embryo showed no AVE induction, though this was likely due to a delay in development as the embryo appeared healthy.

In addition to this, several batches of embryos could not be genotyped. Due to their small size and having been processed for confocal microscopy, genotyping the E5.5 embryos was a difficult process. Of 26 additional embryos of unknown genotype, all showed normal migration.

7.2.1.2 Some *Vangl2*$^{lp/lp}$ embryos exhibit delayed development

Three of eight homozygous *Vangl2*$^{lp/lp}$ mutants showed a delayed phenotype. The AVE fully migrated in two of these three delayed embryos, but they retained a distinctly E5.5-E5.75 morphology, with a more cylindrical appearance and remaining smaller than batch-mates. One embryo had not induced AVE, even at E6.0, however it appeared healthy, and exhibited an E5.25 morphology. All other five Vangl2$^{lp/lp}$ embryos exhibited normal staging.

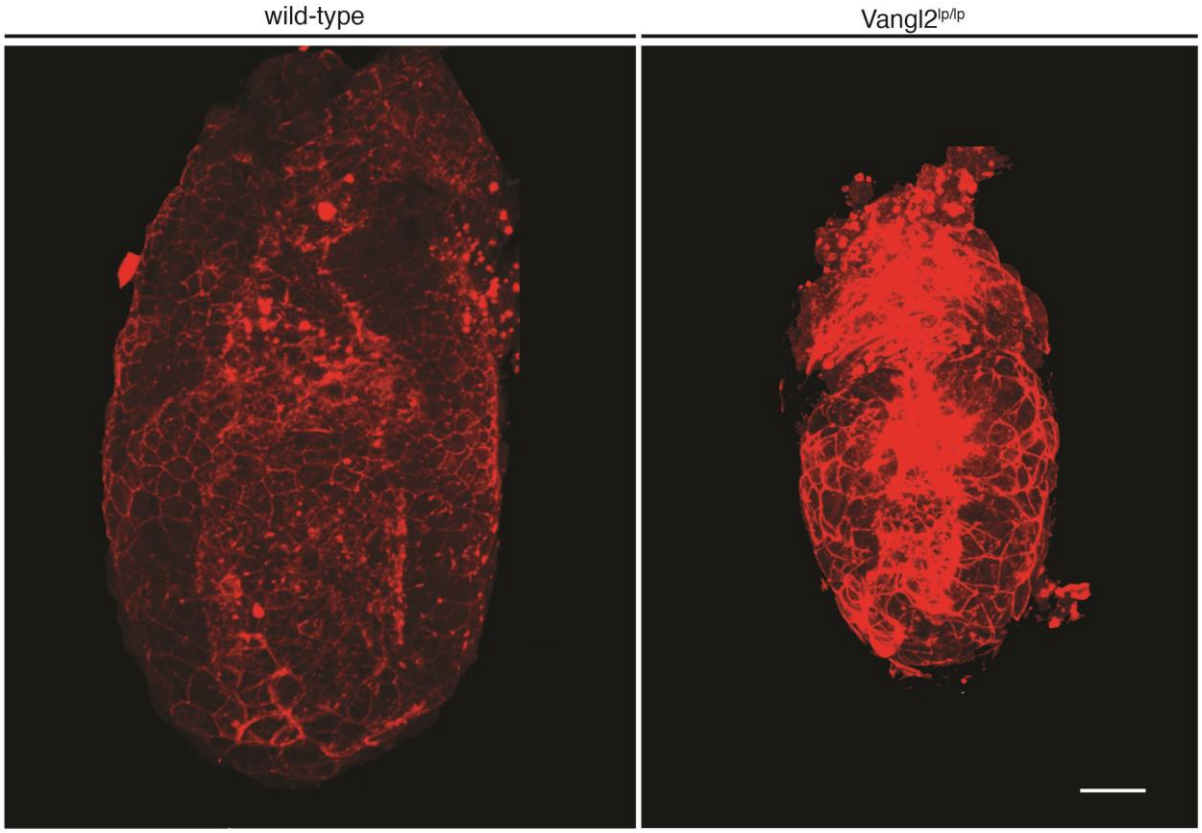


Figure 7.2: Size comparison between Vangl2$^{lp/lp}$ and wild-type embryos

Maximum intensity projection rendering of Vangl2$^{lp/lp}$ mutant (right) and wild-type (left) batch-mate embryos. Three of eight homozygous Looptail mutants exhibited a delayed phenotype. Embryos were fixed and stained with phalloidin at E6.0. Scale bar = 30 μm

7.2.2 Investigating the role of β-arrestin2 in migration of the AVE

7.2.2.1 β-arrestin2 is expressed in E5.5 and E6.5 embryos

I initially examined expression of β-arrestin2 in the egg cylinder stage embryo by RT-PCR at E5.5 and E6.5, using E14.5 brain tissue as a positive control. To obtain enough material for the reverse transcriptase, I pooled embryos for each sample of E5.5 (n = 10) and E6.5 (n = 7) investigation.

The PCR was carried out on the resultant cDNA using primers I designed to specifically amplify β-arrestin2. The primers were designed to span an intron so that they would be less likely to amplify from any contaminating genomic DNA. In addition I performed a standard RT negative control. I performed an RT-PCR against actin as a positive control.

The RT-PCR established the presence of β-arrestin2 at E5.5 and E6.5. A positive actin band at the expected size was seen at all three stages, though it was somewhat faint in the E5.5 sample. The RT negative control was clean for all three samples. The PCR for β-arrestin2 showed bands of the expected size at E5.5 and E6.5, verifying expression at these stages (Figure 7.3).

In the E14.5 sample the band for β-arrestin2 was much fainter than that of E5.5 and E6.5. There was also an unexpected band at 1,200bp that could not be explained by alternative splicing of β-arrestin2. Because this band was not present in the E5.5 and E6.5 stages of interest, this was not followed up. E5.5 showed the expected 300bp band and an additional band at approx. 200bp. E6.5 showed only the 200bp band. These bands can be explained by alternative splicing of β-arrestin2, which is known to have two isoforms that are of similar size.

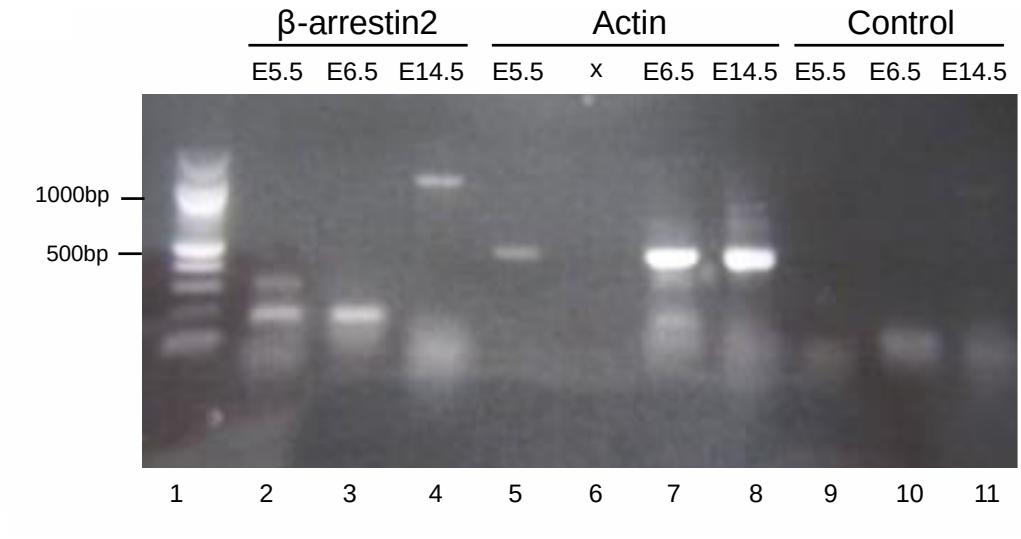


Figure 7.3: RT-PCR analysis of ß-arrestin2 expression at E5.5 and E6.5

Lane 1 contains a 100bp NEB DNA ladder for approximation of DNA gel band size. Lanes 2, 3 and 4 contain the ß-arrestin2 RT-PCR samples for pooled embryos at E5.5, E6.5 and E14.5 (brain tissue only) respectively. Lanes 5, 7 and 8 contain the actin RT-PCR positive control samples for E5.5, E6.5 and E14.5 (brain tissue only), respectively. Lanes 9, 10, and 11 contain the negative control RT-PCR samples for pooled embryos at E5.5, E6.5 and E14.5 (brain tissue only), respectively. Lane 6 does not contain a sample.

7.2.2.2 β-arrestin2 immunohistochemistry could not be achieved at the egg cylinder stage

I next performed immunohistochemistry to visualize wild-type expression of β-arrestin2 at various stages of AVE migration. Multiple protocols to optimize conditions for two separate β-arrestin2 antibodies (Aviva/Cell Signalling, see Table 2.1) were investigated, however neither antibody could be optimized to give clean and consistent staining across batches.

At this time, the β-arrestin2 knockout line was unavailable. As such I attempted to confirm mis-staining using the *ROSA26*$^{Lyn\text{-}Celsr1}$ mutant mouse line, which was readily available to the lab. These mice are known to mislocalise Dvl2 in the E6.0 embryo and have impaired PCP signalling, which would likely relocalise β-arrestin2. (Aviva antibody: wild-type n = 12, *ROSA26*$^{Lyn\text{-}Celsr1}$ homozygous mutant n = 9; Cell Signalling antibody: wild-type n = 6, *ROSA26*$^{Lyn\text{-}Celsr1}$ homozygous mutant n = 11) While some embryos showed regional changes, no consistent difference could be seen in these mutants compared to wild-type staining. Results for the Cell Signalling β-arrestin2 testing are shown in Figure 7.4

Further confirmation that the Aviva β-arrestin2 antibody was unsuitable was achieved using the appropriate blocking peptide. A similarly appropriate blocking peptide was not available for the NEB β-arrestin2 antibody.

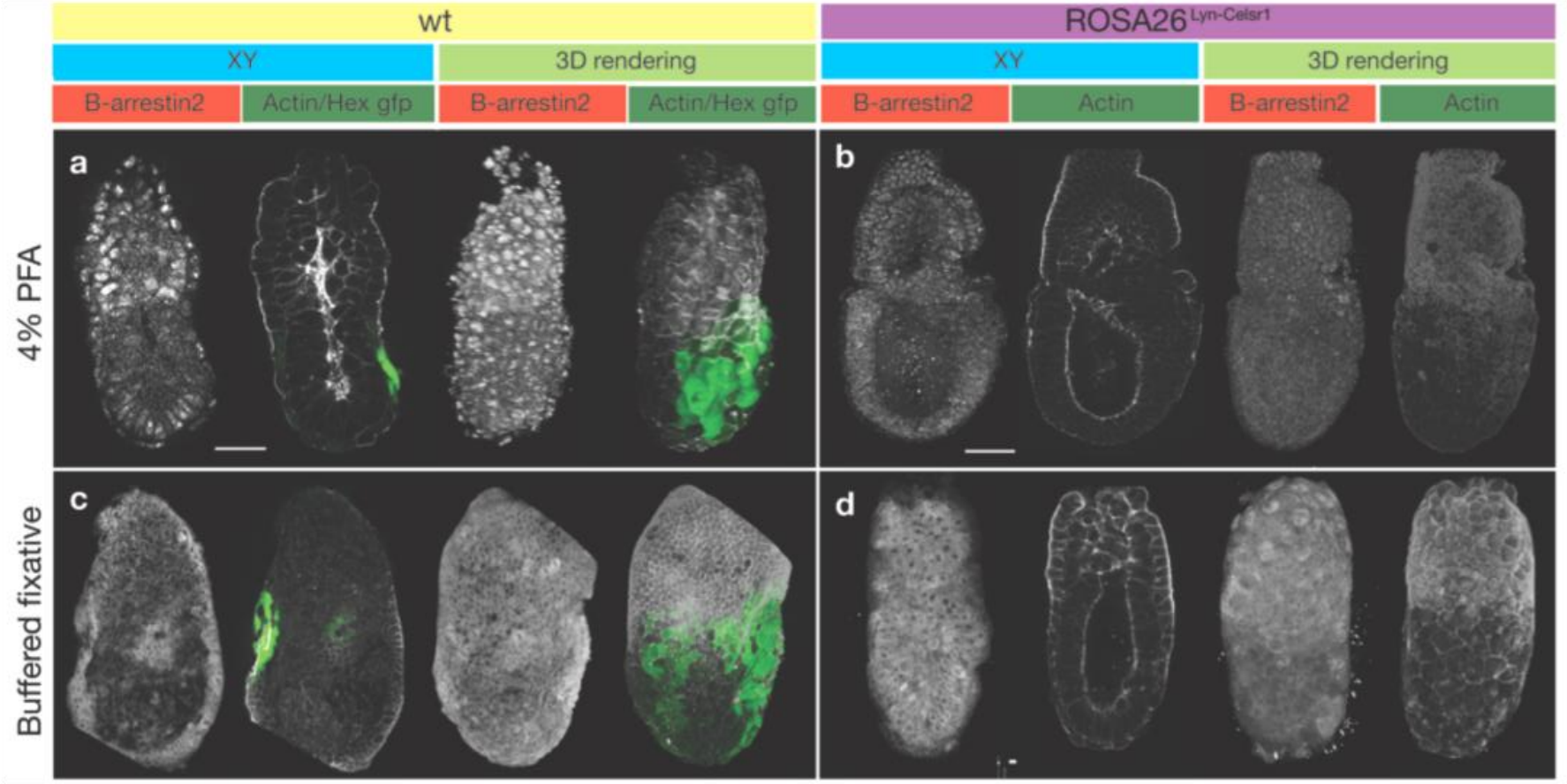


Figure 7.4 Test of the Cell Signalling ß-arrestin2 antibody *(Figure legend overleaf)*

Figure 7.4 Test of the Cell Signalling ß-arrestin2 antibody

E5.75 and E6.25 embryos wild-type (left, yellow header) and homozygous ROSA26$^{Lyn\text{-}Celsr1}$ (right, purple header) were dissected and stained with the Cell Signalling anti-ß-arrestin2 antibody (3857) using both 4% PFA (upper row) fixative and the alternative 'buffered fixative' (lower row), described in Chapter 2.

Block (a) corresponds to wild-type embryos fixed with 4% PFA. Block (b) corresponds to homozygous ROSA26$^{Lyn\text{-}Celsr1}$ mice fixed with 4% PFA. Block (c) corresponds to wild-type embryos fixed with the alternative 'Buffered fixative'. Block (d) corresponds to homozygous ROSA26$^{Lyn\text{-}Celsr1}$ mice fixed with the alternative 'Buffered fixative'. Each block depicts both XY (cyan column) 2D image section and 3D image renderings (light green column), of ß-arrestin2 (red column) and phalloidin (green column) staining.

7.2.2.3 Some β-arrestin2$^{-/-}$ mice exhibit overmigration of the AVE

When a functional antibody could not be established, I re-requested the β-arrestin2 knockout mouse line. When it became available, I bred these mice with the Hex-GFP line described in Chapter 2, establishing a line where mice were heterozygous for the β-arrestin2 deletion and homozygous for the Hex-GFP label. This line was called Arrb2-HexGFP. This ensured that all embryos that were homozygous null for β-arrestin2 would possess GFP labelled AVE cells.

I then dissected pregnant mice from the Arrb2-HexGFP line at E5.5 and analysed the resultant embryos for abnormal AVE behaviour using confocal microscopy. All embryos were then genotyped as described in Chapter 2. 8 homozygous β-arrestin2 null mutants were confirmed by genotyping. 75% of the homozygous β-arrestin2 null mutants (6 of 8) showed an over-migration phenotype reminiscent of *Lefty1*$^{-/-}$ embryos (Figure 7.5)

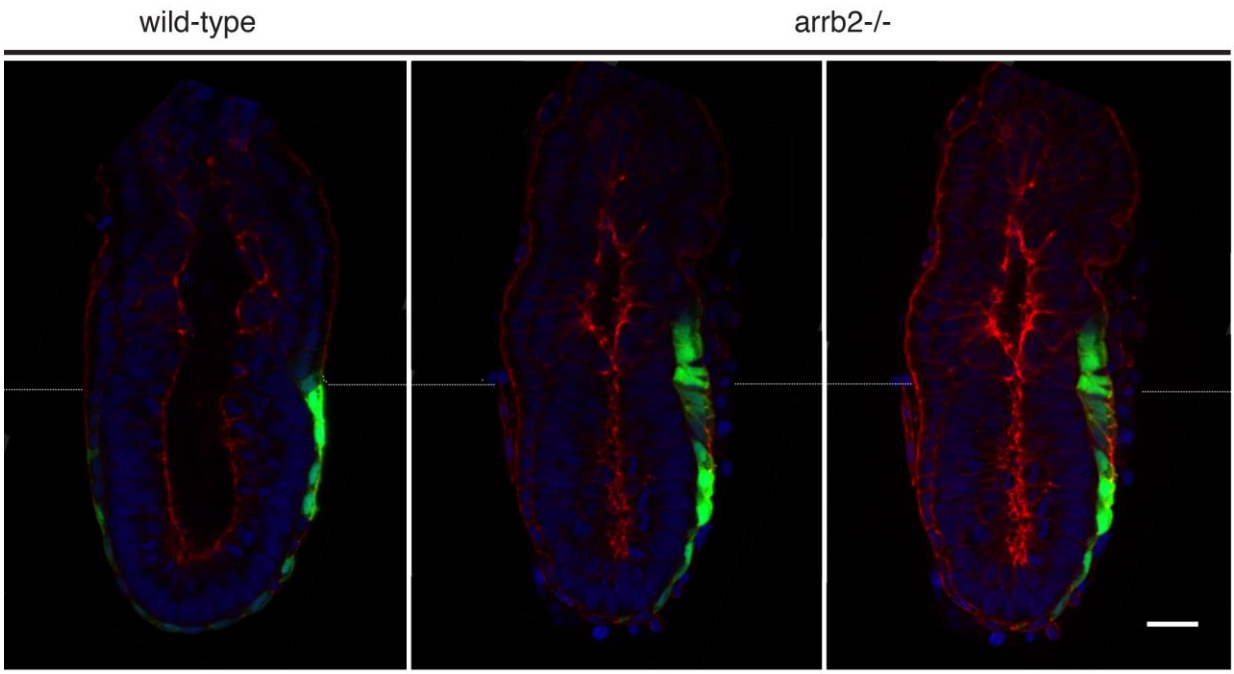


Figure 7.5: AVE overmigration in β-arrestin2 null mutant embryos of the Arrb2-HexGFP line

Optical sections of wild-type (left) and homozygous ß-arrestin2 null (middle, right) embryos of the Arrb2-HexGFP line. For the ß-arrestin2, different Z-levels of the same embryo are shown. Actin is shown in red, Hex-GFP in green and DAPI in blue. Over-migration was seen in 6 of 8 homozygous ß-arrestin2 null embryos.

The dashed line shows the boundary between the epiblast and ExE that wild-type AVE cells do not normally migrate across at this stage.

7.2.3 Disrupting the subcellular localisation of Dvl-2.

I designed and generated gene constructs that will ultimately be used in transient transgenics in order to investigate whether the localisation of Dvl2 has an effect on cell behaviour during AVE migration. These constructs were designed to localise and sequester endogenous Dvl2 protein at the plasma membrane or the mitochondria.

The constructs were based on the Dvl-KM-CAAX and Dvl-MA constructs described in the 2005 paper from Park et al. [259]. Here, endogenous Xenopus Dvl (xDsh) was sequestered to either the cell membrane or the mitochondria by overexpressing an exogenous Dvl protein that was fused to a specific localisation domain. The same localisation domains are used in this case to achieve the same effects with mouse Dvl2:

1. An 18 amino acid fragment of the KRAS protein, known as a CAAX domain [271]. Proteins that terminate with this sequence undergo a series of posttranslational modifications that include polyisoprenylation, endoproteolysis and carboxyl methylation. These modifications make the C-termini of attached proteins hydrophobic, allowing them to be inserted into membranes [272].
2. The Listeria monocytogenes protein ActA has been shown to localize to the mitochondria in eukaryotic cells. 26 amino acids at the C- terminus of the protein are essential for this mitochondrial localisation [273]–[275].

The two generated Dvl-based fusion proteins were Dvl-CAAX and Dvl-MA. Dvl-CAAX leads to the sequestration of endogenous Dvl to the plasma membrane. Dvl-MA is a mitochondrion-tethered version of Dvl2 that sequesters endogenous Dvl2 to the cytoplasm, away from the cell membrane (Figure 7.6)

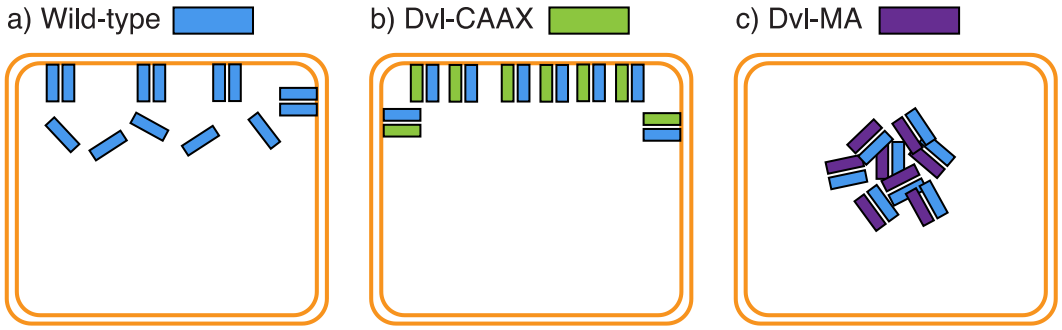


Figure 7.6 Representation of Dvl2 constructs in cells

Wild type cells are depicted in (a), where Dvl2 is recruited to the membrane upon upstream signalling from several pathways. Dvl-CAAX and membrane-sequestered Dvl2 is shown in (b). Dvl-MA and cytoplasm-sequestered Dvl2 is shown in (c).

The full cloning plan for the constructs, as well as justification for each constituent part can be found in Chapter 2. The main components are described below.

- I linked Influenza Hemagglutinin (HA) peptide to Dvl2 to identify where the exogenous protein only is localized. Influenza Hemagglutinin (HA) peptide is a synthetic peptide with an amino acid sequence of N-Tyr-Pro-Tyr-Asp-Val-Pro-Asp-Tyr-Ala-C, which is commonly used as a marker to tag proteins of interest. I included this because the Dvl2 antibodies that have been investigated by our lab to date have been difficult to achieve consistent stainings with. The HA tag would also enable me to distinguish the endogenous from exogenous Dvl2.

- I included tdTomato under the 2A peptide to allow immediate identification of successful transgenics. 2A peptides result in the co-translation of proteins in the same open reading frame, allowing tdTomato and HA-Dvl2 to be expressed together.

- I utilized Human ß-globin genomic sequences at the 3' end as it provides a strong transcriptional termination signal and allows for spacing of the transcript, which has been suggested to enhance stability. The BJ1(CAG- HBG) plasmid was used as a linker/storage vector throughout the plan, as it is a very restriction-site-rich plasmid, which was extremely helpful as *Dvl2* has a very high number of common restriction sites in its sequence.

- I chose TTR and Hex promoter elements to drive the construct. The TTR promoter element drives expression throughout the VE while the Hex promoter drives expression only in AVE cells. This allows testing of whether membrane localisation of Dvl2 in the AVE alone is sufficient

for normal migration.

- I also built a stage into the cloning plan where the construct could be expressed under the CAG promoter, to allow testing of the constructs in cell culture. The six final constructs are shown in Figure 7.7.

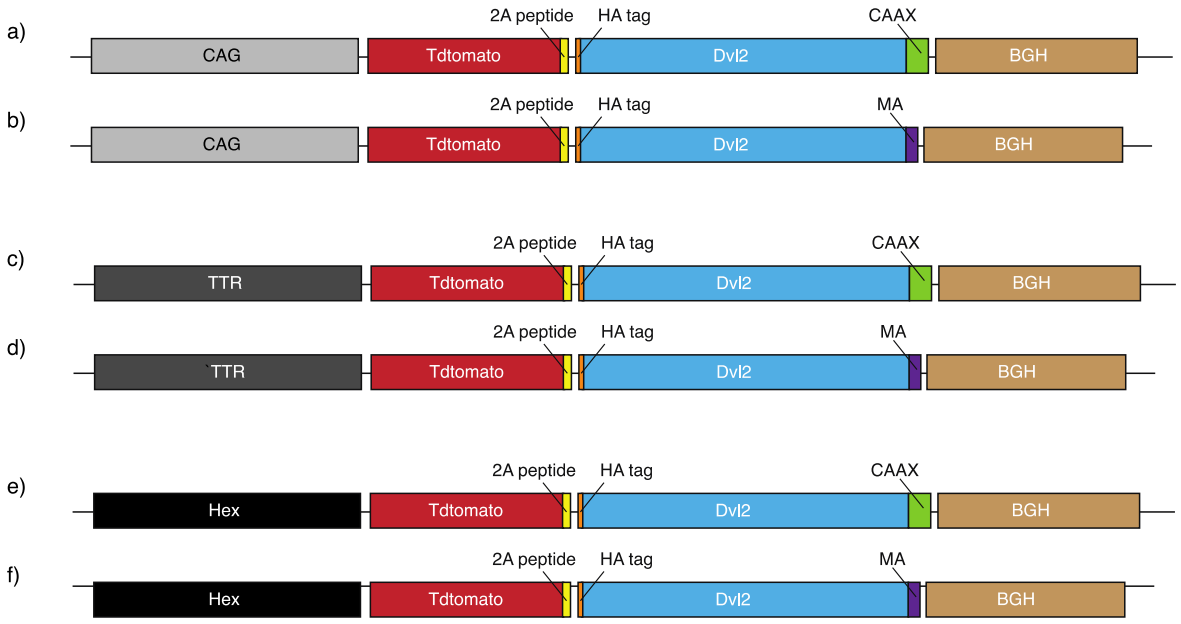


Figure 7.7 Constructs generated for relocalisation of Dvl2

Constructs (a) and (b) contain the CAG promoter which allows expression in HEK293 cells. Constructs (a) and (b) were utilized to test the expression of tdTomato and correct localisation of each form of tagged Dvl2. Constructs (c) and (d) contain the TTR promoter which drives expression in all the cells of the Visceral Endoderm (VE). Constructs (e) and (f) contain the Hex promoter that drives expression in the cells of the Anterior Visceral Endoderm (AVE).

7.2.3.1 Dvl2 mislocalisation constructs function correctly in mammalian cells

Before making transgenics, the constructs were first tested in HEK293 cells. After transfection, cells containing either of the constructs showed the expected tdTomato expression. I fixed the cells and stained with an antibody against the HA tag, to visualise the fusion Dvl2 construct. The CAG-TdTom2A-HA-Dvl2-CAAX-HBG showed the expected membrane localisation of the construct, as visualised using the HA tag. This can be seen in Figure 7.8 (middle row) and Figure 7.9 (top row). The CAG-TdTom2A-HA-Dvl2-MA-HBG showed expected cytoplasmic localisation of the construct, also visualised using the HA tag. This can be seen in Figure 7.8 (bottom row) and Figure 7.9 (bottom row).

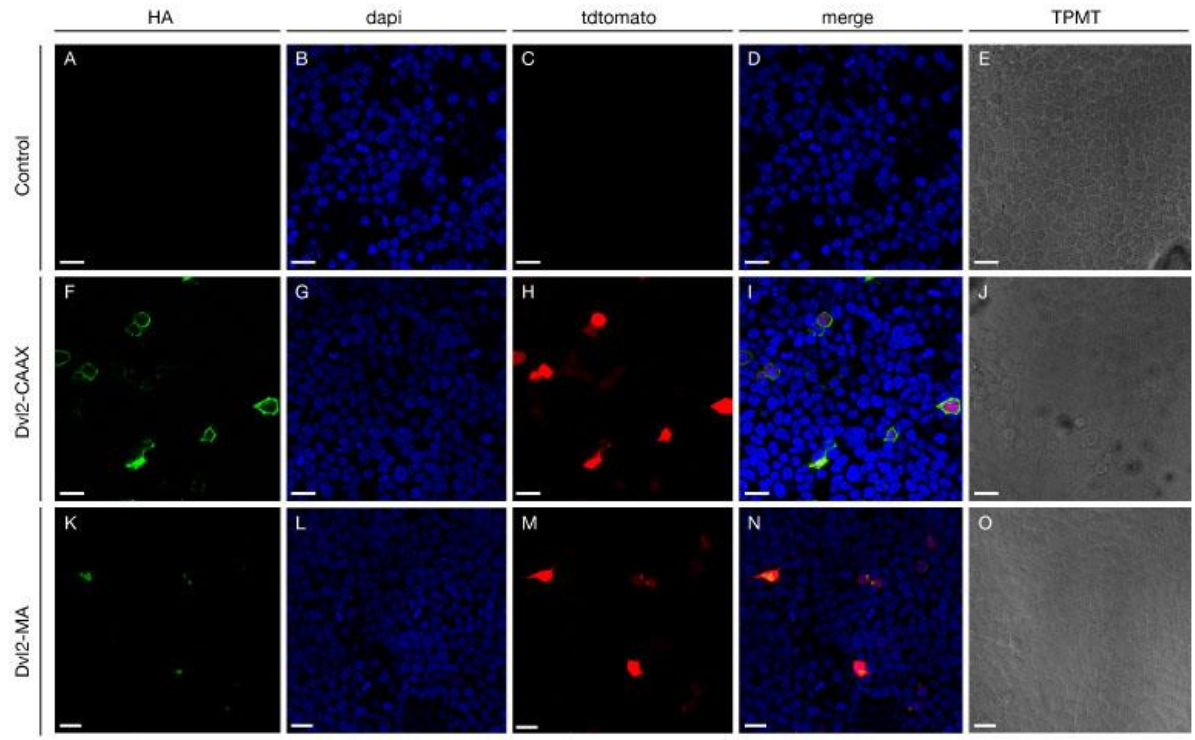


Figure 7.8: Dvl-CAAX and Dvl-MA construct expression in mammalian cells (A)

HEK293 cells transfected with control DNA (top row), the CAG-TdTom2A-HA-Dvl2-CAAX-HBG *construct (middle row) containing the membrane localisation sequence and the* CAG-TdTom2A-HA-Dvl2-MA-HBG *construct (bottom row) containing the mitochondrial localisation sequence. Scale bars = 25um*

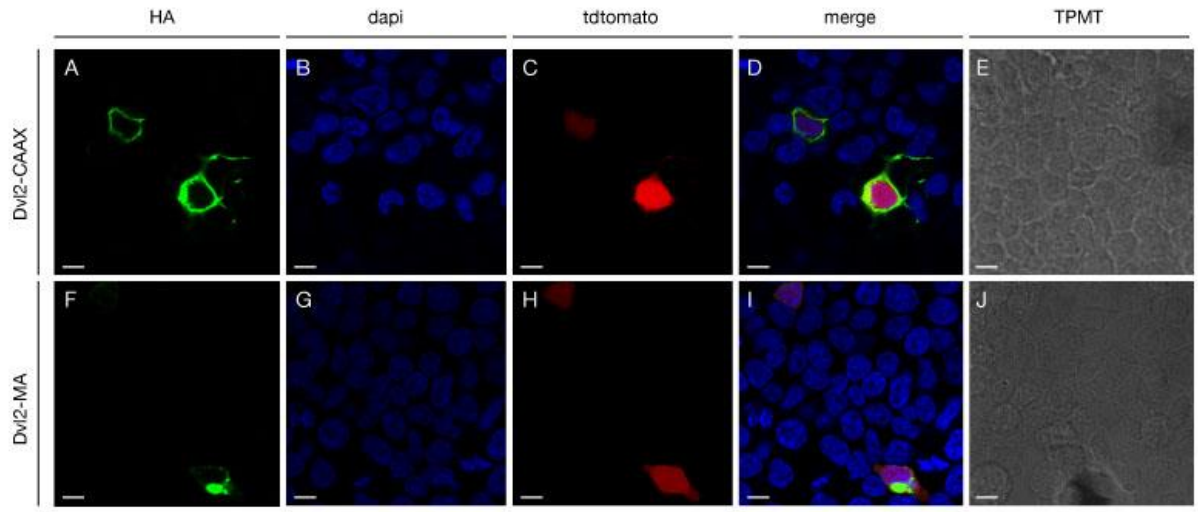


Figure 7.9: Dvl-CAAX and Dvl-MA construct expression in mammalian cells (B)

(Top row) containing the membrane localisation sequence and the CAG-TdTom2A-HA-Dvl2-MA-HBG construct (bottom row) containing the mitochondrial localisation sequence. Scale bars = 10um

7.3 Discussion

7.3.1 Investigation of the role of Vangl2 during AVE migration

I chose Vangl2 as a candidate for investigation for several reasons. Mutations in human Vangl1 and Vangl2 have been linked to human neural tube defects, making the protein of high interest from a clinical perspective [2]. Vangl2 is a core member of the PCP pathway and has been widely established as essential for a broad range of cell coordination processes. There is an abundance of examples of Vangl2 being required for PCP signalling in vertebrates, including convergent extension in Xenopus developing embryos, and neural tube closure in mice [212], [220]. Given the uncoordinated and over-migration phenotype of the *ROSA26*$^{Lyn\text{-}Celsr1}$ mutants, further investigation into the core components of the PCP pathway is warranted to establish the manner in which this pathway is influencing AVE migration [5].

The Looptail mouse line is well established, and has strong phenotypes, due to the additional impeded function of Vangl1 [223]. This made it a good candidate to broadly assess whether defects in Vangl signalling would have a strong effect on AVE migration.

Additionally, given that several mutants show mislocalised Dvl2 alongside a range of migration phenotypes I was keen to further dissect the molecular mechanism controlling Dvl2 at this stage. As such I chose a member of the PCP pathway that interacted with Dvl2 for further investigation. Torben et al. have shown that both mouse Vangl1 and Vangl2 physically interact with all three isoforms of Dvl, making it an ideal candidate for further investigation if an overmigration phenotype had been found [225].

7.3.1.1 Looptail mutants do not display defective AVE migration

The lack of an overt cellular phenotype in the *Vangl2*$^{lp/lp}$ embryos was particularly surprising given that the Looptail mutation not only impairs Vangl2 function, it also has a dominant negative effect that impedes membrane localisation and subsequent functioning of Vangl1. AVE migration occurred in all *Vangl2*$^{lp/lp}$ mutants except for one, though this embryo was delayed and appeared healthy. Uncoordinated cell migration similar to that of the *ROSA26*$^{Lyn\text{-}Celsr1}$ *mutants* was not noted in any of the *Vangl2*$^{lp/lp}$ mutants.

This is particularly interesting, given that Celsr mutant lines such as the Crash (Crsh) and Spincycle (Scy) mice show a large overlap in phenotypes with Looptail mice [123]. It is possible that Vangl2 has redundant function at this stage. It has been shown to genetically interact with several other proteins, producing more severe phenotypes in double mutants and often generating craniorachischisis when double heterozygous mutants are generated.

Examples of these include Vangl1, with Vangl2 and Vangl1 double heterozygotes exhibiting severe developmental defects including craniorachischisis, inner ear defects and cardiac abnormalities. These mutants die at a much earlier stage (E12.5) than Looptail mutants [134]. It would be highly interesting to determine if these double knockout mutants displayed an AVE migration phenotype.

Vangl2 also interacts genetically with Scrb1, with double heterozygous mutants for these proteins exhibiting PCP phenotypes comparable to Vangl2 homozygous mutants [276]. Other genetic interactions of Vangl2 include Ptk7, which generates spina bifida in double heterozygous *Ptk7* and Looptail mutants [277]. Additionally, interaction has been seen with Grhl3, with *Grhl3*$^{-/-}$;*Vangl2*$^{Lp/+}$ mice exhibiting spina bifida. While no phenotype is seen in mice

null for collagen triple helix repeat containing 1 *(Cthrc1)*, exencephaly is produced in *Cthrc1*$^{LacZ/LacZ}$;*Vangl2*$^{Lp/+}$ mutants. It is possible that double mutants of mixed components of the PCP pathway would reveal a migratory phenotype that is being obscured by redundancy [278].

It is also possible that Vangl2 does not play a role in AVE migration, and the PCP pathway is being activated without the need for this protein. This theory is supported by the lack of evidence for asymmetric localisation of Vangl2, or indeed any other PCP protein at this stage. Vangl2 shows membrane enrichment in the Epi-VE, but does not localize to a given side of VE cells. It is possible that the PCP pathway is being activated to utilize the downstream functions of this pathway, not to provide planar cell polarity. Given that Vangl2 is one of the proteins that are required to localize to one region to communicate cell orientation to neighbours in most instances of PCP activity, it stands to reason that it could be bypassed in a scenario where only the cytoskeletal regulatory function of the pathway was needed. This would explain why other members of the PCP pathway show a very distinctive phenotype, yet Vangl2 does not.

This theory is supported by the results from Wang et al., who reported that while *Looptail* homozygous embryos showed failures of PCP signalling in the neuroepithelium and the cochlea, Dvl2 membrane distribution was not affected in the neuroepithelium, despite drastic effects on Dvl2 membrane localisation in the cochlea [121]. As such it is possible that Vangl2 function is not always required for the downstream effects of PCP signalling to be enacted.

7.3.1.2 Some *Vangl2*$^{lp/lp}$ embryos exhibit delayed development

Embryos were dissected at E6.0 to allow for any potential over migration phenotypes to fully occur. Three of the eight *Vangl2*$^{lp/lp}$ embryos displayed delayed development.

Embryos from *Vangl2*$^{lp/+}$ females were often delayed regardless of genotype, however the homozygous mutants showed a smaller size when compared to littermates. Only one of these mutants had not induced AVE. All delayed embryos appeared healthy, despite their delayed phenotype.

This delay was unexpected as embryos have been reported to be found in Mendelian frequencies at E9.5, with homozygous Looptail mutants consistently exhibiting craniorachischisis at this stage [279]. It is possible that the delayed growth is compensated for at a later stage, or the delay is not sufficiently noticeable at the later stages, where the more prominent open neural tube phenotype is typically being assessed.

Overall, the Looptail line proved to have advantages and disadvantages as a genetic tool. While the iconic looped tail of the Lp line, due to a milder neural tube phenotype in heterozygous mice, allows for genotyping mice without PCR, the established heavily penetrant imperforate vagina phenotype limits breeding times significantly. While it is possible that a phenotype subtler than over-migration or uncoordinated cell migration is present in the Looptail mutants, which has yet to be discerned, it is evident that homozygous mutant Looptail mice do not display an AVE over-migration phenotype. Due to the difficulty of genotyping these embryos after scanning, generating large numbers of homozygous mutants which display a subtle or a semi-penetrant phenotype is a project of a much larger scale. Given the time restraints of a D.Phil, I decided to focus efforts elsewhere.

7.3.2 Investigating a role for β-arrestin2 in AVE migration

7.3.2.1 β-arrestin2 immunohistochemistry

The Srinivas lab has previously investigated several components of the core PCP pathway. To date, all share a common attribute in their difficulty to achieve consistent and reliable stains. Vangl2, Daam1 and Dvl2 antibodies have been investigated and all required very large numbers of embryos to achieve satisfactory results, which were achieved after lengthy optimization period for the staining protocol. Antibodies for Celsr1 have also been tested by the lab and proved to be unusable. Given this difficulty, it was unsurprising that consistently reproducible immunohistochemistry could not be achieved for β-arrestin2. This has meant that other approaches need to be taken to investigate the role of β-arrestin2 at this stage.

7.3.2.2 Some β-arrestin2$^{-/-}$ mutants exhibit AVE overmigration

It is highly interesting that the β-arrestin2 phenotype is more penetrant (75%) than those of *Lefty1*$^{-/-}$ and *ROSA26*$^{Lyn\text{-}Celsr1}$. Of the seven *Lefty1* null embryos examined by Trichas et al., five had an AVE migration defect. One of these was a failure of AVE migration, while the other four exhibited overmigration of the AVE. In *ROSA26*$^{Lyn\text{-}Celsr1}$ homozygous mutants, six of eleven embryos showed disrupted migration[5].

Unfortunately, due to the time constraints of the D.Phil, the striking overmigration phenotype seen in the β-arrestin2 homozygous null embryos could not be further investigated. Several approaches could be taken with this line to further understand the role β-arrestin2 is playing at this stage and how the mutant phenotype arises. Given the evidence for an interaction with Dvl2

and the previously demonstrated requirement for xβarr2 in Xenopus convergent extension movements, it is highly likely that Dvl2 signalling is altered in the β-arrestin2 mutants.

Immunohistochemistry using antibodies against Dvl2 and Daam1 would reveal if Barr2 function acts downstream of Dvl2 membrane recruitment, while upstream of Daam1 recruitment, as in Xenopus embryos [269]. Dvl2 and Daam1 antibodies have been established as functional at this stage by the Srinivas lab [5], [140]. While the PCP pathway can require high sample numbers for confident results of immunostaining experiments, this approach would be highly informative. Alternatively, to examine Dvl2 localisation and internalization in live embryos, the β-arrestin2 KO mouse line could be crossed to the Dvl2-EGFP line published by Wang et al. which has been used effectively in the past to demonstrate Dvl2 localisation [280].

Additionally, time-lapse experiments using the new Arrb2-Hex-GFP line would reveal if AVE protrusions had been affected in the absence of β-arrestin2. Typically in mutants where AVE cell protrusions do not occur or are disoriented, AVE migration does not fully occur or occurs in a disorganized manner. Given the overmigration phenotype of the β-arrestin2 mutant line, it would be interesting to see if an upregulation of protrusive behaviour was occurring.

Analysis of cell shape behaviour would also be of interest in β-arrestin2$^{-/-}$ embryos. Given the differences in multiple cell parameters described in Chapters 3 and 4, it is clear that cells of the ExE-VE are different in many ways to those of the Epi-VE. In *Lefty1* null mutants, the cells of the ExE exhibit a more 'Epi-VE like' behaviour, with cells taking on a less hexagonal packing structure than wild-type ExE-VE cells and showing a higher rate of neighbour exchange [140]. Investigation of the cell behaviour in both regions of the

Visceral Endoderm in β-arrestin2 mutants could reveal that changes in ExE-VE cell robustness facilitate migration past the ExE-Epiblast boundary. If this is the case, it would be stronger evidence for the ExE-VEs role as a physical boundary to AVE migration than that of the *Lefty1*$^{-/-}$ mutants, as Lefty1 is an extracellular signalling molecule which might be having a plethora of direct and indirect effects, while β-arrestin2 is intracellular and functions cell autonomously.

The generation of conditional β-arrestin2 mutants where the loss of β-arrestin2 protein is specific to cells of the VE would be highly informative for dissecting the exact role of β-arrestin2 at this stage. If such mutants retained their overmigration phenotype, this would add strongly to the evidence that β-arrestin2 is regulating cell migration and VE cell behaviour in a direct manner. If however this was not the case, conditional mutants for the ExE and epiblast tissues would be useful to determine if the effect on AVE migration is indirect, perhaps via signalling which regulates the underlying basement membrane of the two regions, altering cell tension and subsequent behaviour of distinct areas of the VE.

In several mutant lines where AVE is disrupted, such as *Lefty1* null mutants and *ROSA26*$^{Lyn\text{-}Celsr1}$ mutants, the F-actin shroud that can often be seen in embryos of this stage is diminished or abnormal actin accumulations can be seen in the ExE-VE. It would be highly interesting to examine if this is the case in β-arrestin2 null mutants. Often, the F-actin shroud cannot be seen post-fixation in wild-type embryos, so in order to test for a mutant actin phenotype accurately in β-arrestin2 null embryos, I would suggest that the β-arrestin2 knockout line be crossed to the LifeAct line described in Chapter 2, and the resultant embryos imaged live. This would allow more confident interpretation of any noted phenotype.

It would also be highly interesting to perform stain β-arrestin2$^{-/-}$ embryos using an antibody against phosphorylated ERK. The role of β-arrestins in regulating ERK1/2 signalling is the most explored scaffolding function of these proteins. When activated in β-arrestin-dependent manner, phospho-ERK is active in the cytoplasm, unlike when ERK activated by G proteins, where phospho-ERK relocates to the nucleus [281]. At E6.5 phospho-ERK is seen in this cytoplasmic fashion in the ExE cells of the embryo, while not showing activity in other

regions. This could indicate a role for β-arrestin2 signalling in the cells of the ExE.

7.3.3 Generation of Dvl2 localisation constructs

Unfortunately, due to time constraints, the transient transgenics could not be made within the time-span of this D.Phil. Only one attempt was made to inject the constructs, however this batch was developmentally delayed and unhealthy. Two embryos, however, expressed the TdTomato protein in the VE, indicating that the constructs were expressing their protein products successfully.

The constructs remain an extremely useful tool, and re-injection of the Dvl2-localisation constructs to generate transient transgenics is planned in the coming months. This will be a highly informative experiment, indicating whether localisation of Dvl-2 to the membrane is regulating cell shape and behavioural characteristics that define VE dynamics. An overmigration phenotype in the Dvl-CAAX phenotype would indicate that membrane localized Dvl2 allowed the cells of the VE to adopt a more malleable behaviour, and thus facilitated the migration of the AVE cells into the now-permissive ExE-VE region.

While Dvl2 membrane recruitment is not a characteristic exclusive to PCP signalling, it is known to be required for PCP signalling to occur. Why this is required is currently unknown. Yu at al. have shown role for the internalization of Dvl2 in the activity of PCP signalling. They accomplished this by showing that *Dvl* mutants that are unable to bind AP-2 are unable to activate the PCP pathway [282].

Use of these constructs would give an insight into whether Dvl2 internalization is required for AVE migration. If both localisation to the membrane and localisation to the cytoplasm resulted in failure of migration it would imply that permanent localisation of the protein to this region is not sufficient for PCP signalling to occur correctly at this stage, and that Dvl2 is involved in a more complex signalling pathway than recruitment to the membrane, subsequent activation and downstream signalling from the membrane. This experiment will be particularly of interest in light of the β-arrestin2 null phenotype, given the β-arrestin2 is known to play a role in Dvl2 internalisation.

The differential tissue-dependent localisation of Dvl2 seen in E5.5 and E6.0 embryos could be triggered by a number of events. The most likely to play a role is phosphorylation. Chen et al, showed that Dvl phosphorylation by PKC increases internalization of Dvl in cell culture [268].

Differential ratios of expression of the three *Dvl* isoforms, *Dvl1, Dvl2* and *Dvl3 c*ould affect the cellular localisation of Dvl2. Additionally, varying cofactors at receptor level, the cytoplasmic concentration of Dvl2 relative to other PCP proteins, differences in pH (via ion channels) and selective degradation of pathway members are all known to play roles in regulation of protein activity and localisation and could potentially be involved in this process.

Using the Dvl2 relocalisation constructs, it will be possible to determine whether correct Dvl2 localisation is necessary for AVE migration, and whether correct localisation in the AVE alone is sufficient for normal migration to occur.

The inclusion of the TTR and Hex promoters in separate versions of the constructs will give insight into whether the entire VE is required to correctly coordinate regionally distinct localisation of Dvl2, or only the cells of the AVE.

It is highly likely that the appropriate Dvl2 localisation will be required throughout the VE, as mislocalised Dvl2 is a common factor across several mutants with abnormal migration, which have been discussed in this chapter. Wild-type embryos show regional localisation of Dvl2, as opposed to a specific localisation in the AVE, so it is likely that all the cells of the VE require specific Dvl2 localisation for a permissive or non-permissive cell movement role. It could however be the case that as only the AVE cells are migrating, Dvl2 membrane localisation in non-AVE Epi-VE cells is a side effect of signalling which regulates the AVE and can be inhibited without affecting AVE migration. As such the constructs will give definitive evidence both on the role

of Dvl2 localisation and the cells that is essential to perform this role in.

7.4 Chapter conclusion

In this chapter I have discussed the investigation of two mutant mouse lines, Looptail and β-arrestin2 null. The results of each investigation were highly striking. The lack of a Vangl2 phenotype poses many questions on the role of PCP at this stage, while the overmigration seen in β-arrestin2 confirms a role for this protein in AVE migration, presenting a new player in cellular regulation of the Visceral Endoderm at this stage. I also describe a set of genetic constructs that provide a highly useful tool for further investigation of the PCP pathway in the egg cylinder stage mouse embryo.

8

General Conclusion

From the data presented in Chapters 3 and 4, it can be seen that cells of the Visceral Endoderm do not actively migrate outside of the anterior Epi-VE. In particular, the significantly higher levels of directional migration and neighbour exchange seen in the in the anterior Epi-VE strongly support this.

Global assessment of Visceral Endoderm cells carried out in both 2D and 3D revealed that cells of the Epi-VE are more squamous that those of the ExE-VE. Cells of the anterior Epi-VE showed the most irregular shape, however lateral and posterior Epi-VE were significantly more irregular than that of the ExE-VE. This supports the theory that cells of the Epi-VE facilitate migration of the AVE through rearrangement of their own cell-cell contacts, generating relatively energetically unfavourable structures to facilitate the migration of the AVE [5].

Lateral Epi-VE cells were seen to migrate more than posterior Epi-VE cells, though this was not directional, nor did they show a higher level of neighbour exchange. This indicates that the increased movement of these cells is due to the proximity to the migrating AVE cells. Lateral Epi-VE cells were also seen to be larger than those of the anterior Epi-VE, which was noted in both 2D and 3D data. While this could be interpreted as the cells of the AVE shrinking in size, this is unlikely as cells of the posterior were seen to be of a similar size to those on the anterior when assessed for apical cell surface area. A role for the increased size of lateral Epi-VE cells would be difficult to investigate, however this change in size could play a role in biasing AVE migration towards remaining on the anterior of the embryo.

Evidence from Chapters 3, 4 and 5 support the theory that cells of the ExE-VE form a physical barrier to AVE migration. The ExE-VE cells are seen to be more robust and columnar in 3D, as well as exhibiting a higher shape factor in 2D. They were also shown to exhibit less migration than cells of the Epiblast. Additionally it was shown that AVE cell protrusions from the final point of AVE migration extend into the ExE-VE region, despite cells of the AVE coming to their stereotypical abrupt halt, this further indicates the role of the ExE-VE as a physical barrier. 3D imaging also revealed large effects of the standard embryo fixation process on cellular shape and size. This is highly informative for the community, where fixation is a common technique in the investigation of embryological samples.

A novel method of imaging the distal tip of the embryo revealed cellular projections in the induced unmigrated AVE. These did not show the filopodia-tipped or bifurcated nature often seen during migration. The lack of protrusion characteristics typically associated with migration along a chemical gradient prior to migration supports the evidence for a chemoattractant being involved in AVE migration, rather than the filopodia-tipped and bifurcated processes

being an independently occurring characteristic of AVE cells.

A role for haptotaxis was also indicated by the increased presence of Laminin-α1 in the basement membrane on the anterior side of the Visceral Endoderm during AVE migration. This could be complimentary to the presence of a chemoattractant, or could produce the protrusions seen in the migrating AVE alone. Further investigation into the extent of the role haptotaxis plays in AVE migration would be highly interesting and would reveal previously uncharacterized features of the AVE.

Mass spectrometry was utilized to reveal differences in the regional protein expression and protein phosphorylation at the egg cylinder stage. This has generated many candidates for investigation that will be of benefit to the field. Additionally in this study, the cytoskeleton regulating protein Profilin was seen to have highly dynamic and regionally localized staining in a time series ranging from E5.25 to E6.5. While no upregulation was seen in the cells of the AVE, this demonstrates the rapid nature of cellular changes occurring at this stage and indicates a role for Profilin in the behaviour of non-AVE tissues at this stage.

Finally, investigation of the PCP pathway revealed no AVE migration phenotype in dominant negative mutants for core PCP protein Vangl2. This could indicate a bypassing of asymmetry generation in the activation of PCP signalling. Analysis of other PCP asymmetry generating proteins at this stage would be highly informative to further understand the role of PCP at this stage. An overmigration phenotype was seen in β-arrestin2 null mutants at this stage, adding β-arrestin2 to the cohort of proteins that regulate AVE migration. Given the high likelihood of a role for this protein in the regulation of Dvl2, further investigation of this mutant will contribute to understanding how PCP regulates the behaviour of the cells of the Visceral Endoderm.

References:

[1] P. Ybot-Gonzalez *et al.*, "Convergent extension, planar-cell-polarity signalling and initiation of mouse neural tube closure.," *Development*, vol. 134, no. 4, pp. 789–99, 2007.

[2] D. M. Juriloff and M. J. Harris, "A consideration of the evidence that genetic defects in planar cell polarity contribute to the etiology of human neural tube defects," *Birth Defects Research Part A - Clinical and Molecular Teratology*, vol. 94, no. 10. pp. 824–840, 2012.

[3] E. Scarpa and R. Mayor, "Collective cell migration in development," *J. Cell Biol.*, vol. 212, no. 2, pp. 143–155, 2016.

[4] E. Theveneau and R. Mayor, "Cadherins in collective cell migration of mesenchymal cells," *Current Opinion in Cell Biology*, vol. 24, no. 5. pp. 677–684, 2012.

[5] G. Trichas *et al.*, "Nodal dependent differential localisation of dishevelled-2 demarcates regions of differing cell behaviour in the visceral endoderm," *PLoS Biol*, vol. 9, no. 2, p. e1001019, 2011.

[6] E. Theveneau and R. Mayor, "Neural crest delamination and migration: From epithelium-to-mesenchyme transition to collective cell migration," *Developmental Biology*, vol. 366, no. 1. pp. 34–54, 2012.

[7] D. W. Raible and G. J. Kruse, "Organization of the lateral line system in embryonic zebrafish.," *J. Comp. Neurol.*, vol. 421, no. 2, pp. 189–198, 2000.

[8] J. B. Wallingford and R. M. Harland, "Neural tube closure requires Dishevelled-dependent convergent extension of the midline.," *Development*, vol. 129, no. 24, pp. 5815–25, 2002.

[9] D. Sutherland, C. Samakovlis, and M. A. Krasnow, "branchless encodes a Drosophila FGF homolog that controls tracheal cell migration and the pattern of branching," *Cell*, vol. 87, no. 6, pp. 1091–1101, 1996.

[10] Wikimedia Commons, “Vector diagram of laboratory mouse (black and white).” .

[11] J. E. Dietrich and T. Hiiragi, “Stochastic patterning in the mouse pre-implantation embryo,” *Development*, vol. 134, no. 23, pp. 4219–4231, 2007.

[12] A. Ralston and J. Rossant, “Cdx2 acts downstream of cell polarization to cell-autonomously promote trophectoderm fate in the early mouse embryo,” *Dev. Biol.*, vol. 313, no. 2, pp. 614–629, 2008.

[13] D. Strumpf *et al.*, “Cdx2 is required for correct cell fate specification and differentiation of trophectoderm in the mouse blastocyst.,” *Development*, vol. 132, no. 9, pp. 2093–2102, 2005.

[14] J. Nichols *et al.*, “Formation of pluripotent stem cells in the mammalian embryo depends on the POU transcription factor Oct4,” *Cell*, vol. 95, no. 3, pp. 379–391, 1998.

[15] A. K. Tarkowski and J. Wróblewska, “Development of blastomeres of mouse eggs isolated at the 4- and 8-cell stage.,” *J. Embryol. Exp. Morphol.*, vol. 18, no. 1, pp. 155–180, 1967.

[16] M. H. Johnson and C. A. Ziomek, “The foundation of two distinct cell lineages within the mouse morula,” *Cell*, vol. 24, no. 1, pp. 71–80, 1981.

[17] T. Watanabe, J. S. Biggins, N. B. Tannan, and S. Srinivas, “Limited predictive value of blastomere angle of division in trophectoderm and inner cell mass specification.,” *Development*, vol. 141, no. 11, pp. 2279–88, 2014.

[18] I. Chambers *et al.*, “Functional expression cloning of Nanog, a pluripotency sustaining factor in embryonic stem cells,” *Cell*, vol. 113, no. 5, pp. 643–655, 2003.

[19] K. Mitsui *et al.*, “The homeoprotein nanog is required for maintenance of pluripotency in mouse epiblast and ES cells,” *Cell*, vol. 113, no. 5, pp. 631–642, 2003.

[20] J. Zhang *et al.*, “Sall4 modulates embryonic stem cell pluripotency and

early embryonic development by the transcriptional regulation of Pou5f1.," *Nat. Cell Biol.*, vol. 8, no. 10, pp. 1114–1123, 2006.

[21] C. Chazaud, Y. Yamanaka, T. Pawson, and J. Rossant, "Early Lineage Segregation between Epiblast and Primitive Endoderm in Mouse Blastocysts through the Grb2-MAPK Pathway," *Dev. Cell*, vol. 10, no. 5, pp. 615–624, 2006.

[22] E. Arman, R. Haffner-Krausz, Y. Chen, J. K. Heath, and P. Lonai, "Targeted disruption of fibroblast growth factor (FGF) receptor 2 suggests a role for FGF signaling in pregastrulation mammalian development.," *Proc. Natl. Acad. Sci. U. S. A.*, vol. 95, no. 9, pp. 5082–7, 1998.

[23] B. Feldman, W. Poueymirou, V. E. Papaioannou, T. M. DeChiara, and M. Goldfarb, "Requirement of FGF-4 for Postimplantation Mouse Development," *Science (80-.).*, vol. 267, no. 5195, pp. 246–249, 1995.

[24] B. Plusa, A. Piliszek, S. Frankenberg, J. Artus, and A.-K. Hadjantonakis, "Distinct sequential cell behaviours direct primitive endoderm formation in the mouse blastocyst.," *Development*, vol. 135, no. 18, pp. 3081–91, 2008.

[25] J. Rossant and P. P. L. Tam, "Blastocyst lineage formation, early embryonic asymmetries and axis patterning in the mouse.," *Development*, vol. 136, no. 5, pp. 701–713, 2009.

[26] J. D. Kidder, J. R. Giles, R. H. Foote, M. E. Richmond, and M. Salerno, "Allocation of inner cell mass and trophectoderm cells to the preimplantation blastocyst of the domestic ferret, Mustela putorius furo," *J. Exp. Zool.*, vol. 283, no. 2, pp. 202–209, 1999.

[27] M. Nadijcka and N. Hillman, "Ultrastructural studies of the mouse blastocyst substages," *Development*, vol. 32, no. 3, pp. 675–695, Dec. 1974.

[28] G. S. Kwon, M. Viotti, and A. K. Hadjantonakis, "The Endoderm of the Mouse Embryo Arises by Dynamic Widespread Intercalation of

Embryonic and Extraembryonic Lineages," *Dev. Cell*, vol. 15, no. 4, pp. 509–520, 2008.

[29] M. Guzman-Ayala *et al.*, "Nodal protein processing and fibroblast growth factor 4 synergize to maintain a trophoblast stem cell microenvironment.," *Proc. Natl. Acad. Sci. U. S. A.*, vol. 101, no. 44, pp. 15656–15660, 2004.

[30] T. A. Rodriguez, S. Srinivas, M. P. Clements, J. C. Smith, and R. S. P. Beddington, "Induction and migration of the anterior visceral endoderm is regulated by the extra-embryonic ectoderm.," *Development*, vol. 132, no. 11, pp. 2513–2520, 2005.

[31] G. Trichas *et al.*, "Multi-cellular rosettes in the mouse visceral endoderm facilitate the ordered migration of anterior visceral endoderm cells," *PLoS Biol*, vol. 10, no. 2, p. e1001256, 2012.

[32] C. Chazaud and J. Rossant, "Disruption of early proximodistal patterning and AVE formation in Apc mutants.," *Development*, vol. 133, pp. 3379–3387, 2006.

[33] W. R. Waldrip, E. K. Bikoff, P. A. Hoodless, J. L. Wrana, and E. J. Robertson, "Smad2 signaling in extraembryonic tissues determines anterior-posterior polarity of the early mouse embryo," *Cell*, vol. 92, no. 6, pp. 797–808, 1998.

[34] A. Perea-Gomez *et al.*, "Nodal antaginists in the anterior visceral endoderm prevent the formation of multiple primitive streaks," *Dev. Cell*, vol. 3, no. 5, pp. 745–756, 2002.

[35] J. Huelsken, R. Vogel, V. Brinkmann, B. Erdmann, C. Birchmeier, and W. Birchmeier, "Requirement for β-catenin in anterior-posterior axis formation in mice," *J. Cell Biol.*, vol. 148, no. 3, pp. 567–578, 2000.

[36] N. Ben-Haim *et al.*, "The Nodal Precursor Acting via Activin Receptors Induces Mesoderm by Maintaining a Source of Its Convertases and BMP4," *Dev. Cell*, vol. 11, no. 3, pp. 313–323, 2006.

[37] J. Ding *et al.*, "Cripto is required for correct orientation of the anterior-

posterior axis in the mouse embryo.," *Nature*, vol. 395, no. 6703, pp. 702–707, 1998.

[38] I. Varlet, J. Collignon, and E. J. Robertson, "Nodal Expression in the Primitive Endoderm Is Required for Specification of the Anterior Axis During Mouse Gastrulation.," *Development*, vol. 124, no. 5, pp. 1033–1044, 1997.

[39] D. G. Wilkinson, S. Bhatt, and B. G. Herrmann, "Expression pattern of the mouse T gene and its role in mesoderm formation.," *Nature*, vol. 343, no. 6259, pp. 657–9, 1990.

[40] J. Brennan, C. C. Lu, D. P. Norris, T. a Rodriguez, R. S. Beddington, and E. J. Robertson, "Nodal signalling in the epiblast patterns the early mouse embryo.," *Nature*, vol. 411, no. 6840, pp. 965–969, 2001.

[41] D. Mesnard, M. Guzman-Ayala, and D. B. Constam, "Nodal specifies embryonic visceral endoderm and sustains pluripotent cells in the epiblast before overt axial patterning.," *Development*, vol. 133, no. 13, pp. 2497–2505, 2006.

[42] J. A. Belo *et al.*, "Cerberus-like is a secreted factor with neuralizing activity expressed in the anterior primitive endoderm of the mouse gastrula," *Mech. Dev.*, vol. 68, no. 1–2, pp. 45–57, 1997.

[43] M. Yamamoto *et al.*, "Antagonism between Smad1 and Smad2 signaling determines the site of distal visceral endoderm formation in the mouse embryo," *J. Cell Biol.*, vol. 184, no. 2, pp. 323–334, 2009.

[44] P. Thomas and R. Beddington, "Anterior primitive endoderm may be responsible for patterning the anterior neural plate in the mouse embryo.," *Curr. Biol.*, vol. 6, no. 11, pp. 1487–1496, 1996.

[45] E. Hermesz, S. Mackem, and K. A. Mahon, "Rpx: a novel anterior-restricted homeobox gene progressively activated in the prechordal plate, anterior neural plate and Rathke's pouch of the mouse embryo.," *Development*, vol. 122, no. 1, pp. 41–52, 1996.

[46] P. Q. Thomas, A. Brown, and R. S. Beddington, "Hex: a homeobox gene

revealing peri-implantation asymmetry in the mouse embryo and an early transient marker of endothelial cell precursors.," *Development*, vol. 125, no. 1, pp. 85–94, Jan. 1998.

[47] S. M. Harrison, S. L. Dunwoodie, R. M. Arkell, H. Lehrach, and R. S. Beddington, "Isolation of novel tissue-specific genes from cDNA libraries representing the individual tissue constituents of the gastrulating mouse embryo," *Development*, vol. 121, no. 8, pp. 2479–2489, 1995.

[48] S. Piccolo *et al.*, "The head inducer Cerberus is a multifunctional antagonist of Nodal, BMP and Wnt signals.," *Nature*, vol. 397, pp. 707–710, 1999.

[49] M. Yamamoto *et al.*, "Nodal antagonists regulate formation of the anteroposterior axis of the mouse embryo.," *Nature*, vol. 428, no. 6981, pp. 387–392, 2004.

[50] C. Meno *et al.*, "Two closely-related left-right asymmetrically expressed genes, lefty-1 and lefty-2: their distinct expression domains, chromosomal linkage and direct neuralizing activity in Xenopus embryos.," *Genes Cells*, vol. 2, pp. 513–524, 1997.

[51] S. Srinivas, T. Rodriguez, M. Clements, J. C. Smith, and R. S. P. Beddington, "Active cell migration drives the unilateral movements of the anterior visceral endoderm," *Development*, vol. 131, no. 5, pp. 1157–1164, 2004.

[52] I. Migeotte, T. Omelchenko, A. Hall, and K. V. Anderson, "Rac1-dependent collective cell migration is required for specification of the anterior-posterior body axis of the mouse," *PLoS Biol.*, vol. 8, no. 8, pp. 37–38, 2010.

[53] R. Kalluri and R. A. Weinberg, "The basics of epithelial-mesenchymal transition," *Journal of Clinical Investigation*, vol. 119, no. 6. pp. 1420–1428, 2009.

[54] P. Haas and D. Gilmour, "Chemokine Signaling Mediates Self-

Organizing Tissue Migration in the Zebrafish Lateral Line," *Dev. Cell*, vol. 10, no. 5, pp. 673–680, 2006.

[55] A. Ghysen and C. Dambly-Chaudière, "Development of the zebrafish lateral line," *Current Opinion in Neurobiology*, vol. 14, no. 1. pp. 67–73, 2004.

[56] G. Valentin, P. Haas, and D. Gilmour, "The Chemokine SDF1a Coordinates Tissue Migration through the Spatially Restricted Activation of Cxcr7 and Cxcr4b," *Curr. Biol.*, vol. 17, no. 12, pp. 1026–1031, 2007.

[57] M. Mukhopadhyay *et al.*, "Dickkopf1 Is Required for Embryonic Head Induction and Limb Morphogenesis in the Mouse," *Dev. Cell*, vol. 1, no. 3, pp. 423–434, 2001.

[58] C. Kimura-Yoshida *et al.*, "Canonical Wnt signaling and its antagonist regulate anterior-posterior axis polarization by guiding cell migration in mouse visceral endoderm," *Dev. Cell*, vol. 9, no. 5, pp. 639–650, 2005.

[59] T. Omelchenko, M. A. Rabadan, R. Hernández-Martinez, J. Grego-Bessa, K. V Anderson, and A. Hall, "β-Pix directs collective migration of anterior visceral endoderm cells in the early mouse embryo," *Genes & Dev.*, vol. 28, no. 24, pp. 2764–2777, 2014.

[60] N. Andrew and R. H. Insall, "Chemotaxis in shallow gradients is mediated independently of PtdIns 3-kinase by biased choices between random protrusions.," *Nat. Cell Biol.*, vol. 9, no. 2, pp. 193–200, 2007.

[61] S. J. King *et al.*, "Lamellipodia are crucial for haptotactic sensing and response," *J. Cell Sci.*, vol. 129, no. 12, pp. 2329–2342, Jun. 2016.

[62] J. H. Wen *et al.*, "Haptotaxis is Cell Type Specific and Limited by Substrate Adhesiveness," *Cell. Mol. Bioeng.*, vol. 8, no. 4, pp. 530–542, 2015.

[63] S. P. Amarachintha, K. J. Ryan, M. Cayer, N. S. Boudreau, N. M. Johnson, and C. A. Heckman, "Effect of Cdc42 domains on filopodia sensing, cell orientation, and haptotaxis," *Cell. Signal.*, vol. 27, no. 3,

pp. 683–693, 2015.

[64] S. Carter, “Principles of cell motility: the direction of cell movement and cancer invasion.,” *Nature*, vol. 208, no. 5016, p. 1183, 1965.

[65] B. A. Maldonado and L. T. Furcht, “Epidermal growth factor stimulates integrin-mediated cell migration of cultured human corneal epithelial cells on fibronectin and arginine-glycine-aspartic acid peptide,” *Invest Ophthalmol Vis Sci*, vol. 36, no. 10, pp. 2120–2126, 1995.

[66] S. Aznavoorian, M. L. Stracke, H. Krutzsch, E. Schiffmann, and L. A. Liotta, “Signal transduction for chemotaxis and haptotaxis by matrix molecules in tumor cells,” *J. Cell Biol.*, vol. 110, no. 4, pp. 1427–1438, 1990.

[67] J. B. McCarthy and L. T. Furcht, “Laminin and fibronectin promote the haptotactic migration of B16 mouse melanoma cells in vitro.,” *J. Cell Biol.*, vol. 98, no. 4, pp. 1474–1480, 1984.

[68] L. T. Furcht, J. B. McCarthy, S. L. Palm, M. L. Basara, and J. Enenstein, “Peptide fragments of laminin and fibronectin promote migration (haptotaxis and chemotaxis) of metastatic cells.,” *Ciba Found. Symp.*, vol. 108, pp. 130–145, 1984.

[69] D. K. Olivero and L. T. Furcht, “Type IV collagen, laminin, and fibronectin promote the adhesion and migration of rabbit lens epithelial cells in vitro,” *Investig. Ophthalmol. Vis. Sci.*, vol. 34, no. 10, pp. 2825–2834, 1993.

[70] D. R. Farkas and D. L. Chapman, “Kinked tail mutation results in notochord defects in heterozygotes and distal visceral endoderm defects in homozygotes,” *Dev. Dyn.*, vol. 238, no. 12, pp. 3237–3247, 2009.

[71] N. Gersdorff, M. Müller, S. Otto, R. Poschadel, S. Hübner, and N. Miosge, “Basement membrane composition in the early mouse embryo day 7.,” *Dev. Dyn.*, vol. 233, no. 3, pp. 1140–1148, 2005.

[72] D. Acampora *et al.*, “Forebrain and midbrain regions are deleted in Otx2-/- mutants due to a defective anterior neuroectoderm specification

during gastrulation.," *Development*, vol. 121, no. 10, pp. 3279–3290, 1995.

[73] L. Bally-Cuif, M. Gulisano, V. Broccoli, and E. Boncinelli, "c-otx2 is expressed in two different phases of gastrulation and is sensitive to retinoic acid treatment in chick embryo," *Mech. Dev.*, vol. 49, no. 1–2, pp. 49–63, 1995.

[74] T. A. Yatskievych, S. Pascoe, and P. B. Antin, "Expression of the homebox gene Hex during early stages of chick embryo development," *Mech. Dev.*, vol. 80, no. 1, pp. 107–109, 1999.

[75] P. Q. Thomas, a Brown, and R. S. Beddington, "Hex: a homeobox gene revealing peri-implantation asymmetry in the mouse embryo and an early transient marker of endothelial cell precursors.," *Development*, vol. 125, pp. 85–94, 1998.

[76] S. J. Chou *et al.*, "Conserved regulatory elements establish the dynamic expression of Rpx/HesxI in early vertebrate development," *Dev. Biol.*, vol. 292, no. 2, pp. 533–545, 2006.

[77] F. Bertocchini and C. D. Stern, "The hypoblast of the chick embryo positions the primitive streak by antagonizing nodal signaling," *Dev. Cell*, vol. 3, no. 5, pp. 735–744, 2002.

[78] J. A. Belo *et al.*, "Cerberus-like is a secreted BMP and nodal antagonist not essential for mouse development," *Genesis*, vol. 26, no. 4, pp. 265–270, 2000.

[79] C. D. Stern and K. M. Downs, "The hypoblast (visceral endoderm): an evo-devo perspective.," *Development*, vol. 139, no. 6, pp. 1059–69, 2012.

[80] M. Oshima, H. Oshima, K. Kitagawa, M. Kobayashi, C. Itakura, and M. Taketo, "Loss of Apc heterozygosity and abnormal tissue building in nascent intestinal polyps in mice carrying a truncated Apc gene," *Proc. Natl. Acad. Sci.*, vol. 92, no. 10, pp. 4482–4486, 1995.

[81] J. Bloomekatz, J. Grego-Bessa, I. Migeotte, and K. V Anderson, "Pten regulates collective cell migration during specification of the anterior--

posterior axis of the mouse embryo," *Dev. Biol.*, vol. 364, no. 2, pp. 192–201, 2012.

[82] A. Perea-Gomez *et al.*, "Otx2 is required for visceral endoderm movement and for the restriction of posterior signals in the epiblast of the mouse embryo.," *Development*, vol. 128, no. 5, pp. 753–65, 2001.

[83] C. Bertet, L. Sulak, and T. Lecuit, "Myosin-dependent junction remodelling controls planar cell intercalation and axis elongation.," *Nature*, vol. 429, no. 6992, pp. 667–71, 2004.

[84] J. T. Blankenship, S. T. Backovic, J. S. P. Sanny, O. Weitz, and J. A. Zallen, "Multicellular rosette formation links planar cell polarity to tissue morphogenesis," *Dev. Cell*, vol. 11, no. 4, pp. 459–470, 2006.

[85] J. T. Blankenship, S. T. Backovic, J. P. Sanny, O. Weitz, and J. A. Zallen, "Multicellular Rosette Formation Links Planar Cell Polarity to Tissue Morphogenesis," *Dev. Cell*, vol. 11, no. 4, pp. 459–470, 2006.

[86] G. Trichas *et al.*, "Multi-cellular rosettes in the mouse visceral endoderm facilitate the ordered migration of anterior visceral endoderm cells," *PLoS Biol.*, vol. 10, no. 2, 2012.

[87] J. A. Zallen and J. T. Blankenship, "Multicellular dynamics during epithelial elongation," *Seminars in Cell and Developmental Biology*, vol. 19, no. 3. pp. 263–270, 2008.

[88] F. Tissir *et al.*, "Lack of cadherins Celsr2 and Celsr3 impairs ependymal ciliogenesis, leading to fatal hydrocephalus.," *Nat. Neurosci.*, vol. 13, no. 6, pp. 700–7, 2010.

[89] H. Song *et al.*, "Planar cell polarity breaks bilateral symmetry by controlling ciliary positioning," *Nature*, vol. 466, no. 7304, pp. 378–382, 2010.

[90] J. M. Carvajal-Gonzalez, A.-C. Roman, and M. Mlodzik, "Positioning of centrioles is a conserved readout of Frizzled planar cell polarity signalling," *Nat. Commun.*, vol. 7, p. 11135, 2016.

[91] L. A. Baena-López, A. Baonza, and A. García-Bellido, "The orientation

of cell divisions determines the shape of Drosophila organs," *Curr. Biol.*, vol. 15, no. 18, pp. 1640–1644, 2005.

[92] Y. Gong, C. Mo, and S. E. Fraser, "Planar cell polarity signalling controls cell division orientation during zebrafish gastrulation.," *Nature*, vol. 430, no. 7000, pp. 689–93, 2004.

[93] M. Sgalen *et al.*, "The Fz-Dsh Planar Cell Polarity Pathway Induces Oriented Cell Division via Mud/NuMA in Drosophila and Zebrafish," *Dev. Cell*, vol. 19, no. 5, pp. 740–752, 2010.

[94] D. Devenport and E. Fuchs, "Planar polarization in embryonic epidermis orchestrates global asymmetric morphogenesis of hair follicles.," *Nat. Cell Biol.*, vol. 10, no. 11, pp. 1257–1268, 2008.

[95] L. L. Wong and P. N. Adler, "Tissue polarity genes of Drosophila regulate the subcellular location for prehair initiation in pupal wing cells," *J. Cell Biol.*, vol. 123, no. 1, pp. 209–221, 1993.

[96] D. Gubb and A. Garcia-Bellido, "A genetic analysis of the determination of cuticular polarity during development in Drosophila melanogaster," *J. Embryol. Exp. Morphol.*, vol. 68, pp. 37–57, 1982.

[97] M. Simons and M. Mlodzik, "Planar cell polarity signaling: from fly development to human disease.," *Annu. Rev. Genet.*, vol. 42, pp. 517–40, 2008.

[98] H. Matakatsu and S. S. Blair, "Interactions between Fat and Dachsous and the regulation of planar cell polarity in the Drosophila wing.," *Development*, vol. 131, no. 15, pp. 3785–94, 2004.

[99] H. F. Clark, D. Brentrup, K. Schneitz, A. Bieber, C. Goodman, and M. Noll, "Dachsous encodes a member of the cadherin superfamily that controls imaginai disc morphogenesis in Drosophila," *Genes Dev.*, vol. 9, no. 12, pp. 1530–1542, 1995.

[100] A. Jenny, J. Reynolds-Kenneally, G. Das, M. Burnett, and M. Mlodzik, "Diego and Prickle regulate Frizzled planar cell polarity signalling by competing for Dishevelled binding," *Nat. Cell Biol.*, vol. 7, no. 7, pp.

691–697, 2005.

[101] G. Das, A. Jenny, T. J. Klein, S. Eaton, and M. Mlodzik, “Diego interacts with Prickle and Strabismus/Van Gogh to localize planar cell polarity complexes,” *Development*, vol. 131, no. 18, pp. 4467–4476, 2004.

[102] T. Wolff and G. Rubin, “Strabismus, a novel gene that regulates tissue polarity and cell fate decisions in Drosophila.,” *Development*, vol. 125, no. 6, pp. 1149–1159, 1998.

[103] T. Usui *et al.*, “Flamingo, a seven-pass transmembrane cadherin, regulates planar cell polarity under the control of Frizzled,” *Cell*, vol. 98, no. 5, pp. 585–595, 1999.

[104] J. D. Axelrod, “Unipolar membrane association of Dishevelled mediates Frizzled planar cell polarity signaling,” *Genes & Dev.*, vol. 15, no. 10, pp. 1182–1187, 2001.

[105] R. Bastock, H. Strutt, and D. Strutt, “Strabismus is asymmetrically localised and binds to Prickle and Dishevelled during Drosophila planar polarity patterning,” *Development*, vol. 130, no. 13, pp. 3007–3014, 2003.

[106] A. Jenny, J. Reynolds-Kenneally, G. Das, M. Burnett, and M. Mlodzik, “Diego and Prickle regulate Frizzled planar cell polarity signalling by competing for Dishevelled binding.,” *Nat. Cell Biol.*, vol. 7, no. 7, pp. 691–697, 2005.

[107] G. Das, J. Reynolds-Kenneally, and M. Mlodzik, “The atypical cadherin flamingo links frizzled and notch signaling in planar polarity establishment in the Drosophila eye,” *Dev. Cell*, vol. 2, no. 5, pp. 655–666, 2002.

[108] Y. Bellaïche, M. Gho, J. A. Kaltschmidt, A. H. Brand, and F. Schweisguth, “Frizzled regulates localization of cell-fate determinants and mitotic spindle rotation during asymmetric cell division.,” *Nat. Cell Biol.*, vol. 3, no. 1, pp. 50–7, 2001.

[109] Y. Bellaïche, O. Beaudoin-Massiani, I. Stuttem, and F. Schweisguth, "The planar cell polarity protein Strabismus promotes Pins anterior localization during asymmetric division of sensory organ precursor cells in Drosophila.," *Development*, vol. 131, no. 2, pp. 469–478, 2004.

[110] W. S. Chen *et al.*, "Asymmetric Homotypic Interactions of the Atypical Cadherin Flamingo Mediate Intercellular Polarity Signaling," *Cell*, vol. 133, no. 6, pp. 1093–1105, 2008.

[111] Y. Shimada, S. Yonemura, H. Ohkura, D. Strutt, and T. Uemura, "Polarized transport of Frizzled along the planar microtubule arrays in Drosophila wing epithelium," *Dev. Cell*, vol. 10, no. 2, pp. 209–222, 2006.

[112] M. Matis, D. A. Russler-Germain, Q. Hu, C. J. Tomlin, and J. D. Axelrod, "Microtubules provide directional information for core PCP function," *Elife*, vol. 3, no. August2014, pp. 1–17, 2014.

[113] R. Habas, Y. Kato, and X. He, "Wnt/Frizzled activation of Rho regulates vertebrate gastrulation and requires a novel Formin homology protein Daam1," *Cell*, vol. 107, no. 7, pp. 843–854, 2001.

[114] C. G. Winter *et al.*, "Drosophila Rho-associated kinase (Drok) links Frizzled-mediated planar cell polarity signaling to the actin cytoskeleton," *Cell*, vol. 105, no. 1, pp. 81–91, 2001.

[115] P. N. Adler, R. E. Krasnow, and J. Liu, "Tissue polarity points from cells that have higher Frizzled levels towards cells that have lower Frizzled levels," *Current Biology*, vol. 7, no. 12. pp. 940–949, 1997.

[116] C. M. Karner, R. Chirumamilla, S. Aoki, P. Igarashi, J. B. Wallingford, and T. J. Carroll, "Wnt9b signaling regulates planar cell polarity and kidney tubule morphogenesis," *Nat. Genet.*, vol. 41, no. 7, pp. 793–799, 2009.

[117] C. P. Heisenberg *et al.*, "Silberblick/Wnt11 mediates convergent extension movements during zebrafish gastrulation.," *Nature*, vol. 405, no. 6782, pp. 76–81, 2000.

[118] J. Wu, A.-C. Roman, J. M. Carvajal-Gonzalez, and M. Mlodzik, "Wg and Wnt4 provide long-range directional input to planar cell polarity orientation in Drosophila.," *Nat. Cell Biol.*, vol. 15, no. 9, pp. 1045–55, 2013.

[119] J. B. Wallingford, B. A. Rowning, K. M. Vogeli, U. Rothbächer, S. E. Fraser, and R. M. Harland, "Dishevelled controls cell polarity during Xenopus gastrulation," *Nature*, vol. 405, no. 6782, pp. 81–85, 2000.

[120] J. R. Jessen *et al.*, "Zebrafish trilobite identifies new roles for Strabismus in gastrulation and neuronal movements.," *Nat. Cell Biol.*, vol. 4, no. 8, pp. 610–5, 2002.

[121] J. Wang *et al.*, "Dishevelled genes mediate a conserved mammalian PCP pathway to regulate convergent extension during neurulation," *Development*, vol. 133, no. 9, pp. 1767–1778, 2006.

[122] M. Montcouquiol, R. A. Rachel, P. J. Lanford, N. G. Copeland, N. A. Jenkins, and M. W. Kelley, "Identification of Vangl2 and Scrb1 as planar polarity genes in mammals," *Nature*, vol. 423, no. 6936, pp. 173–177, 2003.

[123] J. A. Curtin *et al.*, "Mutation of Celsr1 disrupts planar polarity of inner ear hair cells and causes severe neural tube defects in the mouse," *Curr. Biol.*, vol. 13, no. 13, pp. 1129–1133, 2003.

[124] N. Guo, C. Hawkins, and J. Nathans, "Frizzled6 controls hair patterning in mice.," *Proc. Natl. Acad. Sci. U. S. A.*, vol. 101, pp. 9277–9281, 2004.

[125] T. Goto and R. Keller, "The planar cell polarity gene strabismus regulates convergence and extension and neural fold closure in Xenopus.," *Dev. Biol.*, vol. 247, no. 1, pp. 165–181, 2002.

[126] T. Nishimura, H. Honda, and M. Takeichi, "Planar cell polarity links axes of spatial dynamics in neural-tube closure," *Cell*, vol. 149, no. 5, pp. 1084–1097, 2012.

[127] A. J. Copp, N. D. E. Greene, and J. N. Murdoch, "The genetic basis of

mammalian neurulation," *Nat. Rev. Genet.*, vol. 4, no. 10, pp. 784–793, 2003.

[128] R. Keller, "Shaping the vertebrate body plan by polarized embryonic cell movements.," *Science*, vol. 298, no. 5600, pp. 1950–1954, 2002.

[129] I. Migeotte, T. Omelchenko, A. Hall, and K. V Anderson, "Rac1-dependent collective cell migration is required for specification of the anterior-posterior body axis of the mouse," *PLoS Biol*, vol. 8, no. 8, p. e1000442, 2010.

[130] N. Smyth *et al.*, "Absence of basement membranes after targeting the LAMC1 gene results in embryonic lethality due to failure of endoderm differentiation," *J. Cell Biol.*, vol. 144, no. 1, pp. 151–160, 1999.

[131] T. a Rodriguez, E. S. Casey, R. M. Harland, J. C. Smith, and R. S. Beddington, "Distinct enhancer elements control Hex expression during gastrulation and early organogenesis.," *Dev. Biol.*, vol. 234, no. 2, pp. 304–16, 2001.

[132] L. C. Strong and W. F. Hollander, "Hereditary loop-tail in the house mouse accompanied by imperforate vagina and with lethal craniorachischisis when homozygous," *J. Hered.*, vol. 40, no. 12, pp. 329–334, 1949.

[133] E. Torban, H.-J. Wang, N. Groulx, and P. Gros, "Independent mutations in mouse Vangl2 that cause neural tube defects in looptail mice impair interaction with members of the Dishevelled family," *J. Biol. Chem.*, vol. 279, no. 50, pp. 52703–52713, 2004.

[134] E. Torban *et al.*, "Genetic interaction between members of the Vangl family causes neural tube defects in mice," *Proc. Natl. Acad. Sci.*, vol. 105, no. 9, pp. 3449–3454, 2008.

[135] L. M. Bohn, R. J. Lefkowitz, R. R. Gainetdinov, K. Peppel, M. G. Caron, and F. T. Lin, "Enhanced morphine analgesia in mice lacking beta-arrestin 2," *Science (80-.).*, vol. 286, no. 5449, pp. 2495–2498, 1999.

[136] J. Riedl *et al.*, "Lifeact: a versatile marker to visualize F-actin.," *Nat.*

Methods, vol. 5, no. 7, pp. 605–7, 2008.

[137] N/A, “International Genetic Standardization (IGS) Program.” [Online]. Available: http://www.criver.com/files/pdfs/rms/rm_rm_r_igs.aspx.

[138] N/A, “CD-1® IGS Mouse Model Information Sheet.” [Online]. Available: http://www.criver.com/files/pdfs/rms/cd1/rm_rm_d_cd1_mouse.aspx.

[139] S. Srinivas, “Imaging cell movements in egg-cylinder stage mouse embryos,” *Cold Spring Harb. Protoc.*, vol. 5, no. 12, 2010.

[140] B. Joyce, “Elucidating the molecular mechanisms underlying cell movements during early embryogenesis,” 2012.

[141] G. Trichas, J. Begbie, and S. Srinivas, “Use of the viral 2A peptide for bicistronic expression in transgenic mice.,” *BMC Biol.*, vol. 6, p. 40, Jan. 2008.

[142] B. Joyce and S. Srinivas, “Cell movements in the egg cylinder stage mouse embryo,” in *Mouse Development*, Springer, 2012, pp. 219–229.

[143] P. J. Keller *et al.*, “Fast, high-contrast imaging of animal development with scanned light sheet-based structured-illumination microscopy.,” *Nat. Methods*, vol. 7, no. 8, pp. 637–42, Aug. 2010.

[144] M. Weber, M. Mickoleit, and J. Huisken, “Light sheet microscopy,” *Methods Cell Biol.*, vol. 123, pp. 193–215, 2014.

[145] C. Sommer and D. W. Gerlich, “Machine learning in cell biology {\textendash} teaching computers to recognize phenotypes,” *J. Cell Sci.*, vol. 126, no. 24, pp. 5529–5539, 2013.

[146] L. J. Mango, “Computer-assisted cervical cancer screening using neural networks,” *Cancer Lett.*, vol. 77, no. 2, pp. 155–162.

[147] K. Z. Mao, P. Zhao, and P.-H. Tan, “Supervised learning-based cell image segmentation for P53 immunohistochemistry,” *IEEE Trans. Biomed. Eng.*, vol. 53, no. 6, pp. 1153–1163, Jun. 2006.

[148] S. Lawrence, C. L. Giles, A. C. Tsoi, and A. D. Back, “Face recognition: a convolutional neural-network approach,” *IEEE Trans. Neural Networks*, vol. 8, no. 1, pp. 98–113, Jan. 1997.

[149] A. K. Jain, J. Mao, and K. M. Mohiuddin, "Artificial neural networks: a tutorial," *Computer (Long. Beach. Calif).*, vol. 29, no. 3, pp. 31–44, Mar. 1996.

[150] D. Ciregan, U. Meier, and J. Schmidhuber, "Multi-column deep neural networks for image classification," in *Computer Vision and Pattern Recognition (CVPR), 2012 IEEE Conference on*, 2012, pp. 3642–3649.

[151] J. Villanueva *et al.*, "F-actin-myosin II inhibitors affect chromaffin granule plasma membrane distance and fusion kinetics by retraction of the cytoskeletal cortex," in *Journal of Molecular Neuroscience*, 2012, vol. 48, no. 2, pp. 328–338.

[152] K. Rehm, L. Panzer, V. van Vliet, E. Genot, and S. Linder, "Drebrin preserves endothelial integrity by stabilizing nectin at adherens junctions.," *J. Cell Sci.*, vol. 126, no. Pt 16, pp. 3756–69, 2013.

[153] M. Deibler, J. P. Spatz, and R. Kemkemer, "Actin fusion proteins alter the dynamics of mechanically induced cytoskeleton rearrangement," *PLoS One*, vol. 6, no. 8, 2011.

[154] A. Fraccaroli *et al.*, "Visualization of Endothelial Actin Cytoskeleton in the Mouse Retina," *PLoS One*, vol. 7, no. 10, 2012.

[155] R. A. Foty and M. S. Steinberg, "The differential adhesion hypothesis: A direct evaluation," *Dev. Biol.*, vol. 278, no. 1, pp. 255–263, 2005.

[156] I. Migeotte, J. Grego-Bessa, and K. V. Anderson, "Rac1 mediates morphogenetic responses to intercellular signals in the gastrulating mouse embryo," *Development*, vol. 138, no. 14, pp. 3011–3020, Jun. 2011.

[157] R. Keller *et al.*, "Mechanisms of convergence and extension by cell intercalation.," *Philos. Trans. R. Soc. Lond. B. Biol. Sci.*, vol. 355, no. 1399, pp. 897–922, 2000.

[158] J. B. Wallingford, B. a Rowning, K. M. Vogeli, U. Rothbächer, S. E. Fraser, and R. M. Harland, "Dishevelled controls cell polarity during Xenopus gastrulation.," *Nature*, vol. 405, no. 6782, pp. 81–5, 2000.

[159] R. Keller, J. Shih, and C. Domingo, “The patterning and functioning of protrusive activity during convergence and extension of the Xenopus organiser.,” *Dev. Suppl.*, vol. 91, pp. 81–91, 1992.

[160] J. Shih and R. Keller, “Cell motility driving mediolateral intercalation in explants of Xenopus laevis.,” *Development*, vol. 116, pp. 901–914, 1992.

[161] J. Shih and R. Keller, “Patterns of cell motility in the organizer and dorsal mesoderm of Xenopus laevis.,” *Development*, vol. 116, pp. 915–930, 1992.

[162] G. Lebreton and J. Casanova, “Specification of leading and trailing cell features during collective migration in the Drosophila trachea,” *J Cell Sci*, vol. 127, no. Pt 2, pp. 465–474, 2014.

[163] A. Domogatskaya, S. Rodin, and K. Tryggvason, “Functional diversity of laminins,” *Annu. Rev. Cell Dev. Biol.*, vol. 28, pp. 523–553, 2012.

[164] E. Klaffky, R. Williams, C. C. Yao, B. Ziober, R. Kramer, and a Sutherland, “Trophoblast-specific expression and function of the integrin alpha 7 subunit in the peri-implantation mouse embryo.,” *Dev. Biol.*, vol. 239, no. 1, pp. 161–175, 2001.

[165] F. Alpy *et al.*, “Generation of a conditionally null allele of the laminin alpha-1 gene,” *Genesis*, vol. 43, no. 2, pp. 59–70, 2005.

[166] L. Gonçalves, M. Filipe, S. Marques, A.-M. Salgueiro, J. D. Becker, and J. A. Belo, “Identification and functional analysis of novel genes expressed in the Anterior Visceral Endoderm.,” *Int. J. Dev. Biol.*, vol. 55, no. 3, pp. 281–95, 2011.

[167] L. N. Johnson, “The regulation of protein phosphorylation,” *Biochem. Soc. Trans.*, vol. 37, no. 4, pp. 627–641, 2009.

[168] S. Ikeda, S. Kishida, H. Yamamoto, H. Murai, S. Koyama, and A. Kikuchi, “Axin, a negative regulator of the Wnt signaling pathway, forms a complex with GSK-3ß and ß-catenin and promotes GSK-3ß-dependent phosphorylation of ß-catenin,” *EMBO J.*, vol. 17, no. 5, pp.

1371–1384, 1998.

[169] M. Kitagawa *et al.*, "An F-box protein, FWD1, mediates ubiquitin-dependent proteolysis of ß-catenin," *EMBO J.*, vol. 18, no. 9, pp. 2401–2410, 1999.

[170] H. Lodish, A. Berk, S. L. Zipursky, P. Matsudaira, D. Baltimore, and J. Darnell, "Overview of the Cell Cycle and Its Control," 2000.

[171] A. H. Kim, G. Khursigara, X. Sun, T. F. Franke, and M. V Chao, "Akt phosphorylates and negatively regulates apoptosis signal-regulating kinase 1," *Mol. Cell. Biol.*, vol. 21, no. 3, pp. 893–901, 2001.

[172] T. Watanabe, H. Hosoya, and S. Yonemura, "Regulation of myosin II dynamics by phosphorylation and dephosphorylation of its light chain in epithelial cells," *Mol. Biol. Cell*, vol. 18, no. 2, pp. 605–616, 2007.

[173] C. Chen *et al.*, "Myosin light chain kinase (MLCK) regulates cell migration in a myosin regulatory light chain phosphorylation-independent mechanism," *J. Biol. Chem.*, vol. 289, no. 41, pp. 28478–28488, 2014.

[174] K. Fumoto, T. Uchimura, T. Iwasaki, U. Kozue, and H. Hosoya, "Phosphorylation of myosin II regulatory light chain is necessary for migration of HeLa cells but not for localization of myosin II at the leading edge," *Biochem. J.*, vol. 370, no. 2, pp. 551–556, 2003.

[175] M. A. Sells, J. T. Boyd, and J. Chernoff, "p21-activated kinase 1 (Pak1) regulates cell motility in mammalian fibroblasts," *J. Cell Biol.*, vol. 145, no. 4, pp. 837–849, 1999.

[176] S. Ray, J. A. Fanti, D. P. Macedo, and M. Larsen, "LIM kinase regulation of cytoskeletal dynamics is required for salivary gland branching morphogenesis," *Mol. Biol. Cell*, vol. 25, no. 16, pp. 2393–2407, 2014.

[177] A. M. Hopkins, A. P. A'Drian, L. M. Winfree, G. T. Brown, M. G. Laukoetter, and A. Nusrat, "Organized migration of epithelial cells requires control of adhesion and protrusion through Rho kinase

effectors," *Am. J. Physiol. Liver Physiol.*, vol. 292, no. 3, pp. G806--G817, 2007.

[178] D. J. C. Pappin, P. Hojrup, and A. J. Bleasby, "Rapid identification of proteins by peptide-mass fingerprinting," *Curr. Biol.*, vol. 3, no. 6, pp. 327–332, 1993.

[179] B. Domon and R. Aebersold, "Mass spectrometry and protein analysis.," *Science*, vol. 312, no. 5771, pp. 212–7, 2006.

[180] P. Casado *et al.*, "Phosphoproteomics data classify hematological cancer cell lines according to tumor type and sensitivity to kinase inhibitors," *Genome Biol.*, vol. 14, no. 4, p. 1, 2013.

[181] M. P. Alcolea, O. Kleiner, and P. R. Cutillas, "Increased confidence in large-scale phosphoproteomics data by complementary mass spectrometric techniques and matching of phosphopeptide data sets," *J. Proteome Res.*, vol. 8, no. 8, pp. 3808–3815, 2009.

[182] H. Mi, S. Poudel, A. Muruganujan, J. T. Casagrande, and P. D. Thomas, "PANTHER version 10: expanded protein families and functions, and analysis tools," *Nucleic Acids Res.*, vol. 44, no. D1, pp. D336--D342, 2016.

[183] M. Kanehisa and S. Goto, "KEGG: kyoto encyclopedia of genes and genomes," *Nucleic Acids Res.*, vol. 28, no. 1, pp. 27–30, 2000.

[184] M. Kanehisa, Y. Sato, M. Kawashima, M. Furumichi, and M. Tanabe, "KEGG as a reference resource for gene and protein annotation," *Nucleic Acids Res.*, p. gkv1070, 2015.

[185] X. Zhou, H. Sasaki, L. Lowe, B. L. M. Hogan, and M. R. Kuehn, "Nodal is a novel TGF-ß-like gene expressed in the mouse node during gastrulation," 1993.

[186] G. Winnier, M. Blessing, P. A. Labosky, and B. L. Hogan, "Bone morphogenetic protein-4 is required for mesoderm formation and patterning in the mouse.," *Genes & Dev.*, vol. 9, no. 17, pp. 2105–2116, 1995.

[187] U. Consortium and others, “UniProt: a hub for protein information,” *Nucleic Acids Res.*, p. gku989, 2014.

[188] M. Magrane, U. Consortium, and others, “UniProt Knowledgebase: a hub of integrated protein data,” *Database*, vol. 2011, p. bar009, 2011.

[189] N. D. E. Greene, P. Stanier, and A. J. Copp, “Genetics of human neural tube defects,” *Hum. Mol. Genet.*, vol. 18, no. R2, pp. R113--R129, 2009.

[190] K. Hayakawa, H. Tatsumi, and M. Sokabe, “Actin filaments function as a tension sensor by tension-dependent binding of cofilin to the filament,” *J. Cell Biol.*, vol. 195, no. 5, pp. 721–727, 2011.

[191] R. M. Ezzell, M. M. Chafel, and P. T. Matsudaira, “Differential localization of villin and fimbrin during development of the mouse visceral endoderm and intestinal epithelium.,” *Development*, vol. 106, no. 2, pp. 407–19, 1989.

[192] C. Meno *et al.*, “lefty-1 is required for left-right determination as a regulator of lefty-2 and nodal,” *Cell*, vol. 94, no. 3, pp. 287–297, 1998.

[193] J. A. Belo *et al.*, “Cerberus-like is a secreted factor with neuralizing activity expressed in the anterior primitive endoderm of the mouse gastrula,” *Mech. Dev.*, vol. 68, no. 1, pp. 45–57, 1997.

[194] M. Blum *et al.*, “Gastrulation in the mouse: the role of the homeobox gene goosecoid,” *Cell*, vol. 69, no. 7, pp. 1097–1106, 1992.

[195] P. Q. Thomas, A. Brown, and R. S. Beddington, “Hex: a homeobox gene revealing peri-implantation asymmetry in the mouse embryo and an early transient marker of endothelial cell precursors,” *Development*, vol. 125, no. 1, pp. 85–94, 1998.

[196] C. Schaniel *et al.*, “Smarcc1/Baf155 Couples Self-Renewal Gene Repression with Changes in Chromatin Structure in Mouse Embryonic Stem Cells,” *Stem Cells*, vol. 27, no. 12, pp. 2979–2991, 2009.

[197] D. W. Stuckey *et al.*, “Coordination of cell proliferation and anterior-posterior axis establishment in the mouse embryo,” *Development*, vol. 138, no. 8, pp. 1521–1530, 2011.

[198] M. L. Soares, M.-E. Torres-Padilla, and M. Zernicka-Goetz, "Bone morphogenetic protein 4 signaling regulates development of the anterior visceral endoderm in the mouse embryo.," *Dev. Growth Differ.*, vol. 50, no. 7, pp. 615–21, 2008.

[199] I. Lassing and U. Lindberg, "Specificity of the interaction between phosphatidylinositol 4, 5-bisphosphate and the profilin: actin complex," *J. Cell. Biochem.*, vol. 37, no. 3, pp. 255–267, 1988.

[200] W. Witke, J. D. Sutherland, A. Sharpe, M. Arai, and D. J. Kwiatkowski, "Profilin I is essential for cell survival and cell division in early mouse development," *Proc. Natl. Acad. Sci.*, vol. 98, no. 7, pp. 3832–3836, 2001.

[201] M.-F. Carlier and D. Pantaloni, "Actin assembly in response to extracellular signals: role of capping proteins, thymosin ß4 and profilin," in *Seminars in cell biology*, 1994, vol. 5, no. 3, pp. 183–191.

[202] T. Finkel, J. A. Theriot, K. R. Dise, G. F. Tomaselli, and P. J. Goldschmidt-Clermont, "Dynamic actin structures stabilized by profilin.," *Proc. Natl. Acad. Sci.*, vol. 91, no. 4, pp. 1510–1514, 1994.

[203] A. K. Wolven, L. D. Belmont, N. M. Mahoney, S. C. Almo, and D. G. Drubin, "In vivo importance of actin nucleotide exchange catalyzed by profilin," *J. Cell Biol.*, vol. 150, no. 4, pp. 895–904, 2000.

[204] T. D. Pollard, L. Blanchoin, and R. D. Mullins, "Molecular mechanisms controlling actin filament dynamics in nonmuscle cells," *Annu. Rev. Biophys. Biomol. Struct.*, vol. 29, no. 1, pp. 545–576, 2000.

[205] T. Johansson, S. Grenklo, and R. Karlsson, "Detection of binding partners to the profilin: actin complex by far Western and mass spectrometry analyses," *Anal. Biochem.*, vol. 335, no. 2, pp. 228–234, 2004.

[206] C. Yang *et al.*, "Profilin enhances Cdc42-induced nucleation of actin polymerization," *J. Cell Biol.*, vol. 150, no. 5, pp. 1001–1012, 2000.

[207] A.-M. C. Yvon, P. Wadsworth, and M. A. Jordan, "Taxol suppresses dynamics of individual microtubules in living human tumor cells," *Mol.*

Biol. Cell, vol. 10, no. 4, pp. 947–959, 1999.

[208] I. Arnal and R. H. Wade, "How does taxol stabilize microtubules?," *Curr. Biol.*, vol. 5, no. 8, pp. 900–908, 1995.

[209] D. Panda, M. A. Jordan, K. C. Chu, and L. Wilson, "Differential effects of vinblastine on polymerization and dynamics at opposite microtubule ends," *J. Biol. Chem.*, vol. 271, no. 47, pp. 29807–29812, 1996.

[210] R. Dhamodharan, M. A. Jordan, D. Thrower, L. Wilson, and P. Wadsworth, "Vinblastine suppresses dynamics of individual microtubules in living interphase cells.," *Mol. Biol. Cell*, vol. 6, no. 9, pp. 1215–1229, 1995.

[211] S. S. Lienkamp *et al.*, "Vertebrate kidney tubules elongate using a planar cell polarity-dependent, rosette-based mechanism of convergent extension," *Nat. Genet.*, vol. 44, no. 12, pp. 1382–1387, 2012.

[212] J. N. Murdoch, K. Doudney, C. Paternotte, A. J. Copp, and P. Stanier, "Severe neural tube defects in the loop-tail mouse result from mutation of Lpp1, a novel gene involved in floor plate specification," *Hum. Mol. Genet.*, vol. 10, no. 22, pp. 2593–2601, 2001.

[213] Z. Kibar, K. J. Vogan, N. Groulx, M. J. Justice, D. A. Underhill, and P. Gros, "Ltap, a mammalian homolog of Drosophila Strabismus/Van Gogh, is altered in the mouse neural tube mutant Loop-tail," *Nat Genet*, vol. 28, no. 3, pp. 251–255, Jul. 2001.

[214] S. Saburi *et al.*, "Loss of Fat4 disrupts PCP signaling and oriented cell division and leads to cystic kidney disease," *Nat. Genet.*, vol. 40, no. 8, pp. 1010–1015, 2008.

[215] D. Qian *et al.*, "Wnt5a functions in planar cell polarity regulation in mice," *Dev. Biol.*, vol. 306, no. 1, pp. 121–133, 2007.

[216] M. Katoh, "Molecular cloning and characterization of Strabismus 2 (STB2).," *Int. J. Oncol.*, vol. 20, no. 5, pp. 993–998, 2002.

[217] M. Park and R. T. Moon, "The planar cell-polarity gene stbm regulates cell behaviour and cell fate in vertebrate embryos," *Nat. Cell Biol.*, vol.

4, no. 1, pp. 20–25, 2002.

[218] A. Jenny, R. S. Darken, P. A. Wilson, and M. Mlodzik, "Prickle and strabismus form a functional complex to generate a correct axis during planar cell polarity signaling," *EMBO J.*, vol. 22, no. 17, pp. 4409–4420, 2003.

[219] A. S. Rawls and T. Wolff, "Strabismus requires Flamingo and Prickle function to regulate tissue polarity in the Drosophila eye," *Development*, vol. 130, no. 9, pp. 1877–1887, 2003.

[220] R. S. Darken, A. M. Scola, A. S. Rakeman, G. Das, M. Mlodzik, and P. A. Wilson, "The planar polarity gene strabismus regulates convergent extension movements in Xenopus," *EMBO J.*, vol. 21, no. 5, pp. 976–985, 2002.

[221] T. Goto, L. Davidson, M. Asashima, and R. Keller, "Planar cell polarity genes regulate polarized extracellular matrix deposition during frog gastrulation," *Curr. Biol.*, vol. 15, no. 8, pp. 787–793, 2005.

[222] N. D. E. Greene, D. Gerrelli, H. W. M. Van Straaten, and A. J. Copp, "Abnormalities of floor plate, notochord and somite differentiation in the loop-tail (Lp) mouse: a model of severe neural tube defects," *Mech. Dev.*, vol. 73, no. 1, pp. 59–72, 1998.

[223] H. Yin, C. O. Copley, L. V Goodrich, and M. R. Deans, "Comparison of phenotypes between different vangl2 mutants demonstrates dominant effects of the Looptail mutation during hair cell development," *PLoS One*, vol. 7, no. 2, p. e31988, 2012.

[224] M. Hashimoto *et al.*, "Planar polarization of node cells determines the rotational axis of node cilia," *Nat. Cell Biol.*, vol. 12, no. 2, pp. 170–176, 2010.

[225] E. Torban *et al.*, "Tissue, cellular and sub-cellular localization of the Vangl2 protein during embryonic development: effect of the Lp mutation," *Gene Expr. Patterns*, vol. 7, no. 3, pp. 346–354, 2007.

[226] E. Belotti *et al.*, "Molecular characterisation of endogenous

Vangl2/Vangl1 heteromeric protein complexes," *PLoS One*, vol. 7, no. 9, p. e46213, 2012.

[227] C. Wansleeben, H. Feitsma, M. Montcouquiol, C. Kroon, E. Cuppen, and F. Meijlink, "Planar cell polarity defects and defective Vangl2 trafficking in mutants for the COPII gene Sec24b," *Development*, vol. 137, no. 7, pp. 1067–1073, 2010.

[228] J. Merte *et al.*, "Sec24b selectively sorts Vangl2 to regulate planar cell polarity during neural tube closure.," *Nat. Cell Biol.*, vol. 12, no. 1, pp. 41-46–8, 2010.

[229] X. He, M. Semenov, K. Tamai, and X. Zeng, "LDL receptor-related proteins 5 and 6 in Wnt/ß-catenin signaling: arrows point the way," *Development*, vol. 131, no. 8, pp. 1663–1677, 2004.

[230] J. Wang and A. Wynshaw-Boris, "The canonical Wnt pathway in early mammalian embryogenesis and stem cell maintenance/differentiation," *Curr. Opin. Genet. & Dev.*, vol. 14, no. 5, pp. 533–539, 2004.

[231] O. G. Fahmy and M. Fahmy, "New mutants report," *Dros Inf Serv*, vol. 33, pp. 82–94, 1959.

[232] J. Klingensmith, R. Nusse, and N. Perrimon, "The Drosophila segment polarity gene dishevelled encodes a novel protein required for response to the wingless signal.," *Genes & Dev.*, vol. 8, no. 1, pp. 118–130, 1994.

[233] H. Theisen, J. Purcell, M. Bennett, D. Kansagara, A. Syed, and J. L. Marsh, "Dishevelled is required during wingless signaling to establish both cell polarity and cell identity.," *Development*, vol. 120, no. 2, pp. 347–60, 1994.

[234] C. Gao and Y.-G. Chen, "Dishevelled: The hub of Wnt signaling," *Cell. Signal.*, vol. 22, no. 5, pp. 717–727, 2010.

[235] L. C. Sheldahl, D. C. Slusarski, P. Pandur, J. R. Miller, M. Kühl, and R. T. Moon, "Dishevelled activates Ca2+ flux, PKC, and CamKII in vertebrate embryos," *J. Cell Biol.*, vol. 161, no. 4, pp. 769–777, 2003.

[236] G.-H. Kim, J.-H. Her, and J.-K. Han, "Ryk cooperates with Frizzled 7 to promote Wnt11-mediated endocytosis and is essential for Xenopus laevis convergent extension movements," *J. Cell Biol.*, vol. 182, no. 6, pp. 1073–1082, 2008.

[237] X. Zhang *et al.*, "Dishevelled promotes axon differentiation by regulating atypical protein kinase C," *Nat. Cell Biol.*, vol. 9, no. 7, pp. 743–754, 2007.

[238] B. C. Mak, H. L. Kenerson, L. D. Aicher, E. A. Barnes, and R. S. Yeung, "Aberrant ß-catenin signaling in tuberous sclerosis," *Am. J. Pathol.*, vol. 167, no. 1, pp. 107–116, 2005.

[239] K. A. Wharton, "Runnin'with the Dvl: proteins that associate with Dsh/Dvl and their significance to Wnt signal transduction," *Dev. Biol.*, vol. 253, no. 1, pp. 1–17, 2003.

[240] H.-C. Wong *et al.*, "Direct binding of the PDZ domain of Dishevelled to a conserved internal sequence in the C-terminal region of Frizzled," *Mol. Cell*, vol. 12, no. 5, pp. 1251–1260, 2003.

[241] C. Punchihewa, A. M. Ferreira, R. Cassell, P. Rodrigues, and N. Fujii, "Sequence requirement and subtype specificity in the high-affinity interaction between human frizzled and dishevelled proteins," *Protein Sci.*, vol. 18, no. 5, pp. 994–1002, 2009.

[242] M. Boutros and M. Mlodzik, "Dishevelled: at the crossroads of divergent intracellular signaling pathways," *Mech. Dev.*, vol. 83, no. 1, pp. 27–37, 1999.

[243] L. Zeng *et al.*, "The mouse Fused locus encodes axin, an inhibitor of the Wnt signaling pathway that regulates embryonic axis formation," *Cell*, vol. 90, no. 1, pp. 181–192, 1997.

[244] M. V. Semënov and M. Snyder, "Human Dishevelled Genes Constitute a DHR-Containing Multigene Family," *Genomics*, vol. 42, no. 2, pp. 302–310, 1997.

[245] J. D. Axelrod, J. R. Miller, J. M. Shulman, R. T. Moon, and N.

Perrimon, “Differential recruitment of Dishevelled provides signaling specificity in the planar cell polarity and Wingless signaling pathways,” *Genes & Dev.*, vol. 12, no. 16, pp. 2610–2622, 1998.

[246] M. Boutros, N. Paricio, D. I. Strutt, and M. Mlodzik, “Dishevelled activates JNK and discriminates between JNK pathways in planar polarity and wingless signaling,” *Cell*, vol. 94, no. 1, pp. 109–118, 1998.

[247] L. Li *et al.*, “Dishevelled proteins lead to two signaling pathways Regulation of LEF-1 and c-Jun N-terminal kinase in mammalian cells,” *J. Biol. Chem.*, vol. 274, no. 1, pp. 129–134, 1999.

[248] M. Simons *et al.*, “Electrochemical cues regulate assembly of the Frizzled/Dishevelled complex at the plasma membrane during planar epithelial polarization,” *Nat. Cell Biol.*, vol. 11, no. 3, pp. 286–294, 2009.

[249] W. Liu *et al.*, “Mechanism of activation of the Formin protein Daam1.,” *Proc. Natl. Acad. Sci. U. S. A.*, vol. 105, no. 1, pp. 210–5, Jan. 2008.

[250] A. S. Alberts, “Diaphanous-related Formin homology proteins,” *Curr. Biol.*, vol. 12, no. 23, p. R796, 2002.

[251] M. Amano, M. Nakayama, and K. Kaibuchi, “Rho-kinase/ROCK: A key regulator of the cytoskeleton and cell polarity,” *Cytoskeleton*, vol. 67, no. 9. pp. 545–554, 2010.

[252] S. B. Rosso, D. Sussman, A. Wynshaw-Boris, and P. C. Salinas, “Wnt signaling through Dishevelled, Rac and JNK regulates dendritic development,” *Nat. Neurosci.*, vol. 8, no. 1, pp. 34–42, 2005.

[253] N. Lijam *et al.*, “Social interaction and sensorimotor gating abnormalities in mice lacking Dvl1,” *Cell*, vol. 90, no. 5, pp. 895–905, 1997.

[254] N. S. Hamblet, “Dishevelled 2 is essential for cardiac outflow tract development, somite segmentation and neural tube closure,” *Development*, vol. 129, no. 24, pp. 5827–5838, Dec. 2002.

[255] S. L. Etheridge *et al.*, “Murine dishevelled 3 functions in redundant pathways with dishevelled 1 and 2 in normal cardiac outflow tract,

cochlea, and neural tube development," *PLoS Genet*, vol. 4, no. 11, p. e1000259, 2008.

[256] A. Wynshaw-Boris, "Dishevelled: In Vivo Roles of a Multifunctional Gene Family During Development," *Curr. Top. Dev. Biol.*, vol. 101, p. 213, 2012.

[257] T. Sinha, B. Wang, S. Evans, A. Wynshaw-Boris, and J. Wang, "Disheveled mediated planar cell polarity signaling is required in the second heart field lineage for outflow tract morphogenesis," *Dev. Biol.*, vol. 370, no. 1, pp. 135–144, 2012.

[258] Y.-N. Lee, Y. Gao, and H. Wang, "Differential mediation of the Wnt canonical pathway by mammalian Dishevelleds-1,-2, and-3," *Cell. Signal.*, vol. 20, no. 2, pp. 443–452, 2008.

[259] T. J. Park, R. S. Gray, A. Sato, R. Habas, and J. B. Wallingford, "Subcellular localization and signaling properties of dishevelled in developing vertebrate embryos," *Curr. Biol.*, vol. 15, no. 11, pp. 1039–1044, 2005.

[260] T. Schwarz-Romond, C. Metcalfe, and M. Bienz, "Dynamic recruitment of axin by Dishevelled protein assemblies," *J Cell Sci*, vol. 120, no. 14, pp. 2402–2412, 2007.

[261] O. A. Mohamed, H. J. Clarke, and D. Dufort, "ß-catenin signaling marks the prospective site of primitive streak formation in the mouse embryo," *Dev. Dyn.*, vol. 231, no. 2, pp. 416–424, 2004.

[262] A. Ferrer-Vaquer, A. Piliszek, G. Tian, R. J. Aho, D. Dufort, and A.-K. Hadjantonakis, "A sensitive and bright single-cell resolution live imaging reporter of Wnt/ss-catenin signaling in the mouse," *BMC Dev. Biol.*, vol. 10, no. 1, p. 1, 2010.

[263] C. Kemp, E. Willems, S. Abdo, L. Lambiv, and L. Leyns, "Expression of all Wnt genes and their secreted antagonists during mouse blastocyst and postimplantation development," *Dev. Dyn.*, vol. 233, no. 3, pp. 1064–1075, 2005.

[264] M. Mcclarrinon *et al.*, "In vivo studies of gene expression via transient transgenesis using lipid-DNA delivery," *DNA Cell Biol.*, vol. 18, no. 7, pp. 533–547, 1999.

[265] L. M. Bohn, R. R. Gainetdinov, F. T. Lin, R. J. Lefkowitz, and M. G. Caron, "Mu-opioid receptor desensitization by beta-arrestin-2 determines morphine tolerance but not dependence.," *Nature*, vol. 408, no. 6813, pp. 720–723, 2000.

[266] M. J. Lohse, J. L. Benovic, J. Codina, M. G. Caron, and R. J. Lefkowitz, "beta-Arrestin: a protein that regulates beta-adrenergic receptor function.," *Science (80-.).*, vol. 248, no. 4962, pp. 1547–50, 1990.

[267] O. B. Goodman *et al.*, "Beta-arrestin acts as a clathrin adaptor in endocytosis of the beta2-adrenergic receptor.," *Nature*, vol. 383, no. 6599, pp. 447–50, 1996.

[268] W. Chen *et al.*, "Dishevelled 2 recruits beta-arrestin 2 to mediate Wnt5A-stimulated endocytosis of Frizzled 4.," *Science*, vol. 301, no. 5638, pp. 1391–4, Sep. 2003.

[269] G.-H. Kim and J.-K. Han, "Essential role for ß-arrestin 2 in the regulation of Xenopus convergent extension movements," *EMBO J.*, vol. 26, no. 10, pp. 2513–2526, 2007.

[270] L. Richardson *et al.*, "EMAGE mouse embryo spatial gene expression database: 2014 update," *Nucleic Acids Res.*, vol. 42, no. D1, 2014.

[271] J. Gao, J. Liao, and G.-Y. Yang, "CAAX-box protein, prenylation process and carcinogenesis," *Am J Transl Res*, vol. 1, no. 3, pp. 312–325, 2009.

[272] E. Choy *et al.*, "Endomembrane trafficking of ras: The CAAX motif targets proteins to the ER and Golgi," *Cell*, vol. 98, no. 1, pp. 69–80, 1999.

[273] C. Kocks, E. Gouin, M. Tabouret, P. Berche, H. Ohayon, and P. Cossart, "L. monocytogenes-induced actin assembly requires the actA gene product, a surface protein," *Cell*, vol. 68, no. 3, pp. 521–531, 1992.

[274] E. Domann *et al.*, "A novel bacterial virulence gene in Listeria

monocytogenes required for host cell microfilament interaction with homology to the proline-rich region of vinculin.," *EMBO J.*, vol. 11, no. 5, p. 1981, 1992.

[275] S. Pistor, T. Chakraborty, K. Niebuhr, E. Domann, and J. Wehland, "The ActA protein of Listeria monocytogenes acts as a nucleator inducing reorganization of the actin cytoskeleton.," *EMBO J.*, vol. 13, no. 4, p. 758, 1994.

[276] J. N. Murdoch *et al.*, "Circletail, a new mouse mutant with severe neural tube defects: chromosomal localization and interaction with the loop-tail mutation.," *Genomics*, vol. 78, no. November, pp. 55–63, 2001.

[277] X. Lu, A. G. M. Borchers, C. Jolicoeur, H. Rayburn, J. C. Baker, and M. Tessier-Lavigne, "PTK7/CCK-4 is a novel regulator of planar cell polarity in vertebrates," *Nature*, vol. 430, no. 6995, pp. 93–98, 2004.

[278] S. Yamamoto *et al.*, "Cthrc1 Selectively Activates the Planar Cell Polarity Pathway of Wnt Signaling by Stabilizing the Wnt-Receptor Complex," *Dev. Cell*, vol. 15, no. 1, pp. 23–36, 2008.

[279] A. J. Copp, I. Checiu, and J. N. Henson, "Developmental basis of severe neural tube defects in the loop-tail (Lp) mutant mouse: use of microsatellite DNA markers to identify embryonic genotype," *Dev. Biol.*, vol. 165, no. 1, pp. 20–29, 1994.

[280] J. Wang *et al.*, "Regulation of polarized extension and planar cell polarity in the cochlea by the vertebrate PCP pathway.," *Nat. Genet.*, vol. 37, no. 9, pp. 980–5, 2005.

[281] S. Ahn, S. K. Shenoy, H. Wei, and R. J. Lefkowitz, "Differential kinetic and spatial patterns of beta-arrestin and G protein-mediated ERK activation by the angiotensin II receptor," *J. Biol. Chem.*, vol. 279, no. 34, pp. 35518–35525, 2004.

[282] A. Yu *et al.*, "Association of Dishevelled with the Clathrin AP-2 Adaptor Is Required for Frizzled Endocytosis and Planar Cell Polarity Signaling," *Dev. Cell*, vol. 12, no. 1, pp. 129–141, 2007.